Targeted treatment approaches and pathogenicity of antibody subclasses in MuSK-myasthenia gravis

by

Michelangelo Cao

Somerville College

A thesis submitted for the degree of Doctor of Philosophy,

Faculty of Medicine, University of Oxford

Michaelmas Term 2021

Abstract

Muscle Specific Kinase myasthenia gravis (MuSK-MG) is an autoimmune disease that impairs neuromuscular transmission leading to muscle fatigability. No targeted medications are currently available, and non-specific immunotherapies are required. MuSK initiates a phosphorylation cascade regulating the clustering of acetylcholine receptors (AChRs) at the neuromuscular junction (NMJ). SH2 domain-containing phosphatase (SHP2) negatively regulates the pathway inhibiting MuSK activation. In MuSK-MG, monovalent IgG4 autoantibodies block MuSK phosphorylation dispersing AChR clusters. The role of the smaller population of divalent MuSK IgG1, 2 and 3 antibodies is still undefined. The aims of the study were a) to test *in vitro* and *in vivo* SHP2 inhibition by NSC-87877 evaluating its efficacy in counteracting the effects of MuSK-Abs; b) to investigate the pathogenic contribution of MuSK IgG1-3-Abs.

Protein phosphorylation and AChR clustering were studied in different cell lines exposed to NSC-87877, and to either patients' purified MuSK-Ab subclasses or anti-MuSK monoclonals. NSC-87877 was tested for safety and efficacy in wild-type mice and a model of AChR deficiency syndrome. Effects of MuSK IgG1-3 were evaluated on impairment of the MuSK-Lrp4 interaction required for MuSK activation, and on the cytoskeleton activation necessary for cluster maturation. RNA transcriptomic analysis was performed to look for changes in intracellular pathways.

In vitro, NSC-87877 increased MuSK phosphorylation protecting AChR clusters from dispersal in the presence of all MuSK-Ab subclasses. Functional *MUSK* was required for the effectiveness of the drug. *In vivo*, no side effects were observed but the available genetice myasthenic syndrome models did not improve. Divalent MuSK antibodies activated the phosphorylation cascade but failed to sustain cluster maturation, impairing MuSK-Lrp4 interaction and cytoskeleton rearrangements. Transcriptomic analysis did

not detect specific changes that could inform on the mechanisms. In conclusion, SHP2 inhibition showed promising results *in vitro*, although more studies are needed *in vivo* to evaluate its potential effectiveness. Although the exact mechanisms of MuSK IgG1-3 antibodies were not identified, the work in this thesis confirms their potential pathogenic role in MuSK-MG that requires further investigation.

Acknowledgements

To Professor David Beeson, my supervisor, for his quiet and reassuring presence, and Professor Angela Vincent for her constant encouragement to be an independent thinker.

To Judith Cossins and Richard Webster, my second supervisors, for teaching me the importance of being critical of my own work and for the thorough proofreading of my Thesis.

To Isabel, Saif, Yin, Susan, Pedro, An, Mirela, Hakan, and David for being friends and not just colleagues.

To Leila, for having been by my side during the writing of all my four theses.

To Mum and Dad, for giving me a dream to achieve.

To my little Didi, for the world she is about to discover.

And to Wei Wei, for being my everything.

Table of contents

Chapter 1: Introduction……...1

1.1) General concepts on neurological autoimmune disorders…….....1

1.2) Myasthenia gravis……...5

SECTION I: Clinical features of myasthenia gravis: epidemiology, symptoms, diagnosis, and treatment

1.3) Myasthenia gravis with antibodies against the acetylcholine receptor (AChR-MG)…….....6

1.3.1) Epidemiology…….....6

1.3.2) Clinical features…….....8

1.3.3) Clinical subtypes……...10

1.3.4) Diagnosis……...11

1.3.5) Therapy…….....13

1.4) Myasthenia gravis with antibodies against the Muscle Specific Kinase (MuSK-MG)…….....17

1.4.1) Epidemiology……17

1.4.2) Clinical features…….…17

1.4.3) Diagnosis…….....19

1.4.4) Therapy…….….20

1.5) Seronegative myasthenia and the significance of Lrp4 antibodies…….....23

SECTION II: Pathophysiology of myasthenia gravis

1.6) Structure and physiology of the neuromuscular junction…….…….....24

1.6.1) Development of the neuromuscular junction and the agrin-Lrp4-MuSK pathway…….……...…….24

1.6.2) Transmission of the signal and clustering of the acetylcholine receptors…….……..30

1.6.3) Additional regulator pathways of the AChR clustering……35

1.6.4) Negative regulation of AChR clustering……...39

1.7) Pathophysiology of myasthenia gravis……..41

1.7.1) AChR-MG…….41

1.7.1.1) Pathogenic mechanisms of AChR antibodies……..41

1.7.1.2) Role of the thymus in AChR-MG……....43
1.7.2) MuSK-MG…….....44
1.7.2.1) Discovery of antibodies and pathogenicity studies…….....44
1.7.2.2) Another player of the game: the IgG1, 2 and 3 subclass antibodies……...…….....50
1.8) Initial steps towards a better understanding of the pathogenic mechanism of MuSK-MG and the development of a targeted treatment…….....51

Chapter 2: Materials and Methods……..55
2.1) Tissue culture……..55
2.2) NSC-87877…….56
Molecular biology techniques…….....56
2.3) Plasmids……..56
2.4) General principles of cell transfection……58
2.5) DOK7 wild type and DOK7 1124_1127dupTGCC overexpressing C2C12s……..……..63
2.6) Creation of Musk mutant cell lines…….....64
2.7) RNA extraction……...65
2.8) RNA sequencing analysis……...66
Protein and antibody purification techniques…….....67
2.9) Generation and Nickel-affinity purification of MuSK on HEK 293T……..……67
2.10) Generation and Nickel-affinity purification of MuSK on Drosophila S2 cells……...……...68
2.11) Samples of MuSK-myasthenia patients……....69
2.12) Purification of MuSK antibodies…….....69
Pull-down techniques……....71
2.13) Protein immunoprecipitation from cultured cells…….71
2.14) Co-immunoprecipitation of MuSK and LRP4 from transfected HEK cells……...……....72
2.15) Immunoprecipitation of MuSK from *ex vivo* muscle specimens……73
2.16) Pull-down of surface AChRs for phosphorylation analysis…….74
2.17) Immunoprecipitation of active Rho GTPase……....74
SDS-PAGE, western blotting and other protein analysis techniques……...75
2.18) SDS-Polyacrylamide gel electrophoresis (SDS-PAGE)……..75

2.19) Western blotting……...76
2.20) Densitometry analysis……..77
2.21) Dot blots……...79
2.22) Protein concentration determination by BCA colorimetric assay……79
2.23) Detection of active Rac1 GTPase by ELISA……....80
Immunohistochemistry techniques……....81
2.24) AChR clustering assay……..81
2.25) Immunostaining for rapsyn and actin filaments……...82
2.26) Cell-based assay……...82
Radioactive immunoassays……...83
2.27) MuSK radioimmunoassay…….83
2.28) Quantification of AChR membrane expression with radioactive assay…...84
2.29) Competition assay to estimate concentration of purified MuSK……..84
Animal work……..85
2.30) Animal welfare, breeding and genotyping……85
2.31) Clinical assessment of the mice……87
Statistical analysis…….87

Chapter 3: *In vitro* effects of SHP2 inhibition by NSC-87877……...92
3.1) Introduction…….92
3.2) Results…….93
3.2.1) Agrin production and titration…….93
3.2.2) Titration of the effects of NSC-87877 on MuSK Phosphorylation and AChR clustering……...95
3.2.3) MuSK phosphorylation time-course……...97
3.2.4) MuSK and AChR membrane expression……99
3.2.5) Effect of SHP2 inhibition on *MUSK* mutant cell lines…….101
3.2.6) Effects of SHP2 inhibition on DOK7 wild type and DOK7 1124_1127dupTGCC overexpressing C2C12s……..103
3.2.7) Modification in gene expression induced by NSC-87877……108
3.2.8) Production of MuSK IgG.…….111
3.2.8.1) IgG purification chromatography……...111
3.2.8.2) Cell based assay (CBA) to access efficacy of MuSK subclasses purification…….……..113
3.2.8.3) Radioimmunoassay (RIA)……..113

3.2.8.4) Additional purification of MuSK IgG1-3 subclasses…….116
3.2.8.5) Dot blots to access efficacy of MuSK subclasses Purification……...122
3.2.9) MuSK immunoprecipitation comparison between purified MuSK antibodies and commercial anti-MuSK AF562…….125
3.2.10) Testing NSC-87877 with MuSK antibodies……...127
3.3) Discussion…….129

Chapter 4: Safety and efficacy of NSC-87877 *in vivo* and purification of recombinant MuSK for active immunisation……...135
4.1) Introduction……..135
4.2) Results…….....137
4.2.1) MuSK immunoprecipitation from *ex vivo* specimens…….....137
4.2.2) Treatment trial with NSC-87877 in wild type mice……...…..139
4.2.3) MuSK phosphorylation analysis in AChR deficiency syndrome model mice……..……...…...141
4.2.4) Treatment with NSC-87877 does not improve the clinical phenotype of the AChR deficiency model…….....…...143
4.2.5) Purification of recombinant MuSK……...145
4.2.6) Active immunisation of the mice……..153
4.3) Discussion…….155

Chapter 5: Testing the monoclonal anti-MuSK antibodies…….161
5.1) Introduction……...161
5.2) Results……...162
5.2.1) Radioimmunoprecipitation assay (RIA) of MuSK monoclonal antibodies…….162
5.2.2) The monoclonal anti-MuSK antibodies inhibited AChR clustering….164
5.2.3) The monoclonal anti-MuSK antibodies increased MuSK phosphorylation……..……..167
5.2.4) Monoclonal MuSK antibodies induced AChR microclusters but failed to induce full cluster maturation……..171
5.2.5) Attempts to evaluate MuSK internalisation by monoclonal antibodies……...…….....173
5.3) Discussion…….176

Chapter 6: Differential effects of IgG subclasses on pathogenic mechanisms of MuSK myasthenia……...183
6.1) Introduction…….183
6.2) Results…….185
6.2.1) MuSK IgG1-3 and IgG4 had an opposite effect on MuSK and DOK7 phosphorylation……..185
6.2.2) Optimisation of AChR pull-down for phosphorylation analysis…….187
6.2.3) Agrin and MuSK IgG1-3 induced a similar phosphorylation time course for MuSK, DOK7 and βAChR…….189
6.2.4) MuSK antibody subclasses induced AChR microclusters but failed to sustain full cluster maturation……191
6.2.5) Staining of rapsyn and β-actin on C2C12 myotubes……...196
6.2.6) Co-localization between rapsyn and AChR microclusters is reduced compared to fully-formed clusters……..199
6.2.7) β-actin intracytoplasmic inclusions were present after exposure to MuSK antibodies……..202
6.2.8) MuSK IgG1-3 and IgG4 activated Rho GTPase…….204
6.2.9) Optimisation of MuSK-Lrp4 co-immunoprecipitation……...207
6.2.10) MuSK IgG1-3 partially reduced Lrp4-MuSK interaction…….....213
6.2.11) Transcriptional modifications induced by MuSK antibodies……214
6.3) Discussion……...224

Chapter 7: Discussion……...234

Bibliography……..243

List of figures

Figure 1.1. Lrp4-MuSK-DOK7 structures and interactions……..28
Figure 1.2. MuSK interactions with Wnt and BM4……..29
Figure 1.3. Schematic representation of the neuromuscular junction and the clustering pathway of acetylcholine receptors (AChRs)……...32
Figure 1.4. Negative regulators of the AChR pathways……...36
Figure 1.5. Structure of IgG4 subclass antibodies and mechanism of Fab arm exchange……..46
Figure 1.6. Proposed pathological mechanisms of MuSK autoantibodies at the neuromuscular junction……..49
Figure 1.7. Structure of NSC-87877 and its binding site on SHP2……...53
Figure 2.1. Structure of the pSecTagB plasmid carrying the gene for soluble agrin - short rat form……..59
Figure 2.2. Structure of the pEGFP-N1 plasmid with EGFP gene substituted with m-Cherry and attached to the C-terminus of human MuSK……..59
Figure 2.3. Structure of the pcDNA 3.1 hygro(+) plasmid carrying the soluble human MuSK ectodomain (aa22-452) with a His-tag sequence at the C-terminus…….60
Figure 2.4. Structure of the pMT/BiP/V5-HisA plasmid carrying the soluble human MuSK ectodomain (aa22-452) with a His-tag sequence at the C-terminus……..60
Figure 2.5. Structure of pcDNA 3.1 hygro(-) plasmid carrying the human LRP4 gene……....61
Figure 2.6. Structure of pcDNA 3.1 hygro(+) plasmid carrying the human gene for the β subunit of the AChR (CHRNB1)……..61
Figure 2.7. Structure of pBabe-PURO-EGFP plasmid carrying the human DOK7 Wild Type gene…….62
Figure 2.8. Structure of pBabe-PURO-EGFP plasmid carrying the human DOK7 1124_1127dupTGCC mutant gene……...62
Figure 2.9. Example of western blot densitometry quantification……78
Figure 2.10. Genotype analysis of AChR-deficiency syndrome animal model……88
Figure 3.1. Titration of agrin on AChR clustering……94
Figure 3.2. SHP2 inhibition by NSC-87877 induces MuSK phosphorylation and AChR clustering…….....96
Figure 3.3. Agrin counteracts the inhibitory effects of high concentration

of NSC-87877 on MuSK phosphorylation and AChR clustering……..98
Figure 3.4. Agrin and NSC-87877 induces a similar MuSK phosphorylation time course……...100
Figure 3.5. In the C2C12 myotubes, NSC-87877 increases the membrane expression of AChRs while MuSK expression remains unchanged……102
Figure 3.6. SHP2 inhibition by NSC-87877 has no effect on MuSK phosphorylation and AChR clustering in MuSK KO and *MUSK* p.C317R myotubes……...104
Figure 3.7. The mutant DOK7 1124_1127dupTGCC generates a truncated non-functional protein……106
Figure 3.8. SHP2 inhibition by NSC-87877 increases MuSK phosphorylation and AChR clustering in *DOK7* overexpressing myotubes but has no effect on the DOK7 1124_1127dupTGCC……...108
Figure 3.9. Elution profiles of purified IgG antibody fractions……..112
Figure 3.10. Cell-based assay to verify purity of MuSK antibody subclass preparations……114
Figure 3.11. Titration of MuSK antibody subclasses by radioactive immunoassay...115
Figure 3.12. Screening of MuSK IgG1-3 antibody positivity by Cell Based Assay..118
Figure 3.13. MuSK-ab titration for initial screening of patients…….119
Figure 3.14. Purification of antibody subclasses and titration of MuSK antibodies by RIA……..121
Figure 3.15. Dot blots to evaluate purity of IgG antibody subclass preparations…...124
Figure 3.16. MuSK immunoprecipitation comparison in the presence and absence of commercial anti-MuSK AF562 using patients' purified IgG4……..126
Figure 3.17. NSC-87877 protects MuSK phosphorylation from MuSK Total IgG and IgG4, and prevents AChR clustering dispersal in the presence of all MuSK IgG subclasses…….128
Figure 4.1. MuSK immunoprecipitation from ex vivo specimens……..138
Figure 4.2. Treatment trial with NSC-87877 in wild type mice……..140
Figure 4.3. MuSK phosphorylation analysis in AChR deficiency syndrome model mice (γ model)……..142
Figure 4.4. Two different treatment protocols with NSC-87877 did not improve the clinical phenotype of the AChR deficiency model……..144

Figure 4.5. Purification of MuSK extracellular domain expressed in

HEK 293T cells……146
Figure 4.6. Purification of ecto-MuSK in Drosophila S2 cells……...150
Figure 4.7. Diagram of the protocol to create the MuSK-MG active immunisation model……154
Figure 5.1. Radioimmunoprecipitation assay (RIA) of MuSK monoclonal antibodies……..163
Figure 5.2. Effect of monoclonal MuSK antibodies on AChR clustering……..168
Figure 5.3. Effect of monoclonal MuSK antibodies on MuSK phosphorylation……169
Figure 5.4. Qualitative differences between fully-formed AChR clusters and microclusters……172
Figure 5.5. Monoclonal MuSK antibodies induced AChR microclusters but failed to induce full cluster formation……..174
Figure 5.6. Staining of MuSK on myotubes with monoclonal antibodies……..175
Figure 5.7. Staining attempt of MuSK on myotubes with monoclonal antibodies….177
Figure 6.1. IgG1-3 and IgG4 had an opposite effect on MuSK and DOK7 phosphorylation……186
Figure 6.2. Optimisation of AChR pull-down for phosphorylation analysis……..188
Figure 6.3. Agrin and MuSK IgG1-3 induced a similar phosphorylation time course for MuSK, DOK7 and βAChR…….190
Figure 6.4. MuSK antibody subclasses induced AChR microclusters but failed to sustain full cluster maturation……..192
Figure 6.5. MuSK IgG1-3 partially increased AChR microclusters overtime but not fully-matured clusters…….194
Figure 6.6. MuSK IgG1-3 partially reduced AChR membrane expression……195
Figure 6.7. SHP2 inhibition increased both micro- and fully-formed AChR clusters in the presence of MuSK antibodies……..197
Figure 6.8. Optimisation of rapsyn and β-actin staining on C2C12 myotubes……...198
Figure 6.9. Optimisation of β-actin staining on C2C12 myotubes…….200
Figure 6.10. Co-localization between rapsyn and AChR microclusters is reduced…201
Figure 6.11. Altered structure of b-actin with intracytoplasmatic inclusions was detected in the presence of MuSK antibodies……203
Figure 6.12. MuSK IgG1-3 and IgG4 activate of Rho GTPase……..205
Figure 6.13. Agrin and MuSK IgG1-3 did not activate Rac1 GTPase……...208
Figure 6.14. Detection of Lrp4 on transfected HEK cells……..209
Figure 6.15. Optimisation of MuSK-Lrp4 co-immunoprecipitation from

HEK 293 cells and C2C12 myotubes……211
Figure 6.16. MuSK IgG1-3 partially reduced MuSK-Lrp4 interaction……..215
Figure 6.17. Transcriptional modifications induced by agrin on C2C12 myotubes...218
Figure 6.18. Transcriptional modifications induced by MuSK IgG1-3 on C2C12 myotubes……225

List of tables

Table 2.1. List of antibodies……89
Table 2.2 List of Materials……..90
Table 3.1. Genes modified significantly by NSC-87877 compared to DMEM……109
Table 3.2. Genes modified significantly by NSC-87877 compared to agrin……110
Table 3.3. Summary of total IgG and IgG subclasses purification……....117
Table 3.4. MuSK antibodies titration by RIA of the plasma samples from patients 4, 5, 6, 8, and 10……..120
Table 3.5. Summary of IgG subclasses purification from pooled MuSK-MG patients' plasma……123
Table 4.1. Volumes and protein concentrations of ecto-MuSK purification in HEK 293T cells……148
Table 4.2. Volumes and protein concentrations of ecto-MuSK purification in Drosphila S2 cells……152
Table 5.1. MuSK monoclonal antibodies titration by RIA……165
Table 5.2. Estimated concentration of monoclonal anti-MuSK antibodies……...166
Table 6.1. Genes modified by agrin compared to DMEM……217
Table 6.2. Genes and corresponding protein products up- and down-regulated by both MuSK IgG1-3 and total IgG from a healthy individual……...219
Table 6.3. Genes and corresponding protein products selectively upregulated by MuSK IgG1-3……...220
Table 6.4. Genes and corresponding protein products selectively downregulated by MuSK IgG1-3……..221

Chapter 1

Introduction

The focus of this thesis is myasthenia gravis with antibodies against Muscle Specific Kinase (MuSK-MG), an autoimmune disorder that was identified as a distinct nosographic entity only twenty years ago. The pathogenic mechanisms underlying MuSK-MG are still not completely defined, but are thought to be mainly caused by a specific subclass of autoantibodies (IgG4) which are not commonly associated with other autoimmune diseases. In addition, no specific treatments are currently available for MuSK-MG, except long-term immunosuppression. This study aimed to test a potential therapeutic approach to target the specific pathogenic effects of MuSK antibodies, and to further characterise the mechanism of action of the IgG1, 2 and 3 antibody subclasses also found in the disease.

1.1) Neurological autoimmune disorders

The dysregulation of the immune system with the consequent loss of self-tolerance is responsible for several different disorders that affect the nervous system. Each one of these diseases differs from the others in terms of epidemiology, clinical manifestations, pathophysiology, and response to treatment. Multiple sclerosis, myasthenia gravis, limbic encephalitis, Guillain-Barré syndrome are just a few names that exemplify the variety of diseases grouped under the common denominator of "autoimmunity".

From a clinical perspective, these disorders can be classified according to the part of the nervous system targeted by the autoimmune process. The central and peripheral nervous systems express many different antigens and the concomitant involvement of the two is uncommon (with the exception of Morvan's syndrome). Clinical manifestations are related to the neural area affected and to the pathogenic mechanism

underlying each individual disease. For example, when the cerebral cortex is primarily involved, symptoms are consistent with epileptic seizures, behavioural changes, and cognitive impairment defining the clinical picture of limbic encephalitis. A pathological process that targets the oligodendrocytes or astrocytes inducing central demyelination (e.g. multiple sclerosis and neuromyelitis optica) will cause focal and disseminated neurological signs with selective and often asymmetric muscle weakness, numbness, diplopia, ataxia, hyperreflexia and spasticity. Conversely, when the myelin layers of the peripheral Schwann cells are involved (e.g. Guillain-Barre' syndrome and Chronic Inflammatory Demyelinating Polyneuropathy – CIDP), the clinical picture will be consistent with a peripheral neuropathy with predominant distal-more-than-proximal muscle weakness, atrophy, hypotonia, sensory loss, paraesthesias, and neuropathic pain. Muscle hyperexcitability with neuromyotonia, together with autonomic dysfunction, epileptic seizures and behavioural changes define Morvan's fibrillary chorea, in which autoantibodies target the proteins of the voltage-gated potassium channel complex. Finally, the impairment of the neuromuscular junction, either pre- or post-synaptic, will determine the typical fluctuating weakness and fatigability characteristic of myasthenic disorders.

Several antigens have been identified over the years and are targeted by specific autoantibodies. Depending on their topographic expression, they can be summarised as following:

- Antigens expressed on the soma of the neurons: receptors for N-methyl-D-aspartate (NMDAR), α-amino-3-hydroxy-5-methyl-4-isoxazolepropionic acid (AMPAR), gamma-amino butyric acid (GABAR), and glutamic acid decarboxylase (GAD). Antibodies to these are clinically associated with limbic encephalitis (NMDAR, AMPAR, and GABAR), and autoimmune cerebellitis (GAD);

- Antigens expressed at the nodes of Ranvier: voltage-gated potassium channel complex (VGKC) proteins contactin-associated protein 2 (CASPR2) and leucine-rich glioma-inactivated 1 (LGI1) – and other paranodal protein such as neurofascins (Nfasc-155, Nfasc-140, Nfasc-186), contactin-1 (CNTN1) and contactin-associated protein 1 (CASPR1). Antibodies directed against these antigens are responsible for Morvan's chorea (CASPR2), limbic encephalitis (LGI1), and different peripheral inflammatory neuropathies;
- Antigens expressed on the glial cells (either central or peripheral): aquaporin 4 (AQP4), myelin oligodendrocyte glycoprotein (MOG), myelin-associated glycoprotein (MAG), and different gangliosides (GMs). Autoantibodies against these antigens have been identified in patients with neuromyelitis optica (AQP4 and MOG), ADEM syndrome (MOG), Distal Acquired Demyelinating Symmetric Neuropathy (MAG), Guillain-Barre' syndrome and other inflammatory peripheral neuropathies (GMs);
- Antigens expressed at the neuromuscular junction: voltage-gated calcium channel (presynaptic), acetylcholine receptor (AChR) and muscle specific kinase (MuSK) (postsynaptic) in the Lambert-Eaton myasthenic syndrome and myasthenia gravis.

Notably, despite the significant advances that have been achieved in the understanding of the pathogenic mechanisms underlying each individual disease, the initial cause that triggers the loss of self-tolerance and the consequent attack to the body's own antigens remains elusive. As for many other multifactorial diseases (such as tumours, hypertension, diabetes), a combination of genetic predisposition (represented mainly by the Human Leucocyte Antigen (HLA, Histocompatibility Complex) and environmental factors (such as viral and bacterial infections, or exposure to other non-

biological substances) is likely to be responsible for the development of autoimmune disorders in an individual (reviewed in (Bodis, Toth et al. 2018, Rojas, Restrepo-Jimenez et al. 2018)).

With the relevant exception of multiple sclerosis – in which the autoimmune process is driven by the cellular immunity of T lymphocytes (Halpern, Bakouche et al. 1969) – the majority of the other syndromes is mediated by humoral immunity including autoantibodies produced by autoreactive B lymphocytes. The identification of the different antibodies in patients' samples (specifically plasma and/or cerebro-spinal fluid) has become the gold standard to confirm a clinical diagnostic suspicion, thanks to the significant improvement in sensitivity and specificity of the modern detection techniques (such as cell-based assays).

Pathophysiological *in vitro* and *in vivo* studies are essential to determine how specific autoantibodies cause the clinical manifestations of individual diseases. These would depend on the intrinsic function of the target antigen, and the subclass of antibody involved in the autoimmune process. In this respect, IgG of the 1, 2 and 3 subclasses are known to activate the complement cascade leading to tissue damage, and to reduce the antigen membrane expression by inducing its internalisation through divalent binding (reviewed in (Vidarsson, Dekkers et al. 2014)). However, while most of the aforementioned antigens are targeted by IgG1-3 antibodies, an increasing number of neurological syndromes are now recognised as IgG4-mediated, including limbic encephalitis, Morvan's chorea, MuSK myasthenia, and CNTN1 inflammatory neuropathy (Irani, Pettingill et al. 2012, Huijbers, Zhang et al. 2013, Devaux, Miura et al. 2016). In these cases, novel pathogenic models have been proposed (such as direct interference of the antigen function) to explain the effect of IgG4 antibodies which are unable to activate complement and to bind divalently to their antigen (reviewed in (Koneczny 2018)).

A deeper understanding of the specific pathogenic processes triggered by individual antibodies is necessary not only to widen our knowledge regarding the pathophysiology of these diseases, but also to provide the basis for the development of targeted treatments to use in the everyday clinical practise.

1.2) Myasthenia gravis

Among the several autoimmune disorders that affect the nervous systems, myasthenia gravis (MG) is one of the most studied and better understood, thanks to the intense research carried out over the past 50 years and the accessibility of the neuromuscular junction (NMJ) for experimental purposes. Myasthenia gravis can be considered a paradigm of antibody-mediated diseases and the pathogenic mechanisms underlying the symptoms have provided a wide understanding of the role of the different IgG subclasses and how they cause impairment of the NMJ.

Myasthenia is a heterogeneous disorder with respects to its clinical manifestations and pathogenic mechanisms. However, all forms of myasthenia have in common the post-synaptic impairment of neuromuscular transmission, which leads to the typical clinical features of the disease. These consist of fluctuating weakness and fatigability of the skeletal muscles, which deteriorate during exertion and improve with rest. Range of symptom severity is wide, from mild and inconstant involvement of the ocular muscles to life-threatening respiratory and swallowing impairment.

Two proteins expressed at the NMJ, the acetylcholine receptor (AChR) and the muscle specific kinase (MuSK), represent the main targets of autoantibodies and define the two major subtypes of myasthenia. Antibodies against a third protein of the NMJ, the low-density-lipoprotein receptor-related protein 4 (Lrp4), have also been reported and their pathogenic potential suggested by different *in vitro* and *in vivo* studies. However, their clinical relevance remains debatable. Finally, it is worth mentioning that

a myasthenic-like disorder, the Lambert-Eaton syndrome (LEMS), is associated with autoantibodies against the voltage-gated calcium channel expressed on the terminal of the motor neuron axon. For this reason, the impairment of the neuromuscular transmission is pre-synaptic differentiating LEMS from MG (Eaton and Lambert 1957).

The epidemiology, symptom distribution, severity, and response to treatment of the different forms of myasthenia vary according to which antibody is responsible for the disease. Therefore, antibody identification represents a fundamental step to confirm the initial clinical suspicion and to choose the most effective therapy.

Among neurological disorders, myasthenia gravis is usually regarded as a treatable disease with different therapeutic options including steroids, immunosuppressant and immunomodulatory drugs. Although these treatments are often effective to control symptoms, they lack specificity and might cause a wide range of side effects as they target the whole immune system. This is particularly true for the form of myasthenia caused by antibodies against MuSK, which is typically more severe and more resistant to treatments compared to the form sustained by antibodies against AChR.

SECTION I: Clinical features of myasthenia gravis: epidemiology, symptoms, diagnosis, and treatment

1.3) Myasthenia gravis with antibodies against the acetylcholine receptor (AChR-MG)

1.3.1) Epidemiology

Due to its clinical and immunological heterogeneity, it is difficult to make a precise estimation of the real prevalence and incidence of myasthenia. If we consider the disease as a whole, a meta-analysis that pooled 55 studies performed between 1950 and 2007 around the world showed an overall incidence rate of 5.3:1000000 population/year and a prevalence rate of 77.7 cases/1000000 population (Carr, Cardwell et al. 2010).

Notably, the prevalence of myasthenia has been rising over the last 40 years, and this could be due to a more accurate diagnosis (following the introduction of the radioimmunoassay to detect antibody titres), the recognition of the disease in older people, better health care of the patients (which live longer), and more precise epidemiological studies.

The variations in incidence and prevalence rates observed among the studies of the meta-analysis represent evidence of the heterogeneous background of myasthenia. Age of onset, gender and geographical distribution vary significantly according to HLA genotypes, thymus involvement, and type of antibodies that sustain the disease. In North America and Europe, *HLA-DR3* and *B8* alleles are strongly associated with AChR-MG with early onset and thymic hyperplasia (Compston, Vincent et al. 1980, Janer, Cowland et al. 1999) whereas late-onset cases are weakly associated with *HLA-DR2* and *B7* (Giraud, Vandiedonck et al. 2008). *HLA-DR9* allele represents a risk factor in Asian people with a higher infantile onset (<15 years of age) particularly in China and Japan (Matsuki, Juji et al. 1990, Yu, Hawkins et al. 1992, Chen, Chiu et al. 1993, Zhang, Yang et al. 2007).

With respect to genders, males present the peak of incidence after the age of 60, whilst females have a bimodal distribution with two different peaks, one between the second and third decade of life, and the second after menopause at a similar age to men (Vincent, Bowen et al. 2003, Heldal, Owe et al. 2009, Carr, Cardwell et al. 2010) indicating a potential correlation with the disease and fertility hormones. There is also evidence that the incidence of AChR-MG is increasing among elders, and this is unlikely related only to a prolonged life expectancy (Phillips and Torner 1996, Vincent, Clover et al. 2003, Somnier 2005, Matsui, Nakane et al. 2009, Carr, Cardwell et al. 2010, Pakzad, Aziz et al. 2011).

1.3.2) Clinical features

Myasthenia gravis was first described in 1672 by Thomas Willis who reported the case of a woman with a fluctuating palsy of her limbs and tongue (Hughes 2005). In his book "De anima brutorum", Willis draws an accurate picture of the basic symptoms that characterise myasthenia writing that "*those who be in trouble with a scarcity of spirits, are able at first rising in the morning to walk, move their arms this way and that, or to lift up a weight with strength; but before noon, the stores of spirits which influenced the muscles being almost spent, they are scarce able to move hand or foot*".

The name myasthenia gravis was coined in late 19th century fusing the Greek words "*μῦς*" (muscle) and "*ἀσθένεια*" (weakness). The Latin adjective "*gravis*" was added to highlight the severity that in the past characterised the prognosis of the disease, almost inevitably fatal, when no treatment was available (Keesey 2002).

Patients affected by myasthenia present a fluctuating weakness that involves the skeletal muscles in a typical and usually recognisable pattern. Fatigue of eye, limb, or bulbar/respiratory muscles worsens with exercise and improves with rest, sometimes with full recovery. Therefore, symptoms could be mild or even absent during the first hours after awakening and tend to worsen during the day with a characteristic circadian pattern.

In 60% to 85% of patients, the onset of the disease involves the extraocular muscles that control gaze movements (Grob, Brunner et al. 2008, Guptill, Sanders et al. 2011). This causes double vision (diplopia) and droopiness (ptosis) of the eyelids, often asymmetrical, exacerbated by activities that imply focus of the gaze such as reading, watching television and driving. The frequent muscle contraction to finely tune the gaze movements and to maintain opening of the eyelid could be one explanation for the selective susceptibility of the extraocular muscles. Within two years from an ocular onset, between 50% and 80% of AChR-MG patients have generalisation of their

weakness with limb and/or bulbar involvement (Antonio-Santos and Eggenberger 2008). Two years is considered the threshold after which, if the symptoms remain confined to the ocular muscles, it is unlikely that the disease will spread to other muscles (Kerty, Elsais et al. 2014).

In generalised myasthenia, weakness of limb muscles is typically symmetric and more proximal than distal, although cases with prevalent distal and asymmetric involvement have been reported (Nations, Wolfe et al. 1999, Rodolico, Toscano et al. 2002). Impairment of neck and axial muscles is usually associated with the bulbar form of the disease consistent with variable degree of difficulty in swallowing (dysphagia - mainly for fluids and associated sometimes with weight loss), speaking (dysarthria and dysphonia – often with nasal voice), and breathing (dyspnoea) (Meriggioli and Sanders 2009). These symptoms are potentially life-threatening and define a myasthenic crisis when the severity of the exacerbation requires intubation of the airways due to the failure of respiratory muscles (Bedlack, Simel et al. 2005). About 15-20% of myasthenic patients experience this kind of crises at least once during their illness, and, among those, one fifth will have a crisis as the first manifestation of myasthenia (Wendell and Levine 2011). Myasthenia has a relapsing-remitting course. Exacerbations of symptoms are due mainly to intermittent infections, pharmacological treatments for intercurrent diseases (antibiotics, anticonvulsants, statins, anaesthetics, and antihypertensives), too fast withdrawal of immunotherapy, pregnancy and surgery. The disease tends to progress to its highest severity during the first 5 years after its onset and, in this period, crises are also more frequent. After this initial period, myasthenia usually stabilises in terms of general symptomatology and exacerbations while permanent and spontaneous remission occurs in about 10% of cases (Grob, Brunner et al. 2008).

1.3.3) Clinical subtypes

Accounting for about 80% of all myasthenic cases, AChR-MG can be classified into the following groups according to the age of onset and its association with thymic pathology:

- Early-onset myasthenia: the onset is set before the age of 40-50, with female predominance (F:M of 3:1) (Meriggioli and Sanders 2009). Thymic follicular hyperplasia is common, and patients usually respond well to thymectomy. There is a strong association with *HLA-DR3*, *HLA-B8* and with other autoimmune diseases, especially thyroiditis, both in the patient and their families (Compston, Vincent et al. 1980, Mao, Yang et al. 2011, Klein, Marx et al. 2013).
- Late-onset myasthenia: the age of onset is usually considered after 50 years, although this threshold could vary between studies. Males are more affected than females (approx. 1.5:1) and thymic pathology is rare (Aarli 2008, Marx, Pfister et al. 2013). Therefore, thymectomy is usually not indicated. There is a weak association with *HLADR2*, *HLA-B7*, and *HLA-DRB1*15:01* (Compston, Vincent et al. 1980). Alongside AChR-Abs, other antibodies against striated muscle antigens (specifically titin and the ryanodine receptor), interferon-alpha and interleukin 12 are detected in a high proportion of late-onset patients with no thymoma (Buckley, Newsom-Davis et al. 2001). Their pathogenic relevance remains unknown but they are associated with a more severe disease (Romi, Skeie et al. 2000).
- Thymoma-associated myasthenia: this is a paraneoplastic subtype directly sustained by the malignant tumour affecting the thymus. The incidence of thymoma reaches the peak at the age of 50 with no gender predominance (Marx, Pfister et al. 2013). Myasthenic symptoms tend to be more severe compared to non-thymomatous forms. About 10-15% of all myasthenic patients are

thymoma-associated, and virtually all of them have AChR-Abs (Grob, Brunner et al. 2008). In addition, patients with thymoma could have detectable serum AChR-Abs even in the absence of myasthenic symptoms, suggesting the presence of subclinical disease (Vincent and Newsomdavis 1985). Although the titre of AChR-Abs is usually lower in thymoma cases compared to other subgroups of myasthenia, it can rise following thymectomy if immunotherapies are not administered. Antibodies against other muscle intracellular antigens (such as titin, the ryanodine receptor, and rapsyn) are frequently found in patients with thymoma (Agius, Zhu et al. 1998, Buckley, Newsom-Davis et al. 2001, Aarli 2008). Although the finding of these antibodies is also relatively common in late onset cases without an underlying tumour, their detection in young patients is highly suggestive for the presence of thymoma (Buckley, Newsom-Davis et al. 2001).

1.3.4) Diagnosis

The diagnosis of myasthenia is based on clinical symptomatology, neurophysiology recording, and antibody detection. Clinical suspicion arises when the patient describes fluctuating weakness, without concomitant sensory impairment, that improves with rest and that affects skeletal muscles, particularly the eye and proximal limbs.

When performed on clinically affected muscles, electromyography (EMG) with repetitive nerve stimulation is able to support the clinical suspicion. It typically shows a decrement of about 10% in the amplitude of the compound muscle action potential while stimulating the nerve at 2–5 Hz. The sensitivity of this test for generalised MG reaches its maximum (up to 90%) if performed on proximal or facial muscles, but it drops dramatically in the pure ocular disease and when tested on distal muscles such as the abductor digiti quinti (between 30-60%) (Zambelis, Kokotis et al. 2011). The

repetitive stimulation on a single muscle fibre (Single Fiber ElectroMyoGram - SFEMG) provides higher sensitivity and specificity, although it is more operator-dependent and available only in specialised centres. SFEMG analyses the variation of inter-potential interval (jitter) between different muscular fibres. A prolonged jitter value (according to standardised thresholds specific for individual muscles and patient's age (Bromberg and Scott 1994)) is considered abnormal and diagnostic for impairment of neuromuscular transmission. A properly performed SFEMG can reach a very high sensitivity (up to 99%) in the detection of myasthenia gravis (Sanders and Stalberg 1996, Sarrigiannis, Kennett et al. 2006). However, specificity is not as high; abnormal values can be found in primary myopathies and neuropathies (Sarrigiannis, Kennett et al. 2006). Therefore, the results – and the electrophysiological study in general – should be interpreted considering the overall clinical picture and the likelihood of other diagnoses.

Laboratory tests have become progressively more and more important and, nowadays, antibody detection and characterisation represent the gold standard to confirm the diagnosis of myasthenia. Identifying antibody type and their target antigen are not only necessary for diagnostic purposes but can also guide the most appropriate treatment. The radioimmunoprecipitation assays (RIA) is the most available and specific test for detection of AChR-Abs. In generalised MG, its sensitivity is above 85% and reaches almost 100% in patients with thymoma. However, RIA sensitivity drops to 50-60% in detecting pure ocular forms (Oger, Kaufman et al. 1987) although its specificity remains high (virtually 100%) regardless of distribution of the deficit. In this respect, due to its high specificity, a positive RIA is sufficient to confirm a diagnosis of MG. The RIA was first introduced by Lindstrom in 1973 (Patrick, Lindstrom et al. 1973). The acetylcholine receptor is mixed with ^{125}I-α bungarotoxin (a radioactive-labelled snake toxin that binds selectively to the AChR) and, after incubation with the

patient serum, a second antibody is added to precipitate the ^{125}I-α bungarotoxin-AChR-Ab complexes. The radioactive counts are then measured and results are compared to healthy control sera.

Despite the high sensitivity of the RIA, a proportion of patients (10-15%) are not positive. In this respect, the introduction of cell-based assays (CBA) in the last decade has increased the detection rate for all subtypes of MG. CBAs avoid the need for radioactivity and provide a more physiological environment for testing as the antigen is expressed in mammalian cells, allowing appropriate glycosylation, folding and positioning at the cell surface. This permits the detection of autoantibodies with lower antigen affinity and/or concentration. In the CBA, human embryonic kidney-293T (HEK) cells are transfected with the cDNA coding for the AChR to express on the cell surface together with a fluorescent tag. All five of the genes of the AChR subunits (adult type) are transfected together with rapsyn in order to express a full clustered AChR and mirror a more physiological condition compared to the RIA. The AChR CBA is able to identify up to 66% of patients who were previously negative in the conventional RIA, including 50% of the ocular forms, and is particularly useful in differentiating seronegative myasthenia (SNMG) from genetic forms of myasthenia (Leite, Jacob et al. 2008, Jacob, Viegas et al. 2012, Cruz, Al-Hajjar et al. 2015).

1.3.5) Therapy

Among neurological and neuromuscular diseases, myasthenia gravis is one of the few that can be successfully treated providing a complete and stable remission in a significant proportion of patients; in parallel advances in therapy have markedly reduced both mortality and morbidity. Due to our growing understanding of the pathogenic mechanisms that sustain the disease, a variety of treatments has been

developed ranging from symptomatic drugs that improve neuromuscular transmission, to specific immunomodulatory therapies that inhibit the production of antibodies.

Acetylcholinesterase (AChE) inhibitors were the first treatment for myasthenia discovered in the 1930s thanks to the intuition of a clinical fellow, Mary Walker. Recognising that myasthenic symptoms were similar to those caused by curare poisoning, Dr Walker administered an intravenous dose of physostigmine to a myasthenic patient producing a partial and temporary symptom improvement (Pearce 2005). This not only provided the first safe therapy for myasthenic patients but also suggested, for the first time, that the disease was caused by an impairment of the neuromuscular junction. Oral AChE inhibitors are still broadly used as a first-line treatment: acting inside the synaptic cleft, they reduce the enzymatic cleavage of ACh molecules, increasing the total amount of the neurotransmitter and prolonging the time during which ACh can stimulate its receptor.

Corticosteroids are introduced when symptoms are not fully controlled by AChE inhibitors. They have been used effectively for the past 50 years as they suppress the expression of pro-inflammatory cytokines (TNF-α and IL-1), inhibit the transcriptional factor NF-KB reducing leucocyte proliferation, and impair T cell maturation in the thymus (reviewed by (Coutinho and Chapman 2011). Steroids are highly effective in controlling MG symptoms, preventing relapse of the disease, and potentially reducing the risk of generalisation in pure ocular forms (Benatar, Sanders et al. 2012, Kerty, Elsais et al. 2014). However, their prolonged administration causes relevant side effects (hypertension, diabetes, weight gain, and osteoporosis) and the lowest possible dose that maintains pharmacological remission should be used.

Immunosuppressants are added with the purpose of "sparing" steroids in those patients that depend on long-term high doses of steroids. However, a combined therapy is usually needed as all immunosuppressants require several months before becoming

fully effective. Azathioprine is usually the first-line choice for its effectiveness and safety (Bromberg, Wald et al. 1997, Palace, Newsom-Davis et al. 1998). If this is not beneficial or tolerated, second-line immunosuppressants include cyclosporine and mycophenolate mofetil that have been adopted in MG after their wide use in anti-rejection treatment for transplants (Tindall, Phillips et al. 1993, Bonifati and Angelini 1997, Ciafaloni, Nikhar et al. 2000, Meriggioli, Ciafaloni et al. 2003). They are both considered effective but present major and more severe side effects compared to azathioprine (including nephrotoxicity, increased risk of infections and tumours). Methotrexate is also used in myathenia despite that only a single clinical trial has been performed providing no evidence of its sparing-steroid effect (Pasnoor, He et al. 2016). Nevertheless, justification for its application in myasthenic patients comes from its effectiveness in other autoimmune diseases.

Refractory MG patients, in whom at least two independent immunosuppressive treatments have been carried out at therapeutic dosage without benefit, should be considered for treatment with rituximab, a monoclonal chimeric IgG1 that depletes B lymphocytes through specific binding to the CD20 transmembrane antigen (Maddison, McConville et al. 2011, Kaegi, Wuest et al. 2019, Di Stefano, Lupica et al. 2020). Despite the fact that controlled studies have not been done yet, early evidence showed that about two thirds of patients with insufficient response to other immunosuppressive treatments had a significant improvement following rituximab administration. This is particular evident in MuSK-Ab myasthenia as detailed later on in this chapter. The use of other biologic drugs – including monoclonal antibodies that targets CD20, CD40, or the IL6-receptor (Ofatumumab, Iscalimab, Tocilizumab), complement inhibitors (Eculizumab, Zilucoplan), and FcRn antagonists (Efgartigimod) – is still in its infancy with only one (Eculizumab) clinically used as an add-onto treatment for refractory forms of AChR-MG, whereas all the remaining drugs are still undergoing pilot trial

studies ((Howard, Freimer et al. 2017, Howard, Utsugisawa et al. 2017, Jonsson, Pirskanen et al. 2017, Howard, Bril et al. 2019, Waters, Field et al. 2019, Howard, Nowak et al. 2020)).

Severe relapses and life-threatening myasthenic crises require acute treatment with either intravenous immunoglobulins (IVIg) or plasmapheresis. Both are usually highly effective (up to 96% of positive response for plasmapheresis irrespective of patients' antibody status) with a rapid control of the symptoms lasting for about 4-6 weeks (Usmani, Kwan et al. 2019). IVIg are less invasive and usually better tolerated than plasmapheresis with fewer side effects (Ronager, Ravnborg et al. 2001, Zinman, Ng et al. 2007). While the mechanism of action of plasmapheresis is quite intuitive (physical removal of autoantibodies and complement proteins by filtration of patient's plasma), how IVIg actually work is still not fully understood. Cytokine and complement inhibition, competition with autoantibodies, and interference with Fc receptor binding are the main mechanisms suggested (reviewed in (Norris, Kaur et al. 2020)).

Finally, thymectomy represents an important therapeutic procedure in early-onset AChR-MG and thymoma-related MG. Despite being in practice since 1941 (Blalock, Harvey et al. 1941), only one recent randomized trial study has finally provided the evidence that the thymectomy gives substantial clinical benefits in AChR-MG patients showing the necessity of a significantly lower dose of steroids in the thymectomised patient cohort (Wolfe, Kaminski et al. 2016, Wolfe, Kaminski et al. 2019). Importantly, thymectomy has its highest effectiveness within 5 years from disease onset (Gronseth and Barohn 2000). In case of thymoma, the removal of the tumour is necessary to avoid the spreading of the malignancy. However, in this case, thymectomy usually does not provide a significant improvement of muscle weakness as the autoimmune process has already been triggered and sustained by peripheral cells (Hoffacker, Schultz et al. 2000, Buckley, Douek et al. 2001).

1.4) Myasthenia gravis with antibodies against the Muscle Specific Kinase (MuSK-MG)

1.4.1) Epidemiology

Original estimates indicated that myasthenia gravis with antibodies against MuSK was responsible for about 70% of all the AChR-Ab negative cases, although this percentage was found to be dependent greatly on the population studied with significant variations according to country of origin and ethnicity (Vincent and Leite 2005, Oh, Morgan et al. 2009). Due to this variability, its general prevalence is difficult to evaluate, and several epidemiological studies have been carried out since MuSK-Abs were discovered in 2001 (Hoch, McConville et al. 2001). These studies showed that Mediterranean countries (especially Italy, Turkey and Greece) have the highest frequency of cases (Evoli, Tonali et al. 2003, Tsiamalos, Kordas et al. 2009). On the other hand, prevalence is lower among those populations that live at northern latitudes (Niks, Kuks et al. 2007, Vincent, Leite et al. 2008), and higher in people of Afro-American origin (Oh, Morgan et al. 2009). Considering this particular ethno-geographical distribution, together with the association with HLA class II DR14 DQ5 (Niks, Kuks et al. 2006, Bartoccioni, Scuderi et al. 2009, Alahgholi-Hajibehzad, Yilmaz et al. 2013), genetic background is likely to play a significant role in the aetiology of MuSK-MG although other – and still undetermined – environmental factors are also likely to be involved.

With respect to gender distribution, MuSK-MG affects predominantly women (F:M of 9:1), especially young females in their third decade (Evoli, Tonali et al. 2003, Guptill, Sanders et al. 2011) and it is reported rarely in elders and children (Pasnoor, Wolfe et al. 2010, Skjei, Lennon et al. 2013).

1.4.2) Clinical features

From a clinical point of view, MuSK-MG presents the same fluctuating involvement of the skeletal muscles already described for AChR-MG. However, in MuSK-MG patients,

symptom fluctuation may be subtler and, therefore, not noticed. In addition, proximal limb involvement can be mild or even absent, whereas respiratory distress and other bulbar symptoms (such as difficulty in swallowing, chewing, and speaking) can be severe and rapidly progressive. The misinterpretation of these symptoms, that can mimic the course of a primary myopathy or even a motor neuron disorder (Huijbers, Niks et al. 2016), may contribute to a delay in recognition and treatment.

Involvement of ocular muscles was initially thought to be less prominent in MuSK-MG as mild, symmetrical ophthalmoparesis and ptosis were reported as the only symptom at onset in 36% of MuSK-MG cases (compared to 60% of AChR-MG) (Guptill, Sanders et al. 2011). However, a recent retrospective analysis of Italian patients showed that the involvement of extra-ocular muscles was present in more than 96% of the population studied, with a frequency comparable to AChR-MG, and represents the first manifestation of the disease in almost 60% of cases (Evoli, Alboini et al. 2017). Purely ocular forms are, however, particularly rare – or at least underdiagnosed – as all the patients in the aforementioned study evolved into a generalised disease (Evoli, Alboini et al. 2017).

Involvement of bulbar and respiratory muscles is particular prominent in MuSK-MG patients with a higher frequency of respiratory crises (up to 35% of cases), with prolonged need for mechanical ventilation and hospital admission (Vincent, Bowen et al. 2003, Evoli 2006, Deymeer, Gungor-Tuncer et al. 2007, Ohta, Shigemoto et al. 2007, Pasnoor, Wolfe et al. 2010, Guptill, Sanders et al. 2011, Konig, Stetefeld et al. 2021).

Finally, characteristic of MuSK-MG is the development in patients with long history of severe disease of facial and tongue atrophy (Evoli, Tonali et al. 2003, Farrugia, Robson et al. 2006). When muscle atrophy occurs, it is clinically associated with non-fluctuating weakness, myopathic changes in the electrophysiology recordings, and fatty

tissue infiltration at the muscle MRI scans (Farrugia, Kennett et al. 2006, Farrugia, Kennett et al. 2007, Nikolic, Bacic et al. 2015).

1.4.3) Diagnosis

As already described for AChR-MG, the diagnosis of MuSK-MG is based on its typical clinical features, on the presence of decrement in the repetitive nerve stimulation of affected muscles and, most importantly, on the detection of MuSK antibodies by RIA or CBA. From a clinical perspective, fatigable weakness involving predominantly the bulbar and respiratory muscles, associated with the lack of response – or even the worsening of symptoms – following administration of AChE inhibitors is highly suggestive for a diagnosis of MuSK-MG (Evoli, Tonali et al. 2003, Guptill, Sanders et al. 2011).

Neurophysiology studies can be extremely useful, especially when muscle fatigability is not particularly clear during history collection and physical examination. However, repetitive nerve stimulation and/or single-fibre jitter recording should be performed on muscles with bulbar innervation as they can be negative on limb muscles (Farrugia, Kennett et al. 2006). Misleading signs of denervation and neuromyotonia have also been reported in the presence of MuSK-Abs, complicating further the interpretation of neurophysiology results (Simon, Reddel et al. 2013, Furuta, Ishizawa et al. 2015, Huijbers, Niks et al. 2016).

Serological detection of MuSK-Abs by RIA or CBA is necessary to confirm the diagnosis. In the RIA, the extracellular domain of MuSK is labelled with ^{125}I and used as radioactive antigen (Matthews, Chen et al. 2004). Its specificity reaches 100%, although it is difficult to estimate its sensitivity due to the variability in the proportion of MuSK-MG patients among the different populations studied. Commercial ELISAs for MuSK are also available and occasionally used in research studies although it is

worth noting that a small fraction of MuSK-Ab positive patient sera tested by RIA were not recognized in ELISA (Koneczny, Stevens et al. 2017). Finally, CBA techniques are also available for MuSK-MG in which transfected HEK-293 express MuSK on their membrane. MuSK CBA has increased by 8% the antibody detection in previously RIA double-seronegative patients. Notably, patients positive only in the CBA presented a milder phenotype and less effective clustering inhibition in *in vitro* experiments compared to the those positive in the RIA (Huda, Waters et al. 2017).

1.4.4) Therapy

In broad terms, treatment of MuSK-MG follows the same principles as described above for AChR-MG. However, MuSK-MG is usually more resistant to medications needing higher dose of medications and more prolonged treatment compared to AChR-MG.

With respect to symptomatic drugs, acetylcholinesterase inhibitors are often ineffective in MuSK-MG patients, and can induce exacerbation of symptoms (Evoli, Tonali et al. 2003, Guptill, Sanders et al. 2011). The reason behind this will be discussed in paragraph 1.7.2.1. Conversely, 3,4-diaminopyridine – that improves neuromuscular transmission by increasing the presynaptic release of ACh vesicles – showed promising results when tested in an *in vivo* model (Morsch, Reddel et al. 2013) and when administered on a few selected MuSK-MG patients (Skjei, Lennon et al. 2013, Evoli, Alboini et al. 2016). The β-adrenergic agonists salbutamol and ephedrine have been successfully used in the treatment of congenital myasthenic syndromes, specifically with mutations in *AGRN*, *DOK7*, *COLQ*, and *MUSK* (Lee, Beeson et al. 2018, Owen, Topf et al. 2018), and also showed effectiveness when tested on a MuSK-MG patient (Haran, Schattner et al. 2013). The use of sympathomimetic drugs in myasthenic syndromes is supported by increasing evidence regarding the role of sympathetic innervation in maintaining shape, size and function of NMJs (Khan,

Lustrino et al. 2016). In this study, chemical sympathectomy induced a reduction in size and complexity of the NMJs, and a concomitant decrease in amplitude and time to peak of the compound muscle action potentials (CMAP) in model animals. These effects were rescued by sympathomimetics. Although this treatment approach appears to be promising, randomised clinical trials are still needed to evaluate systematically the potential efficacy and safety in MuSK-MG.

Due to the lack of availability of symptomatic treatments, the cornerstone of MuSK-MG treatment is represented by a combination of corticosteroids and other immunosuppressant medications. Response to steroids is variable and, compared to AChR-MG, a higher proportion of MuSK-MG patients require high doses, prolonged treatment, and concomitant immunosuppression with either azathioprine, mycophenolate or cyclosporine to achieve full control of symptoms (Evoli, Bianchi et al. 2008, Guptill and Sanders 2010, Sanders and Evoli 2010, Evoli, Alboini et al. 2012). Steroids can also worsen the muscle atrophy already significant in MuSK-MG patients (Benveniste, Jacobson et al. 2005, Farrugia, Robson et al. 2006).

One of the most promising pharmacological treatment currently available is represented by rituximab. Its high level of efficacy in MuSK-MG could be due to the fact that IgG4 antibodies sustain the main pathogenic mechanism of the disease (as described in section 1.7.2). Short-lived circulating plasma cells producing IgG4 antibodies (rather than bone marrow–resident long-lived plasma cells) appear be more susceptible to the drug as indicated by studies on other diseases caused by this antibody subclass (such as pemphigus and the so called “IgG4-related disease”, a systemic condition of unknown aetiology consistent with fibrous-inflammatory infiltration affecting several single organs and mediated by polyclonal IgG4-positive plasma cells) in which significant clinical improvement and reduction in antibody titres were observed (Khosroshahi, Bloch et al. 2010, Diaz-Manera, Martinez-Hernandez et al.

2012, Carruthers, Topazian et al. 2015, Kamisawa and Okazaki 2017, Kurihara, Yamagami et al. 2019). The use of rituximab treatment in MuSK-MG is supported by several case reports, local studies and, more recently, by bigger nation-wide group analysis (Hain, Jordan et al. 2006, Khosroshahi, Bloch et al. 2010, Nowak, Dicapua et al. 2011, Diaz-Manera, Martinez-Hernandez et al. 2012, Keung, Robeson et al. 2013, Hehir, Hobson-Webb et al. 2017, Topakian, Zimprich et al. 2019). Currently, rituximab in MuSK-MG has a level IV evidence according to the latest multicentre prospective review conducted by Hehir and colleagues in 2017 (Hehir, Hobson-Webb et al. 2017). Although randomised clinical trials still need to be performed, all the studies conducted so far consistently indicate rituximab's long-lasting effectiveness and safety for MuSK-MG patients, and support an increase of its use in the current clinical practice. Considering the high rate of positive response, it would be advisable that rituximab treatment is considered also for those severe patients who require high level of immunosuppression even if they do not meet the criteria of a refractory disease. On the other hand, only selected patients should undertake rituximab treatment as it implies several risks, in particular the development of JC-virus-related progressive multifocal leukoencephalopathy as reported during the treatment of other autoimmune disorders (reviewed by (Tan and Koralnik 2010).

Treatment of acute relapses and myasthenic crises are usually effectively treated with either IVIg or plasmapheresis. Although considered equal in terms of efficacy (Ronager, Ravnborg et al. 2001), plasma exchange has been reported to be faster and more effective in MuSK-MG and, therefore, should be prioritised (Guptill and Sanders 2010, Pasnoor, Wolfe et al. 2010).

Association with thymus pathology (either thymic hyperplasia or thymoma) has not been reported and, therefore, thymectomy is not indicated (Marx, Pfister et al. 2013, Clifford, Hobson-Webb et al. 2019).

1.5) Seronegative myasthenia and the significance of Lrp4 antibodies

Seronegative myasthenia (SNMG) is defined by the absence of antibodies against AChR and MuSK in patients who have clinical and neurophysiological features of myasthenia. Seronegative cases count for about 15-20% of all the patients, and for roughly 50% of the pure ocular forms (Kerty, Elsais et al. 2014, Hong, Zisimopoulou et al. 2017).

Antibodies against the Low-density-lipoprotein Receptor-related Protein 4 (Lrp4) have been detected in a variable proportion (2-27%) of seronegative patients (Higuchi, Hamuro et al. 2011, Cossins, Belaya et al. 2012, Pevzner, Schoser et al. 2012, Zhang, Tzartos et al. 2012). Different techniques (CBA and ELISA) were used in these studies to estimate the level of Lrp4-Abs, and this could partially account for their incidence variability. Patients with detectable levels of Lrp4-Abs are usually young females with ocular symptoms or mild generalised involvement, whereas the most severe cases often have double positivity with MuSK-Abs (Higuchi, Hamuro et al. 2011, Zisimopoulou, Evangelakou et al. 2014, Marino, Scuderi et al. 2015, Li, Han et al. 2019). No alteration in thymus histology was reported in a series of 4 patients positive for Lrp4-Abs suggesting that thymus involvement unlikely contributes to the pathogenesis of this subtype of myasthenia (Koneczny, Rennspiess et al. 2019).

Lrp4 is upstream of MuSK in the AChR clustering pathway (see below) and mediates MuSK activation, but the clinical relevance of Lrp4 antibodies is still a matter of debate. However, *in vitro* experiments showed that Lrp4-Abs are able to reduce agrin-dependent AChR clustering (Pevzner, Schoser et al. 2012, Zhang, Tzartos et al. 2012) and a passive immunisation model had clinical and neurophysiological myasthenic features (Shen, Lu et al. 2013, Ulusoy, Cavus et al. 2017).

Alongside AChR, MuSK and Lrp4 as the main relevant antigens, several other proteins of the neuromuscular junction, such as agrin, cortactin or collagen Q, have been

proposed as potential targets for antibodies in SNMG (Cossins, Belaya et al. 2012, Gallardo, Martinez-Hernandez et al. 2014, Gasperi, Melms et al. 2014, Katarzyna, Belaya et al. 2015). Low titres of antibodies against agrin have also been reported, although often co-existing with AChR- or MuSK-Abs (Gasperi, Melms et al. 2014, Zhang, Shen et al. 2014). In a recent study, it was found that patients with clinical features of myasthenia and positivity for Lrp4 or agrin antibodies were more severe compared to SNMG, and equally responsive to immunotherapy (Rivner, Quarles et al. 2020). However, despite the increasing number of reports, the specificity of these antibodies is unclear, their potential pathogenic effects unexplored, and clinical relevance still debatable.

SECTION II: Pathophysiology of myasthenia gravis

1.6) Structure and physiology of the neuromuscular junction

The different subtypes of myasthenia gravis have in common an initial dysregulation of the immune system that leads to the production of autoantibodies against different antigens of the neuromuscular junction. AChR-Abs have been showed to cause a direct loss of acetylcholine receptors from the muscle membrane, whereas MuSK-Abs inhibit the AChR clustering pathway by blocking MuSK activation. In order to understand the pathogenic mechanisms that cause these two different forms of myasthenia, the normal structure, development and physiology of the NMJ will be described first.

1.6.1) Development of the neuromuscular junction and the agrin-Lrp4-MuSK pathway

The neuromuscular junction is a chemical synapse between the lower motor nerve and the surface of the skeletal muscle, using acetylcholine as the main neurotransmitter. Due

to its accessibility and to the apparent simplicity of its connections, the NMJ represents a very well-studied and understood model of synaptic transmission.

The formation of the junction requires a complex signalling process, both spatially and temporally, between the motor neuron and the muscle myotubes. The end of this process results in the clustering of acetylcholine receptors on the postsynaptic side, and a differentiated nerve terminal on the presynaptic one (Burden 2002). During embryonic development, the motor nerve, sprouting from the spinal anterior columns, targets the muscle fibres and starts the innervation preferentially where pre-patterned AChR clusters are expressed (Flanagan-Steet, Fox et al. 2005, Panzer, Song et al. 2006). The axon of a single motor nerve innervates multiple muscle fibres generating large motor units. The final dimension of each motor unit is then determined by the intensity of the neural activity (Wyatt and Balice-Gordon 2003, Chung and Lee 2009).

Several proteins are involved in the maturation process and in the maintenance of the structure of the NMJ. For example, laminin-221 and other proteins of the laminin family – which are synthetized by the muscle cell and expressed in the basal lamina – are essential in shaping the final structure of the synapse (Nishimune, Valdez et al. 2008). They contribute to the formation of the junctional folds and balance the growth of the pre-synaptic components of the NMJ, such as the synaptic bouton of the nerve terminal and the Schwann cells (Noakes, Gautam et al. 1995, Patton, Cunningham et al. 2001). In addition, an intricate network of structural proteins located on the sarcolemma (and protruding into the extracellular matrix) creates a robust scaffold that maintains the shape and permits the overall function of the junction. Specifically, the α-/β-dystroglycans mediate the interaction between perlecan, a large proteglycan of the extracellular matrix, the ColQ-MuSK complex, and the proteins of the Wnt family (see below) (Kamimura, Ueno et al. 2013, Arredondo, Lara et al. 2014). In addition, sarcoglycans bind directly to Lrp4 stabilising its membrane expression (Zhao, Shen et

al. 2018). Finally, utrophin and dystrophin contribute with their binding sites for sarcoglycan and dystroglycan complexes to connect the NMJ with the intracellular cytoskeleton scaffolding (reviewed in (Hack, Groh et al. 2000)).

The most important role in both pre- and post-synaptic development of the synapse is played by the agrin-Lrp4-MuSK pathway that leads to the clustering of the AChR receptors. Specifically, the signalling molecule that triggers all the downstream events of the AChR clustering pathway is a heparan-sulfate proteoglycan called agrin, which is secreted by the motor nerve terminal and binds to its receptor, low-density lipoprotein receptor-related protein 4 (Lrp4), expressed on the sarcolemma (Godfrey, Nitkin et al. 1984, McMahan 1990, Glass, Bowen et al. 1996, Zhang, Luo et al. 2008). Lrp4 plays a double role in synapse maturation: it mediates agrin-induced MuSK activation and, through a retrograde-signalling to the motor axon, it contributes to the pre-synaptic maturation increasing the clustering of acetylcholine vesicles (Zhang, Coldefy et al. 2011, Wu, Lu et al. 2012, Yumoto, Kim et al. 2012). Both Lrp4 and MuSK are transmembrane proteins that form a heteromeric tetramer on the muscular sarcolemma. Lrp4 interacts with MuSK even in the absence of agrin, and this basal interaction is sufficient to partially activate MuSK causing the pre-patterning of acetylcholine receptors in myotubes prior to innervation (Arber, Burden et al. 2002, Kummer, Misgeld et al. 2006). Since the innervation process starts where the pre-pattered AChR are located, the secretion of agrin by the motor nerve represents a fundamental step to reinforce the connection between the two sides of the junction, leading to the formation of mature AChR clusters and the establishment of a fully-operational neuromuscular synapse.

When agrin binds to the first β-propeller (BP) domain in the N-terminal of Lrp4 (Zhang, Coldefy et al. 2011), it strengthens a heteromeric tetramer with MuSK in a 2:2 stoichiometry (Figure 1.1). This conformational change in Lrp4-MuSK interaction

triggers the auto- and trans-phosphorylation of MuSK intracytoplasmic domain and the beginning of a phosphorylation cascade that culminates with the clustering of AChRs (Zong, Zhang et al. 2012).

MuSK is a complex protein consisting of three main parts: an extracellular domain, a transmembrane helix, and an intracytoplasmic region (Figure 1.1). The extracellular part has three immunoglobulin-like domains (Ig1, 2 and 3) and a cysteine-rich frizzled domain. The first Ig1 domain is essential as it mediates the interaction with Lrp4 and, together with the Ig2 domain, forms a dimer with another MuSK molecule (Stiegler, Burden et al. 2006, Zhang, Coldefy et al. 2011). In addition, the Ig3 and frizzled domains interact respectively with BMP4 and the proteins of the Wnt family (Strochlic, Falk et al. 2012, Yilmaz, Kattamuri et al. 2016) (Figure 1.2). A hydrophilic transmembrane helix connects the extracellular domains to the intracytoplasmic region that contains the tyrosine kinase. Within the first cytoplasmic juxtamembrane segment, there is a tyrosine residue 533 (Tyr533) that starts the autophosphorylation process that activates MuSK (Herbst and Burden 2000). Three other tyrosine residues located in the kinase domain (Tyr750, Tyr754 and Tyr755) are then phosphorylated in an activation loop (Till, Becerra et al. 2002). Recently, a new phosphorylation site located on the serine 751 (within the tyrosine phosphorylation loop) has been identified (Camurdanoglu, Hrovat et al. 2016). This serine is characterised by a very low autophosphorylation threshold, which is supposed to maintain a basal level of MuSK activation in the absence of agrin important for the pre-patterning of the AChRs.

In order to sustain MuSK activation, the recruitment of an additional adaptor protein, Downstream of Kinase 7 (DOK7), is required. DOK7 presents two main consecutive

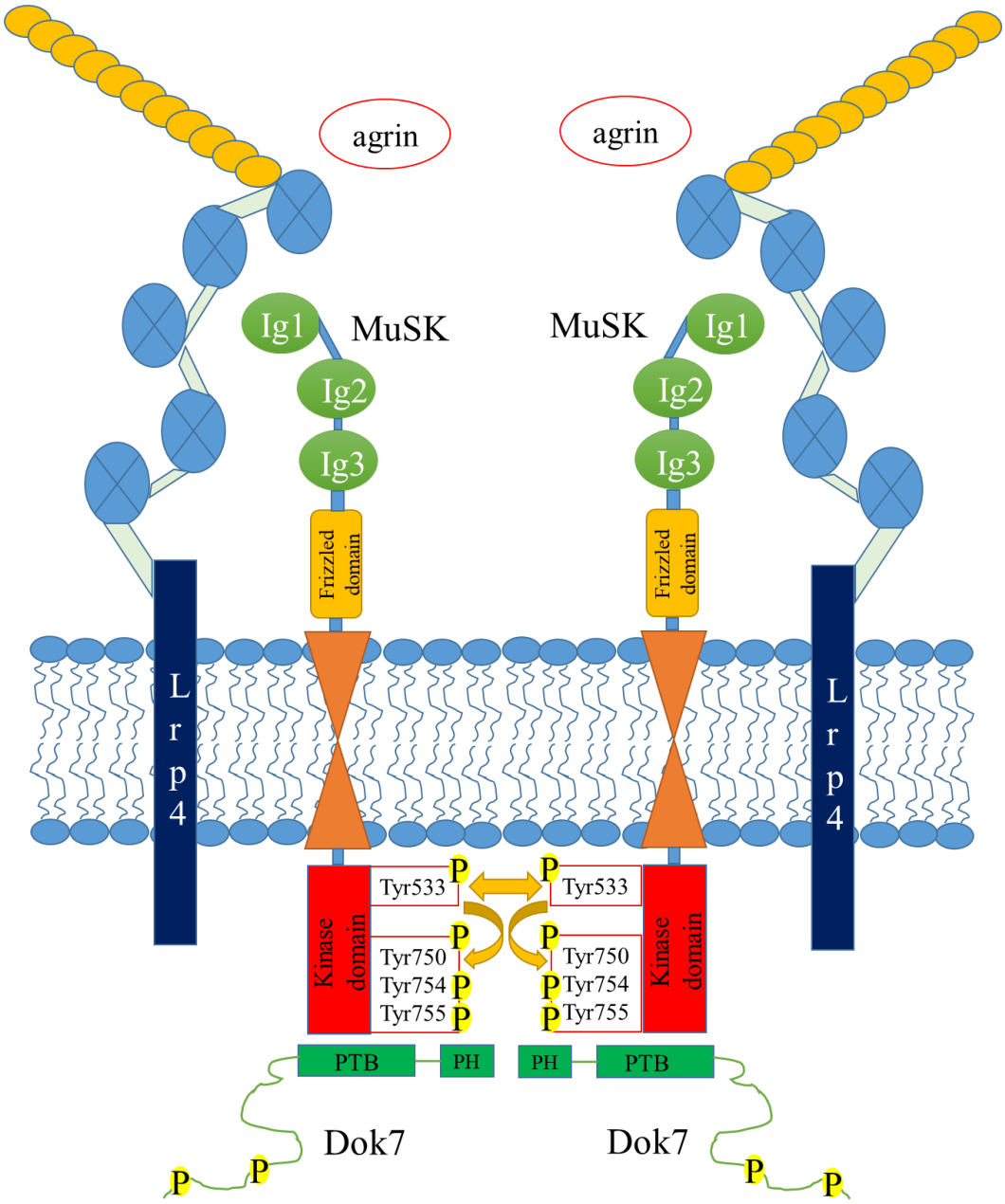


Figure 1.1. Lrp4-MuSK-DOK7 structures and interactions. MuSK consists of an extracellular domain, a transmembrane helix, and an intracytoplasmic region. The extracellular part of the molecule has three immunoglobulin-like domains (Ig1-3) and a cysteine-rich frizzled domain. The first immunoglobulin-like (Ig1) domain mediates the interaction with the extracellular region of Lrp4 (and represents the main immunogenic region for MuSK antibodies). The tyrosine kinase domain of MuSK is located in the intracytoplasmic part of the protein and its juxtamembrane tyrosine residue 533 (Tyr533) starts the autophosphorylation of the MuSK dimer. Three other tyrosine residues (Tyr750, Tyr754 and Tyr755) are then phosphorylated in an activation loop. To sustain MuSK activation, Dok7 is recruited, and binds to Tyr 533 through its PTB domain. The PH domain mediates the dimerisation of Dok7 and also stabilises MuSK dimer. MuSK and Dok7 activates each other triggering, through this reciprocal activation, the intracellular phosphorylation cascade that leads to the clustering of the acetylcholine receptors.

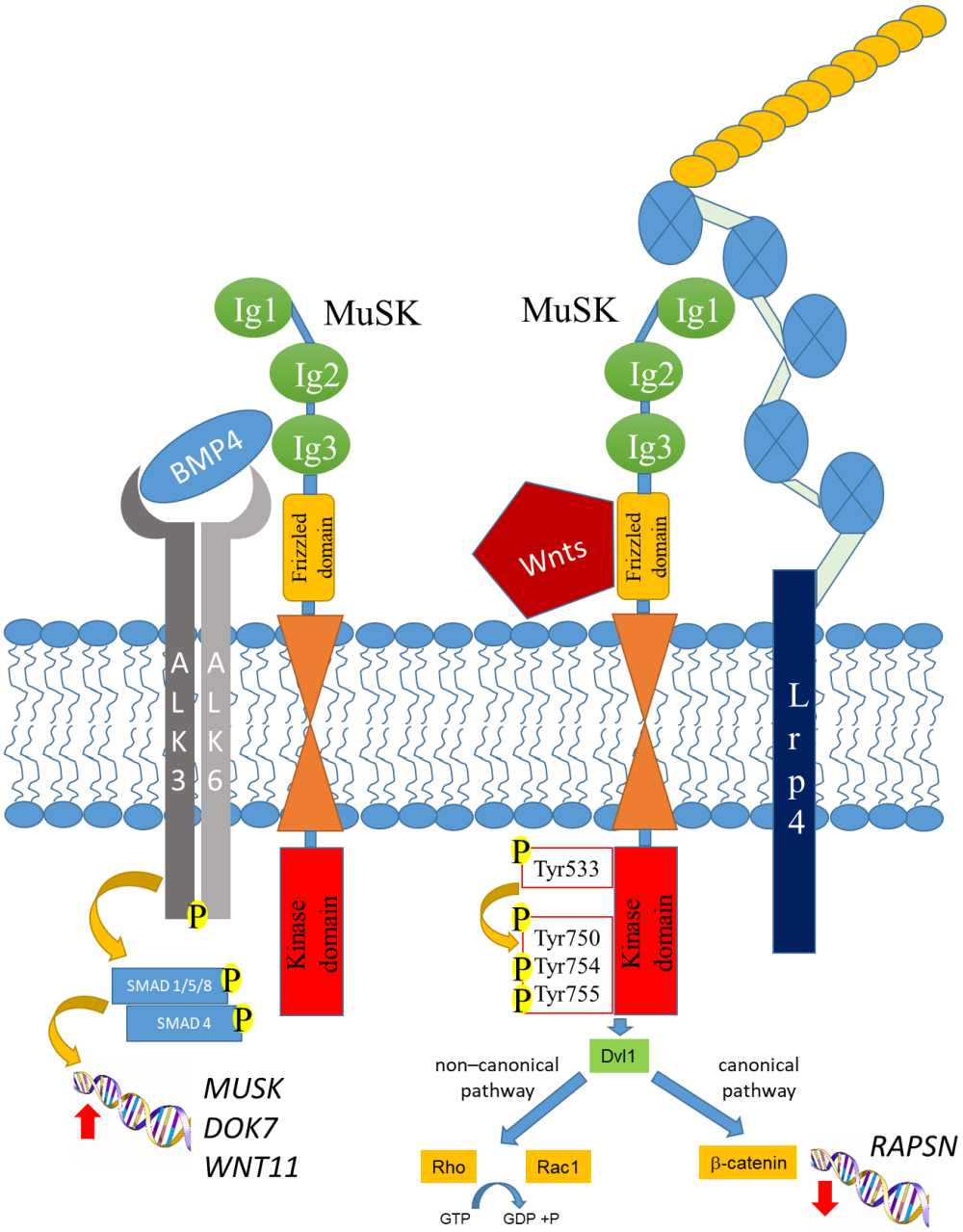


Figure 1.2. MuSK interactions with Wnt and BM4. In addition to the binding to Lrp4 through the Ig1 segment of its extracellular domain, MuSK interacts with other two major complexes involved in the AChR clustering pathway. Through its Ig3 segment. MuSK acts as a coreceptor, together with ALK3 and ALK6, for BMP4 (left). The binding to the ligand, starts a phosphorylation signal mediated by ALK3/6 which enrol the intracellular transcription factor complex SMAD 1/5/8/4 which, after migrating to the cell nucleus, induces the transcription of several effectors including *MUSK*, *DOK7*, and *WNT11* to enhance AChR clustering. Moreover, through its frizzled domain, MuSK can be activated by Wnt proteins. In this case, interaction with Lrp4 seems to be necessary for the transduction of the signal. Wnts activate two different intracellular pathways. The "non-canonical pathway" is thought to sustain the cytoskeleton modifications necessary for the maturation of AChR cluster by activating Rac1 and Rho GTPases. On the other hand, the simultaneous activation of the "canonical pathway" mediated by β-catenin acts as a negative regulator reducing cluster formation by reducing rapsyn expression.

domains, the N-terminal PH and the PTB, followed by a long unstructured region that contains two sites of tyrosine phosphorylation (Figure 1.1). The PTB domain binds directly to phosphorylated Tyr553 of MuSK, while the PH domain mediates the dimerization of DOK7 and stabilises the MuSK dimer to promote trans-phosphorylation of Tyr750, Tyr754 and Tyr755 (Bergamin, Hallock et al. 2010). The role of DOK7 is essential as it operates both upstream and downstream of MuSK. MuSK and DOK7 activate each other, and this reciprocal activation starts the intracellular phosphorylation cascade that causes the clustering of the AChRs.

1.6.2) Transmission of the signal and clustering of the acetylcholine receptors

The downstream parts of the pathway have been only partially defined. Following MuSK-DOK7 activation, more than 200 proteins are thought to undergo phosphorylation modifications as shown in an original proteomic study conducted on C2C12 myotubes (Durnberger, Camurdanoglu et al. 2014). A more recent study, which utilised similar phosphoproteomic techniques, found an agrin-dependent phosphorylation increase in 36 proteins, 13 of them directly dependent on DOK7 as suggested by its selective knock out by CRISPR-Cas9 (Wang, Li et al. 2020). Among these downstream effectors, the most relevant include Crk and Crk-L (Hallock, Xu et al. 2010) and the recently identified annexin A3 (Anxa3) (Wang, Li et al. 2020) which, if mutated, severely impairs the formation of the NMJ and AChR clustering respectively under *in vivo* and *in vitro* conditions. Other downstream kinases and effectors, namely Sorbs-1 and -2, Abl-1 and -2, Scr, Dvl1/PAK1, and the GTPases Rac1 and Rho are subsequently activated playing a substantial role in the transduction of the signal, stabilisation of AChR clusters, and the induction of the cytoskeleton rearrangements (mediated by α-actinin, cortactin, and actin) necessary for cluster maturation (Mittaud, Marangi et al. 2001, Luo, Wang et al. 2002, Finn, Feng et al. 2003, Weston, Gordon et

al. 2003, Dobbins, Luo et al. 2008, Madhavan, Gong et al. 2009, Cartaud, Stetzkowski-Marden et al. 2011, Hallock, Chin et al. 2016, Bai, Guo et al. 2018).

The whole cascade converges into the phosphorylation of the AChR β, γ and δ subunits (Wallace, Qu et al. 1991), and the clustering of the receptors mediated by their interaction with rapsyn. Rapsyn is a structural protein that self-aggregates providing a scaffold, supported by the β-dystroglycans, that anchors the AChRs to the actin cytoskeleton through the mediation of α-actinin and microtubule actin cross-linking factor 1 (MACF1) (Apel, Roberds et al. 1995, Cartaud, Coutant et al. 1998, Borges and Ferns 2001, Dobbins, Luo et al. 2008, Lee, Free et al. 2009, Zuber and Unwin 2013, Oury, Liu et al. 2019, Xing, Jing et al. 2019). The major players and protein interactions of the AChR clustering cascade are summarised in Figure 1.3.

The clustering of the AChRs in a pretzel-like shape, that resembles the form of the nerve terminal, represents the final result of the activation of agrin-Lrp4-MuSK pathway. According to a model of "diffusion-mediated trapping", originally hypothesised in the 1970s through histochemistry studies using fluorescent α-bungarotoxin, the AChRs move freely on the sarcolemma until reaching a trapping site (or sticky zone) where clusters start to form by the accumulation over time of single receptors (Axelrod, Ravdin et al. 1976). This model is supported by a more recent study which utilised new techniques of quantum dots live-cell imagining that track the movements of the AChRs visualising the gradual formation of the clusters (Geng, Zhang et al. 2009). Only clustered receptors are able to respond appropriately to the signal transmitted by the motor nerve terminal and determine muscle contraction.

The acetylcholine receptor located on the muscular sarcolemma is a nicotine type ligand-gate ion channel. The adult receptor is formed by 5 subunits with a stoichiometry of α_2-β-δ-ε, while the foetal form presents a γ subunit instead of the ε one (Mishina, Takai et al. 1986). The subunits are disposed in a circle creating a central pore for the

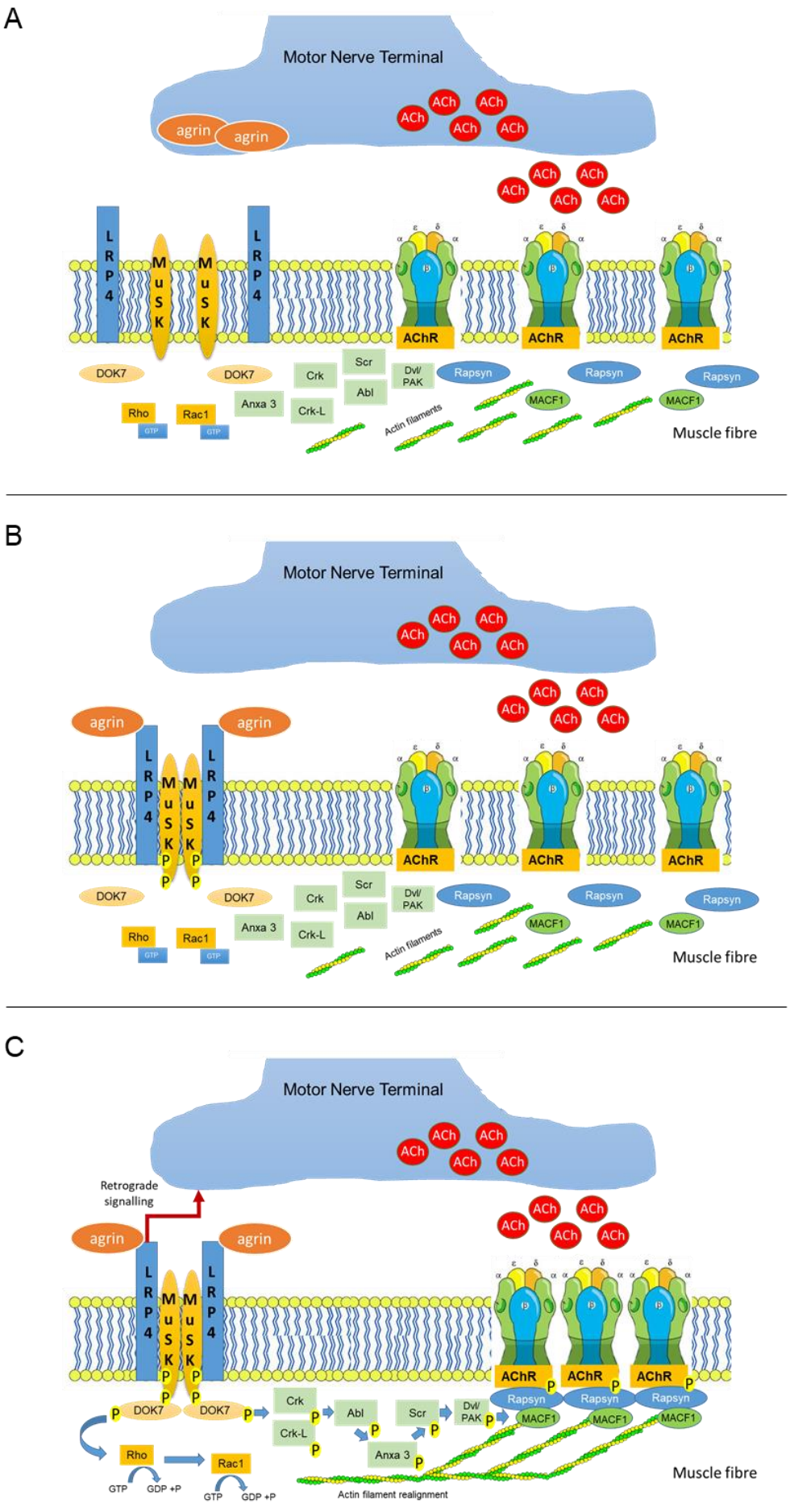

A
Motor Nerve Terminal
ACh
agrin
LRP4
MuSK
AChR
DOK7
Scr
Dvl/ PAK
Rapsyn
Crk
Abl
Anxa 3
Crk-L
Rho
Rac1
GTP
MACF1
Actin filaments
Muscle fibre
B
Motor Nerve Terminal
agrin
LRP4
MuSKPP
AChR
DOK7
Scr
Dvl/ PAK
Rapsyn
Crk
Abl
Anxa 3
Crk-L
Rho
Rac1
GTP
MACF1
Actin filaments
Muscle fibre
C
Motor Nerve Terminal
Retrograde signalling
agrin
LRP4
MuSKPP
AChR
DOK7
Scr
Dvl/ PAK
Rapsyn
Crk
Abl
Crk-L
Anxa 3
Rho
Rac1
GTP
GDP +P
MACF1
Actin filament realignment
Muscle fibre

Figure 1.3. Schematic representation of the neuromuscular junction and the clustering pathway of acetylcholine receptors (AChRs). **(A)** On the muscle post-synaptic membrane, Lrp4 and MuSK form a loose tetramer and, at this stage, AChRs are dispersed along the sarcolemma. **(B)** Agrin is secreted by the motor nerve terminal into the synaptic cleft and interacts with Lrp4 inducing a conformational change in the Lrp4-MuSK tetramer. This leads to MuSK activation through an auto-phosphorylation loop of the tyrosine residues in its intracytoplasmatic domain. **(C)** The recruitment of DOK7 amplifies MuSK phosphorylation and triggers the phosphorylation cascade downstream that involves several intermediate proteins including Crk, Ckr-l, Scr, Abl, Anxa 3, and Dvl/PAK. Concomitantly, a subsidiary pathway leads to cytoskeletal rearrangements through the activation of Rac1 and Rho GTPases. The clustering pathway culminates in the phosphorylation of the subunits of the AChR and the recruitment of rapsyn, which anchors the AChR clusters to the underlying actin filaments. Furthermore, Lrp4 participates in presynaptic development through a retrograde signal which increases the clustering of ACh vesicles in the motor nerve terminal.

passage of the ions. Each subunit carries an extracellular domain, four transmembrane domains (TMD1-4) linked together with intracellular or extracellular loops, and an intracytoplasmic C-terminal end. The binding sites for acetylcholine are in the interface between the extracellular domains of the α–δ and α–ε subunits (Lee, Free et al. 2009, Mukhtasimova, Lee et al. 2009), whereas the intracellular α-helix loops in the α, β, and ε subunits provide the binding areas for rapsyn (Lee, Rudell et al. 2009).

The neurotransmitter acetylcholine (ACh) is secreted in quantal amounts into the synaptic cleft, as firstly suggested by (Katz and Miledi 1965), as the nerve action potential reaches the nerve terminal causing the exocytosis of the ACh vesicles. ACh diffuses into the synaptic cleft and interacts with the receptors on the postsynaptic muscle membrane. When two acetylcholine molecules bind to the AChR, the receptor undergoes a conformational change that opens the channel allowing the entrance of cations, in particular Na^+, into the cell. The influx of cations causes a local depolarisation of the membrane, called the end plate potential (EPP) which then, if the stimulus is enough to reach the threshold of -50 mV (Slater 2015), leads to the generation of an action potential. To ensure a fast and efficient transmission through the synapse, the AChR clustering pathway concentrates the receptors (up to 10000 AChRs per micron^2) on the muscle membrane opposed to the motoneuron terminal (Porter and Barnard 1975, Heuser and Salpeter 1979). AChR density drops to less than 10 per micron^2 just a few micrometres away from the junction. At this concentration, the receptors are too dispersed and, therefore, not able to sustain the transmission of the signal after the binding with the ACh. Conversely, once the action potential is generated in an area with high AChR density, the signal propagates along the sarcolemma, determining the release of calcium from the intracytoplasmic reticulum and, consequently, muscle contraction. The action of acetylcholine is terminated by the enzyme acetylcholinesterase (AChE), within the extracellular matrix, that hydrolyses

acetylcholine to its basic components, choline and acetyl-CoA. AChE is bound to ColQ, a collagen that is arranged as trimers to form a triple helix. AChE binds to the collagen tails of ColQ in the form of tetramers (Krejci, Coussen et al. 1991, Gaspersic, Koritnik et al. 1999). ColQ is located in the extracellular matrix, where it is anchored via MuSK to the synapse (Cartaud, Strochlic et al. 2004) (Figure 1.4 A).

1.6.3) Additional regulator pathways of the AChR clustering

Alongside the main agrin-Lrp4-MuSK cascade, there is increasing evidence that another three complementary pathways contribute to the regulation of the AChR clustering and are activated by neuregulin-1, the Wnt proteins, and BMP4.

Neuregulin-1 is a growth factor secreted by the motor nerve terminal that was found to facilitate AChR clustering by inducing the expression of the ε subunit of the AChR through the activation of the ErbB kinases and the transcription factor Ets-2 (Chu, Moscoso et al. 1995, Jo, Zhu et al. 1995, Moscoso, Chu et al. 1995, Sapru 2001). In addition, it potentiates the effect of agrin on MuSK phosphorylation through the inhibition of the SHP2 phosphatase (see below) (Madhavan, Zhao et al. 2005, Zhao, Qian et al. 2007, Ngo, Cole et al. 2012). The function of neuregulin-1 seems, however, not essential for the development of the NMJ, as the selective knock-down in muscles of the ErbB effectors produces normal synapses (Escher, Lacazette et al. 2005). In addition, its role in the facilitation of AChR clustering was questioned when it was observed that the neuregulin-1 could trigger the dispersal of the clusters in the myotubes (Trinidad and Cohen 2004). However, a later study suggested that this paradoxical effect might be related to an increased turnover of the clusters rather than their direct inhibition (Ngo, Cole et al. 2012).

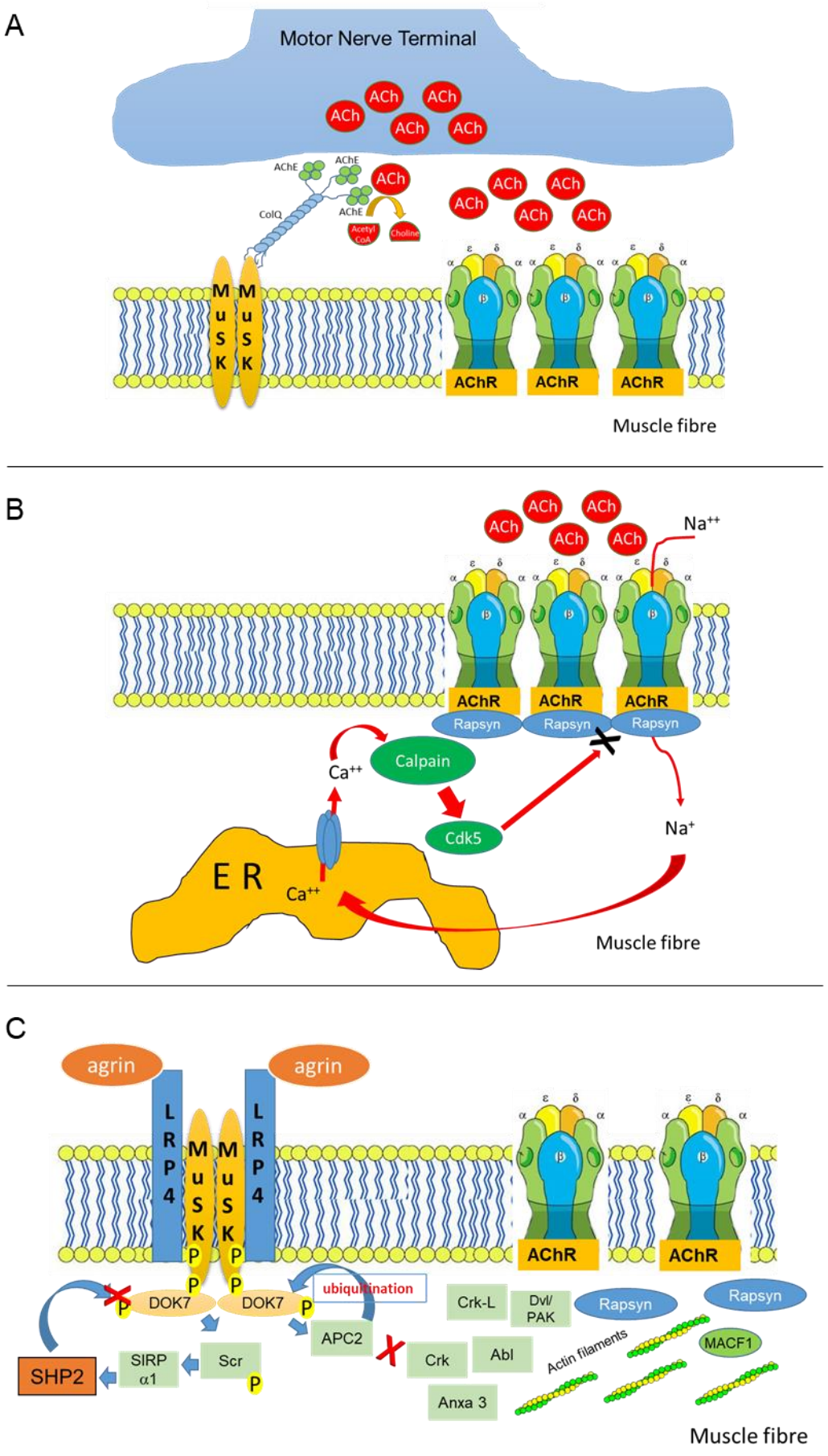

A
Motor Nerve Terminal
ACh
AChE
ColQ
Acetyl CoA
Choline
MuSK
AChR
Muscle fibre
B
Na++
Rapsyn
Calpain
Ca++
Cdk5
Na+
E R
Muscle fibre
C
agrin
LRP4
MuSK
P
DOK7
ubiquitination
APC2
SHP2
SIRP α1
Scr
Crk-L
Dvl/ PAK
Crk
Abl
Anxa 3
Actin filaments
MACF1
Rapsyn
Muscle fibre

Figure 1.4. Negative regulators of the AChR pathways. (A) Via the extracellular matrix (ECM), MuSK interacts with ColQ which, in turn, is attached to tetramers of the enzyme acetylcholinesterase (AChE) responsible for the hydrolysis of acetylcholine (ACh) after its binding to the AChR. The cleavage of acetylcholine into choline and acetyl-CoA avoids the continuous stimulation of the receptor which could induce the desensitisation of the receptor itself. **(B)** Continuous activation of the AChR leads to increased release of Calcium from the endoplasmic reticulum (ER). This, in turn, releases calpain from its physiological inhibition by rapsyn and promotes the dispersal of the AChR mediated by Cdk5. **(C)** Through a negative feedback loop, MuSK is inhibited by the phosphatase SHP2, which is activated by Src and SIRP-a1 after the initiation of the phosphorylation cascade. In a similar manner, APC2 is activated downstream of DOK7 and quenches the phosphorylation signal by inducing the degradation of DOK7 through its ubiquitination.

The Wnt family consists of 19 soluble proteins that guide the tissue development of an organism through differential signal transduction (reviewed by (van Amerongen and Nusse 2009). Wnts' pathway is preserved across different tissues and species, and involves the binding of one specific Wnt to a protein complex containing a transmembrane effector with a frizzled domain connected to a low-density lipoprotein receptor-related protein (Lrp) (Bhanot, Brink et al. 1996, Bilic, Huang et al. 2007). After binding with Wnt, this transmembrane complex activates, in turn, its downstream effectors Dishevelled (Dsh/Dvl), β-catenin/Armadillo and the transcription factors T cell factor (TCF)/Pangolin (Noordermeer, Klingensmith et al. 1994, Siegfried, Wilder et al. 1994, Brunner, Peter et al. 1997). This is also known as "Wnts' canonical pathway". A different, "non-canonical" pathway can also be activated by Wnt-Dvl which, instead of being mediated by β-catenin, involves the activation of the GTPases Rho and Rac for the cytoskeleton rearrangements required for polarity and migration of the cell (Kishida, Yamamoto et al. 2004, Rosso, Sussman et al. 2005). With respect to the NMJ, 5 Wnts have been reported to contribute to the AChR clustering, with Wnt9a and Wnt11 found to be expressed in the developing muscle (Zhang, Liang et al. 2012). Wnts increase MuSK phosphorylation following their binding to its frizzled domain, a function for which Lrp4 is required (Strochlic, Falk et al. 2012, Zhang, Liang et al. 2012). The importance of the Wnt pathway is suggested by the impaired AChR clustering after selective knock-out of Dvl in the muscle cells which, in turn, impairs other downstream effectors such as PAK and APC where the main agrin-Lrp4-MuSK pathway converges (Luo, Wang et al. 2002, Wang, Jing et al. 2003). Wnt stimulation alone seems not sufficient to fully activate the AChR clustering pathway as only cluster precursors (microclusters) were observed after Wnt3 exposure in C2C12 myotubes. This was interpreted as partial activation of the GTPase Rac in the Wnt "non-canonical" pathway (Weston, Gordon et al. 2003, Henriquez, Webb et al. 2008). Conversely, in the same

study of Gordon et al, number and size of AChR clusters were markedly increased by concomitant stimulation by agrin and Wnt3, supporting a cooperation between the two pathways. Interestingly, it has been suggested that different Wnts might inhibit AChR clustering by activating the "canonical" pathway mediated by β-catenin through the suppression of rapsyn expression (Wang, Ruan et al. 2008). A fine tuning between the activity of these regulators and the different members of the Wnt family is responsible to achieve the delicate balance that allows the correct function of the NMJ (reviewed in (Boex, Messeant et al. 2018)).

Finally, recent evidence has emerged regarding the importance of a third pathway regulated by Bone Morphogenic Protein 4 (BMP4) for which MuSK is supposed to act as a co-receptor through its Ig3 domain and the interaction with two other transmembrane type I BMP receptors, ALK3 and ALK6 (Tendijke, Yamashita et al. 1994, Yilmaz, Kattamuri et al. 2016). In C2C12 myotubes, the binding of BMP4 to the complex MuSK-ALK3 induces the transcription of genes involved in AChR clustering including *MUSK*, *DOK7* and *Wnt11* via the activation of the transcription factor complex Smad 1/5/8 and 4 (Yilmaz, Kattamuri et al. 2016). Importantly, these transcriptomic modifications appear to be unrelated to the tyrosine kinase activity of MuSK, indicating an independent and contributory role of BMP4 to the main agrin-Lrp4-MuSK pathway.

1.6.4) Negative regulation of AChR clustering

To prevent the formation of AChR clusters in extrasynaptic sites, and to reduce the risk of tetanic contraction caused by an overstimulation of the muscle, several negative regulators control the clustering pathway and the expression of AChRs on the muscle membrane. The main negative regulator is represented by the continuous muscle stimulation by the release of acetylcholine. Sustained ACh stimulation induces a

prolonged Ca^{++} influx which activates calpain, a protease constitutively inhibited by rapsyn, triggering AChR cluster dispersal mediated by Cdk5 (Lin, Dominguez et al. 2005, Chen, Qian et al. 2007) (Figure 1.4 B). Muscle contraction also leads to a suppression of AChR expression (Tang, Macpherson et al. 2004) and promotes the dispersal of AChR clusters (Lin, Dominguez et al. 2005, Misgeld, Kummer et al. 2005).

Negative regulators and controllers of the membrane expression of AChRs also play a role in avoiding uncontrolled and scattered localisation of the receptors on the muscular sarcolemma, and in directing the clusters close to the nerve terminal where the functional junction should properly develop. For example, it has been recently reported that the anaphase-promoting complex 2 (APC2) is activated early on after the initiation of the agrin-Lrp4-MuSK cascade. APC2 suppresses the phosphorylation signal of MuSK by inducing the ubiquitination of DOK7 and, therefore, its degradation (Chen, Bai et al. 2020) (Figure 1.4 C).

Particularly relevant for the scope of this thesis is another negative regulator of the clustering pathway: SRC homology 2 domain-containing phosphotyrosine phosphatase 2 (SHP2). SHP2 is an intracellular nonreceptor protein tyrosine phosphatase that reduces MuSK phosphorylation in a negative feedback loop through the mediation of Src and SIRPα1 (Madhavan, Zhao et al. 2005, Zhao, Qian et al. 2007) (Figure 1.4 C). It consists of two SH2 domains, a catalytic protein tyrosine phosphatase (PTP) domain, a C-terminal tail with tyrosyl phosphorylation sites (Y542 and Y580), and a proline-rich motif. SHP2 is basally inactive as the N-terminal SH2 region inhibits the catalytic PTP domain, but upon stimulation by tyrosine-phosphorylated docking proteins, SH2 undergoes a conformational change to facilitate phosphatase activation (Cunnick, Mei et al. 2001, Neel, Gu et al. 2003, Alonso, Sasin et al. 2004). SHP2 is enriched at the NMJ, co-localises with AChR clusters, and negatively regulates the expression of AChRs by inhibiting the pathway induced by neuregulin-1 (Tanowitz, Si et al. 1999, Camilleri,

Willmann et al. 2007). SHP2 modulates the activation of MuSK helping the formation and stabilisation of AChR clusters during embryonal development, and avoiding clustering in extrasynaptic sites (Camilleri, Willmann et al. 2007, Qian, Chan et al. 2008). Notably, the role of SHP2 seems to be more supportive than essential for the NMJ formation: an animal model selectively knocked out for SHP2 in muscles presented a normal embryonic development and indistinguishable NMJs compared to wild type controls (Dong, Li et al. 2006). Selective SHP2 inhibitors are commercially available and, considering the role of SHP2 in inhibiting AChR clustering, they might be used for targeted treatment in myasthenic disorders (see below).

1.7) Pathophysiology of myasthenia gravis

The pathogenic mechanisms underlying myasthenia have been investigated intensely over the last five decades and, with the discovery of MuSK antibodies, important differences have emerged between AChR- and MuSK-MG. In the following paragraphs, the pathophysiology of the two forms of myasthenia will be described. and more details will be provided for MuSK-MG as it represents the main focus of this thesis.

1.7.1) AChR-MG

1.7.1.1) Pathogenic mechanisms of AChR antibodies

Myasthenia gravis is associated in more than 80% of the cases with antibodies directed against the AChR (AChR-Abs) which cause extensive damage and destruction of the postsynaptic muscle membrane. AChR antibodies target an epitope around aa 67-76 on the extracellular domain of the AChR α subunit, which is termed the "main immunogenic region" (MIR) and is distinct from the binding site for ACh and α-bungarotoxin (Tzartos and Lindstrom 1980). AChR-Abs are mainly of the IgG1 and IgG3 subclasses and activate the classic complement cascade following their binding to

the receptor (Aharonov, Abramsky et al. 1975, Lennon and Lambert 1981, Vincent and Newsom-Davis 1982, Vincent 2002). Once activated, the complement cascade causes a rapid calcium influx into the muscle cytoplasm with the consequent destruction of the adjacent membrane together with the loss of the AChRs and voltage-gate sodium channels concentrated at the bottom of secondary folds of the sarcolemma (Ruff and Lennon 1998, Tuzun and Christadoss 2013). These latter events determine the reduction in ACh response and the increase of the threshold necessary to trigger the action potential. Another mechanism of action of AChR-Abs is related to their ability to bind two different AChR molecules, through the two MIRs. This divalent binding induces the internalisation of the receptors, increasing their turnover and lysosomal degradation inside the muscle cell (Heinemann, Bevan et al. 1977, Drachman, Angus et al. 1978). Finally, a third pathogenic effect of the antibodies described in a minority of patients' sera, is the direct block of AChR channel function (Burges, Wray et al. 1990).

There are two main adaptive mechanisms actuated by the nerve and the muscle to compensate for the effects of antibody-mediated damage to the junction. First, in the presynaptic terminal, the number of acetylcholine vesicles rise in order to reinforce the amount of neurotransmitter released into the synaptic cleft (Plomp, Vankempen et al. 1995). Furthermore, the muscle increases the transcription of AChR subunit genes in an attempt to replace the receptors that have been lost (Weidoff, Mcnamee et al. 1981). The efficacy of these compensatory mechanisms is likely responsible for the variability and distribution of the symptoms observed among patients. In this respect, it is worth noting that a higher expression of the ε subunit of the AChR has been described in the ocular muscles compared to the foetal γ, and can potentially explain part of their susceptibility in AChR-MG (MacLennan, Beeson et al. 1997),

Although the effects of the AChR-Abs on the NMJ are quite well understood, the very first pathological stages that trigger the disease concerning the loss of tolerance for

the self-antigen are still a matter of speculations. In this respect, a dysregulation of the thymus appears to be fundamental in the development of the disease.

1.7.1.2) Role of the thymus in AChR-MG

Some evidence regarding how the self-tolerance for the AChR is lost comes from a study on the thymic expression of the gene that encodes for the AChR α subunit, *CHRNA1*. A polymorphism of the *CHRNA1* promoter has been associated with early-onset of myasthenia in French and UK populations (Giraud, Taubert et al. 2007). This variant of the *CHRNA1* promoter prevents binding of interferon regulatory factor 8 (IRF8) and reduces the promoter activity in thymic epithelial cells. Therefore, IRF8 together with the *A*uto*I*mmune *RE*gulator (AIRE) modulates the expression of the AChR α subunit and finely balances a tug of war between self-tolerance and autoimmunity.

In early-onset myasthenia, the thymus usually presents lymphofollicular hyperplasia with an increased number of germinal centres and lymphoid follicles. MHC-class II expressing thymic epithelial cells present the unfolded AChR subunits and activate auto-reactive $CD4^+$ T cells (Marx, Pfister et al. 2013). The theory is that T cells sustain the formation of early AChR antibodies that are able to recognise and attack the properly folded AChRs expressed on the membrane of the myoid cells of the thymus. The consequent inflammation, complement activation and release of AChR-Ab/immune complexes cause the activation of other professional antigen presenting cells and initiate an activation loop of $CD4^+$ T cells and the expansion of auto-reactive B cells. Finally, the maturation of B cell receptors leads to the production of high-affinity AChR-Abs and eventually result in the spreading of the autoimmune process to peripheral lymph nodes (Willcox, Leite et al. 2008, Thiruppathi, Rowin et al. 2012). However, this is still

largely speculative, and whether the autoimmune reaction in the thymus is the primary event or a secondary expansion is not yet clear.

In thymoma-related myasthenia, the pathogenic thymic tissue has many features that could impair self-tolerance. The neoplastic epithelial cells express a variety of striatal muscle antigen epitopes, including sequences of the AChR subunits and titin. The theory here is that concomitant reduced expression of both AIRE immune regulator and MHC-class II (Strobel, Chuang et al. 2008) interfere with the correct maturation of regulatory T cells resulting in development of naïve and pre-primed autoreactive T cells in the peripheral blood that further activate autoimmune B cells (Hoffacker, Schultz et al. 2000).

1.7.2) MuSK-MG

1.7.2.1) Discovery of antibodies and pathogenicity studies

The existence of a distinct target for patients with myasthenia who did not have AChR antibodies had been proposed as early as 1976 (Lindstrom, Seybold et al. 1976) and demonstrated, in principle, in 1986 when immunoglobulin preparations from AChR-ab negative myasthenic patients were found to impair neuromuscular function (Mossman, Vincent et al. 1986). Eventually, the existence of an IgG antibody was shown by demonstrating binding of AChR-ab negative patient IgG to the TE671 human immortalised muscle cells (Blaes, Beeson et al. 2000, Scuderi, Marino et al. 2002). In 1996, the Yancopoulos group at Regerneron Inc USA had discovered MuSK as an essential protein in muscle development restricted to the neuromuscular junction (Glass, Bowen et al. 1996, Glass, DeChiara et al. 1996). MuSK was thus a very good candidate for the missing target and this was demonstrated by showing binding to COS cells expressing recombinant MuSK, and by binding to recombinant extracellular domain of MuSK in an ELISA. In addition, MuSK IgG antibodies inhibited agrin-induced AChR

clustering on C2C12 myotubes (Hoch, McConville et al. 2001). MuSK was shown independently to be immunoprecipitated and identified by mass spectroscopy by the Evoli group (Scuderi, Marino et al. 2002) and the approach to immunoprecipitate MuSK from the TE671 cells confirmed and optimised by Littleton et al. in 2009 (Littleton, Dreger et al. 2009).

One of the most intriguing aspects of the pathogenicity of MuSK antibodies resides within the nature of the antibodies themselves. Compared to AChR-MG, where autoantibodies are mainly of the IgG1 and, less frequently, IgG3 subclasses (Vincent and Newsom-Davis 1982), MuSK antibodies are mostly IgG4 (although a smaller population of MuSK IgG1-3 is also present) (McConville, Farrugia et al. 2004). Unlike IgG1-3 antibodies, IgG4 are functionally monovalent (Figure 1.5 A). This is because single amino acid differences between IgG1 and IgG4 in the hinge region of the CH3 backbone allow for greater stereometric flexibility. As a consequence, intrachain (instead of interchain) disulphide bridges are created under reducing conditions, thereby leaving the two half-molecules of IgG4 without a covalent connection (van der Neut Kolfschoten, Schuurman et al. 2007). Further single amino acid differences in the CH3 domain reduce non-covalent interactions between the heavy chains (Figure 1.5 A). Taken together, this allows the Fab-arm exchange phenomenon (reviewed in (Vidarsson, Dekkers et al. 2014)) by which each half-antibody exchanges with another half-antibody randomly selected from the pool of total IgG4 half-antibodies (Figure 1.5 B). As a result, most if not all IgG4 MuSK antibodies are monovalent, rather than divalent, for their antigen (Koneczny, Stevens et al. 2017). This does not allow for divalent-dependent internalisation of the antigen, a mechanism widely recognised in antibody-mediated diseases. Additional single amino acid differences in the CH2 domain of IgG4 render it unable to bind to C1q to activate the complement cascade or FcγR to activate immune cells. Instead, IgG4 antibodies can only block the function of a

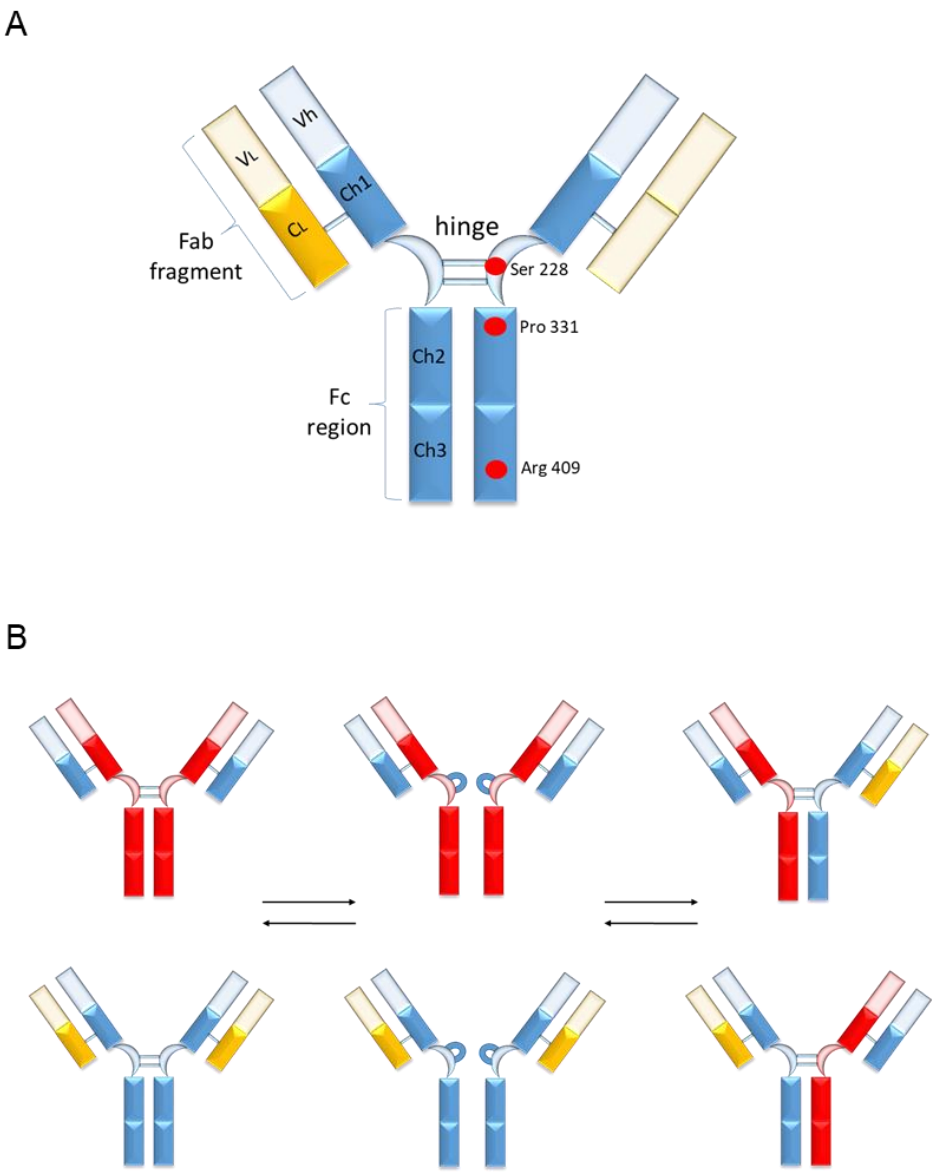


Figure 1.5. Structure of IgG4 subclass antibodies and mechanism of Fab arm exchange. **(A)** IgG4 consists of two heavy (H) and two light (L) chains, each with one variable (V) domain, and one (CL) or three (CH1-CH3) constant domains. In the hinge region, the two heavy chains are connected covalently by two interchain disulphide bridges. The variable domains and the first constant domain form the Fab fragment, which binds the antigen, while the hinge and the CH2-CH3 domains form the Fc region which provides effector function such as binding of C1q or Fc gamma receptors. IgG1 and IgG4 have over 90% sequence homology, but single amino acid differences affect structure and function of the antibody. Three relevant examples are serine at position 228 instead of a proline, allowing for structural flexibility and a switch to intrachain disulfide bridges. Proline at position 331 prevents binding of C1q, and arginine at position 409 leads to reduced non-covalent interactions between the two heavy chains. **(B)** Under reducing conditions (e.g. 1 mM glutathion), IgG4 can undergo Fab-arm exchange. The interchain disulfide bridges change to intrachain disulfide bridges, disconnecting the two half-molecules of the antibody. These then stochastically recombine with other IgG4 half-molecules that recognise different antigens, forming bi-specific antibodies. Under reducing conditions, the different states of IgG4 are in equilibrium.

protein or inhibit its interaction with other proteins (reviewed in (Koneczny 2018)). The two main pathogenic mechanisms characteristic of AChR-MG (antigen internalisation and complement-related damage) are, therefore, not relevant in the IgG4-mediated MuSK-MG and alternative antibody effects needs to be considered.

With the discovery of MuSK as the antigen, both *in vitro* and *in vivo* models provided strong evidence of the pathogenicity of MuSK IgG4 antibodies. Subsequent experiments carried out on different animal models – either passively immunised with MG patients' plasma or actively immunised with purified recombinant MuSK – showed clinical symptoms and/or impaired neuromuscular transmission consistent with the myasthenic phenotype, including muscle weakness and fatigability, reduction of endplate AChR numbers, and reduction of end plate potential (EPP) and miniature EPP amplitudes (Shigemoto, Kubo et al. 2006, Cole, Ghazanfari et al. 2010, Klooster, Plomp et al. 2012, Viegas, Jacobson et al. 2012). Notably, delayed-synapsing muscles (specifically diaphragm, sternomastoid and tibialis posterior), in which synaptogenesis requires a longer period of time to complete, were more severely affected in a MuSK immunised model compared to fast-synapsing muscles (intercostal, adductor longus and tibialis anterior) (Xu, Jha et al. 2006). This suggests that differences in muscle development could affect susceptibility to the effects of MuSK antibodies and might partially explain the clinical pattern of weakness in MuSK-MG.

Insights regarding the pathogenic mechanism by which MuSK antibodies cause myasthenia were provided by further *in vitro* experiments performed on cultured C2C12 myotubes. After incubation of the myotubes with plasma or purified antibodies obtained from MuSK-MG patients, MuSK phosphorylation was markedly reduced and not restored by recombinant agrin (Huijbers, Zhang et al. 2013, Koneczny, Cossins et al. 2013). Moreover, AChR clustering was substantially reduced (Hoch, McConville et al. 2001, Koneczny, Cossins et al. 2013, Huda, Cao et al. 2020).

The inhibition of MuSK phosphorylation was subsequently shown to be dependent on IgG4 antibodies, that prevented binding of Lrp4 to MuSK (Huijbers, Zhang et al. 2013, Koneczny, Cossins et al. 2013) (Figure 1.6 A). They target mainly the first Ig-like domain of MuSK, an epitope located on the extracellular part of the protein which mediates Lrp4-MuSK binding (see above) (McConville, Farrugia et al. 2004, Otsuka, Ito et al. 2015, Huijbers, Vink et al. 2016). According to this pathogenic model, the disruption of the functional tetramer formed by MuSK and Lrp4 prevents MuSK from being activated following agrin-Lrp4 binding (Huijbers, Zhang et al. 2013, Kucukerden, Huda et al. 2016). MuSK is therefore not able to respond to agrin stimulation and, consequently, the entire AChR clustering cascade is inhibited. The on-going turnover of AChRs and dispersal by acetylcholine (see above) leads ultimately to the reduction in AChR clusters on the post-synaptic membrane of the NMJ. Moreover, *in vivo* models of MuSK-MG lack the presynaptic adaptive increase of ACh release (quantal content) observed in AChR-MG models (Mori, Kubo et al. 2012, Viegas, Jacobson et al. 2012, Patel, Oh et al. 2014). A likely explanation is that MuSK antibodies disrupt the retrograde signalling mediated by Lrp4, which increases the release of acetylcholine compensating for the reduction of AChRs. Finally, it is worth mentioning that other epitopes, such as the Ig3 and the frizzled domain of MuSK, were found to be detected by a variable proportion of MuSK antibodies, indicating that the disruption of other pathways – including Wnts and BMP4 – might contribute to the overall pathogenic mechanism of MuSK-MG (Takamori, Nakamura et al. 2013, Huijbers, Vink et al. 2016).

An additional proposed mechanism of MuSK antibodies, that could be available to all autoantibody subclasses (divalent IgG1-3 and monovalent IgG4), is represented by the block of ColQ-MuSK interaction (Figure 1.6 A) (Kawakami, Ito et al. 2011).

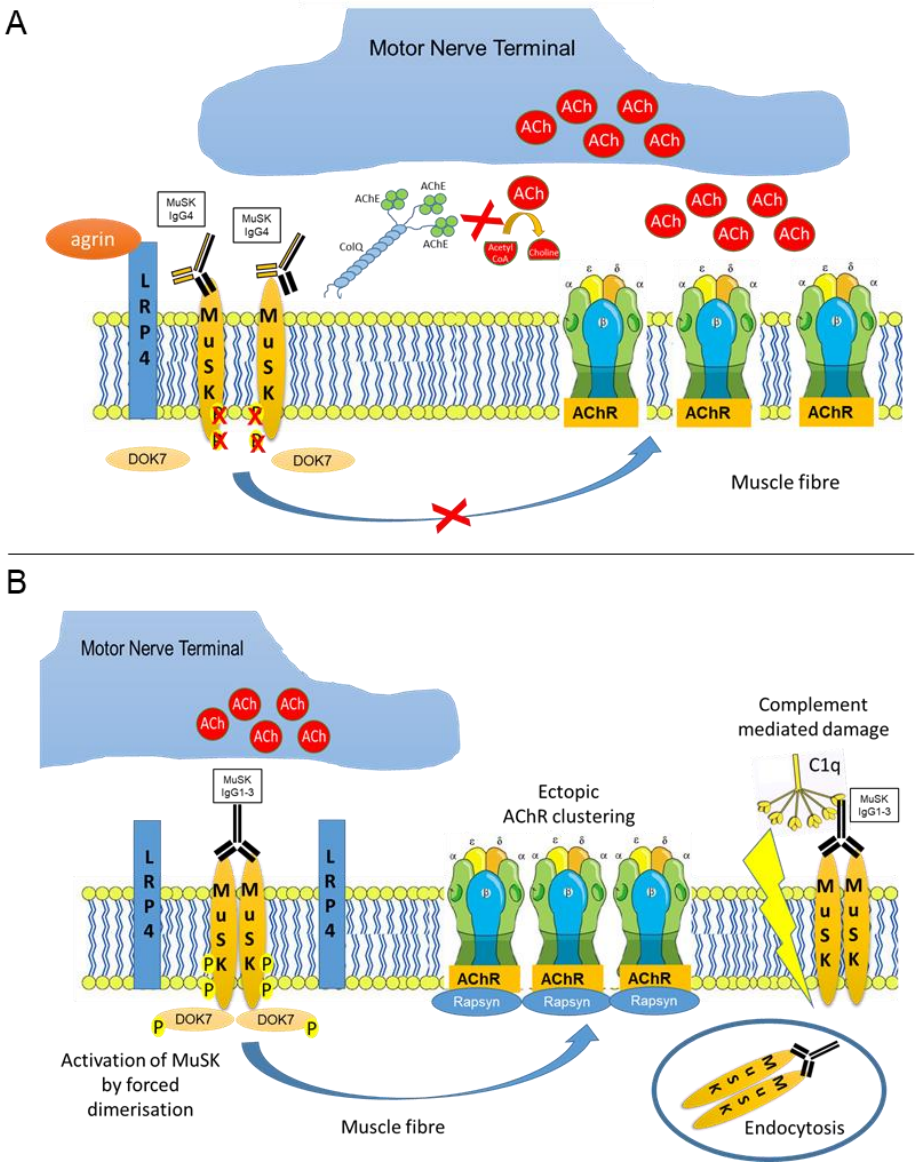


Figure 1.6. Fig 3. Proposed pathological mechanisms of MuSK autoantibodies at the neuromuscular junction. (A) In MuSK-MG, autoantibodies of the IgG4 subclass bind to the ectodomain of MuSK preventing its interaction with LRP4 and therefore block down-stream signalling. The phosphorylation cascade is therefore inhibited causing the ultimate dispersal of AChR clusters. Loss of retrograde signalling mediated by LRP4 may also explain the absence of presynaptic adaptive increase of ACh vesicles observed in MuSK-MG animal models which is otherwise characteristic in AChR-MG. Block of ColQ-MuSK binding by MuSK autoantibodies has been proposed to be a pathogenic mechanism that may lead to a loss of AChE from the ECM at the NMJ. **(B)** Hypothetic pathogenic mechanisms of MuSK IgG1-3. Divalent binding of MuSK antibodies might induce MuSK dimerisation and activation, leading to ectopic, extra-synaptic AChR clusters. These would not participate in neuromuscular transmission as they would lack adjacent motoneuron terminals. For the formation of ectopic AChR clusters, AChRs may also be recruited from synapses thus depleting the NMJ from AChR. *In vivo* MuSK IgG1-3 antibodies may recruit C1q and activate the classical complement pathway, causing complement-mediated damage at the NMJ. Finally, MuSK IgG1-3 could also cross-link MuSK and lead to its internalisation, depleting MuSK from the muscle membrane and causing a loss of agrin-Lrp4-MuSK-DOK7 signal transduction.

This may reduce AChE at the MuSK-MG synapse and, consequently, increase the concentration of ACh within the synapse which would eventually promote dispersal of the receptors. It was proposed that this mechanism could also explain the hypersensitivity to treatment with AChE inhibitors in MuSK-MG patients as, following their administration, the higher amount of ACh released into the synaptic cleft would increase even more the AChR dispersal, which in turn would not be compensated by a functional agrin-Lrp4-MuSK activation (Evoli, Bianchi et al. 2008, Morsch, Reddel et al. 2013).

Finally, an additional pathogenic mechanism of MuSK antibodies might be related to a direct induction of atrophy in the muscles specifically targeted by the disease. In this respect, sera from MuSK-MG patients were found to induce the expression of atrophy factor Muscle RING-Finger protein-1 (MURF-1) in C2C12 myotubes and, selectively, in the masseter of passive-immunised mice, indicating a potential direct link between the antibody effects and the muscular atrophy observed in bulbar muscles of MuSK-MG patients (Benveniste, Jacobson et al. 2005, Farrugia, Robson et al. 2006).

1.7.2.2) Another player of the game: the IgG1, 2 and 3 subclass antibodies

Alongside the prominent and better-characterised MuSK IgG4 antibody population, a variable proportion of MuSK IgG1, 2 and 3 antibodies is usually detectable in most patients. The role and importance of these antibody subclasses is still a matter of debate although there is evidence that IgG1-3 could also actively contribute to the pathogenic process of MuSK-MG. Similar to IgG4, MuSK IgG1-3 are able to disperse agrin-induced AChR clusters in C2C12 myotubes, despite the fact that they do not inhibit the Lrp4-MuSK interaction (Koneczny, Cossins et al. 2013). In the same study, IgG1-3 also prevented DOK7-induced AChR cluster formation on C2C12 myotubes. As DOK7 acts downstream of MuSK, these findings suggest that the effect of MuSK IgG1-3 may not

be limited to the potential disruption of Lrp4-MuSK interaction but could also involve other parts of the AChR clustering pathway. Moreover, complement activation and MuSK endocytosis by cross-linking are other potential mechanisms that have been suggested for MuSK IgG1-3, as already described in AChR-MG, as indicated by the increase of complement breakdown products in MuSK-MG sera and the reduction of MuSK expression on the muscle membrane in passive-immunised mice (Cole, Ghazanfari et al. 2010, Tuzun, Yilmaz et al. 2011).

Additional *in vivo* evidence of IgG1-3 pathogenicity is provided by a model in which a mouse knockout of murine IgG1 – equivalent to human IgG4 – developed myasthenic features when immunised against MuSK. In this case, the immune response was sustained by the murine equivalent of human IgG1-3 antibodies (Kucukerden, Huda et al. 2016) and the authors suggested that both complement activation and direct blocking of Lrp4-MuSK interaction could be the underlying mechanisms of the disease. Current hypotheses regarding the pathogenic mechanisms of MuSK IgG1-3 are summarised in Figure 1.6 B.

1.8) Initial steps towards a better understanding of the pathogenic mechanism of MuSK-MG and the development of a targeted treatment

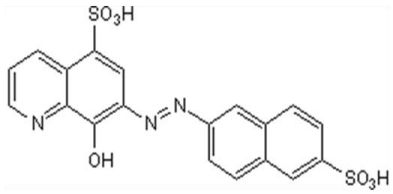
As highlighted in the last paragraphs, there are several questions that remain open regarding the exact pathogenic mechanisms responsible for the development of symptoms in MuSK-MG and the role of individual MuSK-Ab subclasses. This incomplete understanding of the disease also leads to the current lack of specific treatments that could target directly the effects of the MuSK-Abs rather than the immune system as a whole.

In this respect, inducing MuSK activation – directly or by inhibiting its negative regulators – represents one of the possible therapeutic strategies to be considered.As

described above, SRC homology 2 domain containing phosphotyrosine phosphatase 2 (SHP2) represents another possible intracellular target, as it inhibits the AChR clustering pathway acting as a negative regulator of MuSK phosphorylation (Qian, Chan et al. 2008). Notably, apart from its role in the muscle cells, SHP2 also mediates and enhances growth cell signalling in different tissues. It is involved in activation of Erk1/2 MAP kinase by EGF (Deb, Wong et al. 1998), and gain of function mutation of its gene, *PTPN11*, are associated with Noonan's syndrome, juvenile myelomonocytic leukemia, and several types of human malignancies (Bentires-Alj et al, 2004; Tartaglia and Gelb, 2005). For these reasons, SHP2 inhibition has been studied with the aim to understand better tumorigenesis and to develop new antineoplastic drugs (Bunda, Burrell et al. 2015, Grosskopf, Eckert et al. 2015, Schneeberger, Ren et al. 2015, Perez-Fernandez, Lopez-Ruano et al. 2019). In this respect, of particular interest is NSC-87877, a selective SHP 1/2 inhibitor – formed by an aliphatic chain connected through two nitrogen atoms – that binds to the catalytic cleft of SHP2 through hydrogen bonds inhibiting its phosphatase activity (Figure 1.7) (Chen, Sung et al. 2006). In the context of disorders of the neuromuscular junction, the inhibition of SHP2 by NSC-87877 has already been shown to increase AChR clustering in C2C12 mouse myotubes independent of agrin stimulation (Zhao, Qian et al. 2007). These initial findings paved the way for the potential use of SHP2 as a specific target in the treatment of MuSK-MG and represents the core of the research work illustrated in this thesis and detailed in Chapter 3 and 4.

Finally, it is worth considering that the current pathogenic model of the MuSK-MG leans heavily on the role of MuSK IgG4 (Huijbers, Zhang et al. 2013, Koneczny, Cossins et al. 2013), which is the IgG subclass most studied due to its predominance in patients' plasma. However, evidence is increasing to support a significant pathogenic contribution from the less-represented IgG1-3, as these antibodies show similar effects

A



8-Hydroxy-7-[(6-sulfo-2-naphthyl)azo]-5-quinolinesulfonic acid
(NSC 87877)

B

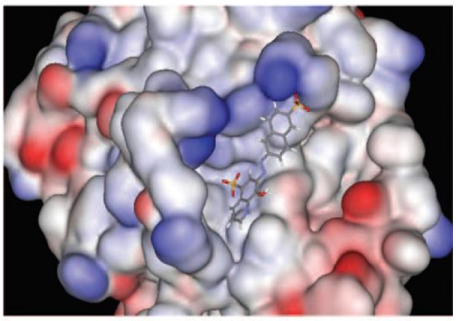


Figure 1.7. Structure of NSC-87877 and its binding site on SHP2. **(A)**: chemical structure of NSC-87877 consisting in 4 aliphatic rings interconnected with a nitrogen bond. **(B)** Molecular model of NSC-87877 binding to the SHP2 PTP domain. The inhibition of the phosphatase is determined by irreversible binding of the drug to the catalytic cleft of the enzyme through hydrogen bonds. Positively charged areas are coloured in blue, and negatively charged areas coloured in red. For NSC-87877, carbon atoms are coloured in grey, oxygen in red, nitrogen in blue, hydrogen in white, and sulphur in yellow (from Chen et al, *Discovery of a novel SHP2 protein tyrosine phosphatase inhibitor*, Mol Pharmacol, 2006)

in disrupting AChR clustering while surprisingly activating MuSK phosphorylation (Koneczny, Cossins et al. 2013, Huijbers, Vergoossen et al. 2019, Takata, Stathopoulos et al. 2019). As mentioned above, the same mechanism appears to be shared by gain-of-function mutations in *MUSK* which have been recently described in a case of congenital myasthenic syndrome (Rodriguez Cruz, Cossins et al. 2020). These recent observations suggest that AChR clustering is disrupted not only by the inhibition of MuSK phosphorylation, but also by MuSK hyperactivation induced by specific mutations or the direct effect of divalent MuSK IgG1-3 antibodies. However, how an increase in MuSK phosphorylation is pathogenic remains unanswered, and the effect of MuSK IgG1-3 subclasses still unexplored. This topic represents the second major focus of this research project and will be explored in Chapter 5 and 6.

There were two main aims of the research project described in this thesis:

1. To study the *in vitro* and *in vivo* effects of a specific SHP2 inhibitor, NSC-87877, which was hypothesised to protect MuSK phosphorylation and AChR clustering from the detrimental effects of MuSK antibodies;
2. To analyse the pathogenic potential of MuSK IgG1-3 antibody subclasses by investigating their action on the MuSK phosphorylation cascade, AChR clustering, and cytoskeletal rearrangements.

Chapter 2

Materials and Methods

2.1) Tissue culture

All tissue culture procedures were carried out in sterile conditions. The following cell lines were purchased from ATCC and used in the experiments described in this thesis: Human embryonic kidney 293T (HEK 293T, CRL-3216); C2C12 mouse immortalised myoblasts (CRL-1772); Phoenix-Ecotropic (ECO) (Human embryonic kidney retrovirus-producing, CRL-3214); Cercopithecus aethiops SV40-transformed-7 (COS-7) (monkey fibroblast-like, CRL-1651); Drosophila Schneider 2 (S2) (embryonic macrophage-like lineage, CRL-1963).

Mammalian cell lines were growth in an adherent monolayer either on T25, T75, or T175 flasks (CLS3289, CLS3290, CLS3292, Corning) at 37°C in an atmosphere of 8% CO_2. Drosophila cells were growth in suspension on Erlenmeyer flasks (Z331627, Corning) with constant agitation in an environment of 25ºC with no CO_2 supplementation.

HEK 293T, COS-7, and Phoenix-ECO cells were grown in Dulbecco-modified essential medium (DMEM) (41966052, Gibco) supplemented with 10% of Foetal Calf Serum (FCS – A15-151P, PAA) with the addition of 100 units/ml of penicillin G, streptomycin, and Amphotericin-B (PSA – 15240096, Invitrogen). C2C12 myoblasts were grown in DMEM supplemented with 15% FCS and 1% PSA. Drosophila S2 cells were grown in Express Five Serum Free Medium (10486025, Thermo Fisher) supplemented with 1% L-glutamine (25030149, Thermo Fisher), 1% PSA, and 10% heat-inactivated FCS (F9665-500ML, Merk).

Mammalian cells were split when reached 70-80% of confluence. Growth medium was aspirated, and the adherent cells washed once with PBS. Cells were then detached

by exposure to trypsin-EDTA (10X solution - T4174, Sigma) diluted in PBS, at 37ºC for 2 minutes (2 ml solution for 75 cm^2 flask, and 5 ml for 175 cm^2 flask). Trypsinised cells were suspended in growth medium, counted in case further seeding in wells was required, and split 1:10 for growth maintenance.

To differentiate myoblasts into myotubes, C2C12s were seeded at a density of 1.5 x 10^5 on 6-well plates (3516, Corning). After 48 hours, growth medium was changed into fusion medium (DMEM containing 2% FCS, 2% Horse Serum (B11-122, PAA), 1% PSA) which was replaced daily until complete differentiation (usually 5-6 days).

2.2) NSC-87877

SHP2 Inhibitor NSC-87877 was purchased from Tocris (2613) and reconstituted as per manufacture's instruction. Dilutions and dosages used for *in vitro* and *in vivo* experiments are indicated in the appropriate sections.

Molecular biology techniques

2.3) Plasmids

All plasmids containing the genomic sequence of proteins of interest (i.e. agrin, MuSK, DOK7, LRP4, and βAChR) were already available in the Neuroscience Lab of Prof David Beeson. According to individual experiments, plasmids were used for transfection and protein expression in the following mammalian cell lines: HEK 293T (for membrane expression in cell-based assays, and soluble extracellular secretion for protein production and purification), Phoenix-ECO (for the creation of retroviral vectors), and COS-7 cells (for the expression of βAChR used as a control in western blots). Stably transfected Drosophila S2 cells were used for the production and purification of MuSK-ectodomain.

The DNA constructs used in this thesis included the following:

- Soluble agrin (short rat form) (Ferns, Campanelli et al. 1993), cloned into a pSecTagB plasmid (Figure 2.1). This truncated form of agrin contains the truncated C-terminus of agrin with a 12 amino acid insert at the x-splice site, a four aminoacid insert at the y-splice site, and an insert of eight aminoacids at the z-splice site. In addition, the recombinant protein contains its own signal peptide, which allows agrin to be secreted as a soluble form. Agrin was produced in HEK 293T and used in all experiments to simulate physiological stimulation inducing MuSK-DOK7 phosphorylation cascade and AChR clustering in C2C12 myotubes.
- Human MuSK with C-terminus mCherry tag, cloned into pEGFP-N1 plasmid (EGFP was substituted with the mCherry sequence by Dr Inga Koneczny in our lab for her DPhil project) (Figure 2.2). This construct was mainly used for immunoprecipitation experiments in co-transfection with LRP4 and, due to the fluorescent mCherry tag, in cell-based assays to test sample positivity for MuSK antibodies.
- Soluble human MuSK ectodomain (aa22-452 plus C-terminus 6 HIS-tag sequence), cloned into a pcDNA 3.1 hygro(+) plasmid (Figure 2.3). Used for production and purification in HEK 293T cells.
- Soluble human MuSK ectodomain (aa22-452), cloned into a pMT/BiP/V5-HisA plasmid (Figure 2.4). In this vector, gene expression is regulated by the MT promoter, which is induced by the addition of copper sulphate. The BiP sequence drives the extracellular secretion of the protein. Finally, the V5-HisA encodes for a His tag necessary for the purification by nickel chromatography. This construct was used for the production and purification of MuSK ectodomain in stably transfected Drosophila S2 cells.

- Human LRP4, with C-terminus GFP tag, cloned into a pcDNA 3.1 hygro(-) plasmid (Figure 2.5). Used for immunoprecipitation experiments on HEK 293T co-transfected with MuSK-mCherry.
- Human β subunit of the AChR, cloned into a pcDNA 3.1 hygro(+) plasmid (Figure 2.6). Used for transfection in COS-7 cells as positive expression control in western blot analysis.
- Human DOK7 Wild Type and DOK7 1124_1127dupTGCC, cloned into retroviral vector pBabe-PURO-EGFP and transfected into retrovirus producing Phoenix-ECO cells (Figure 2.7 and 2.8). Used for overexpression experiments in C2C12 myotubes.

2.4) General principles of cell transfection

Transfection of plasmid DNA was carried out using polyethyleneimine (PEI) as described by Boussif. According to individual experiments, mammalian cells were seeded either on 6-well plates (at 3.5 x 10^5/well), T25 flask (at 3.5 x 10^6), T175 flasks (at 5 x 10^6) and incubated in growth medium for 24h. The following day, cells were transfected with the following amount of plasmid DNA:

- 3 μl DNA (at 1 μg/μl) per well (6-well plates);
- 18 μl DNA (at 1 μg/μl) per T25 flask;
- 42 μl DNA (at 1 μg/μl) per T175 flask;

Plasmid DNA was mixed energetically with a proportionate amount of 20% sterile-filtered glucose (DNA/glucose ratio = 2.4), and PEI (DNA/PEI ratio = 2), added to the final volume of growth medium and incubated for 16h. Supernatant was then aspirated and changed to growth medium. In experiments aimed to produce a soluble protein construct (i.e. agrin and MuSK ectodomain), following 48 hours of transfection, conditioned medium was harvested, collected in cryotubes, and stored at -80ºC. In case



Figure 2.1. Structure of the pSecTagB plasmid carrying the gene for soluble agrin - short rat form

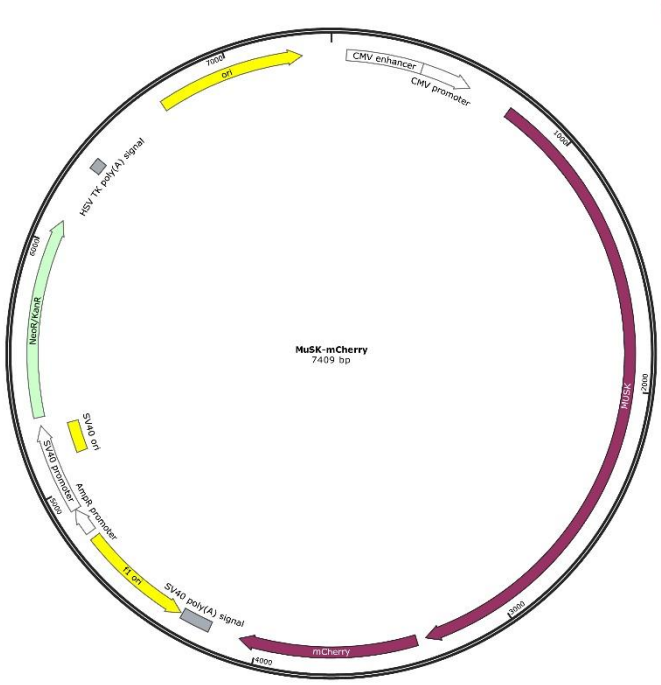


Figure 2.2. Structure of the pEGFP-N1 plasmid with EGFP gene substituted with m-Cherry and attached to the C-terminus of human MuSK

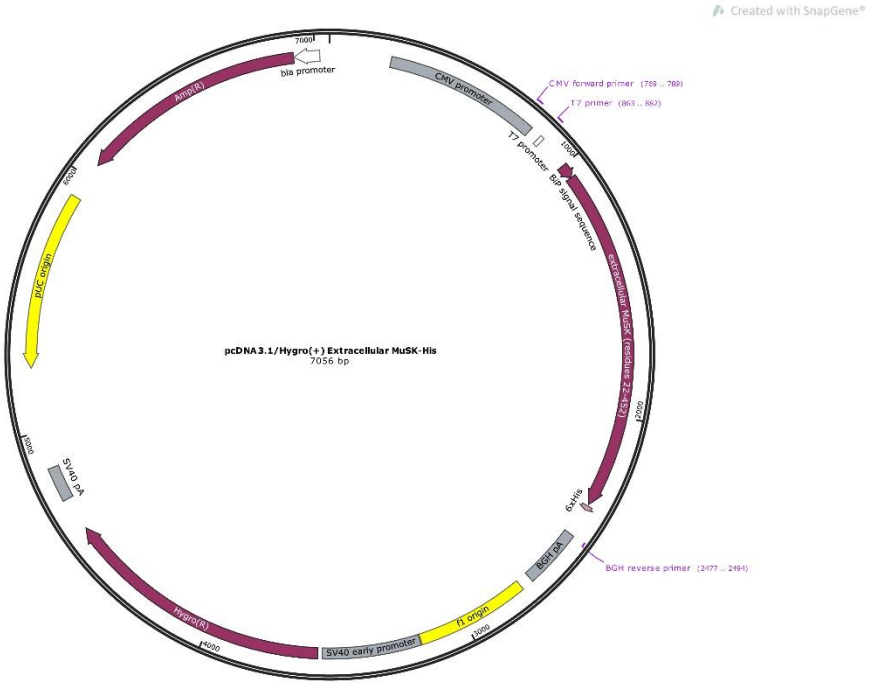


Figure 2.3. Structure of the pcDNA 3.1 hygro(+) plasmid carrying the soluble human MuSK ectodomain (aa22-452) with a His-tag sequence at the C-terminus.

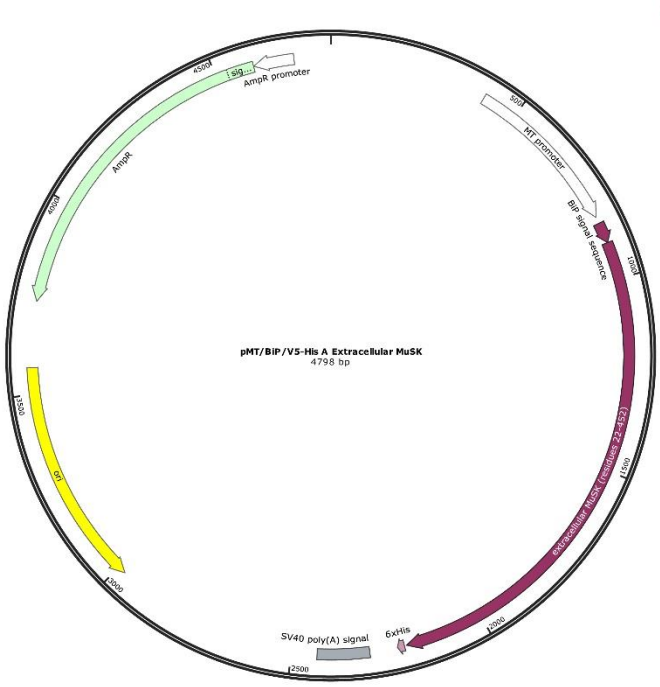


Figure 2.4. Structure of the pMT/BiP/V5-HisA plasmid carrying the soluble human MuSK ectodomain (aa22-452) with a His-tag sequence at the C-terminus.

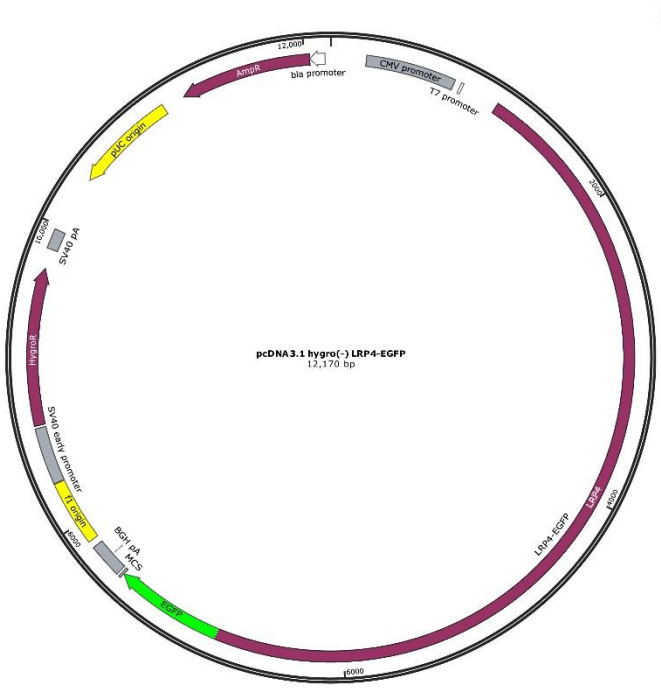


Figure 2.5. Structure of pcDNA 3.1 hygro(-) plasmid carrying the human LRP4 gene.

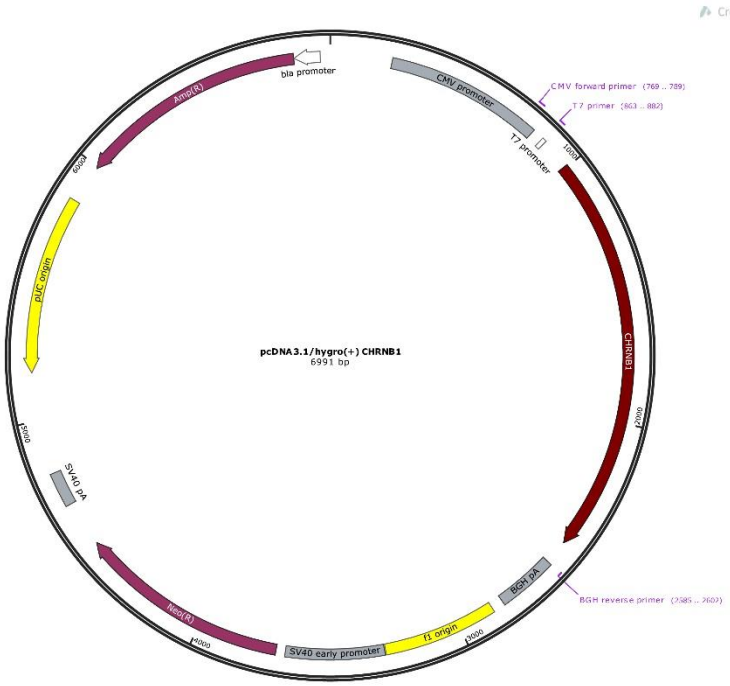


Figure 2.6. Structure of pcDNA 3.1 hygro(+) plasmid carrying the human gene for the β subunit of the AChR (CHRNB1).

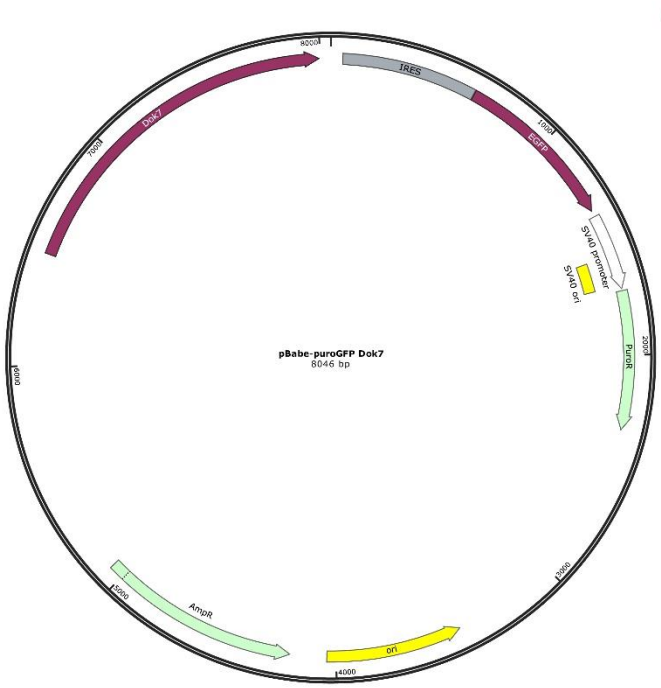


Figure 2.7. Structure of pBabe-PURO-EGFP plasmid carrying the human DOK7 Wild Type gene.

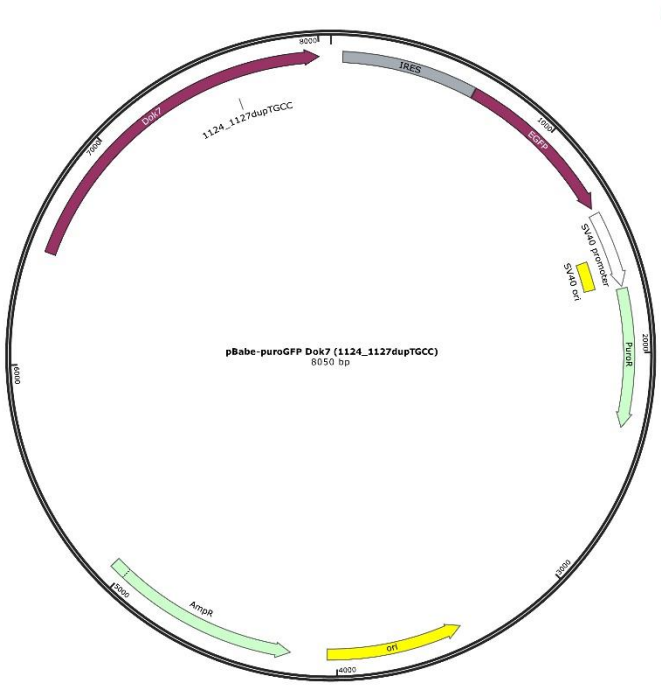


Figure 2.8. Structure of pBabe-PURO-EGFP plasmid carrying the human DOK7 1124_1127dupTGCC mutant gene.

protein construct was necessary for western blot analysis, cells were lysed after 48h from transfection and subjected to SDS-PAGE (see section 2.18). For cell-based assays, methods are described in detail in section 2.25.

2.5) DOK7 wild type and DOK7 1124_1127dupTGCC overexpressing C2C12s

DOK7 overexpressing cell lines were created using a retroviral vector following the methodology previously developed in our lab and described in (Cossins, Liu et al. 2012). Phoenix-ECO retrovirus producer cells were seeded at 2 x 10^6 on a T25 flask in growth medium, and incubated overnight at 37°C. The following day, cells were transfected with 8 μg retroviral vector pBabe-PURO-EGFP-DOK7 or pBabe-PURO-EGFP-DOK7_1124_1127dupTGCC using PEI. After 16h, cells were reseeded into a T75 flask containing growth medium. After 2 days, the medium was harvested, centrifuged to remove cell debris at 2000 rpm for 15 minutes, collected in 1 ml aliquots in cryotubes and stored at -80ºC. C2C12 myoblasts, seeded a day in advance at 5 x 10^4 in a T25 flask, were then infected with 1 ml of harvested medium containing retrovirus and 8 μg/ml of polybrene (sc-134220, Insight Biotechnology). The following day, the medium was replaced with myoblast growth medium, and 2.5 μg/ml of puromycin (P9620, Sigma) was added 72 h after infection to select the infected cells. After 24h, successful infection was confirmed by visualising EGFP expression using an Olympus IX71 fluorescence microscope. After 2-3 days after selection with puromycin, myoblasts were ready to start differentiation into myotubes. Expression of DOK7 WT and DOK7 1124_1127dupTGCC was verified by SDS-PAGE of cell lysates as described in section 2.18.

2.6) Creation of MUSK mutant cell lines

Both cell lines were previously created in our lab by Dr Pedro Rodriguez-Cruz as part of his DPhil research project and used for the purposes of this study thanks to Dr Cruz's kind gift. The methods regarding the creation of both *Musk* mutant cells line are here presented as published in (Huda, Cao et al. 2020, Rodriguez Cruz, Cossins et al. 2020).

The *MUSK* 'knock out' (KO) C2C12 myoblasts were generated with the CRISPR-Cas9 system using standard methods (Ran, Hsu et al. 2013). *MUSK* guide oligonucleotides (Integrated DNA Technologies) were designed and cloned into a modified plasmid pX335-U6-Chimeric_BB-CBh-hSpCas9n-D10A (42335, Addgene). Guide A oligonucleotide sequences were A-forward: 5'-CACCGCATTCTCCCGGATGCTGTAG-3' and A-reverse: 5'-AAACCTACAGCATCCGGGAGAATGC-3'. Guide B oligonucleotide sequences were B-forward: 5'-CACCGCTCCTCACCATTCTGAGCG-3' and B-reverse: 5'-AAACCGCTCAGAATGGTGAGGAGC-3'. A 51 base pare deletion was therefore introduced, which affects the correct splicing of *MUSK* coding sequence. This causes the missing of the whole exome 3 in the final product leading to a non-functional protein. Myoblasts were electroporated with 10 μg of each plasmid using Neon Transfection System (MPK5000, Thermo Fisher), selected with Geneticin antibiotic (10131035, Thermo Fisher), and cloned in 96-well plates using Fluorescence-activated cell sorting (FACS). Clones were screened by Sanger sequencing after PCR of genomic DNA using the primers 5'-TGGTGCTTTGGTTATGGAGCC-3' and 5'-GAGGAGGGGTCTAAGGCTTG-3'. Confirmation of *Musk* KO was conducted by Sanger sequencing after PCR of genomic DNA (primer pair: 5′-TGGTGCTTTGGTTATGGAGCC-3′ and 5′-GAGGAGGGGTCTAAGGCTTG-3′) and western blot analysis of MuSK protein expression.

The *MUSK* p.C317R C2C12 myoblasts were generated by infecting the *Musk* KO cells with a retroviral vector containing the mutant *MUSK* construct. *Musk* mutation was introduced with Quik-Change Multi Site-Directed Mutagenesis Kit (200514, Agilent) and confirmed by Sanger sequencing. The coding sequence for *MUSK* p.C317R was subcloned into the retroviral vector pBabe-PURO-EGFP. Phoenix-ECO retrovirus producer cells were transfected with 10 μg of *MUSK* p.C317R construct, and then grown for 72h in 7 ml of growth medium. A pBabe-PURO-EGFP empty vector was used as a control. The medium was harvested and centrifuged to remove cell debris, collected in 1 ml aliquots in cryotubes and stored at -80ºC. C2C12 *MUSK* KO myoblasts, were then exposed to the retrovirus, selected with puromycin, and finally differentiated into myotubes as described for DOK7 overexpressing cells in section 2.5.

2.7) RNA extraction

Total RNA was extracted from fully differentiated myotubes after exposure to the different compounds/antibody preparations used for individual experiments for 2.5h at 37ºC. After incubation, myotubes were washed 3 times for 5 minutes with differentiation medium, and RNA extracted using TRIzol Reagent (15596026, Thermo Fisher) according to the manufacturer's instructions. Supernatant was removed and 0.5 ml of TRIzol were added to each well pipetting gently to allow homogenisation of the solution. Samples were collected in Eppendorf tubes and left to incubate for 5 minutes at room temperature to permit complete dissociation of the nucleoproteins complex. 0.2 mL of chloroform per 1 mL of TRIzol were added to the samples, mixed for 30 seconds by vortexing, incubated for 2 minutes, and centrifuged for 15 minutes at 12000 g at 4°C. Samples were therefore separated into 3 different phases: a lower red phenol-chloroform one, an interphase containing the DNA, and a colourless upper aqueous phase containing the RNA which was transferred to a new Eppendorf tube. 0.5 mL of

isopropanol per 1 ml of TRIzol were added to the samples, incubated for 10 minutes, and centrifuged for 10 minutes at 12000 g at 4°C. After centrifugation, supernatant was discarded and the pellet containing the RNA resuspended in 1 ml of 75% ethanol per 1 ml of TRIzol. After vortexing, samples were then centrifuged for 5 minutes at 7500 g at 4°C. Supernatant was discarded and the pellet containing the RNA left to air dry for 10 minutes. Finally, the pellet was resuspended in 50 ml of RNase-free water, incubated in a water bath at 55°C for 10 minutes, and then stored at -80°C.

Contaminating genomic DNA was removed using the TURBO DNA-free kit (AM1907, Thermo Fisher) according to manufacturer's instructions. Briefly, 0.1 volume of 10X TURBO DNase Buffer and 1 μL of TURBO DNase Enzyme was added to the RNA and incubated at 37°C for 30 minutes. After vortexing the samples, 2 μL of DNase Inactivation Reagent were added to the solution, mixed thoroughly, and left to incubate for additional 5 minutes at room temperature. Finally, samples were centrifuged at 10000 g for 2 minutes and supernatant containing the RNA transferred to a fresh tube. Concentration and purity of RNA was estimated using a NanoDrop 2000 spectrophotometer (Thermo Fisher), measuring the 260/280 and 260/230 ratios (both ratios should be ≥2 for samples with acceptable acid nucleic purity). Common contaminants are represented by proteins at 280 nm, and carbohydrates and phenol at 230 nm. Quality of samples was finally checked with Agilent Tapestation.

2.8) RNA sequencing analysis

After RNA extraction and purity check of the nucleic acids, 20 μl of each samples (at 50 ng/μl) were sent in triplicates to the company Novogene (UK) for transcriptomic library preparation and sequencing. RNA sequences were aligned to the *mus musculus* genome using STAR (Spliced Alignment to a Reference). Reads were counted using featureCounts and analysed using edgeR (Bioconductor). Data was filtered to exclude

genes with <1 count per million for at least three samples. RNA composition was adjusted using calcNormFactors, and the coefficient of variation and dispersion were estimated. TopTags was used to obtain log-fold change (logFC) data. Bigwig files were created from BAM files for viewing in the UCSC genome browser. The online platform Reatcome was used to analyse the pattern of intracellular pathways and significant interactions within these pathways among the genes modified by each compound.

Protein and antibody purification techniques

2.9) Generation and Nickel-affinity purification of MuSK on HEK 293T

HEK 293T cells were seeded at 5 x 10^6 in 3 T175 flasks. The following day, cells were transfected with a solution of 42 µg pcDNA 3.1 hygro(+) MuSK extracellular domain (ecto-MuSK) (aa22-452 plus C-terminus 6 HIS-tag sequence), 21 µl PEI, 17.5 µl 20% sterile-filtered glucose, 10.5 µl DNase-free water per flask. After 16h from transfection, supernatant was changed to growth medium. Cell medium was then harvested 48h after transfection and centrifuged at 2000 rpm for 10 minutes. 50 ml of pooled supernatant was concentrated 10 times through centrifugal 30 kDa filter devices (Millipore Centriprep YM-30K 4306) and 1X EDTA-free protease inhibitor cocktail (Sigmafast S8830-2TAB) was added. Nickel-chelating resin (ProBond R80115, Thermo Fisher) was washed and activated in native purification buffer (50 mM NaH_2PO_4, 0.5M NaCL, pH 8) according to manufacturer's instruction and incubated with the sample in 1:5 proportion. After 1h incubation at room temperature, sample was loaded into a standard column and flow-through collected. The column was washed 4 times with 10 volumes of washing buffer (native purification buffer plus 50 mM imidazole) until protein OD280, measured with the NanoDrop, reached 0. Finally, target protein was eluted with elution buffer (native purification buffer with 500 mM imidazole) and 15 fractions of 1 ml collected. Samples from each fraction were eluted into SDS sample buffer, subjected

to SDS-PAGE and western blotting (see section 2.18). An additional SDS-PAGE gel was stained with Coomassie solution and elution bands analysed with tandem mass spectrometry (MS-MS) for protein identification.

2.10) Generation and Nickel-affinity purification of MuSK on Drosophila S2 cells

Due to the low yield of purified MuSK obtained with HEK 293T, purification was attempted using a Drosophila S2 cell line stably transfected with ecto-MuSK, which was previously created in our lab by Dr Patrick Waters. Cell culture and subsequent MuSK purification was performed by Dr Weiwei Liu modifying the procedure and buffers as following indicated. Cells were cultured at $1x10^6$/ml in Erlenmeyer flasks with 100 ml growth medium (Express Five SFM, Thermofisher; 1% L-glutamine, 1% PSA, 10% heat-inactivated FCS) plus 100 µl of 25 µg/ml Blasticidin (R210-1, Gibco) for selection. Flasks were kept in constant agitation at 25ºC for 24h. Cells were then induced with 500 µM copper sulphate and allowed to express for 5-6 days. Nickel-chelating resin ProBond was activated in equilibration buffer (50 mM TrisHCl, 0.5M NaCL, 10 mM imidazole, pH 7). Cell conditioned medium was harvested, centrifuged at 4500 rpm for 20 min at 4ºC, and 1X EDTA-free protease inhibitor cocktail was added to the suspension. 200 ml supernatant were incubated for 1h with 2 ml nickel-chelating resin at room temperature, then loaded into a standard column and flow-through collected. The column was washed 4 times with 10 volumes of washing buffer (50 mM TrisHCl, 0.5M NaCL, 20 mM imidazole, pH 7) until the protein OD280, measured with the NanoDrop, reached 0. Finally, target protein was eluted with elution buffer (50 mM TrisHCl, 0.5M NaCL, 250 mM imidazole, pH 7) and 15 fractions of 1 ml collected. Samples from each fraction were eluted into SDS sample buffer, subjected to SDS-PAGE and western blotting (see section 2.18). An additional SDS-PAGE gel was stained with Coomassie solution and elution bands analysed with MS-MS for protein

identification. Final elutions were dialysed against 200 volumes of Hartmann's solution using a SnakeSkin dialysis tubing (10K MWCO, 22 mm, 68100, Thermo Fisher) for 16h at 4C in constant gentle agitation.

2.11) Samples of MuSK-myasthenia patients

Plasmaferesis material was collected, with informed consent, from 10 patients with typical myasthenic symptoms, beneficial response to immunotherapy, and a diagnosis of MuSK-MG confirmed by detection of antibodies by radioimmunoassay (RIA). Collection, storage, and experimental procedures involving patients' samples were carried out in compliance with the Oxfordshire Research Ethics Committee A (07 Q160X/28).

2.12) Purification of MuSK antibodies

IgG purification consists in an affinity matrix chromatography in which plasma from patients is exposed to a resin coupled with protein G sepharose or a specific IgG4 matrix to bind the total IgG or the IgG4 subclass respectively. In the latter case, once the plasma is depleted from the IgG4 antibodies, a second incubation with protein G sepharose is used to purify the remaining IgG1, 2 and 3 antibody subclasses.

Protein G sepharose has a binding capacity for human IgG of 17 mg/ml, and the average IgG concentration in the plasma is about 8-18 mg/ml. This means that, using 10 ml of plasma and 1 ml of matrix, about 1/10 of the total amount of IgG of the original sample should be obtained during the purification process. Conversely, the IgG4 matrix has an antibody binding capacity of 6 mg/ml. The normal concentration of IgG4 in the plasma is usually between 6-10% of the total IgG (about 0.8-1.8 mg/ml). Therefore, from 10 ml of plasma using 1 ml of the matrix, we should be able to purify about 1/2-1/3 of the original IgG4.

For the purification of total IgG, 10 ml of plasma from MuSK-MG patients were centrifuged for 15 minutes at 2000 g and filtered using 0.2 µm syringe filters, diluted 1:2 in PBS and incubated overnight with 2.5 ml of Protein G Sepharose Fast Flow (17-0618-01, Sigma) at 4°C in a rotating shaker. Bead slurry was packed into a column, washed with PBS until the OD280 reached 0, and bound IgG were eluted with 0.1 M glycine, pH 2.3. Twenty elution fractions of 1 ml were collected into Eppendorf tubes containing 150 µl Tris-HCl pH 8.0 to raise the pH, and analysed for protein content by measuring the protein OD280 with the NanoDrop. The fractions with the highest OD280 were pooled, loaded on a SnakeSkin tubing and dialysed overnight against 200 volumes of DMEM for 16h at 4ºC with constant gentle agitation.

For the IgG subclasses purification, IgG4 affinity matrix (CaptureSelect IgG4 Hu Affinity Matrix – 2900.05, Thermo fisher) was used in a similar way as protein G sepharose. 10 ml of plasma from MuSK-MG patients or a healthy individual were centrifuged for 15 minutes at 2000 g and filtered using 0.2 µm syringe filters, diluted 1:2 with PBS, then incubated overnight at 4°C with 1 ml of IgG4 affinity matrix in a rotating shaker. The following day, matrix slurry was packed into a column, washed in PBS until the OD280 reached 0, and IgG4 antibodies eluted with 0.1 M glycine pH 2.3. Twenty fractions of 1 ml were collected into Eppendorf tubes containing 150 µl Tris-HCl pH 8 to neutralize the pH. The flow-through containing IgG1-3 was loaded a second time onto the IgG4 affinity matrix to ensure complete depletion of IgG4. The second flow-through was then incubated overnight 4°C with 2.5 ml protein G sepharose and eluted as previously described for total IgG purification. A final 10 ml elution was collected from both IgG4 and Sepharose Protein G matrix before reconstituting the columns with 5 ml 20% ethanol. The fractions with the highest OD280 of IgG4 and IgG1-3 were pooled, loaded on a SnakeSkin dialysis tubing, and dialysed as above. The fractions with a lower OD280 were pooled together with the final elution from the

column and concentrated using Centriprep 30 kDa centrifugal filter units until reaching a similar concentration of the other fractions previously processed.

The specific purification of MuSK-Abs from the pool of patients' IgG subclasses was not performed, although the concentration of MuSK antibodies in patients' total IgG, IgG4 and IgG1-3 was measured by RIA, and 0.5 nM MuSK-Abs was used in all the experiments described in this thesis. Therefore, the term "purified MuSK-Abs" used in the dedicated sections refers to the measured MuSK-Ab in the patients' total purified fractions of these subclasses.

Pull-down techniques

2.13) Protein immunoprecipitation from cultured cells

Protein G magnetic Dynabeads (10004D, Thermo Fisher) were used in all immunoprecipitation experiments. First, beads were resuspended in the stock solution by gentle rotation at room temperature. For each cell extract obtained from a single well of 6-well plates, 50 μl of beads were used. After positioning the beads on a magnet, the stock solution was removed and beads resuspended in 200 μl of PBS with 0.1% Tween 20 (PBS-Tween) (P1379, Sigma). Afterwards, 5 μg of immunoprecipitation antibody were incubated with the beads for 1h at 4ºC in a rotating shaker. Specifically, goat anti-MuSK AF562 (R&D), mouse anti-DOK7 A-7 (sc-390856, Santa Cruz), mouse anti-AChRα antibody D6 (sc-32253, Santa Cruz) were used to immunoprecipitate MuSK, DOK7, and AChR respectively. Alternatively, patient's own antibodies were used to immunoprecipitate MuSK in those samples directly exposed to antibody preparations purified from MuSK-MG patients.

Cell extract for immunoprecipitation was obtained after completion of individual experiments by lysing the cell in 500 μl/well of ice-cold lysis buffer (10 mM Tris-HCl, 1 mM EDTA, 100 mM NaCl, 1% Triton X-100, 1x protease inhibitor cocktail (P8340,

Sigma), 1x phosphatase inhibitor cocktail (78420, Thermo Fisher)) for 1h at 4ºC in a rotating shaker, followed by centrifugation at 12600 rpm for 10 minutes at 4ºC. Supernatant was then added to the magnetic beads (preincubated with the commercial immunoprecipitation antibody). However, in case immunoprecipitation was targeted only to the proteins expressed on the cell membrane, live cells were exposed to the selected antibodies (either commercial antibodies or purified preparations from MuSK-MG patients) for the duration required by individual experiments, lysed as described above, and then exposed directly to Protein G Dynabeads (50 µl/sample, pre-washed with 200 µl PBS-Tween). Samples were then left incubating overnight at 4ºC in a rotating shaker. The following day, immunoprecipitated beads were subjected to spinning and, after positioning on a magnet, the supernatant was discarded. Beads were then washed once with 200 µl of PBS, eluted in 15 µl of lysis buffer, 11.25 µl of NuPAGE LDS sample buffer (NP0008, Thermo Fisher), and 4.5 µl of NuPAGE Sample Reducing Agent (NP0009, Thermo Fisher), and subjected to SDS-PAGE (see section 2.18).

2.14) Co-immunoprecipitation of MuSK and Lrp4 from transfected HEK cells

MuSK-Lrp4 co-immunoprecipitation described here was adapted and optimised from the method published by (Koneczny, Cossins et al. 2013). HEK 293T cells were seeded at 3.5 x 10^5 on 6-well plates and incubated in growth medium for 16h at 37ºC. The following day, cells were transfected with a total of 3 µg DNA per well of either MuSK-mCherry, Lrp4-EGFP, or a combination of both (cloned into pEGFP-N1 plasmid) as described in section 2.4. Supernatant was aspirated after 16h incubation and replaced with growth medium. After 48h from transfection, cells were exposed to 5 µg anti-MuSK commercial antibody AF562, MuSK purified IgG4 and IgG1-3 (0.5 nM), and healthy control IgG1-3 (at an equal total protein concentration of MuSK antibody

sample) diluted in growth medium and incubated for 2h at 37ºC. Cells were then washed 3 times for 5 minutes with growth medium, lysed with 500 µl ice-cold lysis buffer, vortexed and incubated in ice for 15 minutes. Samples were then centrifuged for 10 minutes at 12600 rpm at 4ºC. 400 µl of supernatant were then incubated with 50 µl of Dynabeads Protein G for 30 minutes at room temperature in constant agitation. Elution and western blot analysis of the samples were performed similarly to other immunoprecipitation experiments as described above in section 2.13. Remaining 100 µl of supernatant were not subjected to immunoprecipitation and used for protein expression comparison.

2.15) Immunoprecipitation of MuSK from ex vivo muscle specimens

To preserve protein phosphorylation, muscle samples (tongue and tibialis anterior) were collected immediately after culling the animals, snap-frozen by direct submersion in isopentane cooled with liquid nitrogen, and stored at -80°C. Frozen muscles were then transferred to a Precellys hard tissue grinding kit tube (MK28R) with 200 µl of ice-cold lysis buffer with protease and phosphatase inhibitor cocktails. Samples were homogenised at 4°C with a Precellys 24 tissue homogeniser (Stretton Scientific) with 2 cycles at 6500 rpm. After homogenisation, samples were left incubating with the lysis buffer for 3h at 4°C in a rotation shaker. After transferring the cell lysate to a glass tube, 10 cycles of sonication (10 seconds of sonication, followed by 30 seconds of rest) were performed on a Bioruptor Pico Sonication System (Diagenode), followed by an additional hour of incubation at 4°C in a rotating shaker.

To remove intrinsic mouse antibodies that could affect immunoprecipitation, samples were precleared with 200 µl of Protein G Dynabeads, previously washed with 500 µl of PBS-Tween, for 6h at 4°C in a rotating shaker. After preclearance, bead supernatant was exposed to 50 µl of Protein G Dynabeads, already prepared for MuSK

immunoprecipitation with 5 μg of anti-MuSK AF562 antibody as previously described. MuSK immunoprecipitation was then carried out as described for cultured cells, incubating the samples with the magnetic beads and the immunoprecipitation antibody for 16h at 4ºC in a rotating shaker, eluted in SDS Sample buffer and Reducing Agent, and finally subjected to SDS-PAGE (see section 2.18).

2.16) Pull-down of surface AChRs for phosphorylation analysis

Membrane AChRs were pulled down from C2C12 myoblasts seeded at 1.5 x 10^5 in 6-well plates and differentiated into myotubes. After incubation with specific compounds or antibody preparations as outlined in individual experiments, cell supernatant was aspirated and myotubes were washed 3 times for 5 minutes with differentiation medium. Myotubes were then exposed to 5 μl of biotin-XX conjugated α-bungarotoxin (B1196, Invitrogen) diluted in 1 ml differentiation medium for 1h at room temperature with gentle agitation. Afterwards, cells were washed 3 additional times for 5 minutes with differentiation medium, and then lysed with the usual ice-cold lysis buffer for 1 hour at 4ºC in a rotating shaker. After spinning for 10 minutes at 12600 rpm, supernatant was incubated with 50 μl of Dynabeads Streptavidin T1 (65601, Thermo Fisher) for 16h at 4ºC in a rotating shaker. Pulled-down streptavidin beads were washed, eluted, and subjected to SDS-PAGE in the same way as described for sample immunoprecipitated with Protein G Dynabeads.

2.17) Immunoprecipitation of active Rho GTPase

Detection of the active form of the GTPase Rho was performed as described by Weston and colleagues (Weston, Gordon et al. 2003) by pulling down active Rho through its specific binding to GST-Rhotekin. A commercial pull-down kit (16116, Invitrogen) was used and optimised. C2C12 myotubes were starved in DMEM with 1% PSA in the

absence of foetal/horse serum for 24h prior to the experiment to reduce the basal GTPase activity, and then incubated with the either medium alone, agrin, or different MuSK antibody preparations for different times (15, 30, 45 minutes) at 37ºC. Cells were immediately placed on ice, rinsed with ice-cold TBS with the addition of 1 mM $MgCl_2$, 0.5 mM $CaCl_2$, and lysed with ice-cold lysis buffer (50 mM Tris HCl, 1% Triton X, 0.5 Na deoxycholide, 0.1% SDS, 500 mM NaCl, 10 mM $MgCl_2$, pH 7.4, 1x protease inhibitor cocktail). Lysates were incubated on ice for 5 min and centrifuged for 15 minutes at 12600 rpm at 4ºC. Supernatant was then incubated for 1h at 4ºC with 100 µl glutathione resin and 100 µl of GST-Rhotekin-RBD as per manufacturer's protocol. Beads were washed 3 times with washing buffer (50 mM TrisHCl, 1% Triton X, 150 mM NaCL, 10 mMgCl2, pH 7.2, 1x protease inhibitor cocktail), eluted into SDS Sample buffer and Reducing agent as described in section 2.13, heated at 100ºC for 10 min, and subjected to SDS-PAGE for western blotting detection. Cell lysates not incubated with GST-Rhotekin-RBD were used as a control for total Rho expression. Differently to what described in the general SDS-PAGE methods in section 2.18, nitrocellulose membranes were blocked with TBS 3% BSA for 2h at room temperature, washed 3 times for 5 minutes with TBS 0.05% Tween 20 and probed overnight at 4ºC with rabbit anti-Rho antibody (1:650 in TBS-Tween 3% BSA). Blots were washed 3 additional times for 5 minutes in TBS 5% BSA, and probed with secondary goat anti-rabbit IgG HRP-conjugate antibody (1:500 in TBS-Tween 5% nonfat dry milk) at room temperature for 1h in constant gentle rotation. Membranes were washed 3 additional times for 5 minutes at room and then developed with enzyme-linked chemiluminescence (ECL) as described in the following section.

SDS-PAGE, western blotting and other protein analysis techniques

2.18) SDS-Polyacrylamide gel electrophoresis (SDS-PAGE)

SDS-PAGE was performed according to standard methods (Laemmli 1970) and following manufacturer's instructions for each specific product. NuPAGE 4-12% Bis-Tris gradient pre-cast electrophoresis gels (NP0321PK2, Thermo Fisher) were used for all the experiment described in this thesis as they provided the size range comprehensive for the detection of all the proteins studied.

In general, 15 μl of cell lysate were dissolved in 11.25 μl of LDS sample buffer, and 4.5 μl of Sample Reducing Agent. Immunoprecipitated samples were processed as described above (see section 2.13). Samples were heated at 100ºC for 10 minutes, followed by vortexing and spinning. 20 μl of each sample were loaded on the gel together with a molecular ladder (according to the molecular weight of the target protein, either SeeBlue or HiMark Pre-Stained Protein Standards, LC5625 and LC5699, Thermo Fisher). Gel was run at a constant voltage (150V) for 1.5 hours in running buffer (NuPAGE MOPS SDS running buffer 20x, NP0001, Thermo Fisher, diluted in distilled water). After electrophoresis, gels were used for western blotting. Alternatively, when protein identification by MS-MS was required, gels were stained and fixed in Coomassie solution (0.25% Coomassie Brilliant Blue R-250, 40% methanol, 10% glacial acetic acid).

2.19) Western blotting

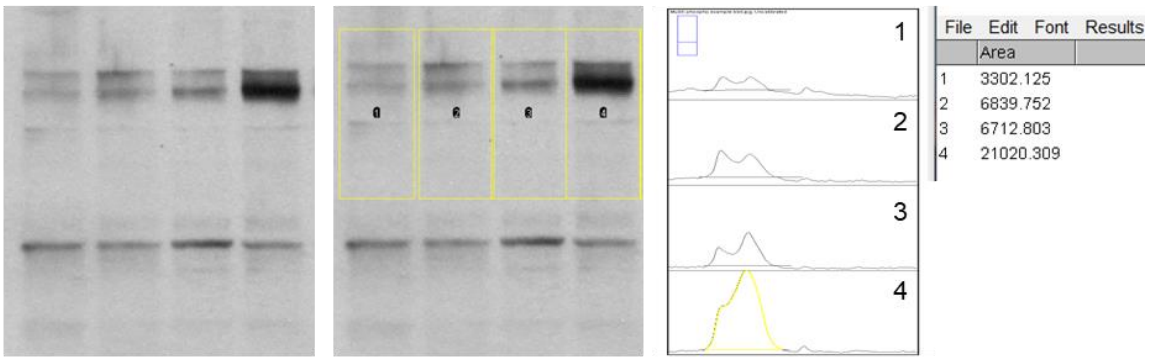
Proteins were transferred electrophoretically to a nitrocellulose membrane (Protran, BA 85, 10401196, Sigma) in transfer buffer (NuPAGE MOPS SDS transfer buffer 20x NP0006-1, Thermo Fisher, diluted in distilled water with 20% methanol) at 30V constant voltage for 2.5h. Blots were blocked in blocking buffer (5% BSA in PBS with 0.1% Tween 20 (PBS-Tween)) for 1h at room temperature on a rocking platform. Primary and secondary horseradish peroxidase (HRP)-conjugated antibodies were usually incubated in 1% BSA PBS-Tween for 1 hour at room temperature, followed by

washing with PBS-Tween with constant rocking 3 times for 5 minutes. Blots were developed exposing the membrane to enzyme-linked chemiluminescence (Amersham ECL - RPN2209, VWR) for the detection of HRP-conjugated antibodies. In case the western blot had to be reprobed for different proteins, the nitrocellulose membrane was exposed to stripping buffer (20 mL SDS 10%; 6.25 mL Tris HCl, pH 6.8, 0.5 M; 73.75 mL Milli-Q water; 0.8 mL β-mercaptoethanol (25351.182, VWR)) at 55ºC for 30 minutes in constant gentle agitation. Afterwards, the membrane was washed in current water for 2h, rinsed in PDB-Tween for 5 minutes at room temperature, and finally stored in PBS at 4ºC. Type and concentration of the antibodies used in specific western blots are given in table 2.1.

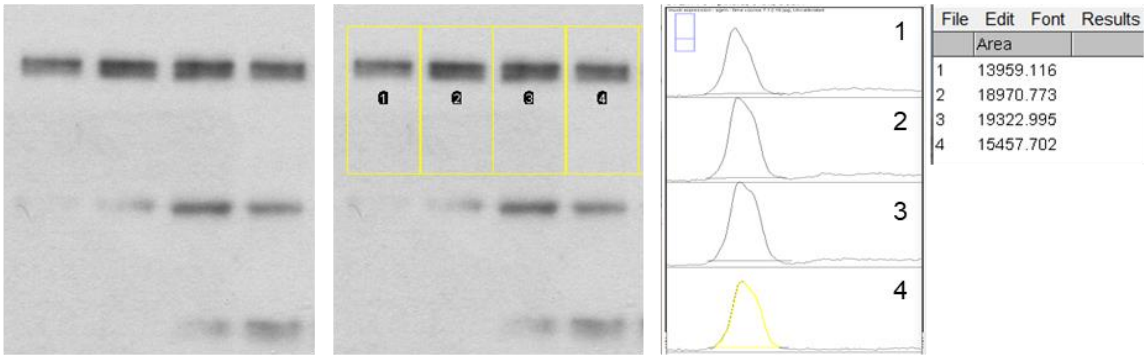
2.20) Densitometry analysis

Band densitometry was analysed using ImageJ software, and levels of phosphorylated (or activated) proteins were normalized to total protein expression (Figure 2.9). ECL-exposed films were digitalised using a Canon scanner (CanoScan LiDE 220) at 300 dpi resolution and analysed as a 16-bit monochrome image. Each column of the blot was selected by drawing a vertical rectangular area that included the band of interest and its surrounding background. Once all the columns were selected with an area of the same size, the software calculated automatically the density of each column. In the graph, the density of the background is represented by a horizontal tremulous line, whereas the band of interest corresponds to a peak. The density of the band was then calculated measuring the area of the peak after substracting the background. The values obtained were essentially arbitrary numbers which do not have a measurement unit. They are generated by the software according to the contrast and brightness of the pixels of the band compared to the background, and are therefore unique for individual blots. This generated a certain degree of intra- and inter-experimental variability when two blots

A. Phospho-tyrosine blot



B. MuSK expression blot



C

Band densitometry measures

P-Tyrosine	Protein expression (MuSK)	P-Tyr / MuSK
3302.125	12959.116	0.2548109
6839.752	18970.779	0.3605414
6712.803	19322.995	0.3473997
21020.309	15457.702	1.359859

Figure 2.9. Example of western blot densitometry quantification. **A)** The blot probed for the phosphorylated tyrosine residues is first digitalised at high resolution (300 dpi) creating a 16-bit monochrome image (left). Each column is selected with a rectangular area of the same size which includes the desired protein band (in this case at 97 kDa) and part of the background (middle). The calculated values of individual columns are represented in a graph (right) where the area underneath the peak corresponds to the density of the band from which the value of the background is subtracted. **B)** The nitrocellulose membrane is stripped and re-probed for the protein of interest (in this case MuSK) to estimate its expression, and the blot analysed in the same way as described. **C)** To obtain the normalised phosphorylation level, the density values of the phospho-tyrosine protein is divided to the values of the total protein expression. The numbers generated by the ImageJ software are arbitrary and are calculated according to the contrast and brightness of individual blots. This partially explains the intra- and interexperimental variability observed when comparing separate blots, or the same blot probed with different antibodies.

were compared, especially when measuring the ratio between protein phosphorylation and expression.

2.21) Dot blots

Dot blots were used primarily to verify the purity of IgG subclass preparations and test for potential contamination. Original plasma, flow-through, washes and purification elutions were tested against corresponding and complementary IgG subclasses. 5 µl of each samples were absorbed directly on a nitrocellulose membrane. The membrane was left do dry for 30 minutes at room temperature after absorption, then blocked with PBS-Tween 5% BSA for 1h at room temperature on a rocking platform, and finally washed 3 times for 5 minutes with PBS-Tween. Depending on individual experimental condition, dot blots were probed either directly with a rabbit anti-human HRP antibody (1:1000) (P0214, Dako) or with a secondary mouse anti-human IgG4 antibody (1:250; I7385, Sigma) for 1h at room temperature. For the latter, after 3 additional washes for 5 minutes with PBS-Tween 20, the membrane was finally probed with a tertiary goat anti-mouse HRP antibody (1:1000) (P0447, Dako).

2.22) Protein concentration determination by BCA colorimetric assay

When the protein concentration needed to be determined more precisely compared to the OD280 reading offered by the NanoDrop, a BCA Protein assay kit (23225, Thermo Fisher) was used according to manufacturer's instructions. This assay measures the colorimetric changes induced by the biding of bicinchoninic acid (BCA) to the cuprous cation (Cu^{1+}) released after the reduction of Cu^{2+} to Cu^{1+} by proteins in an alkaline environment. Briefly, each protein sample was serially diluted in pure water in a total volume of 25 µl in a 96-well plate, and incubated with 200 µl of the Working Reagent (WR provided in the kit) at 37ºC for 30 minutes in the dark. Afterwards, light

absorbsion was measured at 564 nm in an ELISA plate spectrophotometer reader, and plotted against the reading of the BSA standard dilutions provided in the kit.

2.23) Detection of active Rac1 GTPase by ELISA

The active form of Rac1 GTPase was detected using an absorbance method with a dedicated commercial kit (BK128 G-Lisa, Cytoskeleton Inc). 96-well ELISA plates were coated with a GST-Human PAK1-PBD, which binds selectively to the active form of Rac1. C2C12 myotubes were starved in DMEM with 1% PSA in the absence of foetal/horse serum for 24h prior to the experiment to reduce the basal GTPase activity, and then incubated with either medium alone, agrin, or different MuSK antibody preparations for different times (7, 15, 30, 45 minutes) at 37ºC. Cells were immediately placed on ice, rinsed with ice-cold 10 mM phosphate buffer pH 7.4, 140 mM NaCl, 3 mM KCl, and lysed with the ice-cold lysis buffer provided in the kit. Cell lysates were centrifuged at 10000 g for 1 min at 4°C, and 150 µl aliquots of supernatant snap frozen by rapid submersion in liquid nitrogen. Samples were then stored at -80ºC. Additional 20 µl of supernatant were used for protein concentration determination by BCA assay, and final sample concentration adjusted to be within the range 0.25 - 1.0 mg/ml. ELISA plates were prepared as per manufacture's instruction. 100 µl of ice-cold pure water were added to each well of the strips containing GST-Human PAK1-PBD to dissolve the powder and coat the pits. After removing the solution by flicking the plate vigorously, 50 µl of equalised samples were added to each well and incubated on a cold orbital microplate shaker at 400 rpm for 30 minutes at 4°C. Afterwards, the solution was removed by vigorous flicking, and wells washed twice with 200 µl of Wash Buffer at room temperature. 200 µl of Antigen Presenting Buffer were added to each well, and incubated at room temperature for 2 minutes. The solution was then quickly removed and wells washed 3 times with 200 µl of Wash Buffer. 50 µl of anti-Rac1 primary

antibody (diluted to 1:50) was added to each well and incubated on the orbital microplate shaker at 400 rpm for 45 min at room temperature. The solution was again removed quickly by vigorous flicking of the plate, and wells washed 3 times with 200 µl of Washing Buffer. Then, 50 µl of secondary antibody (diluted to 1:100) were added to each well and incubated on the microplate shaker at 400 rpm for 45 min at room temperature. After quick removal of the solution and 3 additional washes, 50 µl of HRP detection reagent were added to each well and incubated at room temperature for 20 minutes. Finally, the reaction was stopped by adding to the wells 50 µl of HRP Stop Buffer, and absorbance at 490 nm measured on an ELISA plate spectrophotometer.

Immunohistochemistry techniques

2.24) AChR clustering assay

C2C12 myoblasts were seeded at a density of 1.5 x 10^5 per well into 6-wells plates and differentiated into myotubes. Cells were then exposed to the different compounds/MuSK antibody preparations – diluted in differentiation medium – for 16h at 37ºC to induce AChR clustering. The following day, cell supernatant was removed by aspiration, and cells were washed 3 times for 5 minutes with differentiation medium. Myotubes were then incubated with Alexa Flour 594-conjugated α-bungarotoxin (B13422, Invitrogen) diluted 1:1000 in differentiation medium for 1h at 37°C to stain the AChR clusters. Afterwards, supernatant was removed and myotubes washed 3 times for 5 minutes in differentiation medium. Cells were fixed in 3% formaldehyde (F003, TAAB) washed 3 additional times with PBS for 5 minutes, and finally stored in PBS at 4°C. Twenty microscopy fields containing myotubes were randomly selected with bright field, and red fluorescent images were captured using an Olympus IX71 fluorescence microscope and Simple PCI (Digital Pixel) software. Images were analysed for AChR cluster number and size using Image J software.

2.25) Immunostaining for rapsyn and actin filaments

Fully-differentiated C2C12 myotubes were exposed to different compounds/MuSK antibody preparations according to individual experiments, for 16h at 37ºC to induce AChR clustering. Myotubes were first stained for AChR clusters with Alexa Fluor 594 α-bungarotoxin as described in the above section 2.23, and then permeabilised and fixed with ice-cold acetone for 5 minutes. Cells were washed in PBS 3 times for 5 minutes, blocked with PBS 1% BSA for 30 minutes at room temperature in gentle constant agitation, and then probed with mouse anti-rapsyn [1234] antibody (1:500 diluted in PBS 1% BSA) (ab58662 – Abcam). Following 3 additional washes for 5 minutes with PBS 1% BSA, myotubes were stained in parallel with secondary Alexa Fluor 488 goat anti-mouse IgG (1:750) (ab150117, Abcam) and Alexa Fluor Plus 405 Phalloidin (1:1000) (A30104, Thermo Fisher) both diluted in PBS 1% BSA, for 1h at room temperature. Cells were finally washed 3 times in PBS for 5 minutes and stored in PBS at 4ºC. Twenty microscopy fields were acquired for each samples at 80x magnification with a Zeiss LSM 780 upright multi-photon confocal microscope. Slides were coded so that images could be acquired and analysed for qualitative differences by a blinded investigator.

2.26) Cell-based assay

Cell-based assay (CBA) to detect MuSK antibodies in patients' plasma and purified IgG subclass preparations was performed as described in (Huda, Waters et al. 2017), and modified according to the specific experiments illustrated in this thesis. HEK 293T cells were seeded at 1.5 x 10^4 per well in 24-wells plates. The wells were pre-treated with PBS 0.01% poly-L-lysine (PLL - P4832, Sigma) to enhance the attachment of the cells to the surface. The following day, cells were transfected with a solution of 0.6 µg MuSK mCherry as described in section 2.4. Successful transfection was confirmed by

visualising mCherry expression using an Olympus IX71 fluorescence microscope. MuSK transfected HEK cells were then incubated with patients' plasma, or purified MuSK IgG4 and IgG1-3 preparations, in serial dilutions in DMEM-HEPES, 1% PSA, 1% BSA for 1h at room temperature with constant gentle agitation. Cells were then washed 3 times for 5 minutes with 500 µl DMEM-HEPES, 1% PSA, 1% BSA. For detection of antibody subclasses, samples were probed with either a corresponding or complementary mouse anti-human -IgG1, -IgG2, -IgG3, -IgG4 monoclonal antibodies (1:50; I2513, I5635, I7260, I7385, Sigma), diluted in DMEM-HEPES, 1% PSA, 1% BSA, for 1h at room temperature. After washing 3 times for 5 minutes with 500 µl DMEM-HEPES, 1% PSA, 1% BSA, cells were fixed with 3% formaldehyde for 20 minutes and then washed again 3 times for 5 minutes with 500 µl PBS. Finally, cells were incubated with a fluorescent antibody Alexa Fluor 488 either goat anti-mouse (ab150117, Abcam) or goat anti-human (A11013, Invitrogen) (for IgG subclasses and MuSK-MG plasma respectively) at 1:750 dilution for 1h at room temperature in the dark with constant gentle agitation. Cells were washed 3 times for 5 minutes with 500 µl PBS and stored in PBS at 4ºC. Images were captured at 80x magnification using Olympus IX71 fluorescence microscope with Simple PCI (Digital Pixel).

Radioactive immunoassays

2.27) MuSK radioimmunoassay

MuSK antibody concentrations in plasma samples and purification fractions were determined by radioimmunoassay (RIA) as described in (McConville, Farrugia et al. 2004). Samples were serially diluted 5-fold in PTX (0.02M PBS, 0.1% Triton X) to a total volume of 50 µl and incubated with 50 µl of ^{125}I labelled MuSK overnight at 4°C. 50 µl of anti-human IgG (PE004.X, Binding Site) and 5 µl of healthy control serum were then added and incubated at room temperature until precipitation was visible

(approximately 60 minutes). After addition of 500 µl PTX, the samples were centrifuged 5 minutes at 10000 rpm at room temperature, washed 3 times with 500 µl PTX, and then cpm were measured with a Wallac Wizard gamma-counter. MuSK antibody concentrations were calculated using the following equation:

$$x\ nM = \frac{(cpm\ sample - cpm\ control) \times decay\ factor}{(Vol.\ sample\ (\mu l) \times specific\ activity)\ (Ci/mmol) \times counter\ efficiency \times 2.22}$$

assuming a counter efficiency of 0.815.

2.28) Quantification of AChR membrane expression with radioactive assay

Myotubes were exposed to different compounds/preparation according to individual experiments. Cells were then exposed to ^{125}I-bungarotoxin at a concentration equivalent to 10^6 cpm/min/ml/sample for 1 hour at room temperature in a rocking platform. Supernatant was then removed, cells washed 3 times for 5 minutes with differentiation medium, and then exposed to extraction buffer (10 mM Tris, 100 mM NaCl, 1 mM EDTA, 1% Triton X100). Cell extract was finally collected in Eppendorf tubes and radioactive counts, corresponding to the precipitated membrane AChRs, measured by the Wallac Wizard gamma-counter.

2.29) Competition assay to estimate concentration of purified MuSK

Serial dilutions of the purified preparation of MuSK-ectodomain were incubated overnight at 4ºC with 50 µl of ^{125}I-MuSK, and a fixed dilution of MuSK-MG plasma (1:200), which was known from previous experiments to give 50% of the maximal radioactive counts. The following day, the experiment followed the same protocol for

the standard MuSK RIA as described above. Total cpm were measured by the Wallac Wizard gamma-counter and concentration of MuSK estimated using the following equation: [MuSK] = 41.1 μCi/μg of MuSK

Considering that 50 μl ^{125}I MuSK = 2.43 x 10^{-2} μCi

Animal work

2.30) Animal welfare, breeding and genotyping

All laboratory animals were handled and treated in compliance to the standard requirements for animal welfare for housing and care outlined and published by the UK Home Office (https://www.gov.uk/government/publications/code-of-practice-for-the-housing-and-care-of-animals-bred-supplied-or-used-for-scientific-purposes). Experimental procedures were carried out at the University of Oxford under the project licence PPL 30/3455, and personal licence No I9038D75C.

C57BL/6 Wild Type mice were purchased at the desired age (10 weeks) from the Oxford Biomedical Service (BMS), and used directly in the scheduled experiments without requiring additional breeding.

A mouse model which reflects a human congenital myasthenic syndrome consistent with AChR deficiency was generated in house by Cossins and colleagues in 2004, and was available for the project presented in this thesis. In this model, C57BL/6 mice constitutively express the human AChR γ-subunit (hγ+) under a skeletal muscle α-actin promotor in an AChR ε-subunit 'knock-out' background (mε-/-). Progeny harbouring hγ+mε+/- were mated to siblings of the same genotype to generate litters containing mice with the human γ-subunit transgene in an ε-/- background (hγ+mε-/-). Genotype analysis to detect the presence of the genes for the γ and ε subunits, and the neomycin resistance gene, was performed by Polymerase Chain Reaction (PCR) of genomic DNA, as previously described by Cossins and colleagues (Cossins, Webster et al. 2004).

Specifically, PCR was performed on earlobe specimens of 0.2 cm diameter collected during ear clipping of the animals (for identification purposes). Specimens were digested in 100 μl of Direct PCR Extraction Reagent (401-E, ViagenBiotech) with 1 μl of Proteinase K (100 mg/ml - P6556, Sigma) and incubated for 16h at 55ºC, followed by further incubation at 95ºC for 45 minutes. The following PCR primers were used:

- Human AChR γ-subunit: 5′-GAGTTAGGGCTGAGCCAGTTCTGTG-3′ and 5′-GTCTGGTGAGGGCAGGTAGGGGCGTG-3′ (which amplify between exons 11 and 12);
- Mouse ε-subunit gene: 5′-CTCTTCGACAATTATGATCCAGA-3′ and 5′-GAGCCGATAGTCGTGCCAGT-3′ (which amplify between exons 2 and 4);
- Neomycin resistance gene: 5′-CAACAGACAATCGGCTGCTCT-3′ and 5′-GAATGGGCAGGTAGCCGGAT-3′.

PCR was carried out according to standard methods (Mullis, Faloona et al. 1986). Reagents included the following: MegaMix Blue (2MMB, Microzone) containing recombinant Taq polymerase in 1.1x reaction buffer (2.75 mM, $MgCl_2$), with 220 μM deoxyrubonucleotide triphosphates (dNTPs – AM8228G, Appleton Woods), blue agarose loading dye and stabiliser. 25 μl MegaMix Blue was mixed with 0.5 μl of each primer (from 100 μM stock) and 1 μl DNA template. Veriti thermal cyclers (Applied Biosystems) were used to carry out the PCR, which was initiated at 95ºC for 3 minutes to denature the template DNA, followed by 30 amplification cycles and a final additional extension step at 72ºC for 5 minutes. Each amplification cycle included a denaturation step at 95ºC for 40 seconds, an annealing step at 62ºC and an extension step at 72ºC for 45 seconds. PCR products were separated on a 1.2% agarose gel, stained with ethidium bromide. Gels were run in 1x TBE buffer (90 mM Tris base, 90 mM Boric acid, 2 mM EDTA) at 60V and visualised under UV light. The DNA molecular marker VI (11062590001, Merk), mixed with a loading dye (Gelpilot 5x –

239901, Qiagen) was used as a size marker. The amplification products γ-subunit, ε-subunit, and neomycin genes were 290 bp, 352 bp, and 333 bp in length respectively.

Model animals were identified by the positive amplification of the γ-subunit and neomycin gene, in the absence of ε product. Therefore, the presence of the neomycin gene indicates an affective substitution of the ε-subunit gene in the animal allele. Conversely, a triple positive PCR result (γ, ε, and neomycin) indicates a heterozygous animal. An example of genotype result is shown in Figure 2.10.

2.31) Clinical assessment of the mice

Mice were assessed and weighed on a regular basis to identify potential general signs of distress (e.g. hunched posture, reduced spontaneous mobility and alertness, shallow breathing, impaired grooming, weight loss). Muscle fatigability was assessed by the inverted screen test. A 50 cm^2 screen of wire mesh (12 mm^2 of 1 mm diameter wire surrounded by a 4 cm deep wooden frame) was used. Mice were placed in the centre of the wire mesh and the screen rotated to inverted position. The screen was held steadily 50 cm above a padded surface. The cumulative hanging time measured with a stopwatch was recorded for 3 subsequent attempts without resting in between. The frequency of the inverted screen assessment varied according to each individual experiment.

Statistical analysis

All data were analysed using GraphPad Prism 7. Data from at least 3 independent experiments (except where stated otherwise) were pooled and analysed as indicated in the appropriate sections. Error bars represent the standard error from the mean. Significance is indicated in all the figures as * for $p<0.05$, ** for $p<0.01$, *** for $p<0.001$, and **** for $p<0.0001$.

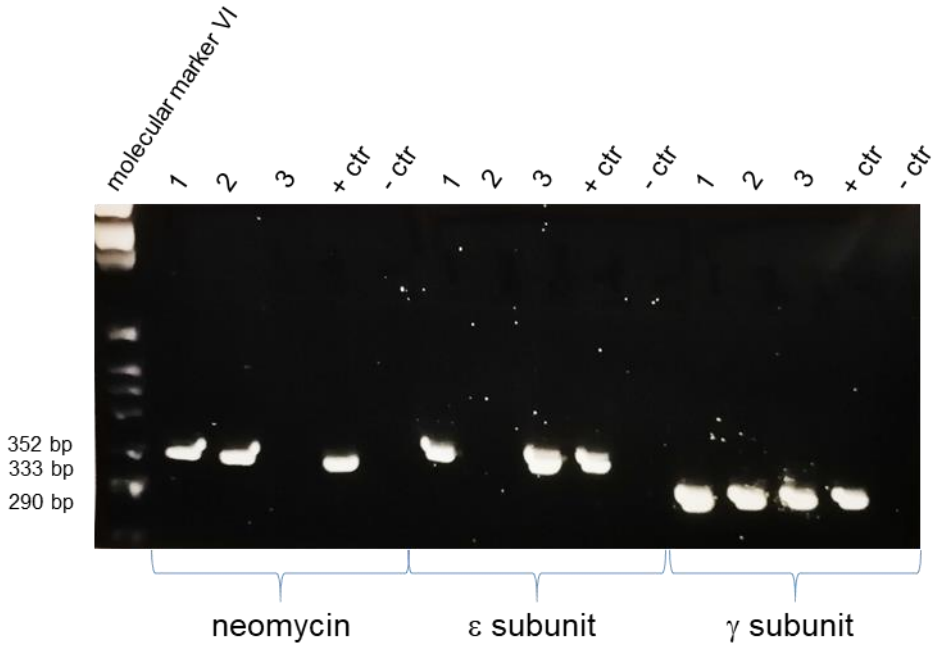


Figure 2.10. Genotype analysis of AChR-deficiency syndrome animal model. Example of agarose gel loaded with the PCR products after amplification of the neomycin, ε and γ subunit genes, stained with ethidium bromide and visualised under UV light. Samples from three animals were analysed. All three genes were detected in mouse #1, identifying it as a heterozygous (carrying one original ε allele, and one substituted with the neomycin gene). In mouse #2, the ε subunit was not detected whereas both neomycin and the γ subunit were present. This identifies the animal as a γ model. Finally, in mouse #3 the neomycin gene was not present, and the analysis showed the positivity only for the ε and γ subunits, identifying the animal as a wild type.

Antibody	Company	Product number	Species	Application	Dilution
Anti P-tyrosine 4G10	Insight Biotech	05-GTX14167	Mouse	WB	1:1000
Anti MuSK	R&S	AF562	Goat	WB	1:100
Anti DOK7	Santa Cruz	SC-390856	Mouse	WB	1:200
Anti AChRβ1 (148)	Santa Cruz	sc-65813	Rat	WB	1:200
Anti AChRδ (C-4)	Santa Cruz	sc-390896	Mouse	WB	1:200
Anti LRP4	Insight Biotech	TA326569	Mouse	WB	1:1000
Anti LRP4	Abcam	N207/27	Mouse	WB	1:500
α-tubulin	Sigma	T5168	Mouse	WB	1:10000
Anti Rho	Invitrogen	16116 (Kit)	Rabbit	WB	1:650
Anti rabbit IgG HRP	Dako	P0448	Goat	WB	1:1000
Anti mouse IgG HRP	Dako	P0447	Goat	WB	1:1000
Anti goat IgG HRP	Dako	P0449	Rabbit	WB	1:1000
Anti rat IgG HRP	Dako	P0450	Rabbit	WB	1:1000
Anti human IgG HRP	Dako	P0214	Rabbit	WB/Dot blot	1:1000
Anti mouse native IgG for IP (HRP)	Abcam	ab131368	Rat	WB	1:1000
Anti rabbit IgG HRP	Invitrogen	16116 (Kit)	Goat	WB	1:500
Anti human IgG1	Sigma	I2513-.2ML	Mouse	CBA/Dot blot	1:50/1:250
Anti human IgG2	Sigma	I5635-.2ML	Mouse	CBA/Dot blot	1:50/1:250
Anti human IgG3	Sigma	I7260-.2ML	Mouse	CBA/Dot blot	1:50/1:250
Anti human IgG4	Sigma	I7385-.2ML	Mouse	CBA/Dot blot	1:50/1:250
Anti-human IgG Alexa Fluor 488	Invitrogen	A11013	Goat	CBA	1:750
Anti-mouse IgG Alexa Fluor 488	Abcam	ab150117	Goat	CBA	1:750
Anti Rapsyn 1234	Santa Cruz	sc-58585	Mouse	IHC	1:500
Anti β-actin	Sigma	A5441	Mouse	IHC	1:500

Table 2.1: Commercial details, applications, and dilutions of antibodies used in the experiments described in this thesis

Product	Company	Product number
^{125}I labelled MuSK	RSR Ltd	MSK/TR
Active Rho Pull-Down and Detection Kit	Thermo Fisher	16116
Alexa Fluor 594 conjugated α-bungarotoxin	Invitrogen	B13423
Alexa Fluor Plus 405 Phalloidin	Thermo Fisher	A30104
Amersham ECL Western blotting system	GE healthcare	RPN2108
Amersham ECL Western blotting reagents	VWR	RPN2209
Anti Human IgG	Binding Site	PE004.X
BCA protein assay Kit	Thermo Fisher	23227
Biotin-XX conjugated α-bungarotoxin	Invitrogen	B1196
Blasticidin	Gibco	R210-1
BSA	Sigma-Aldrich	A7906
C2C12	ATCC	CRL-1772
Centriprep 30 kDa filter devices	Millipore	YM-30K 4306
COS-7	ATCC	CRL-1651
Costar 24-well plates	Corning	3527
Costar 6-well plates	Corning	3516
Costar 96-well plates	Corning	3997
Coomassie Brilliant Blue R-250	Thermo Fisher	20278
Direct PCR Extraction Reagent	ViagenBiotech	401-E
DMEM, high glucose, pyruvate-10 x 500 mL	Gibco	41966052
DNA molecular marker VI	Merk	11062590001
dNTP mix	Appleton Woods	AM8228G
Drosophila S2	ATCC	CRL-1963
Dynabeads MyOne Streptavidin T1-2 mL	Invitrogen	10531265
EDTA pH 8.0	Gibco	15575
Erlenmeyer flask 100 ml	Corning	Z331627
Express Five SFM-1,000 mL	Life technologies	10486025
Fetal bovine serum – heat inactivated	Merk	F9665-500ML
Fetal calf serum	PAA	A15-151
Formaldehyde solution 36%	TAAB	F003
Gelpilot 5x	Qiagen	239901
Geneticin antibiotic	Thermo Fisher	10131035
Hard tissue grinding kit tube	Precellys	MK28R
HEK 293T	ATCC	CRL-3216
HEPES	Sigma	H3375
HiMark Pre-stained High molecular weight protein standard	Invitrogen	LC5699
Horse serum	PAA	B11-122
IgG4 affinity matrix	Captureselect	2900.05
L-Glutamine	Thermo Fisher	25030149
MegaMix Blue	Microzone	2MMB
Nickel affinity column ProBond	Thermo Fisher	R80115
Nitrocellulose membrane Protran BA 85	Sigma	10401196
NSC-87877	Tocris	2613
NuPAGE 4-12% Bis-Tris pre-cast electrophoresis gels	Thermo Fisher	NP0321PK2
NuPage LDS sample buffer	Invitrogen	NP0008
NuPAGE MOPS SDS running buffer	Thermo Fisher	NP0001

(20x)		
NuPage reducing agent	Invitrogen	NP0004
NuPAGE transfer buffer (20x)	Thermo Fisher	NP0006-1
PBS	Oxoid	BK0014G
Penicillin/streptomycin/ amphotericin B solution (100X)	Invitrogen	15240096
Phoenix-ECO	ATCC	CRL-3214
Phosphatase inhibitor cocktail	Thermo Fisher	78420
Poly L-Lysine	Sigma	P4832
Polybrene	Insight Biotechnology Ltd	sc-134220
Protease inhibitor cocktail	Sigma	P8340
Protease inhibitor cocktail – EDTA free	Sigma	S8830-2TAB
Protein G coupled magnetic beads, Dynabeads	Invitrogen	100.03D
Protein G sepharose 4 Fast Flow	Sigma	17-0618-01
Proteinase K	Sigma	P6556
Puromycin	Sigma	P9620
Quik-Change Multi Site-Directed Mutagenesis Kit	Agilent	200514
Rac1 G-LISA Activation Assay	Cytoskeleton Inc.	BK128-S
SeeBlue Plus2 pre-stained protein standards, 3-188 kDa	Invitrogen	LC5925
SnakeSkin Dialysis Tubing, 10K MWCO, 22mm	Thermo scientific	68100
Surface cell culture flasks T175	Corning	CLS3292
Surface cell culture flasks T25	Corning	CLS3289
Surface cell culture flasks T75	Corning	CLS3290
TRIzol Reagent	Invitrogen	15596026
Trypsin-EDTA (10x), liquid	Sigma	T4174
TURBO DNA-free Kit	Thermo Fisher	AM1907
Tween-20	Sigma	P1379
β-mercaptoethanol	VWR	25351.182

Table 2.2: List of all the materials used in the experiments described in this thesis with their commercial details.

Chapter 3

In vitro effects of SHP2 inhibition by NSC-87877

3.1 Introduction

In the current clinical practice, there is an unmet need for an effective treatment that targets specifically the pathogenic mechanisms responsible for MuSK myasthenia. This is particularly evident considering that no symptomatic medications are available – as ACh-esterase inhbitors, usually beneficial in AChR myasthenia, are often ineffective or even detrimental in MuSK-MG patients – whereas high doses of steroids and other immunosuppressive drugs that target the immune system as a whole are necessary to keep disease symptoms under control (Evoli, Tonali et al. 2003, Guptill, Sanders et al. 2011).

According to the most accredited pathogenic model for MuSK-MG, autoantibodies of the IgG4 subclass prevent MuSK activation by blocking its binding with Lrp4 following agrin stimulation (Huijbers, Zhang et al. 2013, Koneczny, Cossins et al. 2013). This would then inhibit the downstream phosphorylation cascade leading to the dispersal of AChR clusters on the muscle membrane. Each step of the AChR clustering pathway could represent a potential pharmacological target for the development of a specific treatment aimed to counteract the effects of MuSK antibodies. In this respect, among the several regulators of the pathway, SH2 domain-containing phosphatase (SHP2) is particularly suitable for our purposes as it acts directly on MuSK in a negative feedback loop, reducing its phosphorylation to modulate formation of AChR clusters during the development of the NMJ (Madhavan, Zhao et al. 2005, Zhao, Qian et al. 2007, Qian, Chan et al. 2008). Notably, it has already been shown that the pharmacological inhibion of SHP2 by the compound NSC-87877 is effective in increasing the number of AChR clusters in C2C12 myotubes independent of agrin stimulation (Zhao, Qian et al. 2007).

However, apart from this initial evidence, the effects of SHP2 inhibition by NSC-87877 on the clustering pathway have not been investigated further, and whether the compound has a direct effect on MuSK phosphorylation, the specificity of its effects on AChR clustering, the potential induction of transcriptional changes and, most importantly, its effectiveness in the presence of MuSK antibodies has not been demonstrated.

3.2) Results

3.2.1) Agrin production and titration

Agrin represents a fundamental component of all the experiments described in this thesis as it provides the physiological stimulation which induces MuSK phosphorylation and, ultimately, AChR clustering. Therefore, agrin was used as the positive control by which to compare the effects of all the different compounds tested, specifically NSC-87877 and MuSK antibodies.

Agrin was produced by transfecting HEK 293T cells with a cDNA plasmid coding for a soluble truncated C-terminus form of the rat protein, which has been shown sufficient to induce AChR clustering (Ferns, Campanelli et al. 1993). Once harvested from the cell medium, agrin was tested at different dilutions on C2C12 myotubes to examine its effects on AChR clustering. Myotubes were exposed to agrin for 16 hours at 37ºC, then fixed in formaldehyde, and finally stained with fluorescent α-bungarotoxin, the snake toxin that binds specifically to the acetylcholine receptors. Myotubes exposed to DMEM were used as a negative control. As expected, there was a direct correlation between the concentration of agrin and the number of AChR clusters (Figure 3.1) at each dilution, agrin significantly increased AChR clustering compared to DMEM

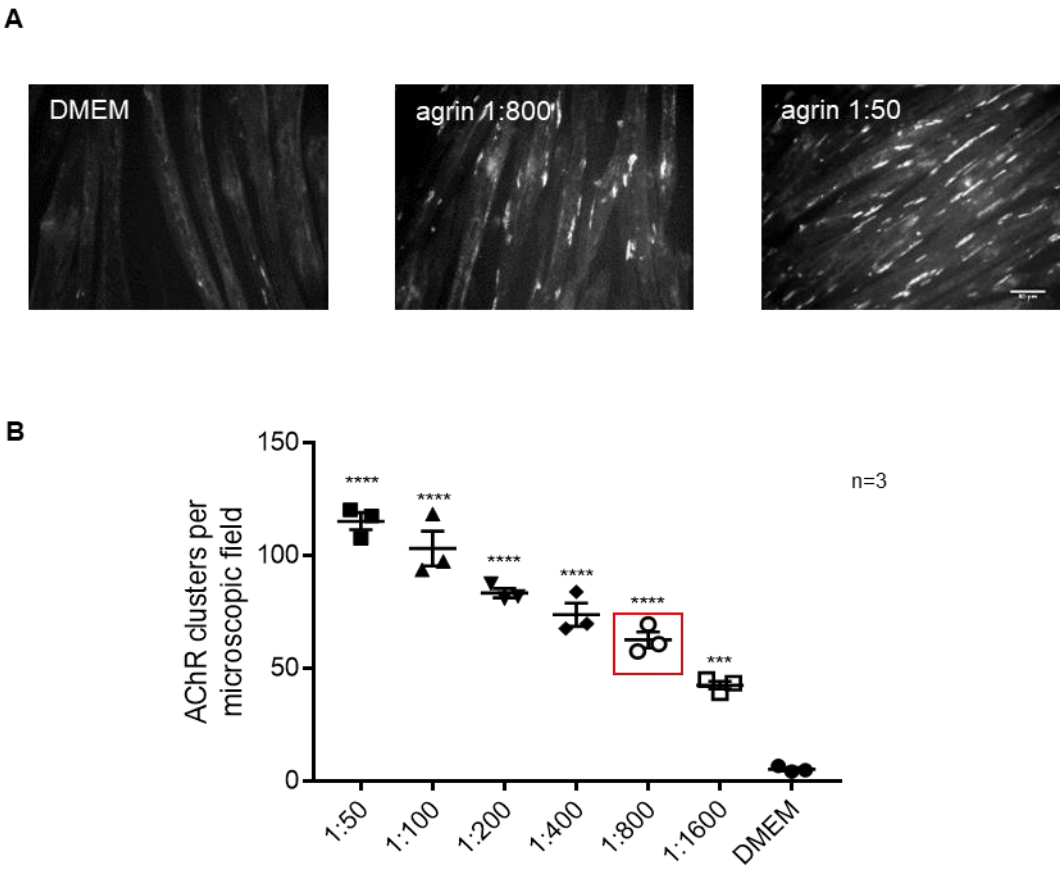


Figure 3.1. Titration of agrin on AChR clustering. **(A)** Representative images of AChR clusters labelled with Alexa Fluor 594 α-bungarotoxin on C2C12 myotubes after overnight exposure to agrin (short rat form, at 1:50 and 1:800 dilutions) and DMEM only. Scale bar represents 50 µm. **(B)** Bar chart of 3 pooled experiments showing the number of AChR clusters for different agrin dilutions. For each experiment, the value indicated on the graph corresponds to the average number of AChR clusters countend in 20 individual microscopic fields. AChR clustering was significantly increased compared to DMEM by each dilution of agrin ($p<0.0001$ for 1:50, 1:100, 1:200, 1:400, 1:800, and $p<0.001$ for 1:1600; one-way ANOVA with Dunnett's multiple comparison test against DMEM; n=3). A non-saturating dilution of agrin (1:800 – indicated in the red box) which produces approximately 50% of AChR clusters was chosen for all subsequent experiments. Mean + SEMs are shown.

($p<0.001$ for each dilution used). A non-saturating dilution of 1:800, which provided approximately 50% of the maximum AChR clusters observed, was used in the experiments described. This non-saturating concentration allowed both positive and negative effects of NSC-87877 and/or MuSK antibodies on both AChR clustering and MuSK phosphorylation.

3.2.2) Titration of the effects of NSC-87877 on MuSK Phosphorylation and AChR clustering

SHP2 inhibition by NSC-87877 has already been shown to induce AChR clustering on C2C12 myotubes independent of agrin, starting from a dosage of 0.1 μM of the drug (Zhao, Qian et al. 2007). However, its effect on MuSK phosphorylation, although presumed, had not been established directly. Therefore, the first experiments titrated the effects on both MuSK phosphorylation and AChR clustering in order to identify the most efficient drug concentration to be used in the future experiments.

MuSK phosphorylation and AChR clustering were studied in parallel, but using different incubation times. First, to study MuSK phosphorylation, increasing concentrations of NSC-87877 were applied to C2C12 myotubes for 40 minutes at 37ºC. Afterwards, myotubes were lysed in ice-cold lysis buffer to preserve protein phosphorylation, and MuSK was immunoprecipitated with Protein G magnetic beads bound to a commercial anti-MuSK antibody (AF562). MuSK phosphorylation was determined by western blotting, probing the precipitate with a monoclonal antibody against phosphotyrosine residues (Figure 3.2A – left). The nitrocellulose membrane was then stripped and reprobed for MuSK, using the same anti-MuSK antibody used for the immunoprecipitation (Figure 3.2A – right). Phosphorylation levels of the bands corresponding to MuSK (97 kDa) were quantified by band densitometry with ImageJ software and then normalised to MuSK expression.

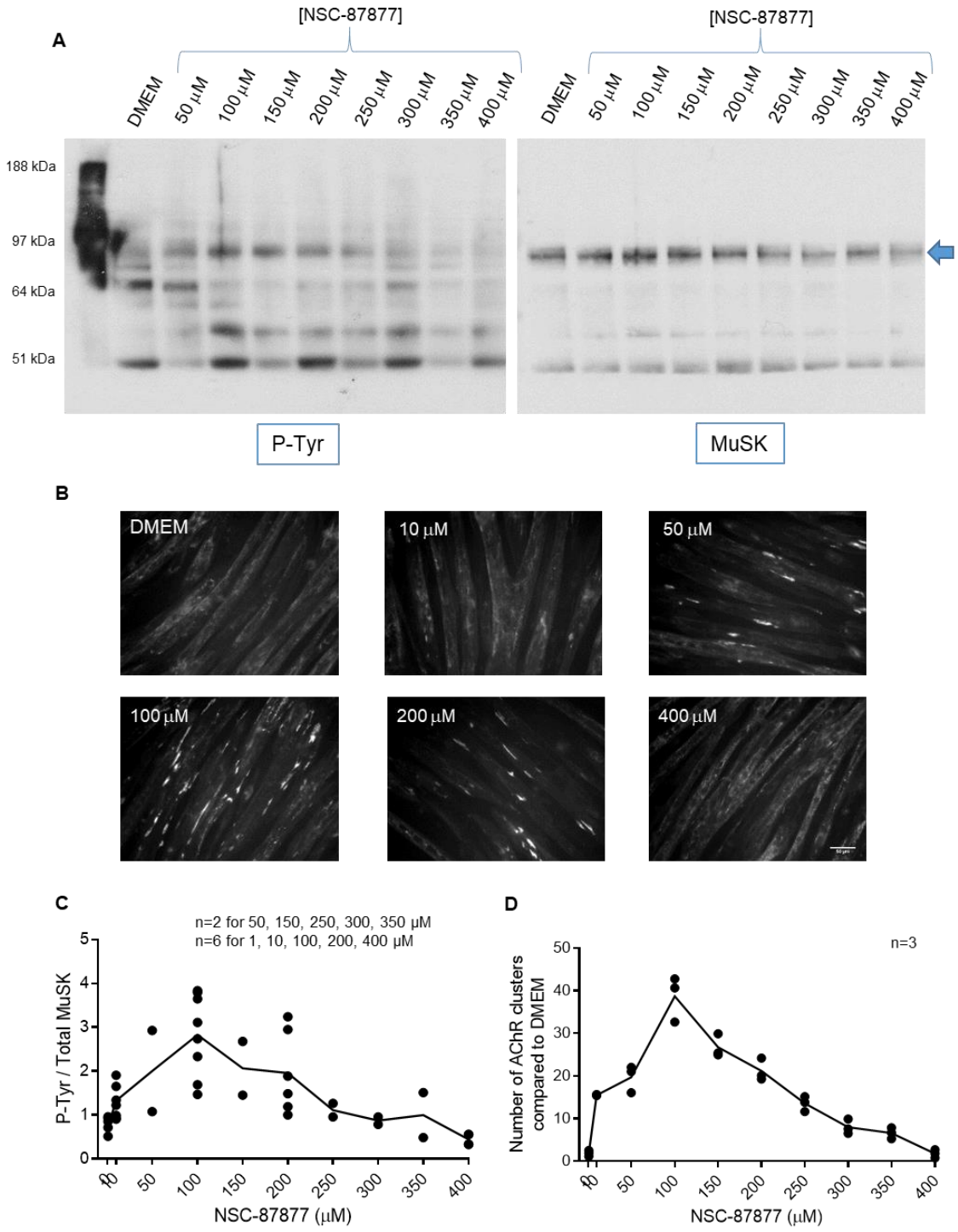


Figure 3.2. SHP2 inhibition by NSC-87877 induces MuSK phosphorylation and AChR clustering. (**A**) Dose-response curve of the effects of SHP2 inhibition on MuSK phosphorylation. Phosphorylation increased progressively reaching a maximal effect at 100 µM of NSC-87877 and decreased at higher concentrations. (**B**) Clustering of AChRs (labelled with Alexa Fluor 594 α-bugaratoxin) in C2C12 myotubes after 16h incubation with DMEM, agrin (1:800), and different concentrations of NSC-87877. The optimal NSC-87877 concentration was 100 µM and phosphorylation and cluster numbers decreased at higher concentrations. (**C, D**) The pooled results of 3 – 6 independent experiments measuring MuSK phosphorylation (**C**) and AChR clusters (**D**) are shown with a scatter. Each dot represents the values obtained from individual experiments.

For the AChR clustering assay, C2C12 myotubes were exposed to the same concentrations of NSC-87877 for 16 hours, followed by formaldehyde fixation and AChR clusters labelled with α-bungarotoxin (Figure 3.1B). AChR clusters were automatically counted using the ImageJ software setting a cluster length threshold of 2.5 μm.

The inhibition of SHP2 resulted in a dose-dependent increase of both MuSK phosphorylation and AChR clustering (Figure 3.2, C and D) with the maximal effect reached at 100 μM. Notably, the efficacy of NSC-87877 started to decrease with higher concentrations and, at 400 μM, phosphorylation and number of clusters were comparable with the basal level observed with DMEM only. However, this paradoxical effect of the drug could be partially reversed by agrin. If agrin (1:800) was added to the myotubes exposed to 400 μM NSC-87877, both MuSK phosphorylation and AChR clustering showed a moderate increase (respectively $p<0.01$ and $p<0.05$ compared to DMEM), despite not reaching the same level induced by agrin alone (Figure 3.3).

3.2.3) MuSK phosphorylation time-course

Phosphorylation is usually a time-dependent signaling event, which starts after stimulation of a receptor by a specific trigger, reaches a plateau, and then gradually fades after forwarding the signal to downstream effector proteins. For this reason, once it was determined that NSC-87877 induces its maximum effect at a dose of 100 μM for the given time of incubation (40 min) tested in the initial experiments, it was necessary to study the modifications over-time of MuSK phosphorylation to identify the most appropriate time window for the experiments, and to evaluate how the effect of the drug compares to the physiological stimulation by agrin.

Myotubes were exposed to NSC-87877 100 μM in the presence or absence of agrin (1:800), from 15 minutes up to 6 hours. MuSK was immunoprecipitated from cell

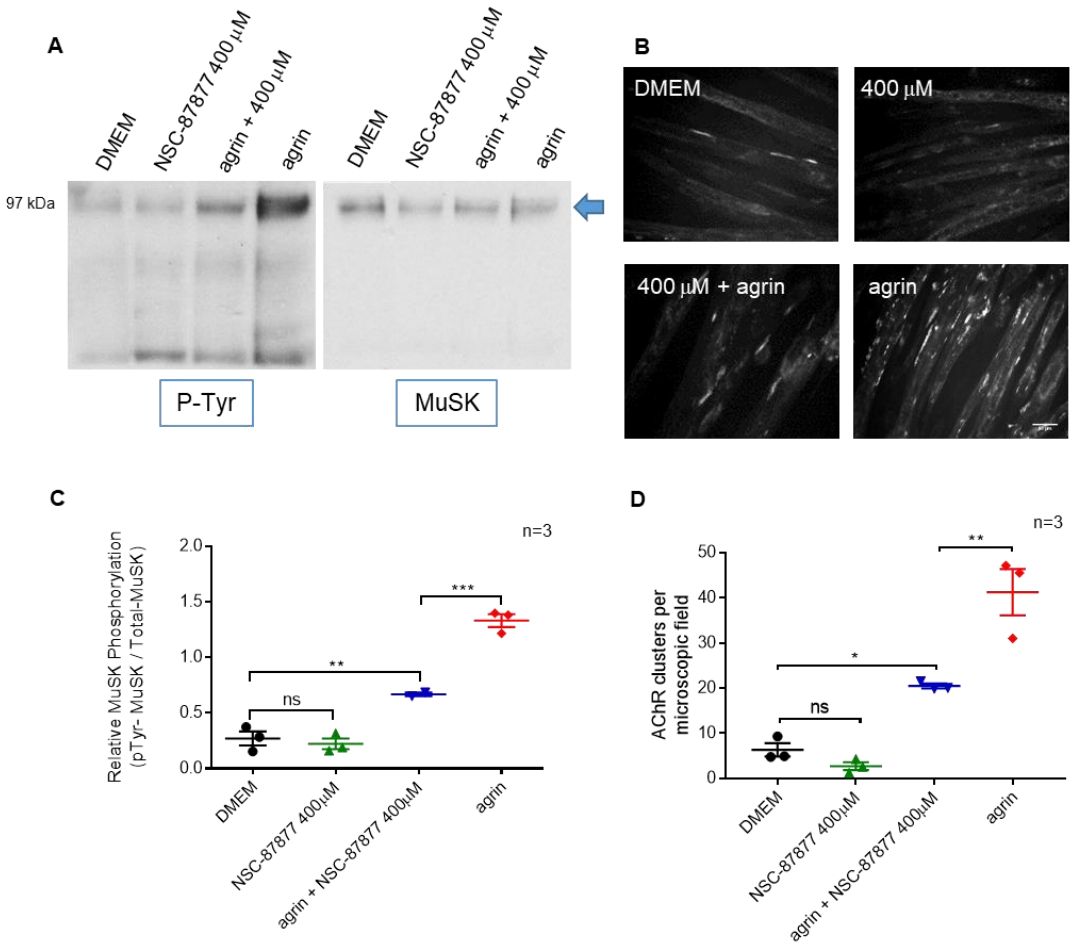


Figure 3.3. Agrin counteracts the inhibitory effects of high concentration of NSC-87877 on MuSK phosphorylation and AChR clustering. (**A**) After incubation with 400 µM NSC-87877, MuSK phosphorylation is similar to DMEM. (**B**) Similarly, after 16h exposure, number of AChR clusters is comparable between DMEM and 400 µM NSC-87877. In the presence of agrin (1:800), an increase in both MuSK phosphorylation and AChR clustering was observed ($p<0.01$ and $p<0.05$ respectively). (**C, D**) The pooled results of 3 independent experiments measuring MuSK phosphorylation (**C**) and AChR clusters (**D**) are shown. Mean + SEMs are shown.

lysates at the end of each time interval (15, 40, 90, 180, 360 minutes), and phosphorylation analysed by western blotting as described above (Figure 3.4A). To minimise cell handling and reduce variability among samples, the incubations with agrin or NSC-87877 were done starting with the samples with the longest incubation time and continuing to those with the shortest exposure; as a result that all cells were lysed and processed at the same time.

In all samples (either exposed to NSC-87877, agrin, or both), MuSK phosphorylation presented a similar activation pattern, increasing progressively and reaching the maximum effect consistently between 40 and 90 minutes (Figure 3.4B). The signal then decreased over time returning to the basal level between 3 and 6 hours. Notably, the level of MuSK phosphorylation was similar after exposure to NSC-87877 or agrin (Figure 3.4B, green and red respectively), whereas the combination of the two (Figure 3.4B, blue) acted synergistically reaching a significantly higher level of phosphorylation ($p<0.05$ and $p<0.01$ at 40' and 90' respectively compared to NSC-87877 alone). On the other hand, the combined action of agrin and NSC-87877 did not make the phosphorylation process faster or longer. The submaximal incubation time of 40 minutes was chosen for the subsequent experiments to allow the detection of subtle changes in MuSK phosphorylation induced by the compound and, ultimately, by MuSK antibodies.

3.2.4) MuSK and AChR membrane expression

Another question was whether, apart from the direct effect on MuSK phosphorylation and AChR clustering, the compound was also able to modify the amount of MuSK and AChRs expressed on the myotube membrane.

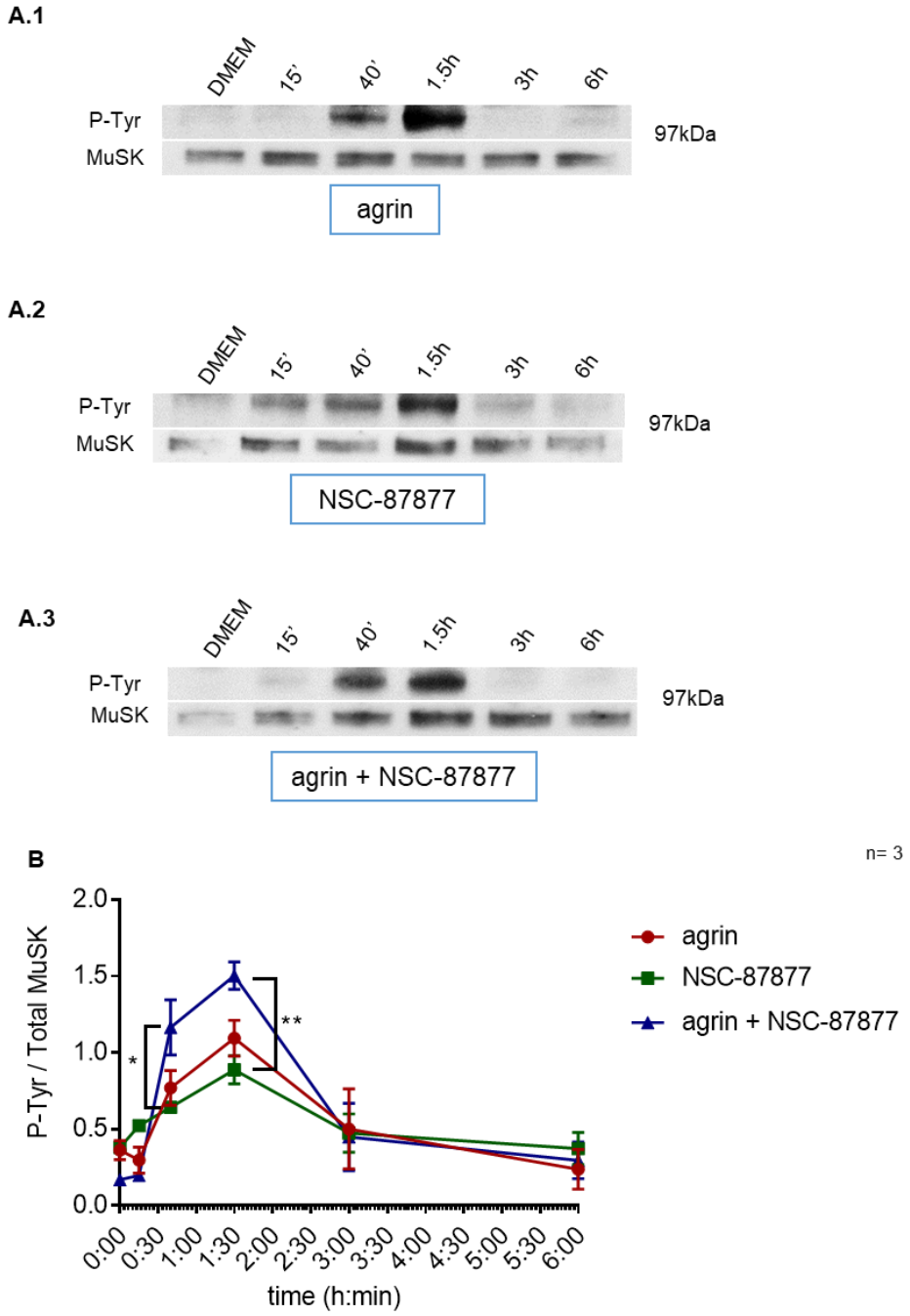


Figure 3.4. Agrin and NSC-87877 induce a similar MuSK phosphorylation time course. **(A)** Representative western blots showing phospho-tyrosine bands (top) and related MuSK expression (bottom) at 97 kDa after incubation with agrin 1:800 **(A.1)**, NSC-87877 100 µm **(A.2)**, and agrin plus NSC-87877 **(A.3)** at different time intervals (from 15 minutes to 6 hours). (**B**) pooled results of 3 experiments showing the variations over time of MuSK phosphorylation after exposure to the different compounds. Both agrin and NSC-87877 induced a time-dependent increase of MuSK phosphorylation reaching the maximal level between 40 and 90 minutes. When combined, NSC-87877 and agrin induced a significant increase of phosphorylation compared to NSC-87877 alone at 40 and 90 minutes. Multiple row comparison with Two-Way ANOVA. Mean + SEMs are shown.

To quantify MuSK membrane expression, myotubes were exposed to NSC-87877 100 μM, in the presence and absence of agrin (1:800) for 16 hours at 37ºC. Afterwards, the cells were exposed to the commercial anti-MuSK antibody (AF562) diluted in growth medium for 1 hour at room temperature followed by cell lysis to immunoprecipitate only the MuSK molecules expressed on the cell membrane. Immunoprecipitation was carried out incubating the cell lysates directly to the Protein G magnetic beads and western blot analysis performed as before (Figure 3.5A – left). A small amount of cell lysate was analysed separately for the detection of α-tubulin (Figure 3.5A – right), against which the level of MuSK expression was normalised. Notably, neither agrin, NSC-87877, nor the combination of both, induced significant changes in the membrane expression of MuSK (Figure 3.5B).

For quantification of membrane AChRs myotubes were exposed to NSC-87877 100 μM, in the presence or absence of agrin, at 37ºC for 16 hours. Cells were then exposed to ^{125}I-bungarotoxin for 1 hour at room temperature, lysed in extraction buffer, and radioactive counts (corresponding to the radioactive toxin bound to membrane AChRs) measured in a Wallac Wizard gamma-counter. Interestingly, NSC-87877 increased the AChR membrane expression compared to DMEM ($p<0.001$) (Figure 3.5C). This was similar to that observerd with agrin, either alone or in combination with NSC-87877.

3.2.5) Effect of SHP2 inhibition on MUSK mutant cell lines

To understand whether the increase on AChR clustering was a direct consequence of MuSK activation induced by the compound, and not by alternative pathways involving phosphorylation, NSC-87877 was tested on two different mutant cell lines in which either MuSK or DOK7 were non-functional.

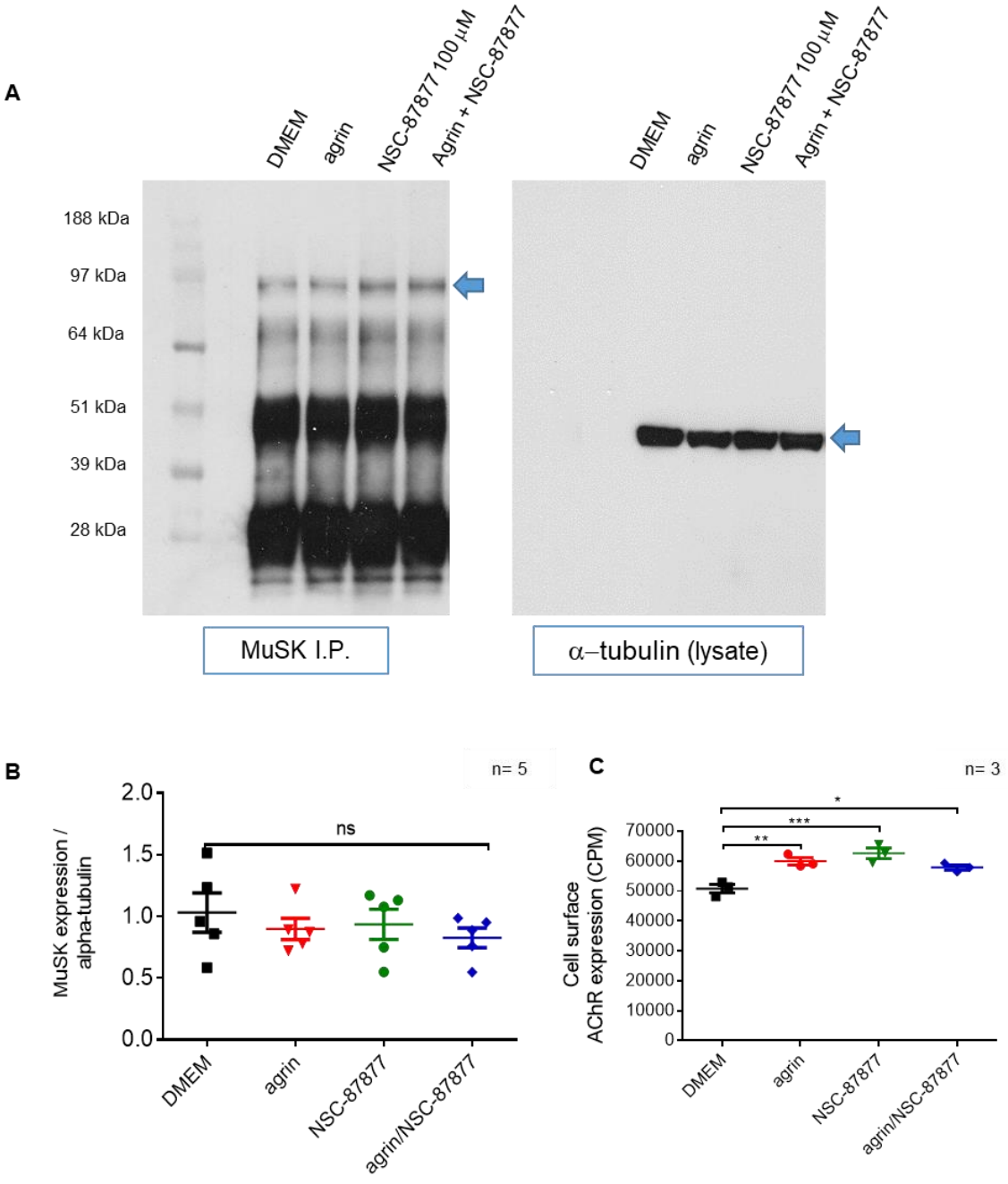


Figure 3.5. In the C2C12 myotubes, NSC-87877 increases the membrane expression of AChRs while MuSK expression remains unchanged. (A) Representative western blots showing expression of MuSK (left - 97 kDa) and α-tubulin (right – 50 kDa) after incubation of the myotubes with NSC-87877, in the presence and absence of agrin for 16h. (**B**) Pooled results of 5 experiments showing the expression of MuSK normalised to the level of α-tubulin. MuSK expression was not modified after exposure to the different compounds **(C)** Pooled results of 3 experiments showing the level of AChR expression on the myotubes' membrane after 16h incubation with NSC-87877, in the presence and absence of agrin. Myotubes were exposed to ^{125}I bungarotoxin to allow binding to AChRs, and total cpm from cell extract (corresponding to the bound bungarotoxin to the receptors) was measured with a gamma counter. NSC-87877 and agrin induced a similar increase of AChR membrane expression compared to DMEM. Mean + SEMs are shown.

MUSK mutant cell lines were created previously by Dr Pedro Rodriguez-Cruz as described fully in the "Materials and Methods" chapter (section 2.6). MuSK phosphorylation and AChR clustering were studied on *MUSK* KO and p.C317R myotubes after exposure to NSC-87877 100 μM, agrin (1:800), or a combination of both. Wild type C2C12 myotubes were used as a control. As above, cells were lysed after 40 minutes of incubation for MuSK phosphorylation, whereas 16 hours of exposure were required to induce full AChR clustering. Western blot analysis (Figure 3.6A) confirmed the complete absence of MuSK in the *MUSK* KO cell line and, consequently, a MuSK phosphorylation signal was not detectable. On the other hand, a MuSK band was observed in the p.C317R mutant myotubes, which run at a slightly smaller size (around 85 kDa compared to the usual 97 kDa), perhaps because the mutant protein corresponded to the human sequence whereas the endogenous MuSK in C2C12 is mouse. An additional explanation is that the p.C317R mutation produces a misfolded protein which undergoes abnormal post-translational modifications (e.g. glycosylation) with consequent smaller molecular size. The phosphorylation signal in the p.C317R mutant was barely detectable and no significant increase was observed after stimulation by either agrin or NSC-87877.

Both *MUSK* KO and p.C317R mutant cell lines were unable to form AChR clusters either spontaneously (wild type myotubes, even in the absence of agrin, usually express few spontaneous clusters around 10 per field), or following stimulation by agrin or NSC-87877 (Figure 3.6B).

3.2.6) Effects of SHP2 inhibition on DOK7 wild type and DOK7 1124_1127dupTGCC overexpressing C2C12s

Once established that NSC-87877 required a functional MuSK for its effect on AChR clustering, the next step was to ask whether DOK7 was also essential for the effect of

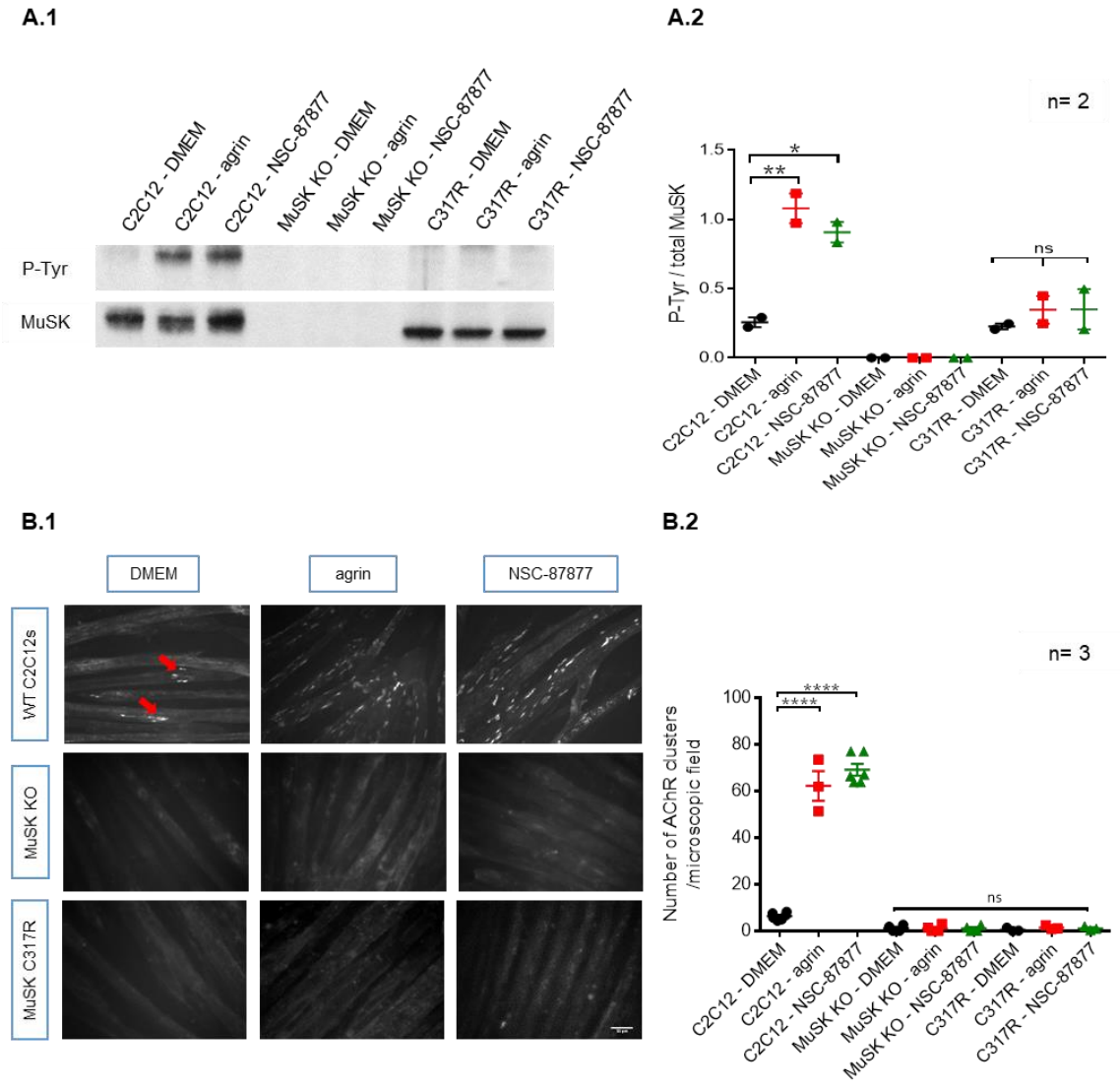


Figure 3.6. SHP2 inhibition by NSC-87877 has no effect on MuSK phosphorylation and AChR clustering in MuSK KO and *MUSK* p.C317R myotubes. (**A.1)** Representative western blots showing bands at 97 kDa for phospho-tyrosine (top) and MuSK expression (bottom) after incubation of MuSK KO and *MUSK* mutant p.C317R myotubes with NSC-87877, in the presence and absence of agrin. In both cell lines, neither agrin nor NSC-87877 induced MuSK phosphorylation. As expected, MuSK expression was not detectable on the MuSK KO myotubes, whereas the mutant MuSK (human) had slightly smaller molecular size compared to the endogenous MuSK of the myotubes. **(A.2)** pooled results of 2 experiments showing the level of phospho-tyrosine MuSK normalised to total MuSK expression. (**B.1**) Clustering of AChRs (labelled with Alexa Fluor 594 α-bungaratoxin) in MuSK KO and *MUSK* p.C317R myotubes after 16 hours incubation with NSC-87877, in the presence and absence of agrin. Spontaneous AChR clusters normally observed on wild type myoutubes (red arrows) were not present in the mutant cell lines and neither agrin nor NSC-87877 induced the formation of the clusters. **(B.2)** Pooled results of 3 experiments showing the average number of AChR clusters per microscopic field in the different cell lines. The number of clusters was not increased on the MuSK KO and *MUSK* p.C317R after exposure to agrin and NSC-87877. Mean + SEMs are shown.

NSC-87877. C2C12 lines either overexpressing wild type DOK7 or 1124_1127dupTGCC DOK7 were used. The lines were established in our lab by Dr Judith Cossins (Cossins, Liu et al. 2012). Notably, the overexpression of the wild type DOK7 (DOK7 WT) induces the formation of a high number of spontaneous AChR clusters on the myotubes, even in the absence of agrin, overriding the need for physiological stimulation of MuSK (Okada, Inoue et al. 2006). On the other hand, the mutant DOK7 1124_1127dupTGCC is non-functional (Beeson, Higuchi et al. 2006) (Figure 3.7A).

As described in full in Chapter 2 (section 2.5), C2C12 myoblasts were infected with the retroviral vector pBabe-PURO-EGFP carrying either DOK7 WT or the mutant 1124_1127dupTGCC, and then differentiated into myotubes for the subsequent experiments with NSC-87877. Efficient overexpression of DOK7 WT and DOK7 1124_1127dupTGCC was confirmed by western blotting on myotube lysates (Figure 3.7B1). In the myotubes expressing DOK7 WT, a strong band of the expected DOK7 size was detected around 50 kDa whereas two bands were detected in the myotubes infected with the mutant variant, a weak one at 50 kDa corresponding to the endogenous DOK7, and a stronger one at 43 kDa corresponding to the truncated protein. In the DOK7 WT overexpressing cells, MuSK phosphorylation was found to be increased compared to the wild type myotubes (Figures 3.7B2), further indicating the role of DOK7 in the retroactive stimulation of MuSK.

Myotubes from the cell line were exposed to NSC-87877 (Figure 3.8). As expected from the preliminary experiments, both MuSK phosphorylation and AChR clusters were induced in the myotubes expressing DOK7 WT, and this was further increased by the addition of NSC-87877 ($p<0.01$ for MuSK phosphorylation, and $p<0.0001$ for AChR

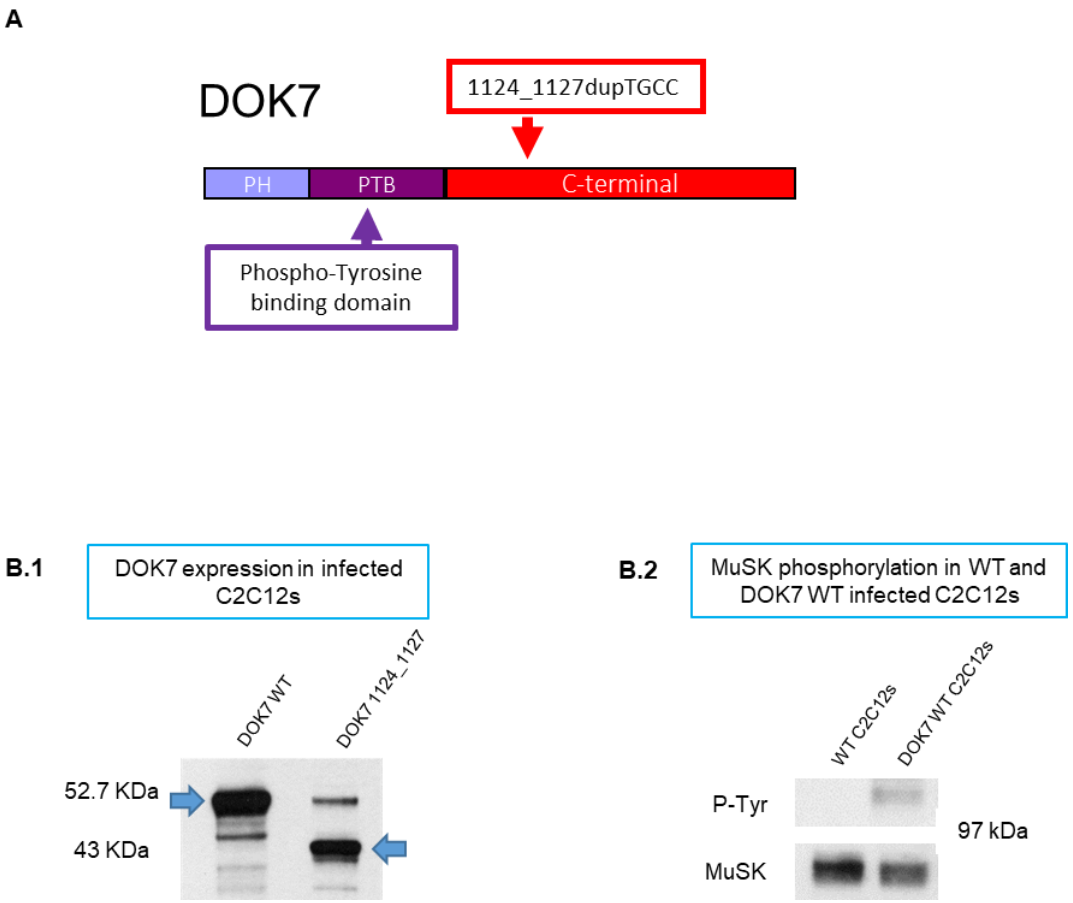


Figure 3.7. The mutant DOK7 1124_1127dupTGCC generates a truncated non-functional protein. (A) Schematic representation of the 3 main protein domains of DOK7. The mutation 1124_1127dupTGCC introduces an early stop codon which causes the creation of a truncated protein. **(B)** Two C2C12 cell lines overexpressing DOK7 WT and DOK7 1124_1127dupTGCC were created by retroviral infection. (**B.1)** Western blot showing the efficient expression of DOK7 WT (52 kDa) and DOK7 1124_1127 (43 kDa) after infection by retroviral vector. **(B.2)** Western blots bands at 97 kDa for phospho-tyrosine (top) and MuSK expression (bottom) showing an increased basal level of MuSK phosphorylation in DOK7 WT overexpressing myotubes compared to wild type C2C12s.

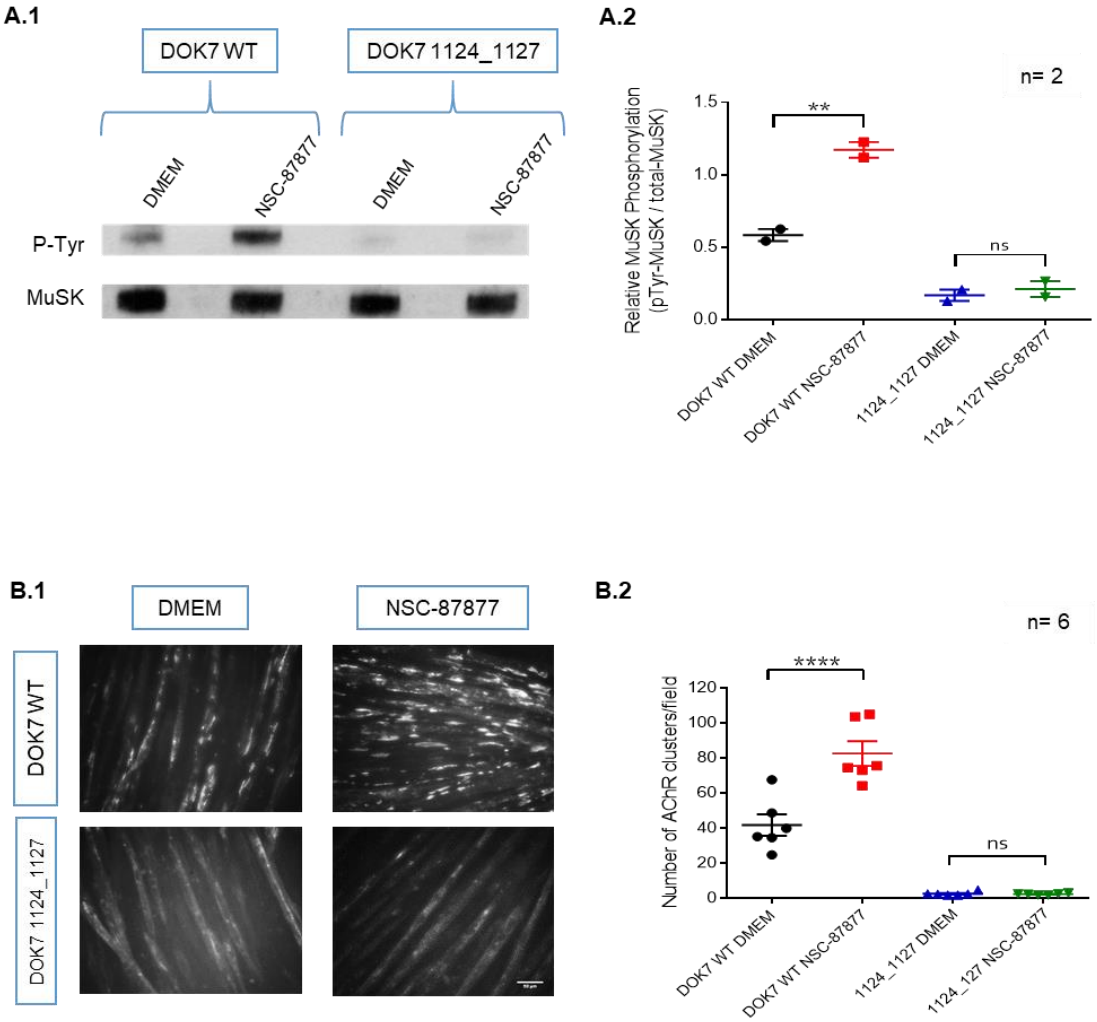


Figure 3.8. SHP2 inhibition by NSC-87877 increases MuSK phosphorylation and AChR clustering in *DOK7* overexpressing myotubes but has no effect on the DOK7 1124_1127dupTGCC. (A.1) Representative western blot showing P-Tyr MuSK (top) and MuSK expression (bottom) after incubation with NSC-87877 of DOK7 WT and DOK7 1124_1127 overexpressing myotubes. **(A.2)** Pooled results of 3 experiments showing that NSC-87877 increases significantly MuSK phosphorylation in DOK7 WT overexpressing myotubes but has no effect in the mutant DOK7 1124_1127. (**B.1**) Clustering of AChRs (labelled with Alexa Fluor 594 α-bugaratoxin) in DOK7 and 1124_1127 overexpressing myotubes after 16 hours incubation with DMEM and NSC-87877. Spontaneous AChR cluster formation is observed in the DOK7 WT myotubes and this is enhanced by NSC-87877. On the contrary, no clusters are observed in the DOK7 1124_1127 mutant and NSC-87877 has no effect. **(B.2)** Pooled results of 6 experiments showing the average number of AChR clusters per microscopic field in the different cell lines. The number of clusters was increased by NSC-87877 on the DOK7 WT cells but not in the mutant 1124_1127dupT. One-way ANOVA was used for multiple comparisons Mean + SEMs are shown.

clustering). Conversely, in the myotubes overexpressing the mutant DOK7, no spontaneous increase in either MuSK phosphorylation or AChR clustering was observed, and the SHP2 inhibition by NSC-87877 had no effect.

3.2.7) Modification in gene expression induced by NSC-87877

An additional question was whether NSC-87877 might have additional effects on the gene transcription of the myotubes alongside the observed upregulation of MuSK phosphorylation. Intracellular RNA was extracted after 2.5 hours of incubation of the myotubes with either DMEM, agrin (1:800), or NSC-87877 100 μM. Samples were then sent in triplicate for full transcriptomic sequencing to the company Novogene. Further analysis was performed using the bioinformatic programmes STAR, featureCounts and edgeR (Bioconductor) to align the RNA sequences according to the *mus musculus* genome, to count the reads for the expression of each gene, and to compare them among the samples to evaluate preferential up- or down-regulation. Only modifications in gene transcription of at least 1 log fold change were considered significant.

Compared to DMEM, 32 genes were upregulated, and 4 downregulated, after exposure to NSC-87877 (Table 3.1). Two genes encoding for proteins for the cytochrome 450 family (Cyp1a1 and Cyp1b1) were among those with the highest increase in expression (up to 6 log fold changes), indicating an induction of the metabolic/detoxicating pathways of the cell. Potentially relevant for the clustering of the AChRs, a significant upregulation was found in the genes encoding for: the neuronal alpha-subunit of the AChR (Chrna10); neuregulin 1 (Nrg1) which contributes to the expression of the postsynaptic AChRs; a negative regulator of the Wnt signalling pathway (Nkd2); and the Actin remodelling regulator (Nhs). The expression of the two cytochromes 450, Chrna10, and Nhs was also found significantly increased when NSC-87877 was compared to agrin, further supporting a specific effect of the SHP2 inhibition for these

Genes	logFC	P value	Protein
Cyp1a1	6.135913	0	Cytocrome P450 a1
Ahrr	3.232608	7.61×10^{-60}	Aryl-Hydrocarbon Receptor Repressor
Cyp1b1	2.343582	5.26×10^{-139}	Cytocrome P450 b1
Slc39a10	2.12387	3.92×10^{-80}	Zinc transporter 10
Pitpnc1	1.968733	3.63×10^{-23}	Phosphatidylinositol Transfer Protein 1
Foxf1	1.828293	2.11×10^{-11}	Forkhead-Related Transcription Factor 1
Spint1	1.827142	2.40×10^{-14}	Serine petpidase inhibitor
Ptgs2	1.688821	2.07×10^{-15}	Prostaglandin-endoperoxide synthase 2
Plscr2	1.668236	2.32×10^{-31}	Phospholipid scramblase 2
Ptx3	1.666378	1.52×10^{-16}	Pentraxin 3
Ccno	1.581287	5.95×10^{-09}	Cyclin O
Cxcl5	1.467134	1.40×10^{-06}	Epithelial-derived neutrophil-activating peptide 78
Hs3st3b1	1.436702	2.75×10^{-07}	Heparan sulfate glucosamine 3-O-sulfotransferase
Aldh3a1	1.321833	1.12×10^{-32}	Aldehyde dehydrogenase
Smox	1.313207	1.69×10^{-43}	Spermine Oxidase
Chrna10	1.209237	0.000108	Acetylcholine Receptor subunit alpha
Cbln1	1.193545	1.10×10^{-05}	Precerebellin precursor
Edn1	1.178337	1.24×10^{-05}	Endothelin 1
4931440P22Rik	1.153714	3.91×10^{-05}	Uncharacterized protein
Slco4a1	1.143555	1.32×10^{-11}	Solute Carrier Organic Anion Transporter
Col27a1	1.11778	7.23×10^{-07}	Collagen Type XXVII Alpha 1 Chain
Nkd2	1.109142	9.09×10^{-23}	NKD Inhibitor Of WNT Signaling Pathway 2
Tns4	1.094775	7.68×10^{-06}	Tensin 4
AA474331	1.073392	0.000902	Major Facilitator Superfamily Domain Containing
Nqo1	1.052523	7.09×10^{-09}	NAD(P)H dehydrogenase
Ch25h	1.042119	6.23×10^{-12}	Cholesterol 25-Hydroxylase
Mertk	1.035114	7.68×10^{-08}	MER Proto-Oncogene, Tyrosine Kinase
Tiparp	1.030483	4.09 x10-33	Poly(ADP-ribose) polymerase
Nrg1	1.020846	6.39×10^{-11}	Neuregulin 1
Slfn2	1.011415	0.000959	Schlafen Family Member 12
Gm2694	1.00731	0.000155	Uncharacterized protein
Nhs	1.000404	0.000247	NHS Actin Remodeling Regulator
Gm4636	-1.09455	2.55×10^{-06}	Uncharacterized protein
Spon1	-1.18124	0.000153	Spondin 1
Snord69	-1.22989	2.97×10^{-05}	small nucleolar RNA, C/D box 69
Slc30a1	-2.94246	9.98×10^{-88}	Zinc Transporter 1

Table 3.1. Genes modified significantly by NSC-87877 compared to DMEM. Log-fold changes (logFC), P value, and encoded protein are indicated for each gene. In red are highlighted the genes which might contribute to the regulation of the AChR pathway.

Genes	logFC	P value	Protein
Cyp1a1	6.065479	0	Cytocrome P450
Ahrr	3.699384	3.07×10^{-77}	Aryl-Hydrocarbon Receptor Repressor
Cyp1b1	2.332992	3.55×10^{-129}	Cytocrome P450
Slc39a10	2.049529	4.35×10^{-68}	Zinc transporter 10
Pitpnc1	1.850389	3.46×10^{-22}	Phosphatidylinositol Transfer Protein 1
Spint1	1.706028	8.88×10^{-14}	Serine petpidase inhibitor
Plscr2	1.548968	4.20×10^{-20}	Phospholipid Scramblase
Ptgs2	1.518701	3.49×10^{-11}	Prostaglandin-Endoperoxide Synthase 2
Ptx3	1.347446	2.88×10^{-12}	Pentraxin 3
Smox	1.34159	4.06×10^{-46}	Spermine Oxidase
Chrna10	1.311474	4.05×10^{-05}	Acetylcholine Receptor subunit alpha
9130008F23Rik	1.309478	1.90×10^{-06}	Chromosome 6 Open Reading Frame 141
Il12rb1	1.279894	5.79×10^{-11}	Interleukin 12 Receptor Subunit Beta 1
Ccno	1.27667	1.69×10^{-06}	Cyclin O
Nhs	1.261822	6.40×10^{-06}	NHS Actin Remodeling Regulator
Foxf1	1.226711	6.52×10^{-07}	Forkhead Box F1
Hs3st3b1	1.205682	8.14×10^{-06}	Heparan Sulfate-Glucosamine 3-Sulfotransferase
Slco4a1	1.180428	3.75×10^{-12}	Solute Carrier Organic Anion Transporter
Nebl	1.162988	0.00017	Nebulette
Aldh3a1	1.156909	9.70×10^{-33}	Aldehyde Dehydrogenase 3 Family Member A1
Tns4	1.138493	9.69×10^{-05}	Tensin 4
Tiparp	1.091235	1.03×10^{-37}	Poly(ADP-ribose) polymerase
AI607873	1.061902	8.65×10^{-05}	Tensin 4
Frmd4b	1.051144	7.92×10^{-12}	FERM Domain Containing 4B
Npas4	1.04211	5.34×10^{-05}	Neuronal PAS Domain Protein 4
Rtn4rl2	1.035558	0.001128	Reticulon 4 Receptor Like 2
Sdf2l1	1.030387	2.91×10^{-20}	Stromal Cell Derived Factor 2 Like 1
Ddx58	1.014446	2.27×10^{-11}	DExD/H-Box Helicase 58
Tspan33	1.005074	3.17×10^{-08}	Tetraspanin 33
Ccl7	-1.00039	3.09×10^{-13}	C-C Motif Chemokine Ligand 7
Hs3st1	-1.05136	6.56×10^{-05}	Heparan Sulfate-Glucosamine 3-Sulfotransferase 1
Gm10638	-1.09411	0.000576	Uncharacterised protein
Snord69	-1.16198	0.000163	Small Nucleolar RNA, C/D Box 69
Ccl2	-1.79475	8.15×10^{-19}	C-C Motif Chemokine Ligand 2
Cxcl1	-1.91899	2.29×10^{-10}	C-X-C Motif Chemokine Ligand 1
Slc30a1	-2.92921	7.84×10^{-95}	Solute Carrier Family 30 Member 1

Table 3.2. Genes modified significantly by NSC-87877 compared to agrin. Log-fold changes (logFC), P value, and encoded protein are indicated for each gene. In red are highlighted the genes for which the expression was modified by NSC-87877 when compared to both agrin and DMEM.

genes. Other genes found selectively upregulated by NSC-87877 when compared to both agrin and DMEM are highlighted in red in Table 3.2. Finally, potential interactions among the modified genes were analysed using the online platform Reatcome. However, a dysregulation of specific intracellular pathways was not detected.

3.2.8) Production of MuSK IgG

The next question was whether the compound would retain its stimulatory effect in the presence of MuSK antibodies and, therefore, be able to counteract the pathogenic mechanisms responsible for the onset of myasthenia. Preliminary experiments, carried out in our lab by Dr Saif Huda, had already shown that NSC-87877 was able to preserve AChR clustering on C2C12 myotubes exposed to different dilutions of MuSK-MG patients' sera. Here, the effects of purified MuSK antibody preparations, particularly individual IgG antibody subclasses, were investigated. To maintain consistency with the previous experiments performed by Dr Huda, plasmapheresis materials from three of his patients were selected for IgG purification according to the amount of plasma available. Samples from patients 1 and 2 were used to purify total IgG, IgG4 and IgG1-3 subclasses, whereas material from patient 3 was sufficient to perform only the purification of the individual IgG subclasses.

3.2.8.1) IgG purification chromatography

IgG4 (see Methods) was prepared using an anti-IgG4 matrix and eluted with glycine acid solution (pH 2.3). The first 5-6 fractions (around 1 ml each) usually contain the highest amount of IgG (Figure 3.9) but, to avoid wasting IgG, the later elutions were pooled and further concentrated. After concentration the samples were pooled, dialysed against DMEM and sterile-filtered to avoid potential contamination, and tested for MuSK-antibody concentrations. Meanwhile the flow-through from the matrix was

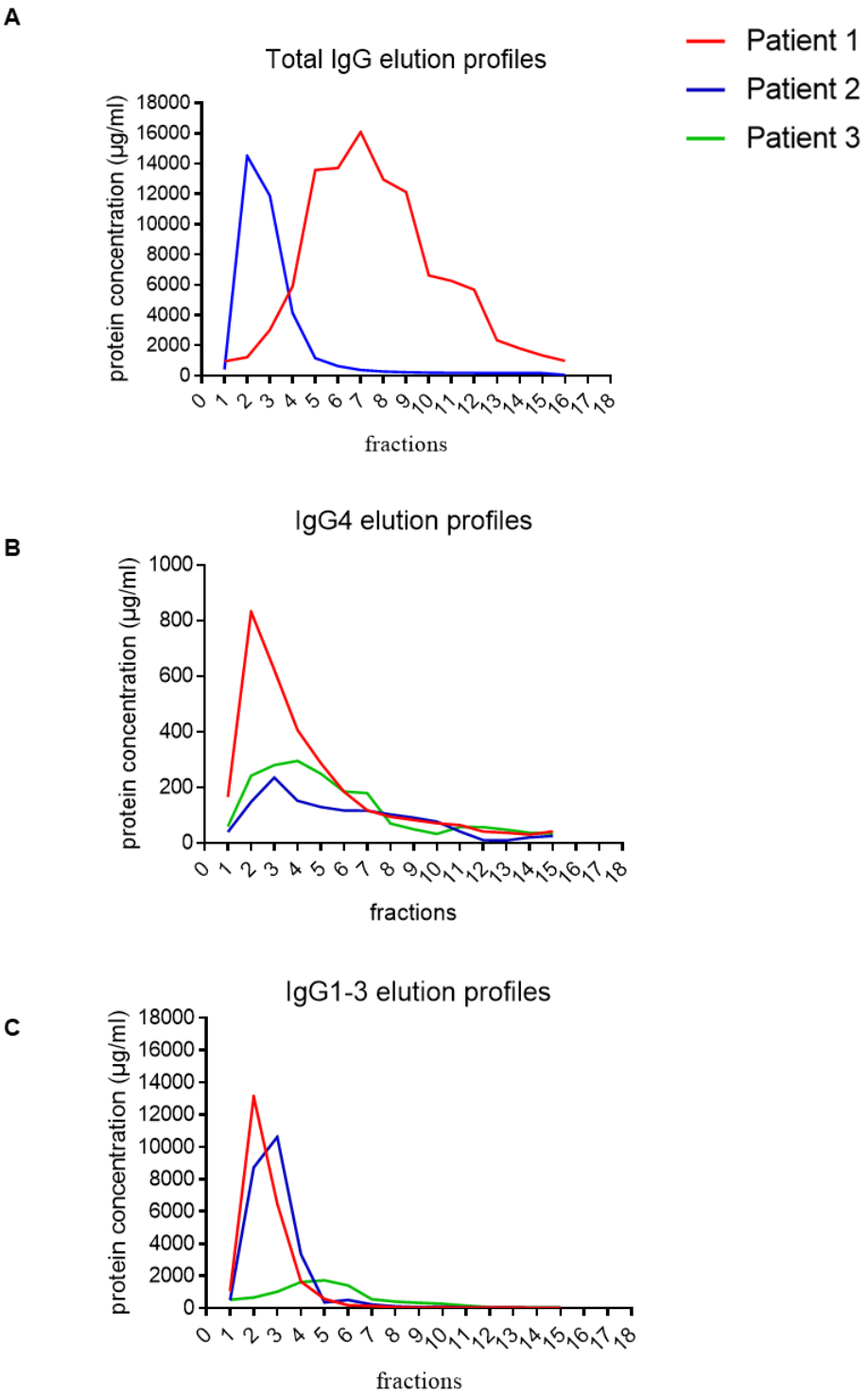


Figure 3.9. Elution profiles of purified IgG antibody fractions. Total IgG **(A)**, IgG4 **(B)**, and IgG1-3 **(C)** were purified from three MuSK-MG patients (in red, blue and green respectively). Total protein concentration was estimated measuring the OD280 absorbance with a NanoDrop and plotted against the corresponding elution fraction.

exposed to a Protein G Sepharose matrix to purify the remaining subclasses which were also concentrated and tested for MuSK-antibody.

3.2.8.2) Cell based assay (CBA) to access efficacy of MuSK subclasses purification

To confirm the fractionation of the subclasses a MuSK cell-based assay was performed. Antibody preparations from each individual MuSK-MG patient containing either IgG4 or IgG1-3 (at 1:25 dilution) were incubated for 2 hours with HEK 293T cells transfected with a recombinant MuSK with a fluorescent C-terminus tag (mCherry) (Figure 3.10 - red). Antibody binding was detected with secondary mouse antibodies directed against the different IgG subclasses, followed by a tertiary 488 fluorescent antibody directed against mouse-IgG (Figure 3.10 – green). Both IgG1-3 and IgG4 preparations showed strong positivity when probed with the corresponding anti-IgG subclasses (Figure 3.10 – top and bottom respectively) with consistent visual co-localisation with the MuSK-mCherry molecules expressed on the cell membrane (Figure 3.10 – merge images). Importantly, when probed with the complementary anti-IgG subclasses, both preparations tested negative (Figure 3.10 – central panels), confirming the absence of undesired IgG subclass contaminants.

3.2.8.3) Radioimmunoassay (RIA)

The MuSK antibodies were titrated against ^{125}I-MuSK and the concentration calculated according to the equation (see previous chapter "materials and methods"). Figure 3.11 shows the titration of MuSK antibodies for the individual patients. The reaching of a plateau in the number of cpm, usually at lower sample dilutions, indicates the saturation level of the assay. The dilution at about half of the maximum cpm, when the curve was essentially linear, was taken to provide a good estimation of the MuSK-ab concentration in the sample (half-maximal binding concentration).

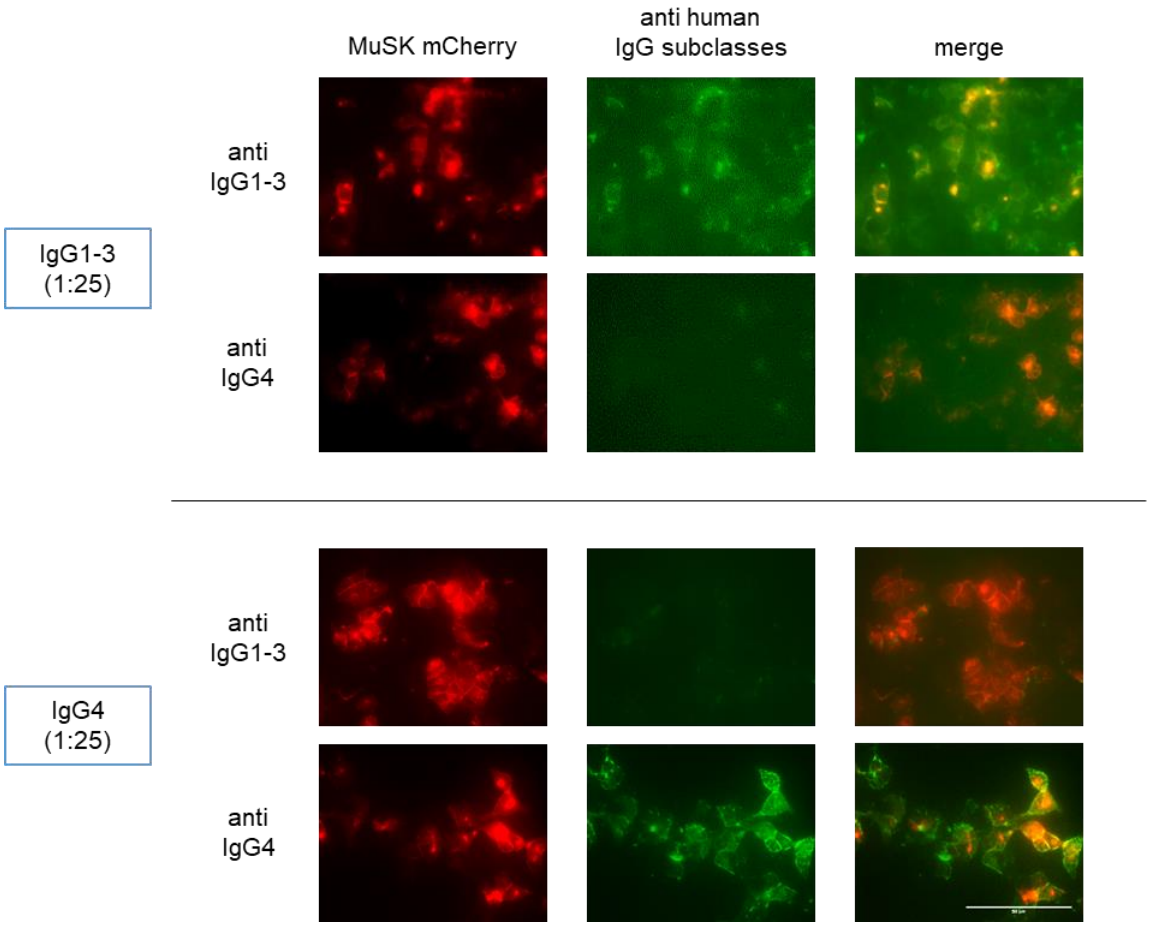


Figure 3.10. Cell-based assay to verify purity of MuSK antibody subclass preparations. HEK 293 cells transfected with MuSK-mCherry (red) and exposed to either IgG1-3 or IgG4 preparations at 1:25 dilution. Samples were then probed with mouse mouse anti-human IgG1, 2, and 3 (pooled together at 1:50 dilution) and anti-IgG4 secondary antibodies (green, after tertiary anti-mouse IgG antibody Alexa Fluor 488). Both IgG1-3 and IgG4 showed strong positivity when probed with their respective anti-subclass antibody. Conversely, when samples were probed for their complementary subclasses, no signal was detected on the surface of the cells confirming purity of the antibody preparations.

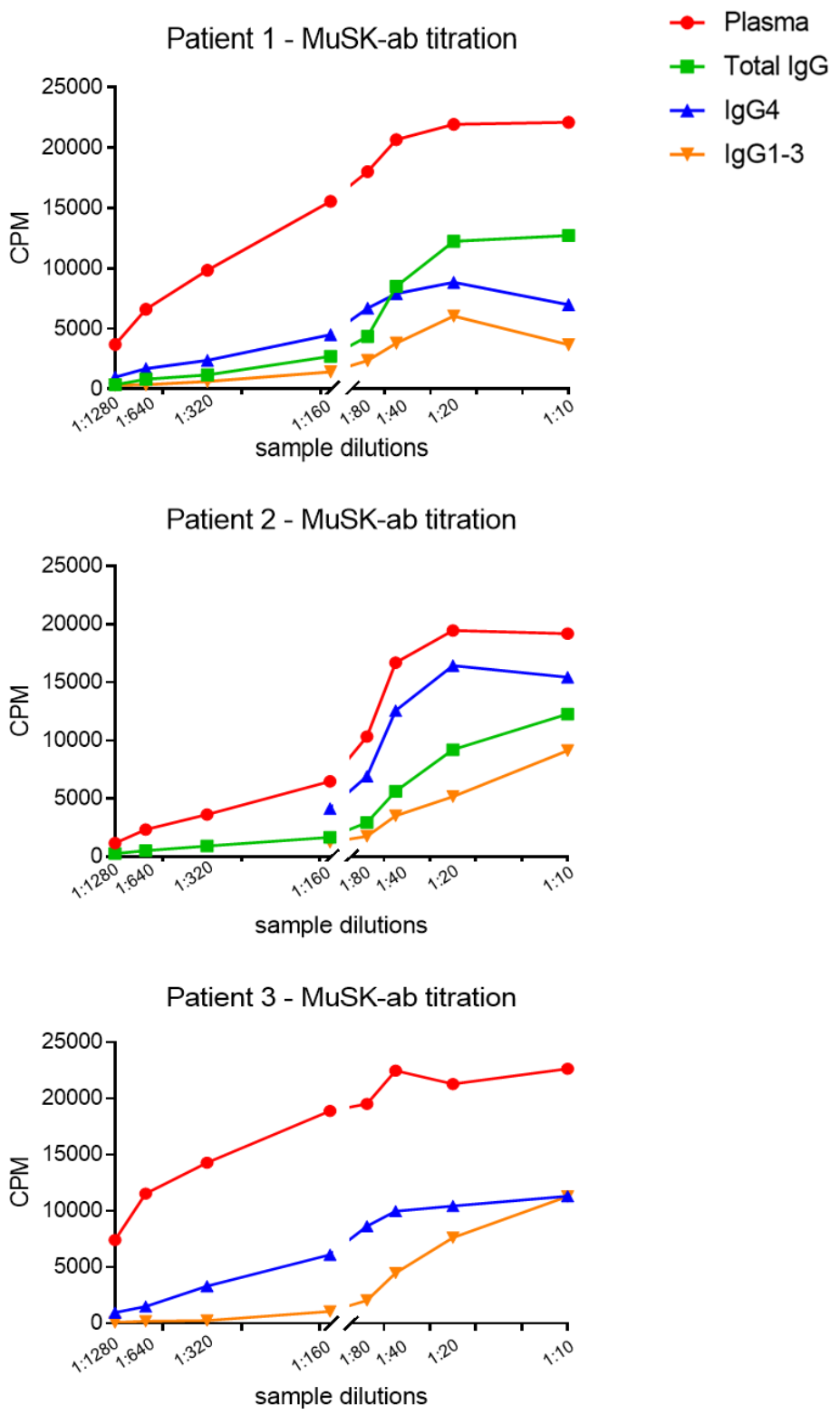


Figure 3.11. Titration of MuSK antibody subclasses by radioactive immunoassay. Half-maximal binding concentration of MuSK-Abs was estimated by radioactive immunoassay (RIA) on both the original plasma and the final antibody preparations obtained after pooling the elution fractions with the highest protein concentration. Antibody titration from plasma (red), total IgG (green), IgG4 (blue) and IgG1-3 (orange) preparations from the three MuSK-MG patients are shown.

The final results and the efficacy of IgG purifications are summarised in Table 3.3. Here are indicated the volumes of the different stages of purification (initial plasma amount, after dilution with PBS, flow-through from total IgG and IgG4 matrix) together with the relative protein concentrations measured with the NanoDrop. As expected, in all patients the half-maximal binding concentration of MuSK IgG4 was significantly higher compared to IgG1-3, suggesting that IgG4 is the most represented subclass in MuSK myasthenia, but both IgG4 and IgG1-3 levels varied among patients.

3.2.8.4) Additional purification of MuSK IgG1-3 subclasses

The first round of purification provided enough material to carry out the initial experiments. However, due to the average low titre of MuSK IgG1-3 in the initial preparations, and the antibody concentration of 0.5 nM utilised in the protocol, additional samples were needed. A sufficient amount of plasmapheresis material was still available from 7 other MuSK-MG patients to perform an additional round of antibody purification. This time, plasma samples were first screened for their positivity for IgG1-3 antibody subclasses. A MuSK CBA was performed using two different dilutions of the original plasma (1:10 and 1:50) (Figure 3.12). Patient 4, 5, 6, 8 and 10 had the strongest positivity for MuSK IgG1-3 at 1:50 dilution of the original plasmas. Estimated antibody concentrations using the radioimmunoprecipitation are indicated in Figure 3.13 and Table 3.4.

Up to 10 ml of plasma from each patient were pooled (final total volume of 42.5 ml) and the IgG4 and IgG1-3 subclasses purified as above (Figure 3.14). To maximise the IgG1-3 elution a final volume of 50 ml of glycine solution was used to elute from the Protein G sepharose.

Patient	Sample	Volume (ml)	OD280 (µg/ml)	Half-maximal binding concentration MuSK-abs (nmol/ml)
1	Plasma	10	29860	11.82
	Plasma + PBS (1:1)	20	14711	
	Flow-through IgG matrix	17.5	7842	
	Total IgG	5	6827	1.31
	Flow-through IgG4 matrix	17.5	11378	
	IgG4	6.5	294	2.86
	IgG1-3	5	6855	0.71
2	Plasma	10	32781	3.9
	Plasma + PBS (1:1)	20	15356	
	Flow-through IgG matrix	18	8245	
	Total IgG	7	4764	0.84
	Flow-through IgG4 matrix	17.5	7629	
	IgG4	7	121	3.12
	IgG1-3	5	7767	0.53
3	Plasma	7.5	63617	27.7
	Plasma + PBS (1:1)	15	36520	
	Flow-through IgG4 matrix	15	15441	
	IgG4	6	643	3.66
	IgG1-3	7	3723	0.6

Table 3.3. Summary of total IgG and IgG subclasses purification for each patient indicating the initial and final volumes with relative protein concentration and half-maximal binding concentration of MuSK-Abs.

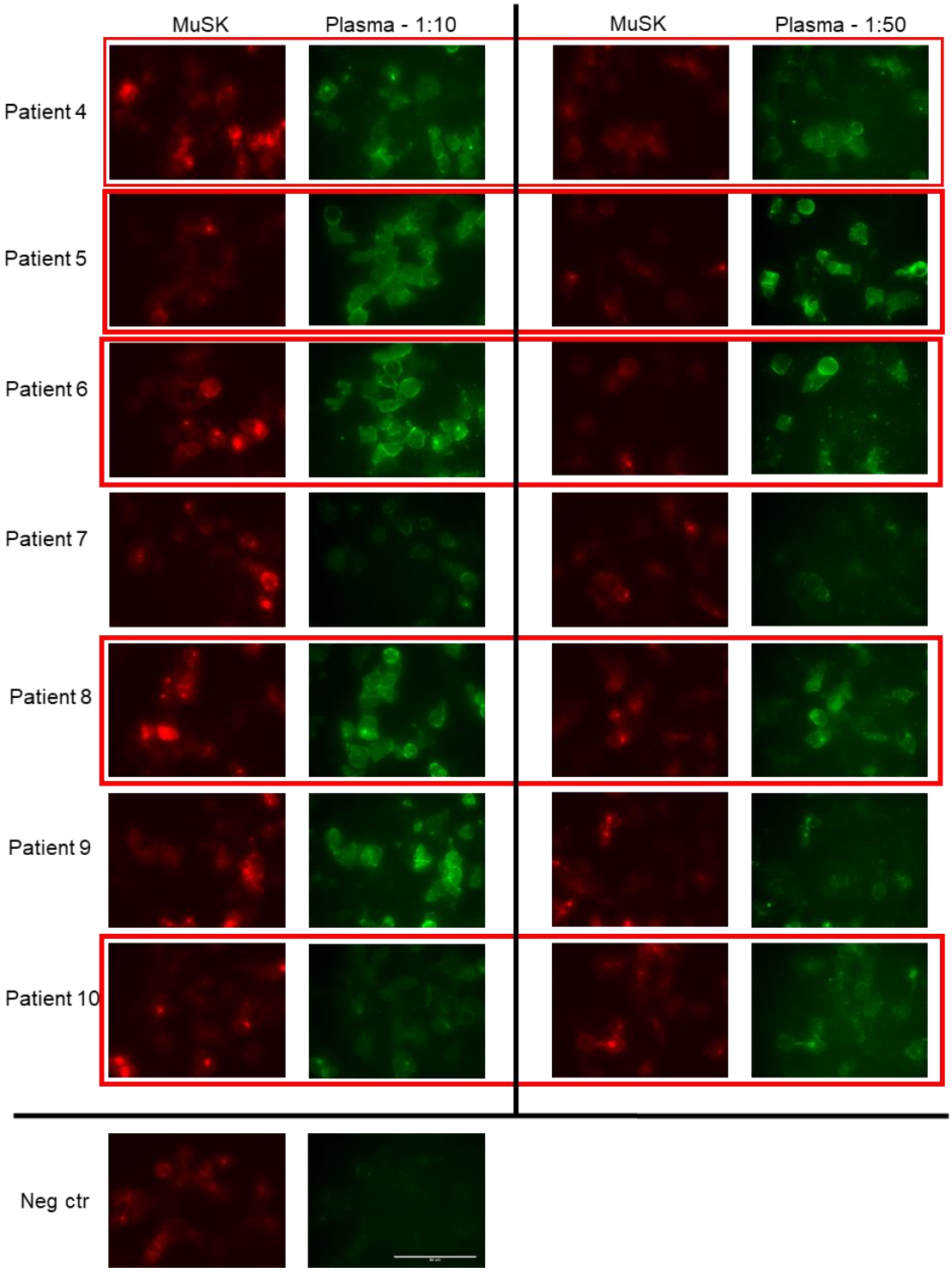


Figure 3.12. Screening of MuSK IgG1-3 antibody positivity by Cell Based Assay. Plasma samples from eight MuSK-MG patients was tested (1:10 and 1:50 dilutions) on HEK 293 cells transfected with MuSK tagged with fluorescent mCherry at the C-terminal (red). Cells were then incubated with mouse anti-human IgG1, IgG2 and IgG3 antibodies (1:50) which, in turn, were probed with a tertiary anti-mouse fluorescent antibody (Alexa Fluor 488 – green). Patients 4, 5, 6, 8, and 10 (indicated by the red boxes) showed the strongest positivity for MuSK IgG1-3 abs at 1:50 dilutions and were selected for subsequent antibody purification.

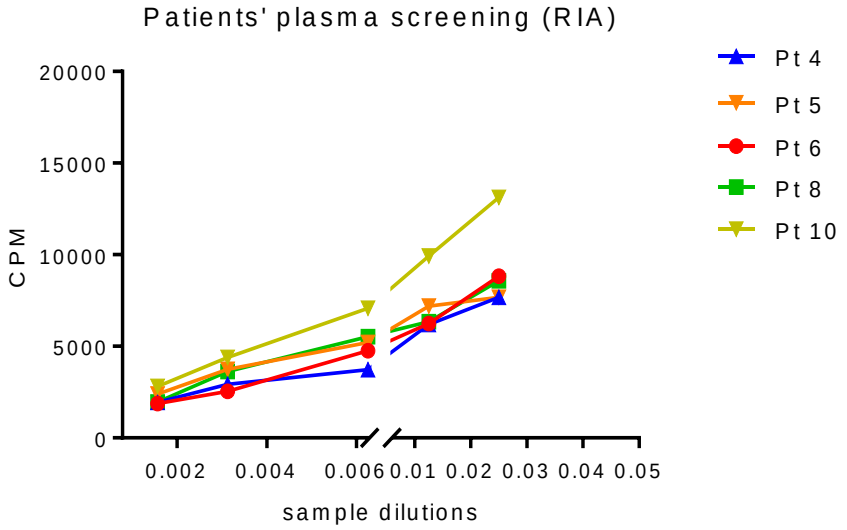


Figure 3.13. MuSK-ab titration for initial screening of patients. MuSK antibody concentration was estimated by radioactive immunoassay (RIA) on plasma samples from patients 4, 5, 6, 8, and 10 (which showed the strongest positivity on the CBA for MuSK IgG1-3 subclasses).

Patient	dilution	CPM	mmol	nmol/ml
4	1/40	7673.4	1.44×10^{-12}	1.15
	1/80	6199.2	1.16×10^{-12}	1.86
	1/160	3717	0.69×10^{-12}	2.23
	1/320	2926.8	0.54×10^{-12}	3.51
	1/640	1942.2	0.36×10^{-12}	4.66
5	1/40	7682.4	1.44×10^{-12}	1.15
	1/80	7194.6	1.35×10^{-12}	2.16
	1/160	5205.6	0.97×10^{-12}	3.12
	1/320	3745.8	0.70×10^{-12}	4.49
	1/640	2395.8	0.45×10^{-12}	5.75
6	1/40	8823.6	1.66×10^{-12}	1.32
	1/80	6247.8	1.17×10^{-12}	1.87
	1/160	4762.8	0.89×10^{-12}	2.86
	1/320	2541.6	0.47×10^{-12}	3.05
	1/640	1882.8	0.35×10^{-12}	4.52
8	1/40	8571.6	1.61×10^{-12}	1.28
	1/80	6348.6	1.19×10^{-12}	1.90
	1/160	5520.6	1.04×10^{-12}	3.31
	1/320	3627	0.68×10^{-12}	4.35
	1/640	1951.2	0.36×10^{-12}	4.68
10	1/40	13129.8	2.46×10^{-12}	1.97
	1/80	9928.76	1.86×10^{-12}	2.98
	1/160	7071.71	1.33×10^{-12}	4.24
	1/320	4393.71	0.82×10^{-12}	5.27
	1/640	2807.65	0.52×10^{-12}	6.74

Table 3.4. MuSK antibodies titration by RIA of the plasma samples from patients 4, 5, 6, 8, and 10. In red are highlighted the dilutions equivalent to half of the highest CPM counts, corresponding to half-maximal binding MuSK-ab concentrations for each sample.

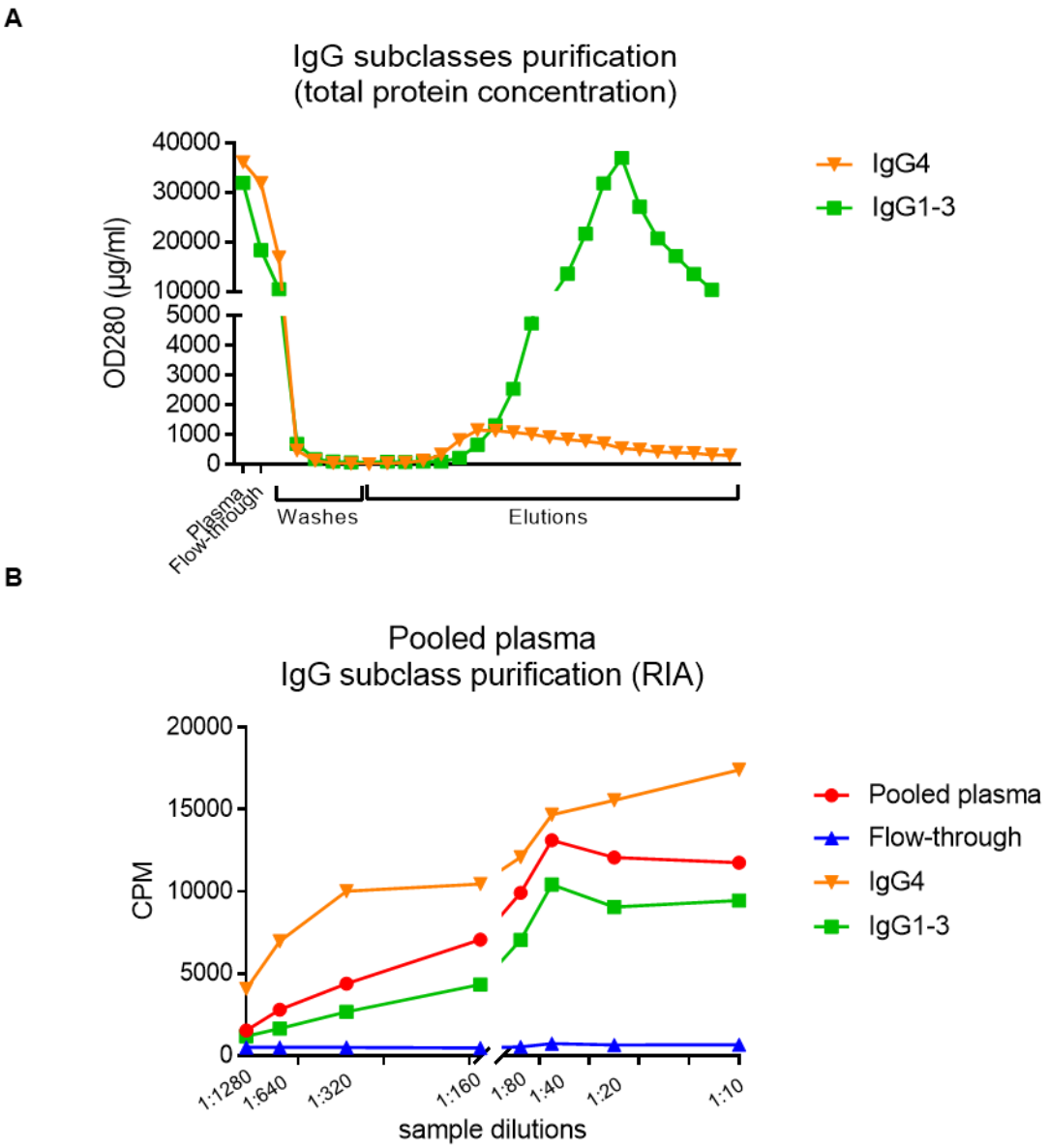


Figure 3.14. Purification of antibody subclasses and titration of MuSK antibodies by RIA. IgG subclasses were purified from plasma pooled from 5 MuSK-MG patients who showed highest IgG1-3 positivity at the CBA. Pooled plasma were incubated first with a specific IgG4 matrix to isolate the IgG4 fraction. The flow-trough from the column was then incubated with Sepharose G to isolate the remaining IgG1, 2 and 3 subclasses. **(A)** Antibody concentration was estimated on each elution fraction measuring the OD280 absorbance by nanodrop. The peak concentration of total IgG1-3 was 40 times higher compared to the IgG4. **(B)** Half-maximal binding concentrations of MuSK IgG4 and IgG1-3 subfractions were then estimated by RIA on the original plasma, flow-through and the pooled elutions. MuSK antibodies were almost not detectable in the flow-through indicating efficient binding to the column. In the final preparations, MuSK IgG4 concentration was about 3.5 fold higher than MuSK IgG1-3.

Finally, all elution fractions were pooled together, concentrated by centrifuge spinning tubes, and dialysed against DMEM. Volume, total protein and MuSK antibody concentrations of original pooled plasma, flow-through and final elutions are indicated in Table 3.5.

3.2.8.5) Dot blots to access efficacy of MuSK subclasses purification

To test for the total IgG in the preparations, the original pooled plasma, flow-through, washes and elution fractions were tested on dot blots detecting with the corresponding and complementary anti-IgG subclasses (Figure 3.15). This different approach was chosen to evaluate whether dot blots could provide similar reliability and sensitivity while requiring less time and materials compared to the CBA. Due to their high concentration, IgG1-3 were detectable in all the samples (including flow-through and washes) and elution fractions from the Protein G column (Figure 3.15A – left). Conversely, a strong positive IgG4 signal was observed only in the original plasma and in the elution fractions from the IgG4 matrix, indicating efficient binding to the matrix and complete depletion of this subclass from the flow-through (after two passages through the matrix) (Figure 3.15A – right). Afterwards, purity of the IgG1-3 preparations was tested probing different dilutions of each purification fraction with antibodies against either total IgG (Figure 3.15B - right) or specific IgG4 subclass (Figure 3.15B - left). The IgG1-3 signal was strong in all dilutions of each sample tested. Conversely, once the samples were probed with the anti-IgG4 antibody, the signal was detected only at the lowest dilutions indicating a very low concentration of IgG4 in the final IgG1-3 preparations. The presence of an IgG4 signal in the flow-through is due to the fact that, in this case, the first passage through the matrix was tested, indicating that a second passage is needed for complete IgG4 depletion.

Sample	Volume (ml)	OD280 (μg/ml)	MuSK-ab half-maximal binding concentration (nmol/l)
Pooled plasma	42.5	36302	5.28
Flow-through	40.5	32770	0.286
IgG4	4.5	2042	8.4
IgG1-3	7.3	5557	2.365

Table 3.5. Summary of IgG subclasses purification from pooled MuSK-MG patients' plasma. Volumes of the different purification steps with relative protein concentration and half-maximal binding concentration of MuSK antibodies are indicated.

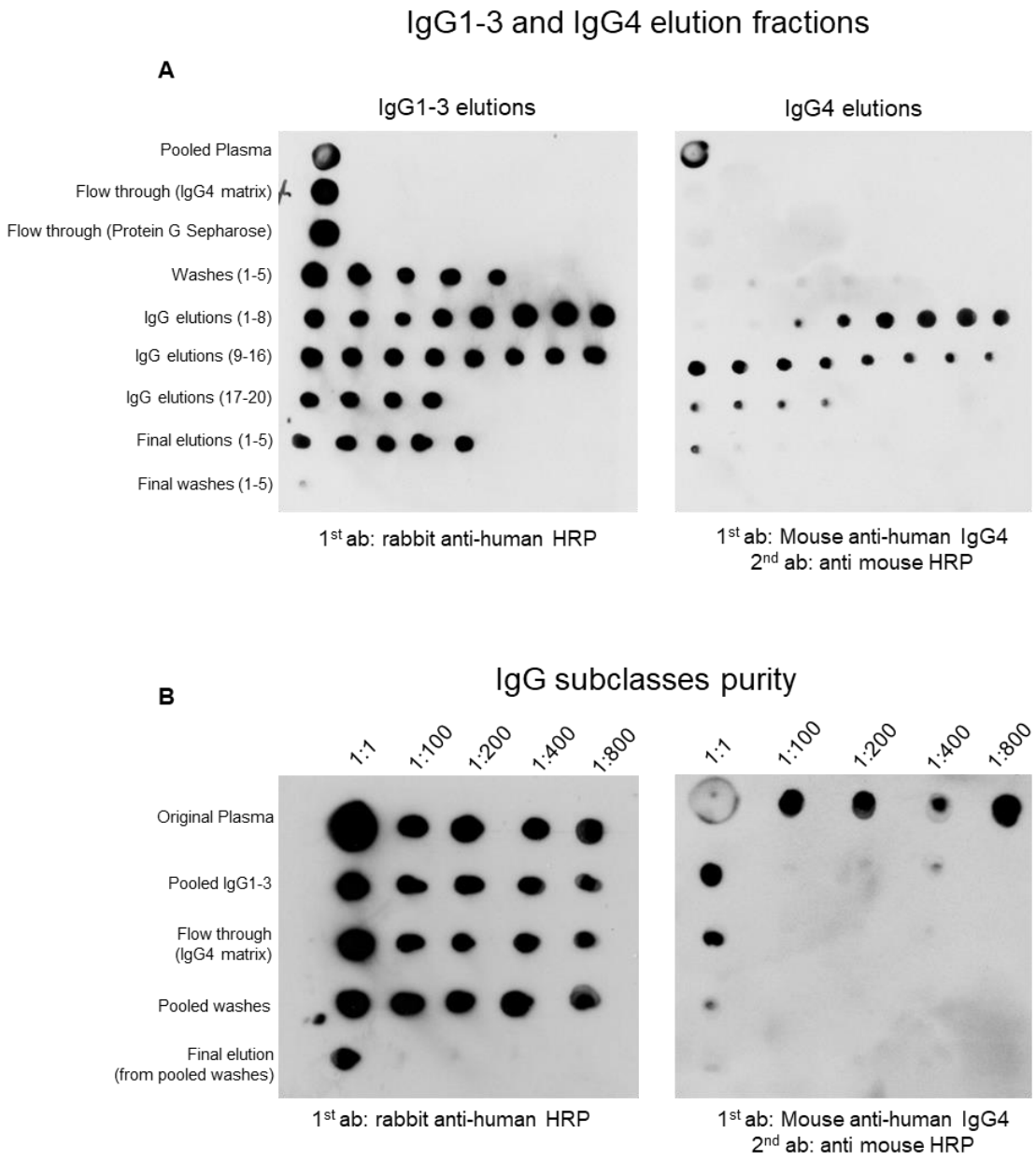


Figure 3.15. Dot blots to evaluate purity of IgG antibody subclass preparations. **(A)** 5 µl of each purification fraction were absorbed directly on a nitrocellulose membrane. After blocking with BSA, the membrane was probed with an anti-human HRP antibody (left) or with a secondary mouse-anti human IgG4 antibody (right) to evaluate the efficacy of the selective IgG4 matrix. IgG4 were detectable only in the original plasma and the elutions with the intensity of the signal correlating to the OD280 concentration measured with the NanoDrop. **(B)** Different dilutions of the purification fractions and pooled elutions of the IgG1-3 were tested on dot blots as described above. Pooled IgG1-3 showed a strong signal in all dilutions when probed with a non-specific anti-human IgG antibody (left). However, after probing with the anti-human IgG4 antibody (right), a positivity was observed only in the non diluted IgG1-3 fraction (the signal was not detectable in all the remaining dilutions) indicating a very low concentration of IgG4 in the final IgG1-3 preparation.

3.2.9 MuSK immunoprecipitation comparison between purified MuSK antibodies and commercial anti-MuSK AF562

Before proceeding with the experiments involving SHP2 inhibition, it was necessary to test how effective the patients' antibodies were at immunoprecipitating MuSK, and comparing with precipitation with the commercial anti MuSK antibody AF562. This was important because (a) only the molecules of MuSK that were interacting with the patients' antibodies should be evaluated in the experiments whereas (b) the DMEM and agrin controls had to be immunoprecipitated with the commercial antibody AF562. Myotubes were pre-incubated with purified MuSK IgG4 fractions for 30 minutes and then stimulated with agrin for additional 40 minutes. Cell lysates were then incubated either directly with the protein G magnetic beads (to immunoprecipitate MuSK using only the patients' own antibodies) or with the beads pre-incubated with the commercial anti-MuSK AF562 (for agrin and DMEM controls, and comparisons among patients' samples). Notably, in the presence of both patients' antibodies and AF562, the western blot bands corresponding to the expression of MuSK were stronger compared to patients' antibody alone, suggesting a more efficient immunoprecipitation with the commercial antibody (Figure 3.16A). However, when the results of the phosphorylated MuSK were normalised to the total MuSK expression, no significant differences were observed between the two methods of immunoprecipitation (Figure 3.16B). This suggests that the addition of AF562 does not interfere with MuSK phosphorylation, and that the commercial antibody can be used for the immunoprecipitation of agrin and DMEM controls reliably and comparably to the samples incubated with patients' antibodies alone.

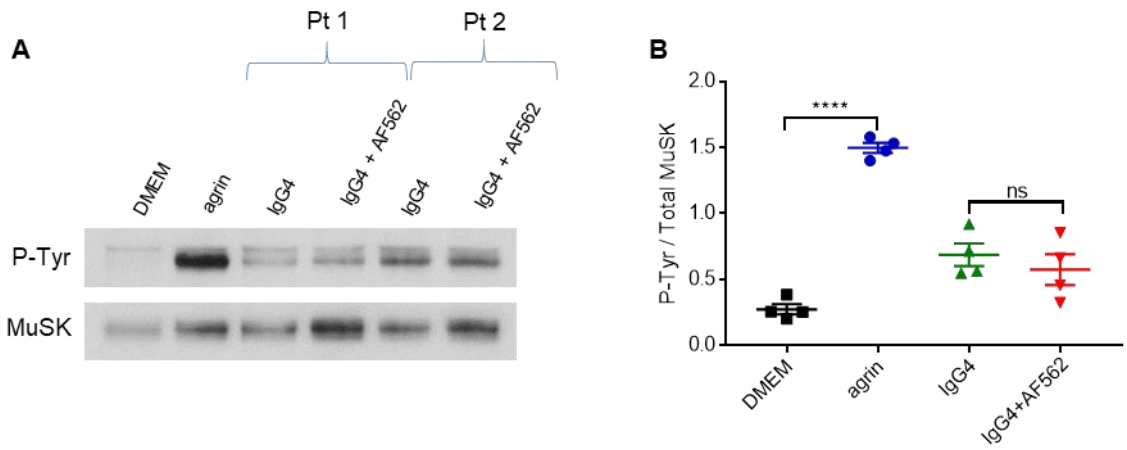


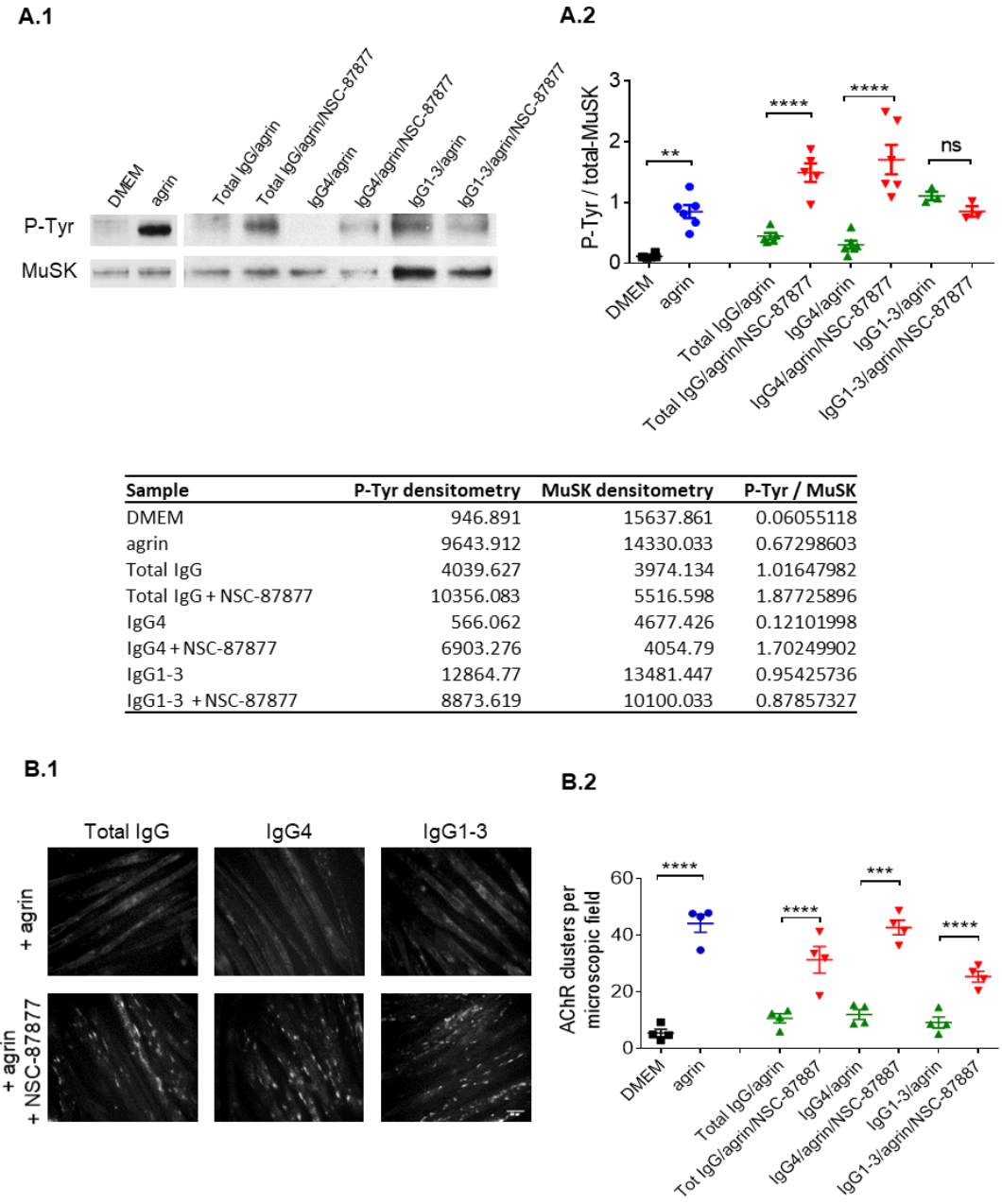
Figure 3.16. MuSK immunoprecipitation comparison in the presence and absence of commercial anti-MuSK AF562 using patients' purified IgG4. Myotubes were pre-incubated for 30 minutes with purified IgG4 fractions (1:5 dilution) and phosphorylation was induced by adding agrin 1:800 for 40 minutes. MuSK was then immunoprecipitated from cell lysate directly with patients' antibodies or pre-incubating the Protein G beads with commercial anti-MuSK AF562. **(A)** In the representative western blot, MuSK expression is higher in the presence of AF562, suggesting a more efficient immunoprecipitation with the commercial antibody. However, the phosphorylated-MuSK/total-MuSK ratio **(B)** did not show any significant difference between AF562 and patients' antibodies alone.

3.2.10 Testing NSC-87877 with MuSK antibodies

Finally, the selective effects of MuSK-MG IgG subclasses on MuSK phosphorylation and AChR clustering were tested in the presence and absence of NSC-87877 to evaluate the potential therapeutic action of SHP2 inhibition. C2C12 myotubes were pre-exposed to 0.5 nM of purified total MuSK-IgG, IgG1-3 and IgG4 for 30 minutes to allow the antibodies to bind to MuSK, prior to the addition of agrin at 1:800 dilution. NSC-87877 100 µM was added at the same time as agrin. After 40 minutes of exposure, the cells were lysed and incubated directly with protein G magnetic beads to immunoprecipitate MuSK using the purified antibodies from the patients. In those samples incubated only with DMEM or agrin (negative and positive control respectively), MuSK immunoprecipitation was carried out as previously described using the anti-MuSK commercial antibody AF562 pre-incubated with the protein G beads.

As expected, MuSK-IgG and IgG4 prevented MuSK activation physiologically induced by the presence of agrin. However, the addition of NSC-87877 caused a dramatic increase in MuSK phosphorylation overwhelming the inhibitory effects of Total IgG and IgG4 antibodies ($p<0.0001$) (Figure 3.17A). Conversely, MuSK phosphorylation was not affected by IgG1-3 and, even more notably, the SHP inhibition did not show any effect.

An AChR clustering experiment was conducted in parallel with the phosphorylation analysis. Myotubes were exposed to the same amount (0.5 nM) of each MuSK IgG subclass and, after 30 minutes of incubation, agrin and NSC-87877 were added to the medium. After overnight incubation, the AChR clusters were counted. Notably, all MuSK IgG subclasses prevented the formation of AChR clusters despite the presence of agrin, including the IgG1-3 that did not appear to have any effect on MuSK phosphorylation (Figure 3.17B). In this case, SHP2 inhibition by NSC-87877 increased AChR clustering in all the samples ($p<0.01$ compared total IgG, $p<0.05$ to IgG1-3,



Sample	P-Tyr densitometry	MuSK densitometry	P-Tyr / MuSK
DMEM	946.891	15637.861	0.06055118
agrin	9643.912	14330.033	0.67298603
Total IgG	4039.627	3974.134	1.01647982
Total IgG + NSC-87877	10356.083	5516.598	1.87725896
IgG4	566.062	4677.426	0.12101998
IgG4 + NSC-87877	6903.276	4054.79	1.70249902
IgG1-3	12864.77	13481.447	0.95425736
IgG1-3 + NSC-87877	8873.619	10100.033	0.87857327

Figure 3.17. NSC-87877 protects MuSK phosphorylation from MuSK Total IgG and IgG4, and prevents AChR clustering dispersal in the presence of all MuSK IgG subclasses. Agrin-stimulated myotubes were exposed to purified MuSK Total IgG, IgG4, and IgG1-3 antibodies (adjusted to 0.5 nM) in the absence and presence of NSC-87877. **(A.1)** Example of phosphorylation blots. MuSK was immunoprecipitated by anti-MuSK AF562 in agrin and DMEM controls, and directly by patients' own antibodies in the other samples. Densitometry results of the representative western blot are indicated in the table below the graphs. (**A.2**) Pooled densitometry results show that Total IgG and IgG4 inhibited MuSK phosphorylation and this was increased substantially by NSC-87877. Conversely, IgG1-3 did not inhibit MuSK phosphorylation and NSC-87877 had no effect. **(B)** Agrin-stimulated myotubes were exposed for 16 hours to MuSK IgG antibody subclasses and stained for AChR clustering with fluorescent α-bungarotoxin. (**B.1**) Examples of AChR clusters. **(B.2)** Pooled results show that all IgG subclass fractions, including IgG1-3, inhibited the formation of AChR clusters, which in each case were increased by NSC-87877. Two-sided t tests were used for comparisons at each IgG concentration. Mean + SEMs are shown.

$p<0.001$ to IgG4) showing a therapeutic effect regardless of the individual MuSK antibody subclass.

3.3 Discussion

The experiments described in this chapter represent a continuation of the preliminary research work carried out in our lab by Dr Saif Huda who firstly studied the effects of SHP2 inhibition on AChR clustering in the presence of plasma from MuSK-MG patients. In order to preserve interexperimental consistency, particular attention was paid to use the same materials of Dr Huda including cell lines, antibodies, plasmids, and plasma samples from myasthenic patients. For this reason, the short form of agrin was chosen instead of the full-length protein for the physiological stimulation of MuSK. Agrin's effects were titrated measuring the number of AChR clusters induced by serial dilutions of the protein. As mentioned above, the dilution that provided a 50% increase of the clusters (1:800) was chosen for all the subsequent experiment as, being submaximal, it allowed a more sensitive detection and comparison of the effects induced by the inhibition of SHP2. AChR clusters were counted automatically using a macro of the ImageJ software which discriminates the clusters from the background of the myotubes according to the pixels' brightness and size. This guarantees a higher intra- and inter-experimental consistency as the cluster number is less influenced by the intrinsic human bias related to manual counting.

The quantification of the western blots to estimate the phosphorylation level of MuSK was, however, less straightforward. Despite the fact that all the experimental procedures were performed rigorously and consistently, the immunoprecipitation of MuSK showed variability among samples for both phosphorylation and expression of the protein. This was likely related to the intrinsic quality of the differentiated myotubes, the efficacy of the cell lysis, and the stripping of the nitrocellulose membrane. In addition, due to the

low volume (about 50 µl) of the immunoprecipitated sample and the instability of the phosphorylation signal, a loading correction according to the protein concentration (estimated by BCA assay) was considered not appropriate. Instead, the normalised result was obtained calculating the ratio between the density of the phosphorylation band and the corresponding level of protein expression in the stripped blot. Due to the immunoprecipitation variability, however, each blot required different developing times to provide a non-saturating appearance of the bands for a reliable densitometry measurement. Moreover, to evaluate correctly the density analysis, variations in contrast and brightness of each blot should be considered when comparing different images (as described in detail in Chapter 2). This interexperimental variability explains why it was difficult to provide representative western blots that matched the quantitative scatter plots.

Initial experiments were carried out to determine which posology and incubation time were the most appropriate to evaluate the effect of NSC-87877 on MuSK phosphorylation and AChR clustering. The initial incubation time of 40 minutes was decided according to previous studies (Herbst and Burden 2000, Huijbers, Zhang et al. 2013) and further confirmed by a time-course experiment. NSC-87877 determined a dose-dependent increase of both MuSK phosphorylation and AChR clustering, consistently reaching the maximal effect at a concentration of 100 µM. This complements the original observations by Zhao and colleagues in which a significant increase in AChR clustering was observed at 0.1 – 1 µM of the compound (Zhao, Qian et al. 2007). Notably, higher concentrations showed no effectiveness and caused an opposite, paradoxical effect suggesting a loss of specificity in the mechanism of action of NSC-87877. Nevertheless, the addition of agrin was still able to activate MuSK even at the highest concentration of NSC-87877 tested.

During the phosphorylation time-course, both NSC-87877 and agrin activated MuSK in a similar pattern, with a progressive increase in the phosphorylation signal reaching the maximal level between 40 and 90 minutes. When the myotubes were exposed to NSC-87877 and agrin simultaneously, the combined effect was significantly higher compared to NSC-87877 alone, suggesting a synergistically effect in the activation of the clustering pathway.

The membrane expression of MuSK was found to be unmodified by SHP2 inhibition. This could be due to a potential bias introduced by normalising the level of immunoprecipitated MuSK to the α-tubulin which is present only in the total cell lysate (and not in the immunoprecipitated fraction). Therefore, correlation between the levels of the two proteins needs further investigation. On the other hand, agrin and NSC-87877 (individually and when combined together) increased the membrane expression of the AChRs in the radioactive assay. This might be related to a more efficient binding and precipitation of the clustered receptors to the radioactive bungarotoxin, although a direct transcriptional upregulation could also be involved. It was previously suggested that SHP2 reduces the expression of AChRs by inhibiting the neuregulin pathway (Tanowitz, Si et al. 1999) and this is supported by our RNA sequencing results in which NSC-87877 increased the expression of neuregulin-1 and the neuronal variant of the AChR–α subunit.

SHP2 inhibition by NSC-87877 had no effect in the *MUSK KO* and mutant cell lines in activating the clustering pathway, supporting the hypothesis that MuSK is essential for the formation of AChR clusters, and that the main mechanism of action of the compound relies on targeting MuSK phosphorylation. In addition, even in the presence of a functional MuSK, DOK7 was required for NSC-87877 to be effective. Notably, in the mutant *DOK7* cell line, the endogenous *DOK7* WT was still expressed alongside the 1124_1127dupTGCC mutation. However, as shown in the western blot (Figure 3.7B1),

the expression of the truncated protein was markedly higher compared to the endogenous wild type, indicating that the mutant DOK7 was the dominant form. This unbalanced expression in favour of the mutant DOK7 likely prevented the interaction between the wild type protein and MuSK, suppressing the stimulation of the AChR pathway induced by NSC-87877.

As shown by the transcriptomic analysis, the myotubes reacted to the exposure to NSC-87877 by inducing genes involved in the cell metabolism with the likely aim of eliminating the drug and its metabolites, as this is the primary function of the members of the Cytochrome P450 family (Manikandan and Nagini 2018) which were found to be among the genes with the highest upregulation after exposure to NSC-87877. This is not surprising considering the molecular structure of NSC-87877, which is a xenobiotic chemical with 4 aromatic-carbon rings. This also explains the upregulation of the second most expressed protein, Aryl-Hydrocarbon Receptor Repressor, which is likely induced to balance the activity of the cytrochromes (Yamamoto, Ihara et al. 2004). The upregulation of other molecules such as Zinc Transporter 10, Phosphatidylinositol Transfer Protein 1, Prostaglandin-Endoperoxide Synthase 2, and Pentraxin 3 indicates the activation of other detoxicating processes and the production of acute-phase proteins linked to inflammation (Alles, Bottazzi et al. 1994, Garner, Hunt et al. 2012, Gao, Zhao et al. 2017).

Only a few genes among those modified by NSC-87877 showed possible direct connections with the AChR clustering pathway. Specifically, the neuronal isoform of the α-subunit of the AChR (Chrna10) was found significantly upregulated. In humans, this isoform is expressed mainly in the neuroepitelium of the inner ear and in lymphoid cells, and the meaning of its upregulation in the myotubes remains unclear (Lustig, Peng et al. 2001). On the other hand, a previous study (Tanowitz, Si et al. 1999) observed an upregulation of the εAChR following SHP2 inhibition but no direct evidence of this was

found in the current transcriptomic analysis. It is worth noting, however, that the concomitant upregulation of Neuregulin-1 by NSC-87877 might indicate that the ε subunit is upregulated indirectly by the drug through the mediation of Neuregulin itself (which has been associated with the increased expression of the εAChR through the activation of the ErbB/Erk kinases (Tansey, Chu et al. 1996, Yang, Huang et al. 2005)). Moreover, The NKD Inhibitor Of Wnt Signaling Pathway 2 was also upregulated by NSC-87877, which suggests the activation of an additional negative feedback regulation as the Wnt pathway is supposed to co-operate with MuSK in the activation of the AChR clustering pathway (Henriquez, Webb et al. 2008, Wang, Ruan et al. 2008).

As expected, the purification of MuSK antibody subclasses showed a marked prevalence of the IgG4 subtype compared to the IgG1, 2 and 3. An antibody concentration of 0.5 nM was chosen as, at this concentration, the level of immunoprecipitated MuSK was comparable between patients' antibodies and the commercial AF562. This antibody concentration was suitable for studying the effects of MuSK IgG4, considering their high yield obtained during purification. However, in order to use the same concentration of MuSK IgG1-3, a significant amount of sample (up to 500 μl of undiluted preparation for each experiment) was necessary. This led to a shortage of materials from the patients initially used for antibody purification. Attempts to scale down the experiments to reduce the volume of material needed (using 24- instead of 6-well plates) resulted in unreliable immunoprecipitation results. A second round of purification was therefore required, and the yield of IgG1-3 antibody was improved by pooling together the samples from 5 additional patients, selected according to their higher positivity for MuSK IgG1-3 in the CBA. In addition, the dot blots resulted to be a quicker and more sensitive method to determine the efficacy of the antibody purification compared to the CBA.

In the final experiments illustrated in this chapter, the myotubes were incubated with the different MuSK antibody subclasses followed by exposure to NSC-87877, to study whether the compound was able to protect the AChR clusters from the detrimental effects of the antibodies. The inhibition of SHP2 significantly increased MuSK phosphorylation despite the presence of MuSK Total IgG and IgG4. The dispersal of AChR clusters was prevented in all the samples, including the IgG1-3, as previously observed by Koneczny and colleagues (Koneczny, Cossins et al. 2013). Notably, MuSK IgG1-3 did not reduce MuSK phosphorylation whereas they were still able to disperse the AChR clusters. In this case, NSC-87877 did not modify significantly MuSK phosphorylation although it was still able to prevent the dispersal of AChR clusters induced by the MuSK IgG1-3. From a technical perspective, it is worth mentioning that the immunoprecipitation of MuSK in the IgG1-3 sample was initially unsuccessful due the high concentration of non-specific IgG1-3 in the preparation, which competes with the MuSK antibodies for the binding to the Protein G beads. This was prevented by the addition of a washing step after incubating the myotubes with the sample and before cell lysis, to eliminate the soluble antibodies not bound to MuSK.

The results illustrated in this chapter provide initial *in vitro* evidence to support the inhibition of SHP2 by NSC-87877 as a therapeutic strategy in MuSK myasthenia. The next chapter will further develop this aspect of the project by studying the effectiveness and safety of NSC-87877 in different *in vivo* models. In addition, several questions arised regarding the pathogenic mechanisms by which MuSK IgG1-3 impair AChR clustering without apparently affecting MuSK phosphorylation. These aspects will be will be further investigated in Chapter 5 and 6 of this thesis.

Chapter 4

Safety and efficacy of NSC-87877 *in vivo* and purification of recombinant MuSK for active immunisation

4.1) Introduction

Considering the promising results in the myotubes shown by NSC-87877 in improving MuSK phosphorylation and AChR clustering even in the presence of MuSK antibodies, the next step was to test whether the compound was safe to be administred *in vivo* and, most importantly, whether it was effective in increasing MuSK phosphorylation in both wild type and myasthenic animals.

SHP2 inhibition (by NSC-87877 or other similar compounds) already showed efficacy as a potential therapy in different tumour models due to the involvement of SHP2 in promoting cell replication (Li, Kang et al. 2014, Bunda, Burrell et al. 2015, Shi, Ma et al. 2015, Dayot, Speisky et al. 2018). Although this therapeutic strategy improved the clinical phenotype in each model tested, with no recorded side effects, only one study showed a direct increase of protein phosphorylation (p53) after intraperitoneal injection of NSC-87877 at 30 mg/kg in a neuroblastoma model (Shi, Ma et al. 2015). Moreover, the dose of the drug was extremely variable among the studies – from 1 mg/kg to 30 mg/kg – and it was determined empirically in the absence of standardised methods to measure its concentration and efficacy.

Notably, the inhibition of SHP2 has never been tested in myasthenic models of either autoimmune or congenital aetiology. In this respect, in order to widen the range of potential therapeutic targets, it was decided to include in the experimental testing a model of AChR deficiency syndrome (γ mouse) that was created in house in 2004 (Cossins, Webster et al. 2004). This is one of the most common form of congenital

myasthenia with an autosomal recessive inheritance in which mutations of the ε subunit impair the function of the adult AChR, with consequent reduced density of the clusters and defect of neuromuscular transmission. A partial function of the receptor is guaranteed by the sustained expression of the foetal γ subunit that compensates for the defective ε (Engel, Ohno et al. 2003). A mouse model ressembling this condition was created by introducing null mutations in the ε subunit gene and overexpressing the human γ subunit in the animal (Cossins, Webster et al. 2004). The transfection of the human γ was necessary as the homozygous *null* ε determines a severe phenotype with the death of the mice after few days after birth, which does not reflect the milder course observed in humans (Missias, Mudd et al. 1997). As the shape and size of the muscle endplates are disrupted in the γ model (Vincent, Cullcandy et al. 1981), it was hypothesised that the sustained activation of MuSK by NSC-87877 might improve the myasthenic phenotype by increasing the AChR clustering and, in this way, theoretically compensating for its deficiency.

Finally, several *in vivo* models of MuSK-MG have been created in the past by either passive or active immunisation (Benveniste, Jacobson et al. 2005, Shigemoto, Kubo et al. 2006, Cole, Reddel et al. 2008, Mori, Kubo et al. 2012, Viegas, Jacobson et al. 2012, Patel, Oh et al. 2014). For the current project, the active immunisation approach was most appropriate, and the extracellular domain of MuSK (ecto-MuSK) purified for this purpose. In this respect, ecto-MuSK has already been shown to be sufficient in inducing the myasthenic phenotype in previous studies (Shigemoto, Kubo et al. 2006, Viegas, Jacobson et al. 2012). However, as it was not possible to pursue independently this route in our lab due to restrictions in the animal project licence, a collaboration was established with Prof. Erdem Tüzün in Istanbul, who has long experience in creating and studying different models of experimental autoimmune myasthenia gravis (EAMG)

(Tuzun, Scott et al. 2003, Tuzun, Berrih-Aknin et al. 2015, Kucukerden, Huda et al. 2016, Ulusoy, Cavus et al. 2017).

4.2) Results

4.2.1) MuSK immunoprecipitation from ex vivo specimens

The immunoprecipitation protocol used to pull down MuSK from cultured cells needed to be optimised for reliable detection of MuSK in *ex vivo* specimens. To preserve phosphorylation, muscle samples from adult wild type C57BL/6 mice (> 8 weeks old, either male or female) were snap-frozen within seconds of culling and dissection. Samples were then subjected to mechanical homogenisation, sonication, and prolonged chemical lysis for 4 hours. As described in Chapter 3 for cultured cells, lysed samples were immunoprecipitated with Protein G magnetic beads pre-incubated with the commercial anti-MuSK AF562, and MuSK expression analysed by western blotting (Figure 4.1A, B). These first attempts provided variable results when MuSK was pulled down from the tibialis anterior, whereas a more promising band at 97 kDa corresponding to MuSK was observed consistently in the tongue specimens (Figure 4.1A).

To further optimise the *ex vivo* immunoprecipitation and improve detection of the MuSK pulled down, a pre-clearing step was introduced before incubating the samples with the anti-MuSK antibody. For these, lysates were first exposed to the Protein G beads in order to remove the endogenous mouse antibodies present in the tissue which can interfere with the specific MuSK immunoprecipitation. As shown in Figure 4.1B, the pre-clearance improved markedly the overall cleanliness of the western blot, avoiding the detection of non-specific bands (present in the non-precleared samples at 65 and 55 kDa), and providing a stronger MuSK signal in the tongue specimen (Figure 4.1B – left columns). Specificity of MuSK immunoprecipitation was also supported by

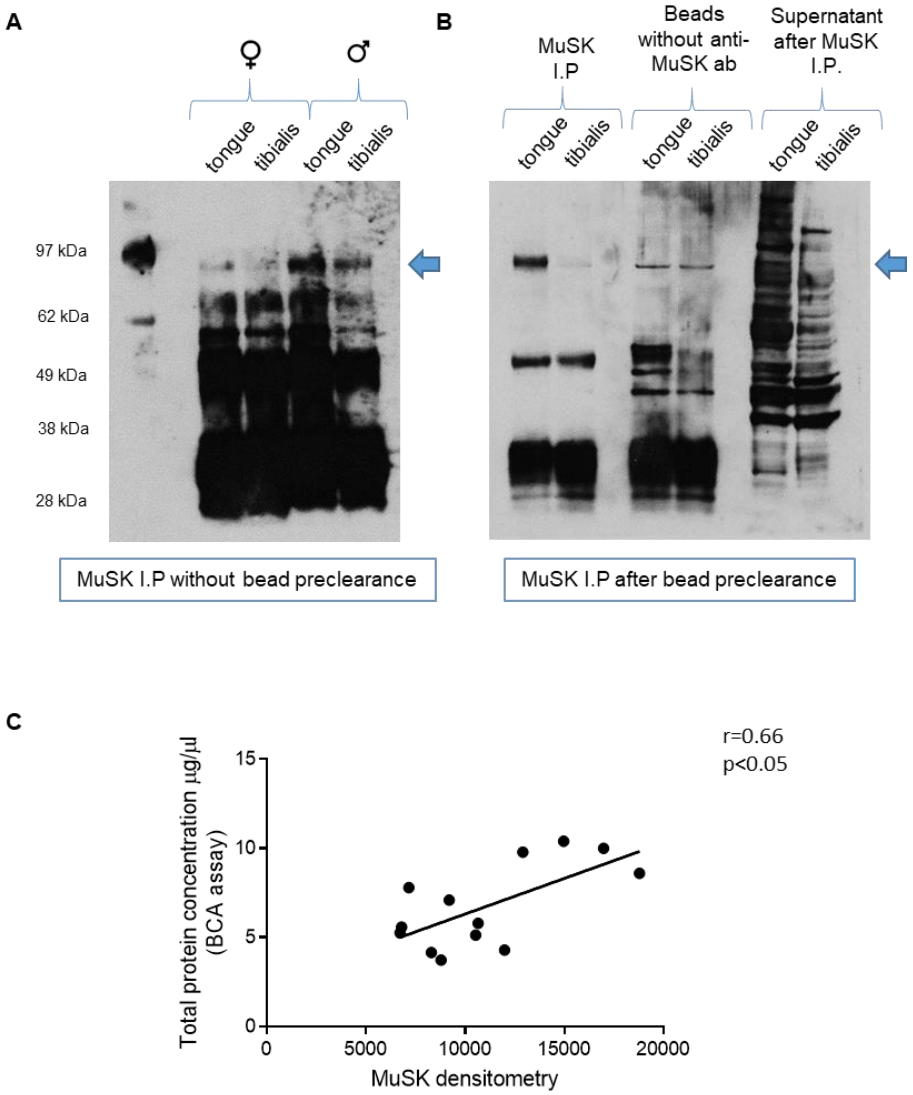


Figure 4.1. MuSK immunoprecipitation from ex vivo specimens. (A) A first attempt to immunoprecipitate MuSK from ex vivo specimens was performed on two different muscle types (tongue and tibialis anterior) after homogenisation and sonication of snap-frozen samples. MuSK was immunoprecipitated with Protein G Dynabeads pre-incubated with anti-MuSK AF562. Tongue specimens from male animals showed initial promising results with a strong band at 97 kDa corresponding to MuSK. **(B)** In order to improve the immunoprecipitation efficacy and selectivity, samples were then precleared with Protein G Dynabeads for 6 hours to reduce the amount of the animal's own antibodies prior incubation with the anti-MuSK commercial AF562 antibody for specific pull-down. Following this additional step, the immunoprecipitation blot appears much clearer and confirms the tongue as the best muscle in which MuSK could be detected. In the control sample with the beads without anti-MuSK AF562 there was a mild band at 97 kDa suggesting minor non-specific binding. Conversely, several non-specific bands were detected in the beads' supernatant. Although a faint signal is present at the correct size of 97 kDa, it is not possible to determine whether that band corresponds to MuSK or to a different protein that runs at the same molecular size which is also detected by the antibody. **(C)** A linear correlation ($r=0.66$; $p<0.05$) was found between the density of the western blot bands of immunoprecipitated MuSK from tongue samples and the total protein concentration in the muscle lysate measured by BCA assay.

the absence of a MuSK band in the supernatant of the IP beads (Figure 4.1B – right columns). In addition, to rule out that the band corresponding to MuSK was not caused by a non-specific, antibody-independent pull-down, samples incubated directly with the Protein G beads (in the absence of the antibody against MuSK) were processed and probed under the same experimental conditions (Figure 4.1B – central columns). A faint band was detected at 97 kDa, although its appearance was different in intensity and shape to that with anti-MuSK and was considered irrelevant.

Finally, the amount of immunoprecipitated MuSK was related to the protein concentration in the tissue lysates. The total protein concentration was measured in the lysates of 13 tongue specimens by colourimetric BCA assay and plotted against the density of the MuSK band calculated with ImageJ software (Figure 4.1C). A linear correlation was found ($r=0.66$; $p<0.05$) suggesting that the amount of immunoprecipitated MuSK broadly reflected that originally present in the tissue.

4.2.2) Treatment trial with NSC-87877 in wild type mice

Once the immunoprecipitation protocol was optimised, the next experimental step was to evaluate whether the administration of NSC-87877 was safe to use in the animals and was able to increase MuSK phosphorylation. A total of 16 C57BL/6 wild type mice (8 males and 8 females) of 10-weeks of age were divided into 4 cohorts of 4 animals each, with an equal distribution of males and females. NSC-87877 was administered with daily intraperitoneal injection for 7 days at 3 different dosages (30, 60, and 120 mg/kg), with the fourth cohort treated with SHAM (0.9% saline solution). The mice were weighed daily and inspected for any clinical sign of distress, such as reduced mobility, arched posture, respiratory impairment, or piloerection. For the duration of the treatment with NSC-87877, all the animals looked healthy, with normal behaviour and without showing any visible distress, adverse reactions or weight loss (Figure 4.2A).

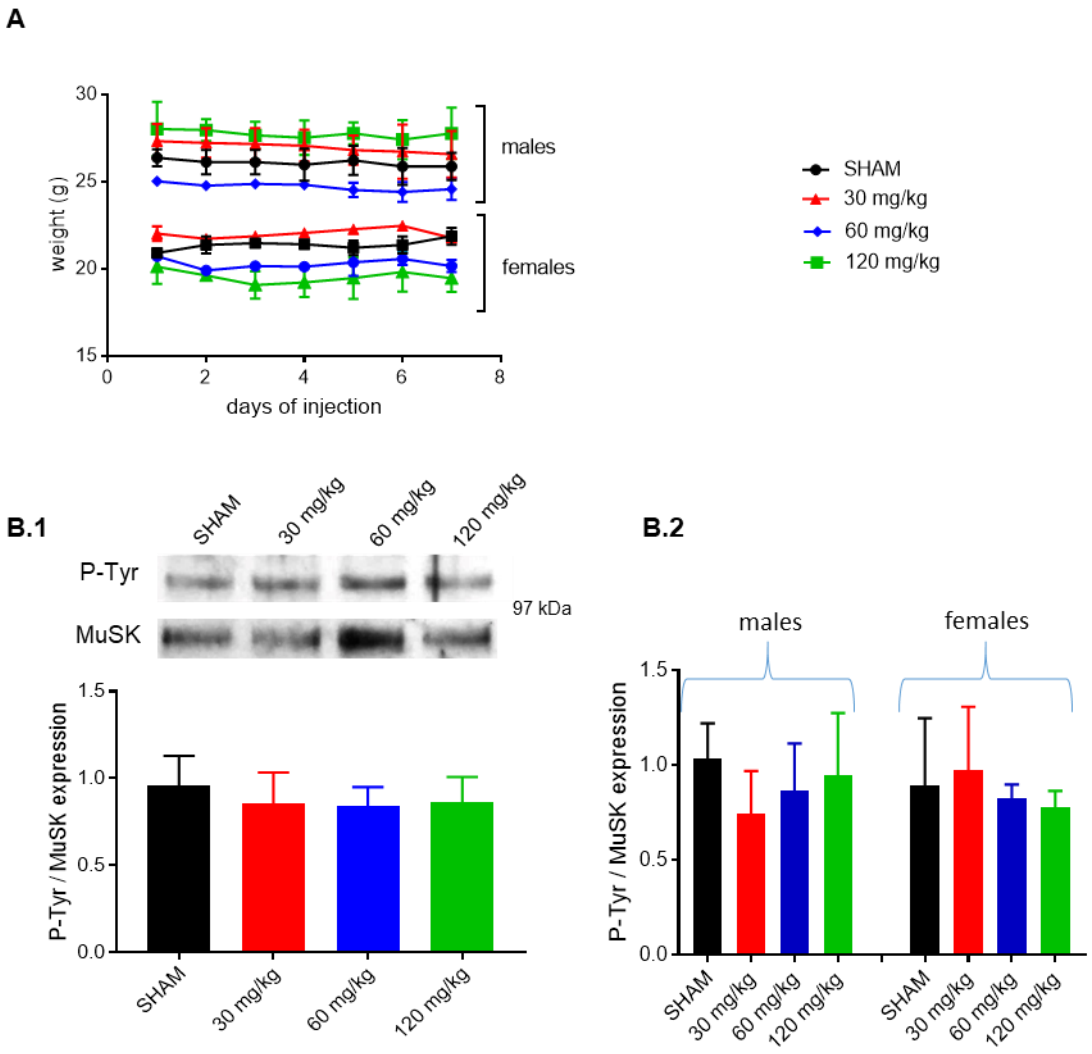


Figure 4.2. Treatment trial with NSC-87877 in wild type mice. Daily injections of NSC-87877 (30, 60, and 120 mg/kg) or an equal volume of SHAM, were administered for 7 days to 4 cohorts of 10-weeks old C57BL/6 wild type mice (2 males and 2 females in each cohort). Mice did not show any distress, side effects and weigh loss **(A)** during drug administration. However, MuSK phosphorylation analysis of tongue specimens did not show any significant difference among the 4 cohorts **(B.1)** and between sexes **(B.2)**. One-way ANOVA with multiple comparison against SHAM.

When MuSK phosphorylation was analysed in the *ex vivo* specimens, however, no significant differences were found between treated and untreated animals, regardless of the dosage of the SHP2 inhibitor (Figure 4.2B1). A similar result was observed when the data were analysed dividing the animals according to their gender (Figure 4.2B2).

4.2.3) MuSK phosphorylation analysis in AChR deficiency syndrome model mice

The phosphorylation results of the previous experiment raised the question as to whether a wild type mouse is an appropriate model to test the SHP2 inhibitor. Under physiological conditions MuSK could be already maximally activated by agrin, and further increase in its phosphorylation by NSC-87877 might not be achievable. As a model of autoimmune MuSK myasthenia was not available, further testing of the drug was performed on a congenital myasthenia model of AChR deficiency syndrome (γ model) readily available in our lab.

First, MuSK phosphorylation was measured in the γ model to evaluate whether its level was changed. A total of 10 animals (5 γ models, and 5 littermate C57BL/6 wild type controls) were culled at the age of 10 weeks and MuSK phosphorylation analysed in the tongue specimens. As shown in Figure 4.3A, MuSK phosphorylation was mildly decreased ($p<0.05$) in the affected animals compared with the wild type mice, representing a possible candidate for the treatment with NSC-87877.

As protein phosphorylation is usually a quick intracellular process, a pilot study was performed to test potential short-term effects of SHP2 inhibition. 6 γ model animals were equally subdivided in two groups, one injected with a single dose (30 mg/kg) of NSC-87877, and the other with a corresponding volume of SHAM (Figure 4.3B). The mice were culled 3 hours after drug administration, and tongue specimens collected immediately afterwards. However, when MuSK phosphorylation levels were analysed, there were no differences between treated and untreated animals.

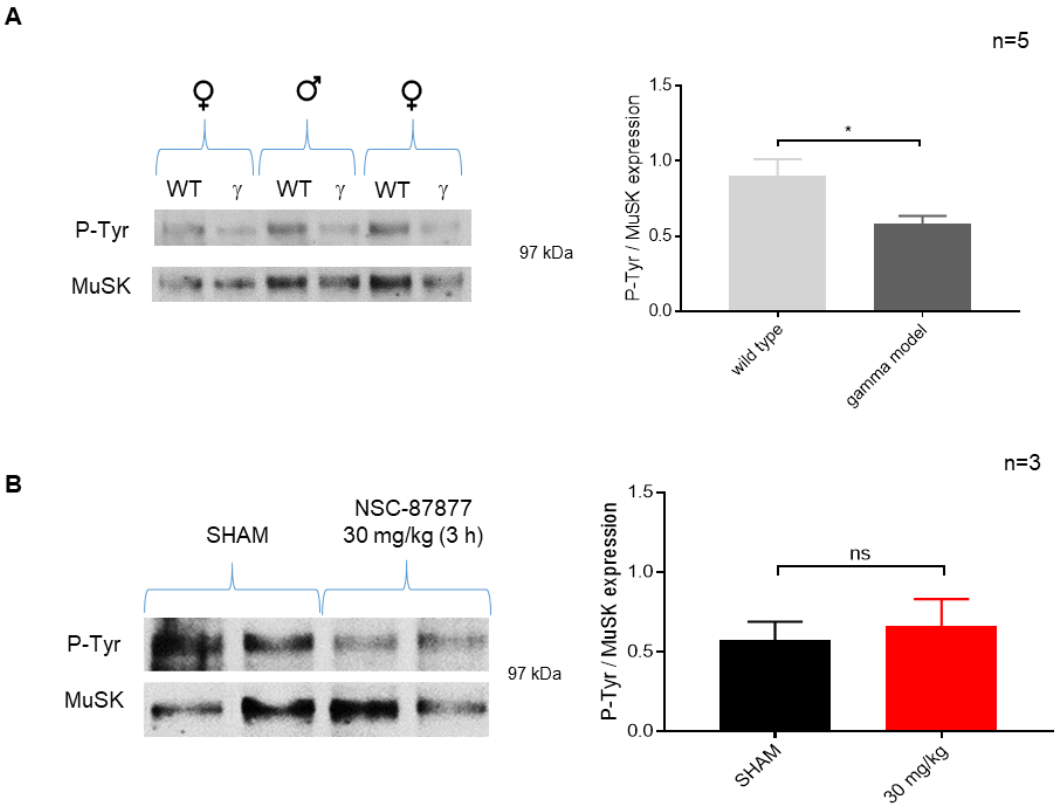


Figure 4.3. MuSK phosphorylation analysis in AChR deficiency syndrome model mice (γ model). Muscle specimens (tongue) were collected from 5 wild type and 5 AChR deficiency syndrome model mice (10 weeks old) and MuSK immunoprecipitated from muscle lysates. **(A)** MuSK phosphorylation decreased in the mice expressing the γ subunit ($p<0.05$, Student's t). **(B)** A pilot trial with a single dose of NSC-87877 30 mg/kg was performed in 3 AChR deficiency model mice. Samples were collected 3 hours after drug administration and analysis performed on tongue specimens. No significant difference was found in MuSK phosphorylation levels between treated and untreated animals. Statistical analysis was carried out using unpaired t-test.

4.2.4) Treatment with NSC-87877 does not improve the clinical phenotype of the AChR deficiency model

To evaluate potential long term clinical effects of the NSC-87877, two additional treatment protocols were tested on the γ model. In the first study (Figure 4.4A), 6 male model mice of 9 weeks of age were equally divided into two cohorts and treated either with 10 mg/kg of NSC-87877 or SHAM. At this age, mice are starting to express the myasthenic phenotype and their muscle strength decreases progressively until reaching a plateau when they are 12 weeks old (Cossins, Webster et al. 2004). After randomly dividing the mice in the two groups, their baseline fatigable weakness was evaluated with the inverted screen test. This also helped to accustom the animals to the handling and to the inverted screen, allowing for more reliable measurements. NSC-87877 was injected intraperitoneally daily for 21 consecutive days, and the mice were weighed and assessed every 2 days with the inverted screen test. No differences were observed in the cumulative hanging time between treated and untreated animals, and the drug did not slow or prevent the deterioration in muscle strength over time (Figure 4.4A1). Notably, the weight gain in the mice treated with NSC-87877 was lower compared to the animals injected with SHAM, although the difference was not statistically significant (Figure 4.4A2).

A second treatment protocol was tested on 4 model mice of 15 weeks of age, when the myasthenic phenotype is fully expressed (Figure 4.4B). The mice were subdivided in two groups and treated for 1 week with daily intraperitoneal injections either of NSC-87877 30 mg/kg or SHAM. Similar to the previous protocol, mice were subjected to the inverted screen test 4 days before starting the administration of the drug to accustom them to the handling and to record the baseline level of muscle fatigability. After starting the treatment, the animals were assessed and weighed every day, and cumulative measurements using the inverted screen test were recorded immediately

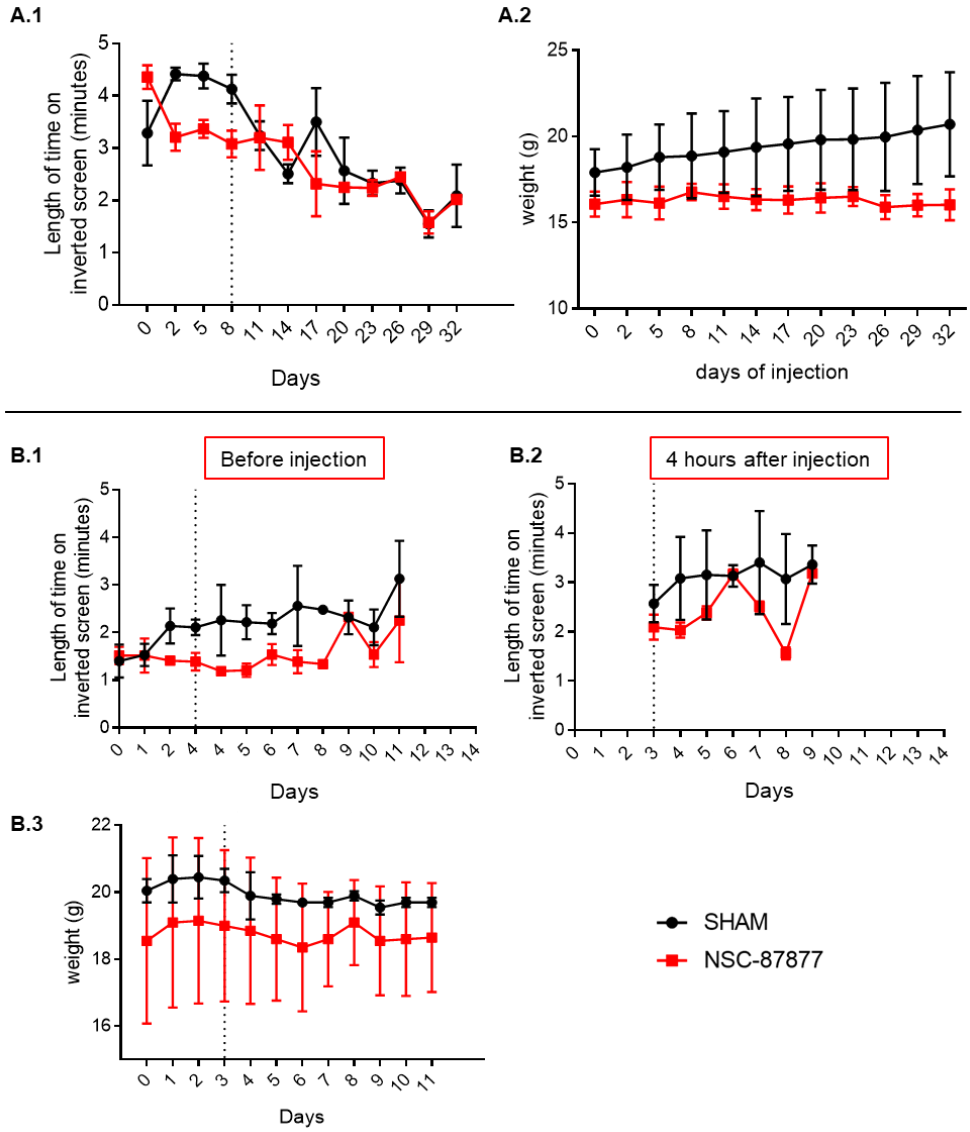
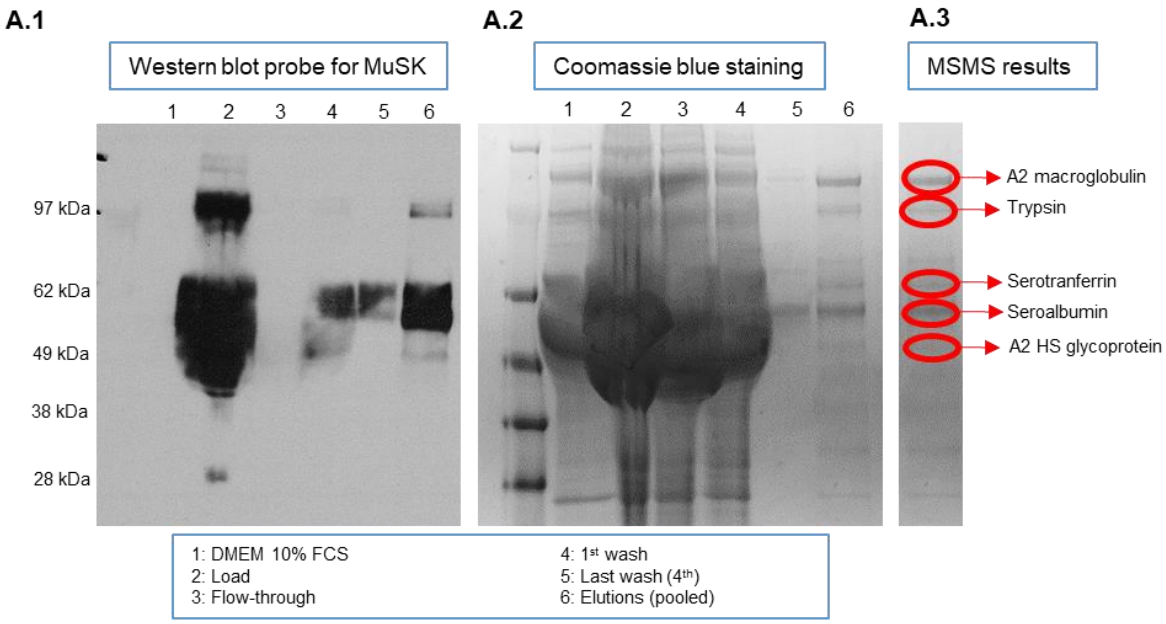


Figure 4.4. Two different treatment protocols with NSC-87877 did not improve the clinical phenotype of the AChR deficiency model. (A) From a cohort of 6 model mice (all males – 9 weeks old), 3 animals were injected with NSC-87877 10 mg/kg, and the remaining 3 with an equivalent volume of SHAM. From day 1 to day 8, an inverted screen test was performed to accustom the animals to handling and to record the baseline values for each mouse. Injections started on day 9 (vertical dotted line) and were performed daily for 21 days. **(A.1)** No differences were observed in the cumulative hanging time (3 subsequent attempts without resting) between the two groups. **(A.2)** Mice injected with NSC-87877 did not gain weight during the administration of NSC-87877 compared to those injected with SHAM. **(B)** A second treatment protocol was performed in 2 model mice (15 weeks old) which were injected daily with NSC-87877 30 mg/kg or SHAM from day 4 (dotted line) to day 12. Inverted screen test hanging time was recorded daily immediately before **(B.1**) and 4h after **(B.2)** drug administration**.** Mice treated with NSC-87877 did not show any significant improvement and hanging times were comparable to pre-treatment values or to the controls. On average, both treated and untreated mice performed better 4h after injection likely due to the circadian rhythm of the animals. No differences were found between the weight of treated and untreated mice **(B.3**) although treated mice were smaller on average. Grouped statistical analysis was carried out with multiple t-tests comparing the two cohorts at each time point.

before the injection, and 4 hours after injection, to evaluate potential short lasting effects of the drug. Despite the increased dosage of the drug compared to the previous protocol, the mice treated with NSC-87877 did not show any improvement in their strength (Figure 4.4B1), although both treated and SHAM treated mice performed better 4 hours after injection (Figure 4.4B2). All animals maintained a stable weight with minimal variations during the whole duration of the experiment regardless of their treatment, and no statistical difference was observed between the two groups (Figure 4.4B3).

4.2.5) Purification of recombinant MuSK

The lack of positive results obtained in wild type and AChR deficiency animals highlighted the need to test the compound in a proper *in vivo* model of MuSK-MG, for which NSC-87877 had previously shown encouraging data in the *in vitro* work (see Chapter 3). An active immunisation approach was chosen. A first attempt to produce and purify the amount of recombinant MuSK needed for the immunisation was performed by inducing a transient expression of the MuSK extracellular domain (ecto-MuSK) in HEK 293T cells (Figure 4.5). Ecto-MuSK is secreted into the culture medium, and a tag sequence of 6 histidine residues was included at the C-terminus to allow for the purification by metal (nickel) ion affinity chromatography. 500 ml of conditioned medium was collected 48 hours after transfection, concentrated about 10-fold, and then exposed to the nickel resin. To eliminate potential contaminants with low-affinity binding to the resin, the column was washed with a solution with low imidazole concentration (10 mM), and then exposed to a high concentration (500 mM) imidazole to elute the MuSK protein. The volumes and concentrations measured with the NanoDrop of each purification fraction are indicated in Table 4.1. Western blot analysis (Figure 4.5A1) of the purification fractions (load, flow-through, first and last


A.1
Western blot probe for MuSK
1 2 3 4 5 6
97 kDa
62 kDa
49 kDa
38 kDa
28 kDa
A.2
Coomassie blue staining
1 2 3 4 5 6
A.3
MSMS results
A2 macroglobulin
Trypsin
Serotranferrin
Seroalbumin
A2 HS glycoprotein
1: DMEM 10% FCS
2: Load
3: Flow-through
4: 1st wash
5: Last wash (4th)
6: Elutions (pooled)

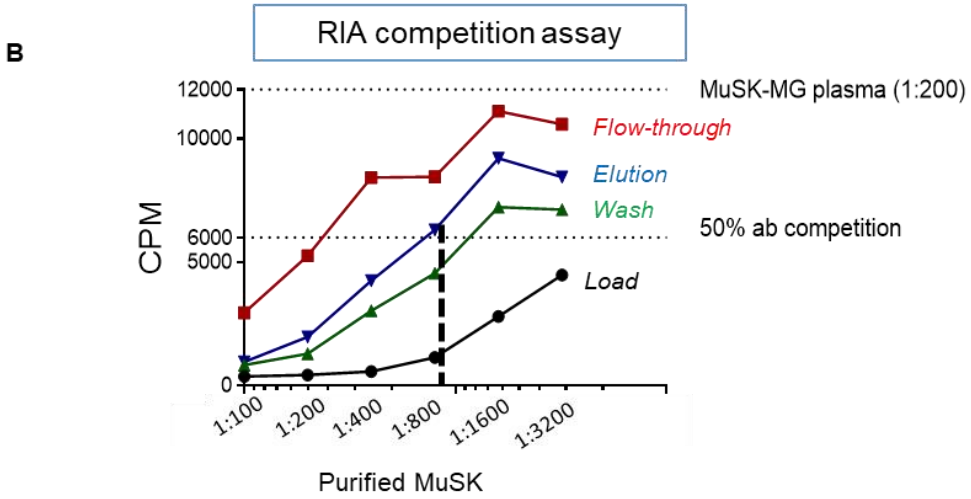

B
RIA competition assay
12000
10000
6000
5000
0
CPM
MuSK-MG plasma (1:200)
Flow-through
Elution
Wash
50% ab competition
Load
1:100
1:200
1:400
1:800
1:1600
1:3200
Purified MuSK

Figure 4.5. Purification of MuSK extracellular domain expressed in HEK 293T cells. HEK 293T cells were transiently transfected with MuSK extracellular domain (ecto-MuSK) expressed with a C-terminus HIS-tag and MuSK purification attempted by nickel chromatography. **(A)** Load, flow-through, washes, and final elution of the nickel column were run on SDS-page. Western blot **(A.1)** probed for MuSK level showed that MuSK was highly expressed in the load (2^{nd} lane) and absent in the flow-through (3^{rd} lane), indicating efficient binding of the recombinant protein to the nickel column. A faint MuSK band was present in the washes (4^{th} and 5^{th} lanes) with a stronger band in the eluted fraction (6^{th} lane). A concomitant gel was stained for Coomassie **(A.2).** A protein pattern comparable to that observed in the DMEM with FCS (1st lane) was present in all the fraction (2^{nd}-4^{th} lanes) until the final wash (5^{th} lane). Five major bands were detected in the elution fraction (6^{th} lane) and analysed through MS/MS **(A.3).** However, MS/MS showed only contaminating proteins, with albumin from the FCF running at a similar size to ecto-MuSK (around 55 kDa). **(B)** In a RIA competition assay, 5 ml of each purification fraction were serially diluted (1:100 - 1:3200) and incubated with ^{125}I-MuSK and MuSK-MG plasma (1:200 – which could immunoprecipitate about 12000 CPM – about 3.6 times less compared to the 43249 nominal CPM ^{125}I-MuSK). Among the different fractions, the load showed the greatest competition for the ^{125}I-MuSK resulting in CPM below 6000 at every dilution. The flow-through showed the weakest competition indicating efficient binding of the MuSK present in the load to the column, whereas the wash and the elution were not very different. At 1:800 dilution of purified MuSK 50% competition was achieved in the elution fraction, indicating about 2.62 $x10^{-3}$ mg/ml of MuSK in the elution (see text for detailed calculation). However, the wash fraction showed greater competition than the elution itself indicating that a significant amount of the target protein was lost before the column elution.

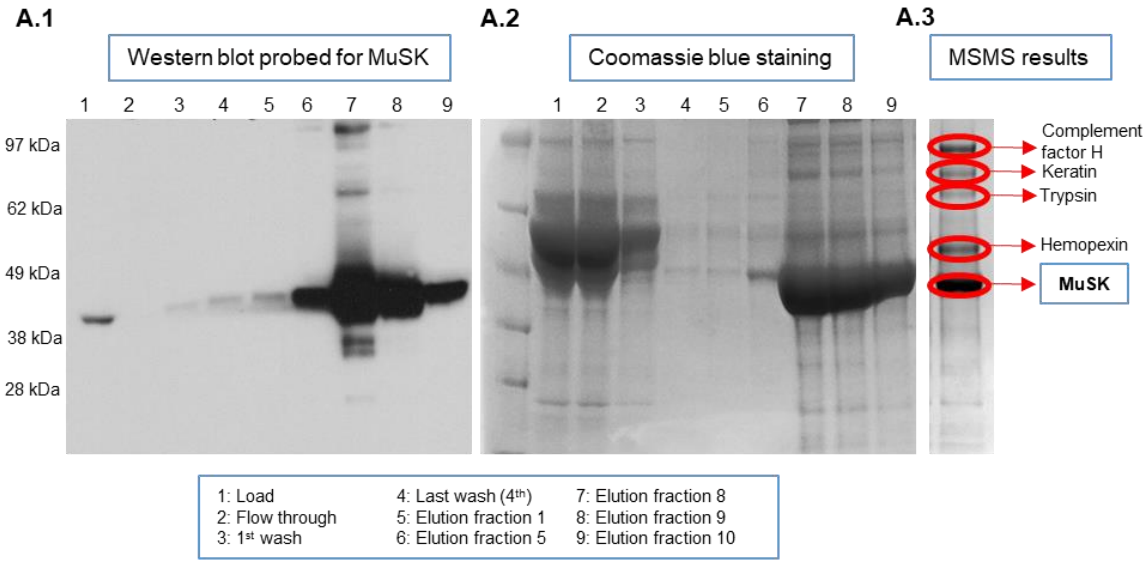
Sample	Volume (ml)	OD280 (μg/ml)
Load	500	3489
Concentrated load	35	23539
Flow-through	35	21062
Wash 1	45	2470
Wash 2	45	247
Wash 3	45	13
Wash 4	45	3
Elution	10	170

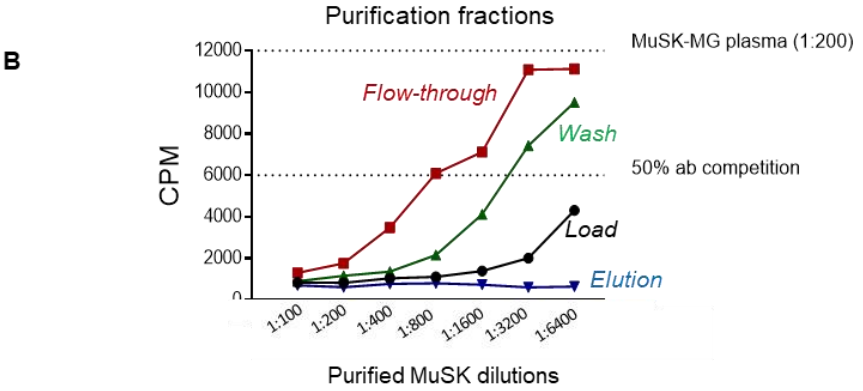
Table 4.1. Summary of the volumes and protein concentrations measured with the NanoDrop (OD290) for each fraction during ecto-MuSK purification in HEK 293T cells.

washes, and pooled final elution) showed that ecto-MuSK, which migrates at approximately around 55 kDa, was strongly detectable in the load and absent in the flow through, indicating efficient binding to the nickel column. The size of ecto-MuSK was predicted to be 49 kDa according to the aminoacid sequence of the plasmid, and the difference observed in the blot is likely related to post-translational modifications of the protein. A faint MuSK band was present in the washes, and a stronger signal was observed in the final elution. A second gel was stained with Coomassie (Figure 4.5A2) and all the protein bands visible in the final elution were sent for MS/MS analysis. However, despite detection of a signal of the appropriate size on the western blot, the MS/MS analysis showed the presence of only contaminating proteins, and predominantly albumin which runs at similar size to ecto-MuSK (Figure 4.5A3).

To quantify more precisely the actual concentration of MuSK in the samples, a competitive RIA was performed. Specifically, considering that the activity of ^{125}I-MuSK in the original batch was 41.1 μCi/μg, the estimated concentration of recombinant MuSK in the elution was 2.62 x10^{-3} μg/μl, for an amount of 26.2 μg (in the total elution volume of 10000 μl). Unfortunately, this does not represent an adequate amount for immunisations.

An alternative Drosophila S2 cell line, stably-transfected with ecto-MuSK, was used to achieve a better yield of recombinant MuSK. This model was kindly provided by Dr Patrick Waters, who previously created it for the original immunisation experiments carried out by Viegas and colleagues in 2012 (Viegas, Jacobson et al. 2012). The Drosophila cells were grown by Dr Wei Liu in our lab, who purified MuSK from the culture supernatants by nickel chromatography as described above (Figure 4.6). The volumes and concentrations of each purification fraction are indicated in Table 4.2. As shown in the western blotting, a small amount of MuSK was detectable in the washes but most of the protein was eluted in the 7th elution fraction (Figure 4.6A1).


A.1
Western blot probed for MuSK
A.2
Coomassie blue staining
A.3
MSMS results
1 2 3 4 5 6 7 8 9
97 kDa
62 kDa
49 kDa
38 kDa
28 kDa
Complement factor H
Keratin
Trypsin
Hemopexin
MuSK
1: Load
2: Flow through
3: 1st wash
4: Last wash (4th)
5: Elution fraction 1
6: Elution fraction 5
7: Elution fraction 8
8: Elution fraction 9
9: Elution fraction 10


B
Purification fractions
MuSK-MG plasma (1:200)
Flow-through
Wash
Load
Elution
50% ab competition
CPM
12000
10000
8000
6000
4000
2000
0
1:100
1:200
1:400
1:800
1:1600
1:3200
1:6400
Purified MuSK dilutions

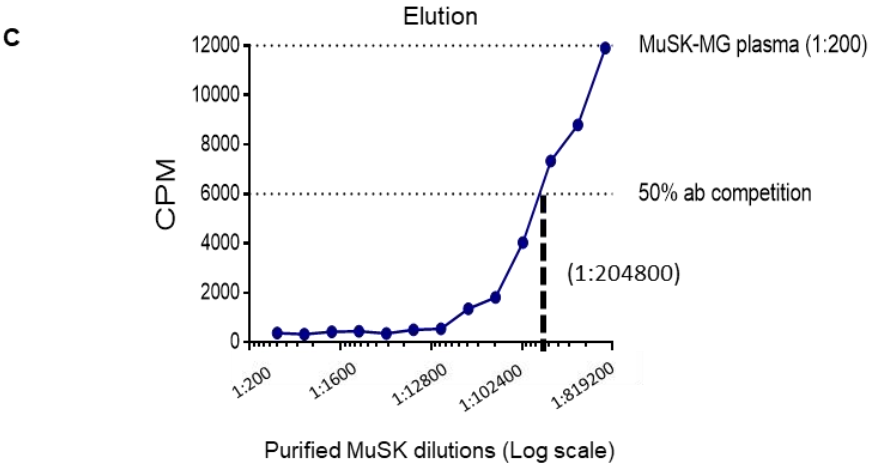

C
Elution
MuSK-MG plasma (1:200)
50% ab competition
(1:204800)
CPM
12000
10000
8000
6000
4000
2000
0
1:200
1:1600
1:12800
1:102400
1:819200
Purified MuSK dilutions (Log scale)

Figure 4.6. Purification of ecto-MuSK in Drosophila S2 cells. **(A)** Drosophila S2 cells were stably-transfected with HIS-tag ecto-MuSK and MuSK purified by nickel chromatography. **(A.1)** Western blot probed for MuSK showed presence of MuSK in the load (1st lane) and not in the flow-through (3rd lane), indicating efficient binding to the nickel column. A faint MuSK band appeared in the washes (3th and 4th lanes) becoming stronger it the elutions (5th – 9th lanes) with a peak in the 8th elution fraction. In parallel Coomassie staining, the load (1st lane) and flow-through had similar protein patterns with less in the washes (3rd and 4th lanes). Most of the MuSK protein was eluted in the 8th elution. **(A.3)** MS/MS on the bands of the pooled elution fractions confirmed the presence of MuSK ectodomain (predicted size of 49 kDa). **(B)** In the RIA competition assay, purification fractions were serially diluted (1:200 – 1:12800) and incubated with ^{125}I-MuSK and MuSK-MG plasma (1:200) as in Figure 4.5. **(B.2)** At the highest dilution (1:12800) of the elution fraction, immunoprecipitation of ^{125}I-MuSK was still completely inhibited. The elution fraction was retested at higher dilutions (up to 1:819200). **(B.2)** At a 1:204800 dilution of purified MuSK, 50% competition was achieved indicating 0.67 mg/ml (see text for detailed calculation).

Sample	Volume (ml)	OD280 (μg/ml)
Load	800	4259
Flow-through	800	4119
Wash 1	30	1469
Wash 2	30	684
Wash 3	30	189
Wash 4	30	134
Elution (pooled)	6	1055

Table 4.2. Summary of the volumes and protein concentrations measured with the NanoDrop (OD280) for each fraction during ecto-MuSK purification in Drosphila S2 cells.

This time, the MuSK band corresponded to the expected size of 49 kDa predicted according to the plasmid sequence. The difference in size compared to that of the HEK cell model is likely due to variations in the mammalian protein's post-translational modifications, which are not carried out in the insect cells. The MS/MS analysis confirmed the presence of MuSK in the corresponding band of the gel stained with Coomassie (Figure 4.6A2 and 3). Using the RIA competition assay, 50% competition between ^{125}I-MuSK and the purified ecto-MuSK was reached at 1:204800 dilution of the recombinant protein indicating a concentration 0.67 μg/μl, for a total amount of 4.02 mg of protein for 6 ml of final elution volume (Figure 4.6B and C), very suitable for immunisations. Considering the high yield of MuSK protein achieved, the pooled elution was then sterile filtered and dialysed against Hartman solution for the immunisations.

4.2.6) Active immunisation of the mice

A first immunisation trial was performed by our collaborator in Istanbul, Prof Erdem Tüzün. 15 Balb/c adult mice were immunised following the protocol outlined in (Ulusoy, Kim et al. 2014) (Figure 4.7A). The animals were divided into two groups. The first consisted of 10 mice injected subcutaneously with 40 μg of MuSK in the presence of Complete Freund's Adjuvant (CFA). The second included 5 mice injected with SHAM containing only CFA with PBS. After 28 days, a booster immunisation in CFA was given. Only 3 out of the 10 mice of the immunised cohort developed a myasthenic phenotype of grade 1 (corresponding to a mild decrease in the mouse spontaneous activity with reduced grip strength) within the following 7 days, and as planned a second booster was performed after a further 28 days. This time, in the first 3 animals the condition worsened to grade 2 (muscle fatigue at rest) and 4 additional mice developed a grade 1 phenotype.

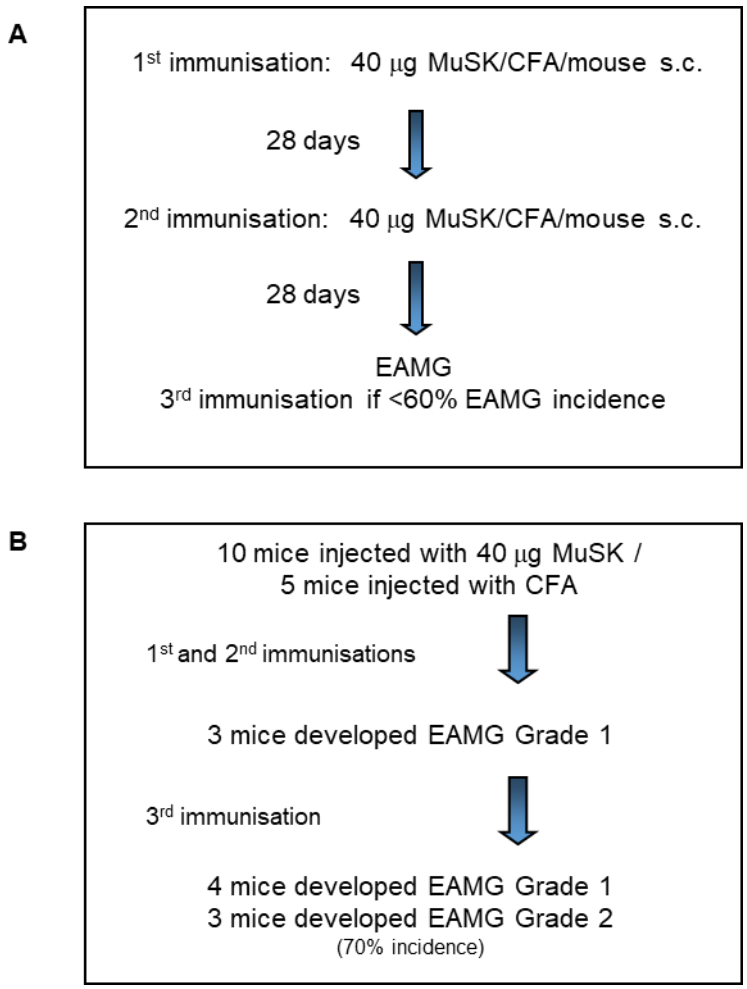


Figure 4.7. Diagram of the protocol to create the MuSK-MG active immunisation model. (A) An initial dose of 40 mg of MuSK ecto-domain (purified as previously described) to be injected subcutaneously in one of the paws of the mouse (BALB/c) with Complete Freund Adjuvant (CFA). A second boost to be performed after 28 days. A final third boost only if the incidence of experimental autoimmune myasthenia (EAMG) animals is lower than 60% of the total number. **(B)** Pilot study of active immunisation involving a total number of 15 mice: 10 immunised with 40 mg ecto-MuSK and CFA, 5 with CFS alone. After the 1st and 2nd immunisation, only 3 mice developed EAMG grade 1. A third boost was necessary to obtain a total number of 7 model mice (4 with EAMG grade 1, and 3 with EAMG grade 2). Performed by Prof Erdem Tüzün, University of Istanbul.

As expected, none of the animals injected with SHAM developed myasthenic features. The final incidence of EAMG achieved was that 70% of the immunised mice developed grade 1 or grade 2 disease (Figure 4.7B).

4.3) Discussion

As described in Chapter 3, SHP2 inhibition by NSC-87877 showed encouraging results in counteracting the effects of the autoantibodies in an *in vitro* model of MuSK-MG. The next experimental step was, therefore, to evaluate its efficacy *in vivo*. However, previously NSC-87877 had been tested in only a small number of animal models – mainly in tumour-related diseases – and data regarding safety and potential therapeutic dosages were limited. In addition, the immunoprecipitation protocol was tailored for cultured cells, and further optimisation was needed in the *ex-vivo* muscle to achieve reliable measurements. The results described in this chapter are, therefore, mainly methodological; they show the optimisation of the immunoprecipitation of MuSK, attempts to identify an effective dose of the compound to use in the animal models, and purification of recombinant MuSK for the creation of an active immunisation model of MuSK-MG.

Immunoprecipitation of MuSK and reliable detection of its phosphorylation level proved to be a challenging task in *ex vivo* samples. Compared to cultured cells, which can be easily lysed due to their loose intercellular binding and the absence of structured connective matrix, *ex vivo* specimens required a longer, multiphasic process to achieve a good level of homogenisation and lysis. This was achieved by mechanical grinding, prolonged (4 h) chemical lysis in a small volume of lysis buffer – to maximise protein concentration – and sonication of the samples for complete membrane disruption. Despite these considerations, the initial attempts to immunoprecipitate MuSK from the muscle specimens proved unreliable, with either complete absence or wide variations in

the amount of MuSK precipitated. In particular, immunoprecipitation was unsuccessful mainly in the tibialis samples, whereas more consistent results were obtained for the tongue. In fact, although Punga et al had reported less MuSK mRNA in the masseter and sternomastoid suggesting that a reduced expression might explain the more severe involvement in the bulbar muscles (Punga, Lin et al. 2011), MuSK protein was previously shown to be better expressed in the tongue compared to the tibialis (Viegas, Jacobson et al. 2012). This fits with the relatively selective impairment of the tongue, with severe weakness and atrophy, in MuSK-MG patients (Farrugia, Robson et al. 2006) although the relationship between MuSK expression and weakness or atrophy is not well investigated.

Improvement in the efficacy of MuSK immunoprecipitation was obtained when a preclearance step was added to the process. When the muscle specimen is harvested, it contains around 10% of mouse IgG from the vessels and the extravascular fluid. This endogenous IgG binds to the Protein G beads alongside the anti-MuSK commercial antibody, potentially pulling down other non-specific proteins. In this respect, the lysate pre-clearance facilitated the immunoprecipitation by eliminating the endogenous IgG and other contaminants that might bind directly to the beads, and potentially decreasing additional non-specific binding to the anti-MuSK antibody itself. Three useful improvements were observed following the lysate preclearance. First, fewer non-specific bands were detected on the western blot. Second, more MuSK was pulled down with a reduction in the exposure times needed for detection (with consequent cleaner blots). Third, MuSK immunoprecipitation was more consistently successful at least for the tongue specimens. Efficacy and specificity of the pull down was supported by the absence of a specific MuSK band in the supernatant from the immunoprecipitated Protein G beads, and in the samples incubated directly with the beads in the absence of the anti-MuSK antibody. Notably, a correlation was found between the density of the

MuSK band and the total protein concentration of the original samples, encouraging evidence of reliability in comparing samples from different animals. It is worth mentioning that the phosphorylation signal was well preserved during the whole process and always detectable when the immunoprecipitation of MuSK was successful. This was guaranteed by the immediate harvesting and snap-freezing of the muscles after culling the animals, by the addition of the phosphatase inhibitor cocktail in the lysis buffer, and by processing the samples at a constant temperature of 4ºC.

Once the immunoprecipitation protocol was optimised, the safety and efficacy of NSC-87877 were evaluated in wild type mice. An arbitrary starting dose of 30 mg/kg was chosen as it was effective in increasing p53 phosphorylation in a neuroblastoma model (Shi, Ma et al. 2015). Two additional doses (60 and 120 mg/kg) were also tested. However, MuSK phosphorylation did not change at any of the doses. It was possible that in wild type mice, MuSK phosphorylation is already maximal and further increases cannot be achieved by SHP2 inhibition. This hypothesis is supported by a previous study in which an increase of phosphorylation was not observed in wild type mice after stimulating MuSK with a specific monoclonal antibody (Cantor, Zhang et al. 2018). Another possible explanation is that the dose administered was too high, causing a detrimental effect on MuSK, which was subsequently counteracted by an upregulation in the secretion of agrin in a homeostatic feedback mechanism to preserve the integrity of the pathway. In the C2C12 model (see Chapter 3), where high concentrations of NSC-87877 failed to increase MuSK phosphorylation, the addition of agrin partially reversed this detrimental effect. Notwithstanding the lack of positive results on MuSK phosphorylation, no major side effects or adverse events were detected at the physical examination of the animals – even at high doses of NSC-87877 – providing reassurance regarding the *in vivo* safety of the compound.

Three treatment protocols with different dosages of NSC-87877 were then tested in a congenital model of AChR deficiency syndrome. However, despite the fact that MuSK phosphorylation was lower in the muscles from this model compared to the wild type muscle, no changes were measured when the short-term effects of the drug were analysed after culling the animals 3 hours after its administration. Moreover, no improvement in muscle fatigability was observed when the model mice were subjected to two prolonged treatment trials (the better performance observed at the second inverted screen test performed in the late afternoon hours is likely due to the circadian rhythm of the animals, which makes them more active at that time of the day, rather than a short term effect of NSC-87877 as no differences between treated and non-treated animals were detected). Only muscle fatigability and weight of the mice were evaluated at this stage, as it was thought unnecessary to embark on the difficult and time consuming analysis of MuSK phosphorylation in the absence of a clear improvement of the mouse phenotype.

One of the main limitations of this set of experiments was related to the small number of animals used for each protocol, which makes it hard to evaluate any potential statistical significance. The number of mice was kept at minimum according to the three "Rs" (replacement, reduction, and refinement) as these were pilot studies from which full scale experiments would have taken place if there were initial encouraging trends. An additional limitation of the experiments is the uncertainty regarding which dose of NSC-87877 to use in the trials. As suggested by the *in vitro* results, the therapeutic window of NSC-87877 is likely to be narrow as a paradoxical effect on MuSK phosphorylation was observed at concentrations higher than 100 μM (see Chapter 3). Unfortunately, it is not possible to convert this concentration to an accurate mg/kg dosage, and data regarding the metabolism and pharmacokinetic properties of NSC-87877 are still not described in the literature.

The absence of positive results in these initial *in vivo* experiments highlighted the need to test NSC-87877 in a more appropriate model of MuSK-MG, for which an active immunisation approach was chosen. In this respect, the first experimental step was to produce and purify a recombinant MuSK to administer to the animals. According to previous immunisation works performed by Jha et al, Shigemoto et al, and by Viegas et al (Jha, Xu et al. 2006, Shigemoto, Kubo et al. 2006, Viegas, Jacobson et al. 2012), the extracellular domain of MuSK (ecto-MuSK) represents a sufficient antigenic stimulus to trigger an effective autoimmune response and induce a myasthenic phenotype in the animals.

Ecto-MuSK was first expressed transiently in mammalian HEK 293T cells using the same transfection technique as that described for cell-based assays. However, despite the high number of transfected plates and the large volume of conditioned medium harvested, the final protein yield was particularly low and insufficient for the immunisations. Although mammalian cells are usually preferred for antigen production, as they are able to express a recombinant protein with their full post-transcriptional changes, the amount of protein produced can often be lower compared to other systems, especially when transfection is transient. In this respect, the stable-transfected line of Drosophila cells was much more effective as shown by the substantive increase in the yield of MuSK observed in western blots, MS/MS analysis, and competitive RIA when the concentration of MuSK increased 256 fold.

Potential further experiments were severely limited by the project licence of our research lab which do not allow the creation of an animal model of experimental autoimmune myasthenia (EAMG), either by active or passive immunisation. Therefore, to verify whether our recombinant MuSK was an effective immunogenic antigen, it was sent for testing to our collaborator in Istanbul, Prof Erdem Tüzün. The pilot experiment showed promising results with up to 70% of the immunised animals developing a

myasthenic phenotype, allowing the possibility of testing NSC-87877 in the autoimmune MuSK-MG model.

Chapter 5

Testing monoclonal anti-MuSK antibodies

5.1) Introduction

After completing the experiments aimed to study the potential role of SHP2 inhibition as a therapeutic strategy in MuSK-MG, the project focused on the pathogenic mechanisms of MuSK antibodies, with a specific interest in evaluating the differences between the predominant MuSK IgG4 and the less characterised IgG1, 2 and 3 subclasses. In this respect, MuSK-MG is known to be mediated mainly by autoantibodies of the IgG4 subclass, which have been shown to be monovalent in their binding to their antigen, after undergoing Fab-arm exchange with other IgG4 of different antigen-specificity under the reducing conditions present in the plasma (McConville, Farrugia et al. 2004, Koneczny, Cossins et al. 2013, Koneczny, Stevens et al. 2017). Due to the structure of their Fc region and the monovalent binding to their antigen, IgG4 do not share the pathogenic mechanisms commonly recognised for IgG1-3 subclasses. Specifically, IgG4 are not able to bind to C1q, which is essential in activating the complement cascade, and they do not cause internalisation of their antigen (Vidarsson, Dekkers et al. 2014). Instead, IgG4 antibodies block protein-protein interactions through direct inhibition and, in the specific case of MuSK-MG, prevent MuSK activation inhibiting its interaction with Lrp4 (Huijbers, Zhang et al. 2013, Koneczny, Cossins et al. 2013, Koneczny 2018).

Notably, all the pathogenicity studies performed so far had to rely on preparations of MuSK antibodies purified from patients' samples, with the intrinsic limitations of this procedure (e.g. contamination with non-specific antibodies and, potentially, with other IgG subclasses, and limited availability of materials). However, due to the high number of circulating MuSK-specific B cells (as indicated by the effectiveness of rituximab

treatment in this form of myasthenia), it became possible, thanks to the advances in the single-cell sorting techniques, to isolate individual plasma cell clones from MuSK-MG patients to selectively produce MuSK monoclonal antibodies (MuSK-mAbs) (Stathopoulos, Kumar et al. 2018, Takata, Stathopoulos et al. 2019). This was achieved by our collaborator in Yale, Prof K. O'Connor, who sent to our lab a selection of the newly produced MuSK-mAbs to test their ability to bind MuSK, and to study their pathogenic potential on MuSK phosphorylation and AChR clustering in the *in vitro* model offered by the C2C12 myotubes. Notably, all the monoclonals were created as divalent, either by substituting their native Fc with an IgG1 or IgG3 backbone, or by preventing the Fab-arm exchange in those antibodies which maintained the original IgG4 structure. For this reason, the monoclonal preparations provided the unique opportunity to evaluate the effects of divalent antibodies on MuSK with high specificity and sensitivity, theoretically resembling the behaviour of the native MuSK IgG1-3 as described in detail in the following paragraphs.

5.2) Results

5.2.1) Radioimmunoprecipitation assay (RIA) of MuSK monoclonal antibodies

A total of 15 different human monoclonal antibodies, derived from control and MG patients and at a nominal concentration of 5 μg/ml, were sent to our lab for blinded testing. Samples were labelled from #A to #O and tested for MuSK antibody positivity by radioimmunoassay (RIA). In the first experiment, each sample was diluted 1:10 from the original 5 μg/ml preparation provided (Figure 5.1 A). An equal amount of plasma (5 μl) from a MuSK-MG patient was used as control. Three monoclonal antibodies (samples #B, #C, and #D) gave a clear positive result although only precipitating around 35-45% of the counts pulled down by the patient's plasma. Samples #A, #E, and #F immunoprecipitated low numbers of counts, only just above the remaining samples

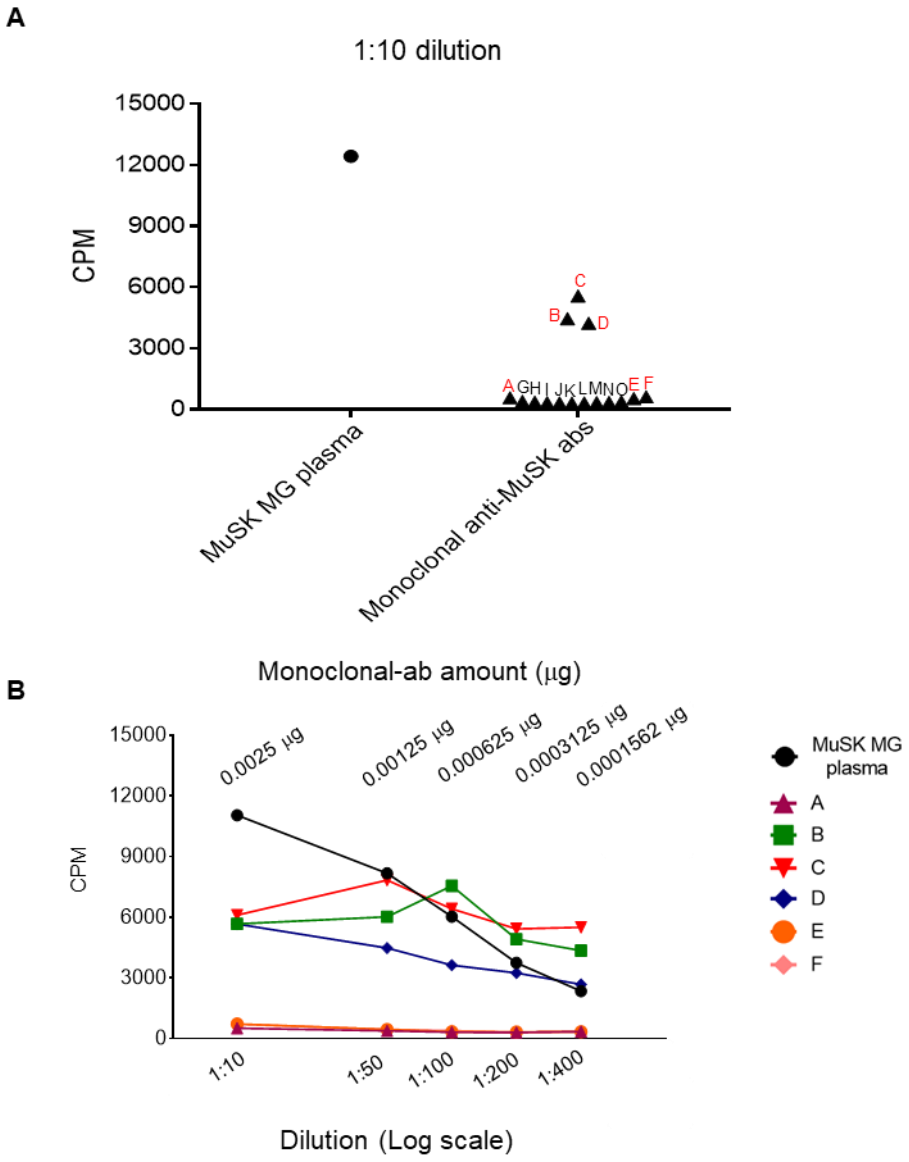


Figure 5.1. Radioimmunoprecipitation assay (RIA) of MuSK monoclonal antibodies. (A) Monoclonal-Abs (#A-#O) were tested blinded in a MuSK RIA at 1:10 dilution of the preparations provided (5 µg/ml). 5 µl of MuSK-MG plasma was used as positive control. Samples #B, #C, and #D were positive and precipitated around 35-45% of the counts of MuSK-MG plasma. Samples #A, #E, and #F immunoprecipitated low numbers of counts, just above samples #G-#O which were subsequently identified as controls. **(B)** RIA for positive samples #A-#F was repeated at different dilutions (1:10, 1:50, 1:100, 1:200, 1:400) to verify their positivity and titrate antibody concentration. Samples #A, #E, and #F became negative at dilutions higher than 1:50. Samples #B, #C, and #D maintained significant positivity, and #B and #C precipitated more MuSK at 1:50 and 1:100 dilutions compared to 1:10.

(which were subsequently identified as controls) in which the CPM was similar to the background level (250-300 CPM). RIA analysis was then repeated for the 6 positive antibodies at different dilutions (1:10, 1:50; 1:100; 1:200; 1:400) to confirm their positivity and estimate their half-maximal binding concentration (Figure 5.1 B). Samples #A, #E, and #F showed no positivity at dilutions higher than 1:50. Conversely, samples #B, #C, and #D maintained significant positivity with #B and #C precipitating more MuSK at higher dilutions (1:50 and 1:100 compared to 1:10). This suggests that the secondary anti-human IgG used to immunoprecipitate the anti-MuSK antibody was insufficient when the monoclonals were present at 1:10. CPM counts and concentrations for each dilution of the MuSK monoclonal antibodies are indicated in Table 5.1 and 5.2.

5.2.2) The monoclonal anti-MuSK antibodies inhibited AChR clustering

To test whether the anti-MuSK monoclonal antibodies shared similar pathogenicity compared to native antibodies isolated from MuSK-MG patients, their effects were tested *in vitro* on C2C12 myotubes. Their ability to inhibit AChR clustering was evaluated first. Cells were pre-exposed to each monoclonal antibody at 1:5 dilution for 30 minutes, and then incubated overnight with agrin to induce the formation of AChR clusters. This dilution was kept the same for all preparations as they had the same nominal concentration of MuSK-Abs (which should have corresponded to 1 μg/ml according to the original 5 μg/ml stated at the arrival of the preparations). However, based on titrations using the RIA, the estimated concentration of MuSK-Abs used in the experiment was 0.014, 1.31, 1.65, 0.8, 0.02, and 0.04 nM for samples #A-#F respectively. Samples incubated with medium only, agrin, or MuSK IgG4 (0.5 nM) purified from a myasthenic patient were used as control. After staining with fluorescent α-bungarotoxin, samples #B-#F (which were all positive by RIA) significantly reduced

Antibody	dilution	CPM	mmol	nmol/ml
MuSK-MG	1/10	11052	2.07×10^{-12}	0.41
	1/50	8182.2	1.53×10^{-12}	1.53
	1/100	6033.8	1.13×10^{-12}	2.26
	1/200	3754.62	0.7×10^{-12}	2.81
	1/400	2351.35	0.44×10^{-12}	3.29
A	1/10	523.088	0.01×10^{-12}	0.02
	1/50	389.216	0.07×10^{-12}	0.07
	1/100	323.866	0.06×10^{-12}	0.12
	1/200	311.216	0.06×10^{-12}	0.23
	1/400	353.336	0.06×10^{-12}	0.53
B	1/10	5680.34	1.06×10^{-12}	0.21
	1/50	6030.01	1.13×10^{-12}	1.13
	1/100	7561.06	1.41×10^{-12}	2.83
	1/200	4926.06	0.92×10^{-12}	3.69
	1/400	4355.81	0.81×10^{-12}	6.54
C	1/10	6111.8	1.14×10^{-12}	0.22
	1/50	7841.4	1.47×10^{-12}	1.47
	1/100	6418.8	1.20×10^{-12}	2.40
	1/200	5435.88	1.02×10^{-12}	4.08
	1/400	5506.79	1.03×10^{-12}	8.26
D	1/10	5675.7	1.06×10^{-12}	0.21
	1/50	4485.65	0.84×10^{-12}	0.84
	1/100	3640.3	0.68×10^{-12}	1.36
	1/200	3255.87	0.61×10^{-12}	2.44
	1/400	2687.07	0.5×10^{-12}	4.03
E	1/10	735.67	0.13×10^{-12}	0.02
	1/50	457.336	0.08×10^{-12}	0.08
	1/100	350.257	0.06×10^{-12}	0.13
	1/200	333.523	0.06×10^{-12}	0.25
	1/400	350	0.06×10^{-12}	0.52
F	1/10	716.2	0.01×10^{-12}	0.02
	1/50	462.399	0.08×10^{-12}	0.08
	1/100	402.2	0.07×10^{-12}	0.15
	1/200	321.176	0.06×10^{-12}	0.24
	1/400	339.088	0.06×10^{-12}	0.50

Table 5.1. MuSK monoclonal antibodies titration by RIA (samples #A-#F). In red are highlighted the dilutions equivalent to roughly half of the highest CPM counts, corresponding to the half-maximal binding concentrations of MuSK antibodies for each sample.

Sample	MuSK-ab concentration (nmol/l)
MuSK-MG plasma	2.26
Monoclonal A	0.07
Monoclonal B	6.54
Monoclonal C	8.26
Monoclonal D	4.03
Monoclonal E	0.13
Monoclonal F	0.24

Table 5.2. Estimated concentration of monoclonal anti-MuSK antibodies according to their RIA results.

the formation of AChR clusters, although less than the purified patient's IgG4. Conversely, #A and the RIA-negative samples #G-#O did not impair AChR clustering as the number of clusters was comparable to that induced by agrin alone (Figure 5.2).

5.2.3) Monoclonal anti-MuSK antibodies increased MuSK phosphorylation

After observing that the monoclonal anti-MuSK antibodies had pathogenic effects in inhibiting AChR clustering, their effect was evaluated on MuSK phosphorylation. Myotubes were pre-incubated with the monoclonal antibodies (1 μg/ml) for 30 minutes to allow their binding to MuSK, followed by exposure to agrin for 40 minutes to induce MuSK phosphorylation. To guarantee equal immunoprecipitation, MuSK was pulled down in all samples with the commercial anti-MuSK AF562, which was pre-incubated with the Protein G magnetic beads prior to exposure to the cell lysate. In contrast with the effects of the patient's MuSK IgG4, which inhibited MuSK phosphorylation as expected, the monoclonal antibodies #B, #C, #D, and #F significantly increased MuSK phosphorylation (Figure 5.3 A), even when compared with agrin alone. Sample #E also increased phosphorylation although statistical significance was not achieved. On the other hand, antibodies #A and #G-#K had no effect on MuSK phosphorylation compared with that induced by agrin.

Following this unexpected finding, the next question was whether the monoclonal antibodies were able to activate MuSK even in the absence of agrin. Therefore, myotubes were exposed to the RIA-positive antibodies #A-#F (at the same concentration as before) for 40 minutes in the absence of agrin. MuSK immunoprecipitation was carried out as described above with the addition of the commercial anti-MuSK AF562. Notably, as shown in the western blot (Figure 5.3 B), the monoclonal antibodies #B, #C, #D, #E and #F had a direct effect on MuSK, inducing an agrin-independent increase of its phosphorylation level.

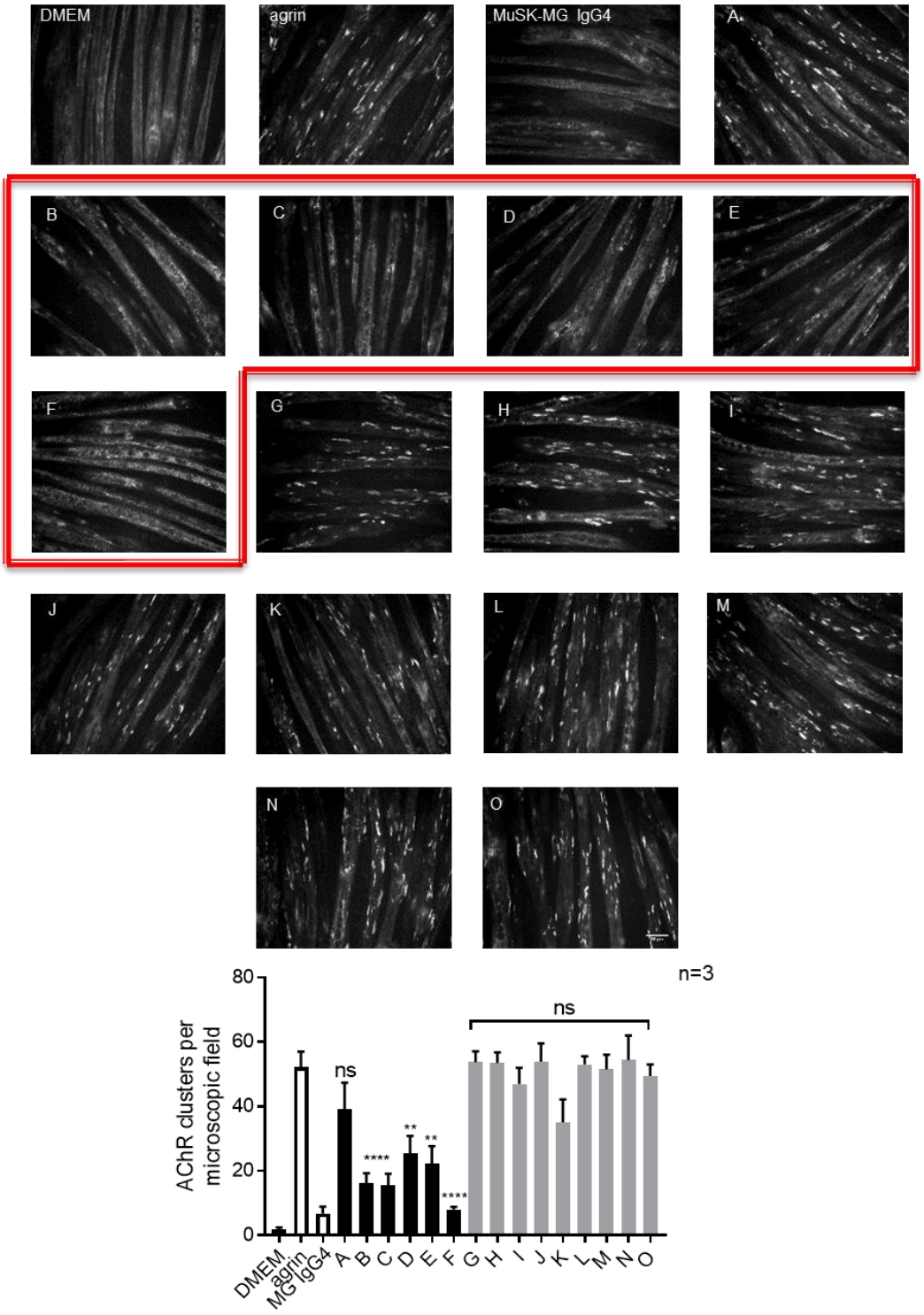


Figure 5.2. Effect of monoclonal MuSK antibodies on AChR clustering. Myotubes were pre-exposed for 30 minutes to mAbs (1:5 dilution, corresponding to an estimated concentration of 0.014, 1.31, 1.65, 0.8, 0.02, and 0.04 nM for samples #A-#F respectively) and then AChR clusters were induced by adding agrin for 16h. MuSK MG IgG4 (0.5 nM) was used as control. Among RIA positive-Abs (black in the bar chart), samples #B, #C, #D, #E and #F prevented clustering. Control antibodies (in grey) and sample #A did not have any effect on cluster number which was similar to the agrin control. Scale bar represents 50 µm. One-way ANOVA with multiple comparisons against agrin was used. Mean + SEMs are shown.

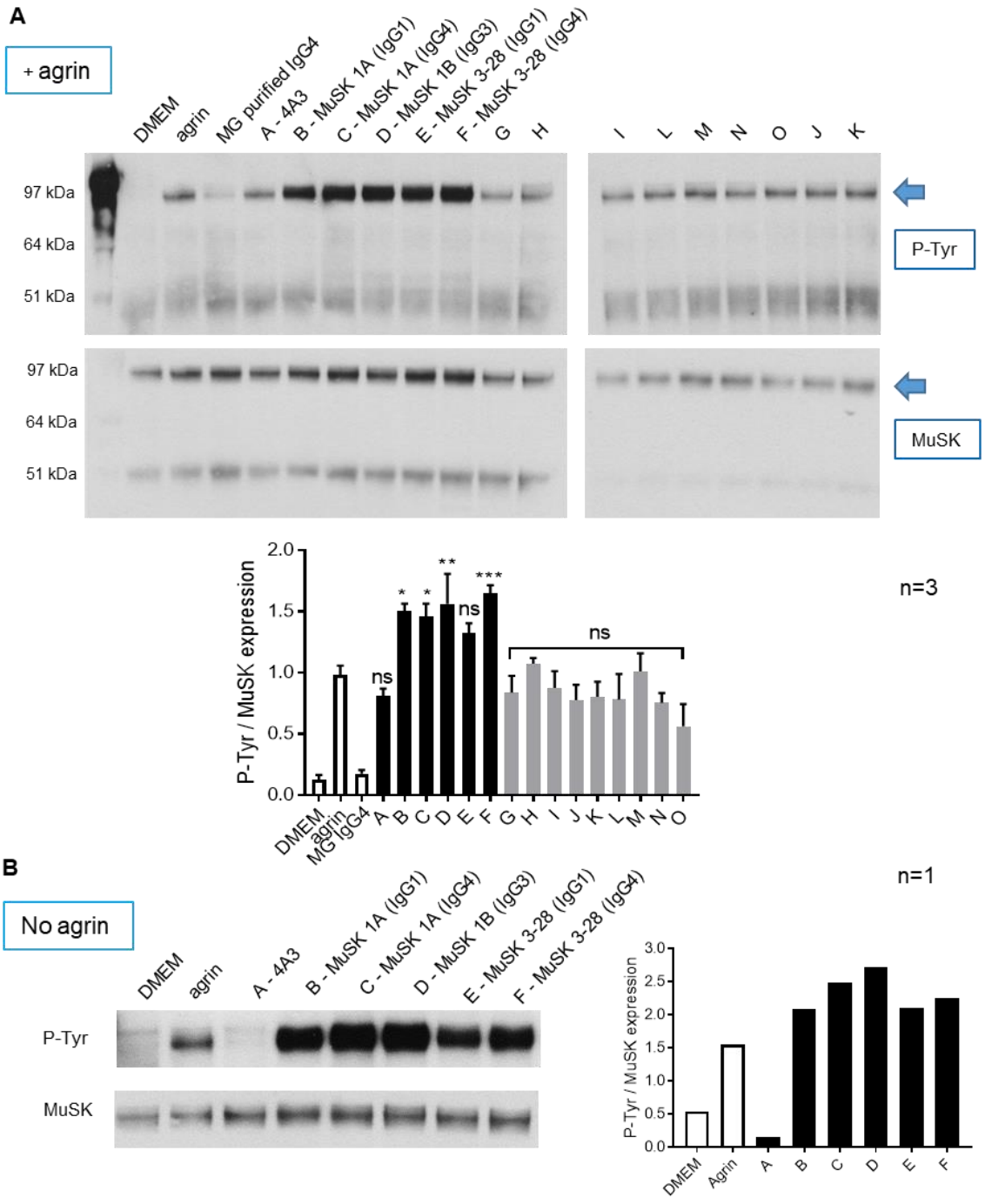

A
+ agrin
DMEM
agrin
MG purified IgG4
A - 4A3
B - MuSK 1A (IgG1)
C - MuSK 1A (IgG4)
D - MuSK 1B (IgG3)
E - MuSK 3-28 (IgG1)
F - MuSK 3-28 (IgG4)
G
H
I
L
M
N
O
J
K
97 kDa
64 kDa
51 kDa
P-Tyr
MuSK
P-Tyr / MuSK expression
n=3
ns
B
No agrin
n=1

Figure 5.3. Effect of monoclonal MuSK antibodies on MuSK phosphorylation. (A) Myotubes were pre-exposed for 30 minutes to mAbs (1:5 dilution, corresponding to an estimated concentration of 0.014, 1.31, 1.65, 0.8, 0.02, and 0.04 nM for samples #A-#F respectively) and then MuSK phosphorylation was induced by adding agrin for 40 minutes. MuSK MG IgG4 (0.5 nM) was used as control. MuSK was immunoprecipitated with commercial anti-MuSK AF562 in all samples. Among RIA positive-Abs (black in the bar chart), samples #B, #C, #D, and #F significantly increased MuSK phosphorylation. Sample #E also increased phosphorylation but did not reach significance. For control antibodies (in grey) and sample #A, MuSK phosphorylation was similar to the agrin control. One-way ANOVA with multiple comparisons against agrin was used. Mean + SEMs are shown**. (B)** Myotubes were then exposed directly to RIA-positive mAbs (1:5 dilution) in the absence of agrin. After 40 minutes incubation, MuSK was immunoprecipitated with commercial anti-MuSK AF562. Samples #B, #C, #D, #E and #F caused an agrin-independent increase of MuSK phosphorylation. Due to scarcity of material, **(B)** was carried out only once. However, the ability of the mAbs to induce MuSK phosphorylation was already indicated by **(A)**, and the new results provided additional evidence regarding their effects independent of agrin. The activation of MuSK induced by mAbs is likely to due with their divalency as monovalent MuSK IgG4 prevented MuSK phosphorylation as shown in **(A)**. IgG backbones are given in the brackets.

Due to the limited availability of materials, this experiment was performed only once considering that the previous results already indicated the ability of the monoclonals to increase MuSK phosphorylation.

At this point, samples were unblinded by Prof O'Connor; antibodies #B and #C originated from the common plasma cell clone 1A, whereas #E and #F came from the clone 3-28. In this respect, antibodies #B and #E were engineered on an IgG1 Fc, whereas #C and #F on the IgG4 Fc. Antibody #D derived from a third clone (1B) and was engineered on a IgG3 Fc. As mentioned above, all antibodies, including the IgG4, were created as divalent and monospecific. Finally, sample #A was an additional control derived from a hybridoma murine monoclonal, 4A3, that recognises human MuSK.

5.2.4) Monoclonal MuSK antibodies induced AChR microclusters but failed to induce full cluster maturation

Due to the discrepancy between the effects of the monoclonal antibodies on AChR clustering and MuSK phosphorylation, further analysis of AChR clusters was carried out evaluating in more detail their number and size. Specifically, a threshold of 3 μm was chosen to separate fully-developed AChR clusters from those which were still in the early phases of maturation immature/developing (so called microclusters) (Figure 5.4) (Weston, Gordon et al. 2003, Geng, Zhang et al. 2009). Myotubes were incubated with the monoclonal antibodies #A-#F in the absence of agrin for 16 hours, and then they were stained with fluorescent α-bungarotoxin. Clusters were counted automatically with ImageJ software differentiating them according to their size between microclusters (≥1 μm and <3 μm) and fully-formed clusters (≥3 μm). MuSK-MG IgG4 and samples #B, #C, #D, #E induced an increase in the number of microclusters which was comparable to that observed with agrin. For sample #F, the number of microclusters

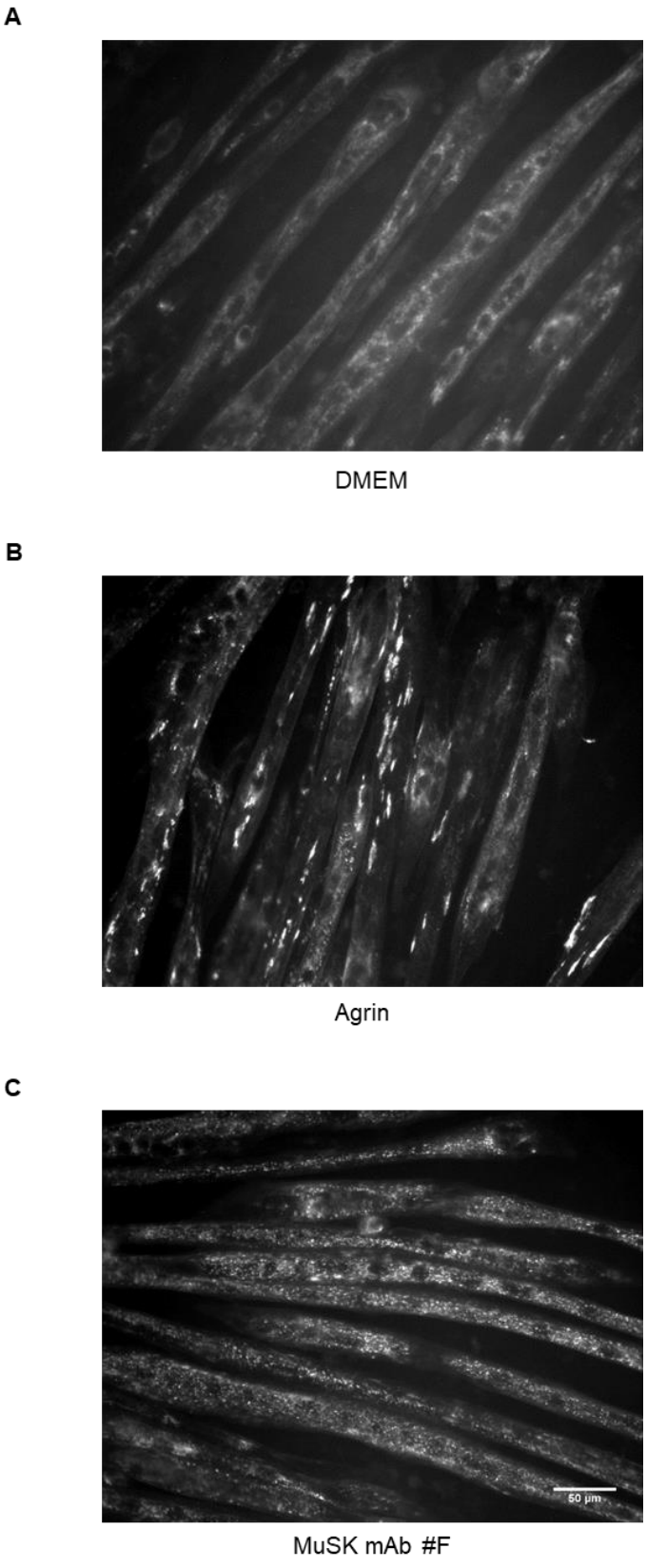


Figure 5.4. Qualitative differences between fully-formed AChR clusters and microclusters. Example images showing the microscopic appearance of **(A)** myotubes exposed to DMEM with no visible AChR clusters, **(B)** normal and fully-developed AChR cluster after 16h incubation with agrin, and **(C)** AChR microclusters after 16h exposure to MuSK mAbs #F. Scale bar represents 50 µm.

was even higher ($p<0.001$ compared to agrin) (Figure 5.5). Conversely, as observed before (Figure 5.2), the number of fully-formed clusters was not increased by the monoclonal antibodies, suggesting an impairment in the cluster maturation.

5.2.5) Attempts to evaluate MuSK internalisation by monoclonal antibodies

As the anti-MuSK monoclonals were created specifically as divalent antibodies, their ability to internalise the membrane-expressed MuSK was tested by immunohistochemistry. In a first attempt, cells were exposed to individual RIA-positive antibodies (#A, #E, #F) at the usual 1:5 dilution and at two different incubation times (1h and 16h). Antibodies #E and #F were chosen for this experiments for three main reasons: first, the amount of preparations available at this point was running low (in particular for high-titre samples #B-#D) and, in order to carry out all the scheduled experiments, a selection was necessary; second, despite their different concentrations, all antibodies showed comparable effects on MuSK phosphorylation and AChR clustering; finally, this first experiment was carried out to probe the possibility of staining MuSK on the myotube surface and the remaining high-titre antibodies #B-#D were reserved in case some promising result was observed and further optimisation was necessary. Sample #A was also used as control because, as mentioned in the previous paragraph, it was different from all the other preparation being a murine chimaera with no demonstrated pathogenic effects. Samples exposed to medium only and antibody #L were used as controls. Myotubes were then either fixed directly with formaldehyde or permeabilised with ice-cold acetone prior to labelling the monoclonals with a secondary fluorescent anti-human antibody (Alexa Fluor 488 – Figure 5.6). Coded images were evaluated by an independent investigator for potential qualitative differences in the staining. Only sample #E showed a diffuse positive staining on the myotube surface, which was not evident with the other antibodies. However, the intensity and localisation

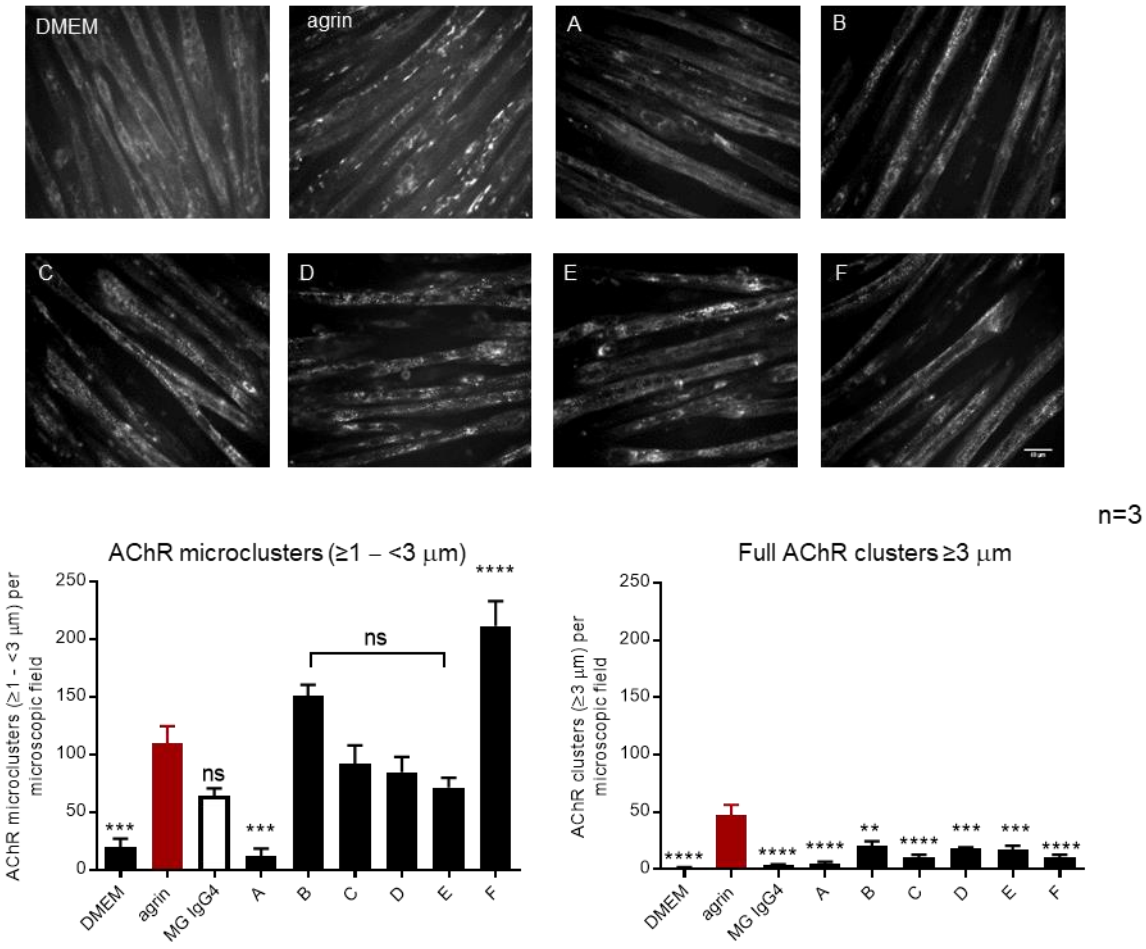


Figure 5.5. Monoclonal MuSK antibodies induced AChR microclusters but failed to induce full cluster formation. Myotubes were exposed overnight to RIA-positive mAbs (1:5 dilution, corresponding to an estimated concentration of 0.014, 1.31, 1.65, 0.8, 0.02, and 0.04 nM for samples #A-#F respectively) in the absence of agrin and AChR clusters stained with Alexa Fluor 594 α-bungarotoxin. MuSK MG IgG4 (0.5 nM) was used as control. Clusters were counted with ImageJ software using different thresholds for cluster length (<3 μm for microclusters; ≥3 μm for fully formed clusters). MuSK-MG IgG4 and mAbs #B, #C, #D, #E and #F caused an increase in the number of microclusters similar to agrin, and this was even more evident for #F. At the same time, all MuSK-Abs failed to induce concomitant maturation into fully formed AChR clusters. Scale bar represents 50 μm. One-way ANOVA with multiple comparisons against agrin was used. Mean + SEMs are shown.

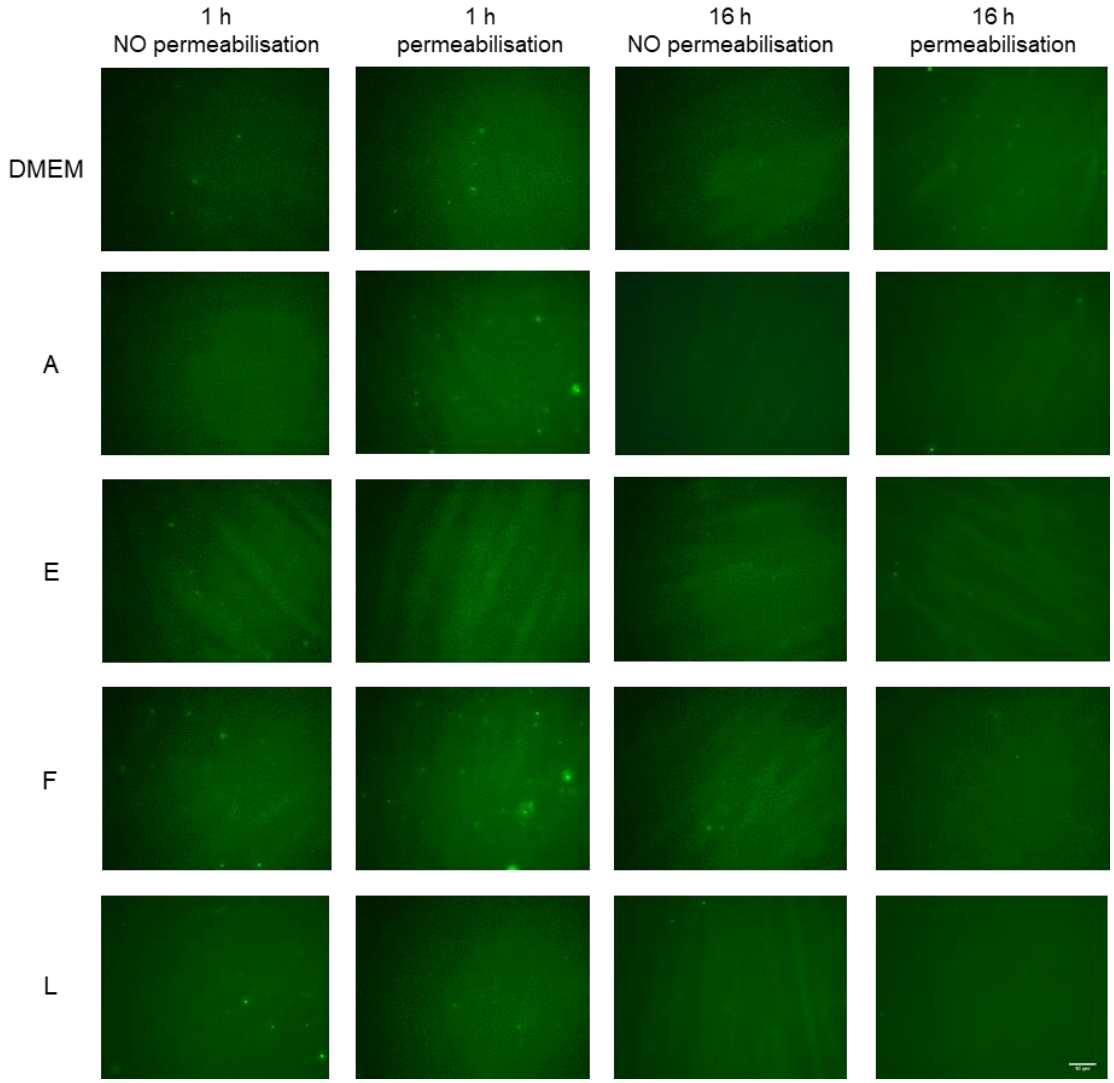


Figure 5.6. Staining of MuSK on myotubes with monoclonal antibodies. C2C12 myotubes were exposed to MuSK mAbs #A, #E, #F, and control antibody #L (1 mg/ml) for 1 hour and 16 hours to evaluate their ability to detect endogenous MuSK. Permeabilisation with triton was performed in parallel to study potential internalisation of the antigen. After fixing, cells were incubated with a fluorescent secondary anti-human antibody (Alexa Fluor 488). Images were evaluated qualitatively by a blinded investigator. Among all the antibodies, only #E showed a more intense staining on the surface of the myotubes and no significant differences were detectable between the different exposure times and permeabilised/non-permeabilised cells. Scale bar represents 50 µm.

of the staining was similar at 1h and 16h time points, and between permeabilised and non-permeabilised cells.

In order to improve the sensitivity of the staining, the experiment was repeated using two different secondary antibodies – before and after cell permeabilisation – to differentiate potential intracellular labelling of internalised monoclonals. Due to scarcity of materials, the remaining monoclonal anti-MuSK antibodies (#B, #D, #E) were pooled together, diluted 1:5, and incubated with the myotubes for either 1h or 16h. Cells were exposed to the first secondary anti-human antibody (Alexa Fluor 594) before fixation, whereas the second anti-human antibody (Alexa Fluor 488) was used afterwards in both permeabilised and non-permeabilised samples. Fixation with formaldehyde and permeabilisation with acetone were conducted in parallel to evaluate potential difference in the staining. In theory, in the non-permeabilised samples, the green fluorescent staining by Alexa Fluor 488 should be markedly dimmer compared to the permeabilised cells as all the MuSK antibody on the cell surface should already be bound to the secondary red Alexa Fluor 594. The combination of the three pooled anti-MuSK monoclonals together with the fluorescent double labelling provided a stronger positivity of the myotubes compared to the control sample (Figure 5.7). However, no qualitative differences were detectable in the green fluorescent staining between the two incubation times, and between permeabilised or non-permeabilised cells.

5.3) Discussion

The availability of monoclonal anti-MuSK antibodies derived from patients' plasma cells provided the unprecedented opportunity to study their pathogenic effects with higher specificity compared to the previous experiments carried out with antibodies purified from plasmapheresis materials of myasthenic patients. In this respect, it was possible to test individual clones of MuSK antibodies without the confusing presence of

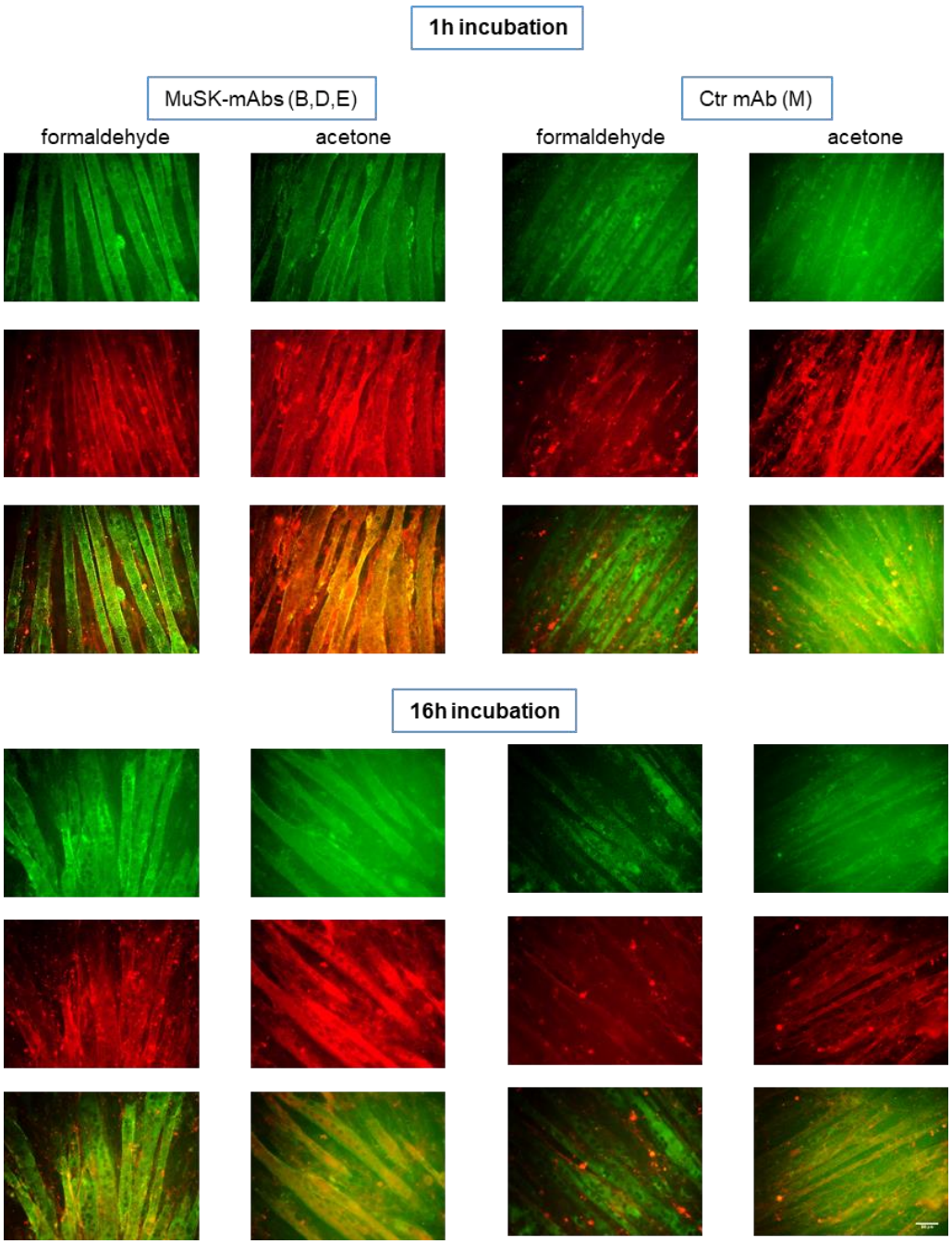


Figure 5.7. Staining attempt of MuSK on myotubes with monoclonal antibodies. C2C12 myotubes were exposed to pooled monoclonal anti-MuSK antibodies (#B, #D, #E) and control antibody #M for 1 hour and 16 hours. Cells were exposed to two different secondary fluorescent anti-human antibodies: Alexa Fluor 594 (red) before fixing with formaldeyde, and Alexa Fluor 488 (green) after permeabilisation with acetone. The green fluorescent antibody was also added to the non-permeabilised cells for comparison purposes. The double staining was aimed to evaluate potential differences in the intensity and localisation of the fluorescent signal by the green antibody in case of effective internalisation of MuSK. Images were qualitatively evaluated by a blinded investigator. A generalised staining of the surface of the myotubes was more defined in the presence of anti-MuSK antibodies compared to the control antibody, and in the red staining in the acetone-fixed samples. However, no detectable differences were observed between the different exposure times and permeabilised/non-permeabilised cells in the green staining, which should have been stronger for potentially internalised antibodies. Scale bar represents 50 µm.

other non-specific antibodies, which contaminate purified preparations from patients' plasma. This is particularly true for the IgG1-3 subclasses that usually represents only a small proportion of the total MuSK antibodies and a very small proportion of total IgG.

Initially, the identities of the monoclonals were unknown but their specificity was evident from the positive results in the MuSK radioimmunoassay. At low dilution (1:10), only 3 (#B, #C, and #D) of the original 15 samples showed a clear positive result at the RIA, whereas additional 3 samples (#A, #E, and #F) were just above the background CPM count (around 250-300) as seen in the control preparations. These results were confirmed when the RIA was repeated at different dilutions to titrate the concentration of the antibodies. Notably, the three samples with the initial strong positive result were able to immunoprecipitate more radioactive MuSK as they were diluted. This apparently paradoxical behaviour suggests that the secondary anti-human antibody, required for the formation and precipitation of the immunocomplexes, was insufficient to bind all the monoclonal present when at high concentration resulting in inefficient immunoprecipitation. However, they never reached the saturation level of the patients' IgG. Interestingly, it was revealed subsequently that all MuSK mAbs recognised a less common antigen located in the Ig2-like sequence of the extracellular domain of MuSK. Conversely, patients' antibodies are polyclonal and, therefore, are direct against multiple antigens of the MuSK molecule (more predominantly the Ig1-like sequence that mediates the interaction between MuSK and Lrp4) ((Huijbers, Vink et al. 2016)). The ability to bind ^{125}I-MuSK in the RIA could have been reduced in the MuSK mAbs as a result of their intrinsic monoclonality and the recognition of an atypical antigenic epitope. In this respect, it is worth noting that samples #E and #F subsequently showed a very strong pathogenic effect on clustering despite the low concentration of MuSK antibodies detected in the immunoprecipitation assay. This was particularly evident for #F, in which the effects were significantly more pronounced

compared to all the other MuSK mAbs. The lack of correlation between antibodies' ability to immunoprecipitate MuSK and, concomitantly, to impair its function might be related to the specific epitope they recognise (and this could be particularly relevant for #E and #F considering that they were created from the same plasma cell clone, but mounting a different IgG backbone). As mentioned above, the Ig2 sequence targeted by the mAbs has been detected less frequently in MuSK-MG patients. It is possible that antibodies against this particular target are not able to bind under the experimental condition of the RIA, requiring a more physiological environment to attach to MuSK (such as the myotube surface). This is indeed the principle behind the cell-based-assay (CBA) and the reason why this it is able to identify myasthenic patients (for both AChR- and MuSK-MG) that are otherwise negative in the traditional RIA (Leite, Jacob et al. 2008, Huda, Waters et al. 2017).

Once the monoclonals were tested on the C2C12 myotubes to evaluate their effects on the AChR clustering, the identity of the samples became evident. Specifically, samples #B-#F, which all showed some degree of positivity in the RIA, inhibited agrin-induced clusters and were confirmed to be the MuSK mAbs. Conversely, the RIA-negative samples #G-#O, which had no pathogenic effect, were derived from non-myasthenic patients. Sample #A, which did not inhibit AChR clustering despite being able to immunoprecipitate MuSK in the RIA, was revealed to be an additional control from a chimaeric humanised anti-MuSK mouse antibody.

In order to understand the peculiar pathogenic effects shown by the MuSK mAbs compared to their native equivalents, it is important to highlight that the monoclonals were created monospecific and divalent, irrespective of their original subclasses. This represents a major difference compared to the native conformation of MuSK IgG4 antibodies which are supposed to exchange their Fab arms with other IgG4 directed against different antigens becoming functionally monovalent (Koneczny, Stevens et al.

2017). In this respect, the divalent MuSK mAbs were expected to behave more similarly to the IgG1-3 subclasses, which are divalent and likely to bind to two different molecules of MuSK at the same time. Indeed, the monoclonals did behave differently compared to their equivalent patient-purified IgG4 when their effects on MuSK were studied. Unexpectedly, all the mAbs activated MuSK, increasing significantly its phosphorylation even in the absence of agrin. This is in contrast to that observed in previous studies (Huijbers, Zhang et al. 2013, Koneczny, Cossins et al. 2013), and in other experiments described in this thesis, where MuSK IgG4 consistently inhibited MuSK phosphorylation by blocking its stimulation by agrin. One possible explanation is that the divalent nature of the monoclonal antibodies induces the dimerisation of two MuSK molecules, triggering their activation. A similar conclusion was reached by Huijbers and colleagues who tested similar MuSK mAb preparations. They observed the same increase of MuSK phosphorylation induced by the divalent IgG4 monoclonal antibodies, although a concomitant mild increase in the number of AChR clusters was also noted. It was therefore hypothesised that the non-physiological activation of MuSK by the mAbs would reduce the overall pathogenicity of the divalent IgG4 compared to their native monovalent equivalents (Huijbers, Vergoossen et al. 2019). This was further supported by a mouse model passively immunised with the MuSK mAbs. A milder phenotype was observed in the presence of the divalent mAbs compared to the monovalent equivalents (Vergoossen, Plomp et al. 2021).

The original study of Huijbers et al, however, did not consider whether the AChR clusters induced by the mAbs were different from that normally observed with physiological agrin stimulation. In the experiments here, the AChR clusters were studied in more detail evaluating their size alongside their number. Specifically, it was observed that while acquiring the images for the initial counting of the clusters, the myotubes exposed to the monoclonals were covered by puntiform aggregates of

acetylcholine receptors, which were absent in the sample incubated with medium only, and much smaller compared to the typical AChR clusters induced by agrin. These small aggregates (<3 μm) were identified as microclusters, which correspond to the initial stages of the AChR cluster formation and maturation (Weston, Gordon et al. 2003, Geng, Zhang et al. 2009). Their number was significantly increased by all the MuSK mAbs whereas, at the same time, the fully-formed clusters were severely inhibited. This suggests an impairment of the cluster maturation which will be further investigated in Chapter 6 where the effects of patient-purified MuSK antibody subclasses will be discussed. It is worth noting that, among all the monoclonals, #F showed the most significant effects in increasing MuSK phosphorylation and AChR microclustering, while severely inhibiting fully-formed AChR clusters. These effects were more pronounced compared to #E, which has the same variable regions as #F but mounted on a backbone of IgG1 rather than #F's IgG4 backbone. In this respect, the higher effectiveness showed by #F might be due to the fact that it resembles more closely the original antibody produced by the native plasma cell from which the mAb was created, with better antigen recognition on the myotube surface.

Finally, due to the divalency of the monoclonal antibodies, it was possible that they might induce the internalisation of the MuSK molecules on the membrane of the myotubes, as an additional and typical pathogenic mechanism shared by divalent IgG subclasses (see Chapter 1, paragraph 1.8). After exposure to the MuSK monoclonal antibodies, myotubes were permeabilised and labelled with a fluorescent anti-human secondary antibody. Overall, the myotubes incubated with the anti-MuSK antibodies showed a diffuse positive staining on their surface, which was not present (or minimally evident) in the control samples, indicating a positive recognition of the surface MuSK. However, permeabilised and non-permeabilised cells showed similar signal enhancement, and no qualitative differences were observed at the two time points

studied. Similar results were also obtained after optimising the technique with a double fluorescent staining (pre- and post-permeabilisation) in the attempt to identify potential internalised antibodies through different colours. However, considering the pattern of staining and the overall appearance of the positive-labelled myotubes, it is likely that immunohistochemistry technique here applied was not sensitive enough to detect the small changes in the fluorescence signal expected for the surface expression or internalisation of the antigen. A potential approach that could have been used to improve the sensitivity of the assay involves newly developed secondary antibodies that become fluorescent only after being internalised by the lysosomes. The fluorescent dye attached to the antibody is, in fact, pH sensitive and is activated by the acid environment inside the lysosomes after the internalisation of the primary-secondary antibody complex (Nath, Godat et al. 2016).

Unfortunately, it was not possible to carry out further experiments due to the reduced availability of the anti-MuSK monoclonals. Instead, MuSK antibodies purified from patients' plasma were used, with their limitations, in the next and final result chapter of this thesis.

Chapter 6

Differential effects of IgG subclasses

on pathogenic mechanisms of MuSK myasthenia

6.1) Introduction

The current and most accredited pathogenic model of MuSK-MG is based solely on the effects of the monovalent MuSK IgG4, which inhibit MuSK phosphorylation by blocking the interaction between MuSK and Lrp4, leading to the dispersal of AChR clusters (Huijbers, Zhang et al. 2013, Koneczny, Cossins et al. 2013). Although MuSK IgG4 antibodies predominate (McConville, Farrugia et al. 2004), lower proportions of divalent MuSK-IgG1-3 exist in most patients, and their pathogenic potential in dispersing AChR clusters has been already suggested *in vitro*, although no evidence was found that these subclasses induce MuSK internalisation or disrupt its binding with Lrp4 (Koneczny, Cossins et al. 2013). Pathogenicity of MuSK IgG1-3 is also supported *in vivo* by a recent mouse model knockout of murine IgG1 (equivalent to human IgG4) which developed a full myasthenic phenotype when immunised against MuSK. In this case, the immune response was sustained by the murine equivalent of human IgG1-3 subclasses (Kucukerden, Huda et al. 2016).

Initial clues regarding the potential pathogenic mechanism by which MuSK IgG1-3 contribute to the development of myasthenia come from the *in vitro* testing of NSC-87877 with the different MuSK-Ab subclasses (see Chapter 3), in which IgG1-3 impaired AChR clustering without modifying MuSK phosphorylation. This was further supported by the finding that the MuSK-mAbs (functionally identical to the native IgG1-3) forcedly induced MuSK phosphorylation likely through their divalent binding (see Chapter 5). This non-physiological activation of the phorphorylation pathway

disrupted the maturation of AChR clusters with the the overall reduction of fully-formed clusters and, concomitantly, increasing the number of cluster precursors.

Different hypothesis could be postulated to explain this apparent paradox. For example, it is possible that the forced activation of MuSK disrupts its interaction with its intracellular effector, DOK7, with the consequent quenching of the phosphorylation signal. In addition, the failing in AChR cluster maturation (with the consequent increase in the number of microclusters) indicates a likely impairment in the subsidiary pathways and effectors that regulates the cytoskeleton rearrangements necessary in the clustering process. These include the time-dependent activation of Rho and Rac1 GTPases, the preservation of the anchoring function of rapsyn, and the integrity of interactions between the MuSK-Lrp4 complex and other structural protein of the sarcolemma and extracellular matrix (Weston, Gordon et al. 2003, Dobbins, Luo et al. 2008, Kamimura, Ueno et al. 2013, Zuber and Unwin 2013, Arredondo, Lara et al. 2014, Bai, Guo et al. 2018, Zhao, Shen et al. 2018). The experiments described in this Chapter will try to address the following questions:

- Do native IgG1-3 purified from MuSK-MG patients have the same effect of MuSK-mAbs on MuSK phosphorylation and AChR clustering?
- Once MuSK is activated by IgG1-3, is the phosphorylation signal forwarded effectively downstream of DOK7 and the rest of the intracellular clustering pathway?
- Is an impairment in the activation of Rho and Rac1 GTPases the reason behind the failing in cluster maturation by MuSK antibodies?
- Do MuSK IgG1-3 affect the recruitment of rapsyn?
- Do MuSK IgG1-3 impair the the binding between MuSK and Lrp4?

6.2) Results

6.2.1) MuSK IgG1-3 and IgG4 had an opposite effect on MuSK and DOK7 phosphorylation

C1C12 myotubes were exposed to purified MuSK antibody subclasses (either IgG1, 2 and 3, or IgG4) at a concentration of 0.5 nM, in the presence and absence of agrin at submaximal dilution (1:800). After 40-minute incubation, protein immunoprecipitation was carried out from cell lysates as described in Chapters 2 and 3. MuSK was pulled down by patients' purified antibodies, whereas the commercial anti-MuSK AF562 was used in the agrin and DMEM controls. DOK7 was immunoprecipitated in parallel with MuSK by adding an anti-DOK7 antibody (A7) to the Protein G beads prior to the cell lysis. Protein phosphorylation was detected by western blotting (Figure 6.1A) and band densitometry performed as described in Chapter 2 (Figure 6.1B).

As expected, MuSK IgG4 inhibited agrin-induced MuSK phosphorylation (Figure 6.1A – left) and, consequently, DOK7 phosphorylation was also reduced (Figure 6.1A – right). No direct effect on either MuSK or DOK7 was induced by IgG4 alone in the absence of agrin. Conversely, phosphorylation of MuSK and DOK7 was significantly increased ($p<0.001$ and $p<0.05$ respectively) in the samples exposed to the IgG1-3 subclasses (Figure 6.1A and B). Notably, phosphorylation was increased even in the absence of agrin, suggesting a direct activation of MuSK induced by the antibodies. In addition, a band at 49 kDa was consistently detected in the phosphorylation blot in the samples exposed to IgG1-3 (Figure 6.1A top left). This is consistent with the size of DOK7 and might indicate that, compared to MuSK IgG4, the IgG1-3 subclasses are able to co-immunoprecipitate DOK7 together with MuSK.

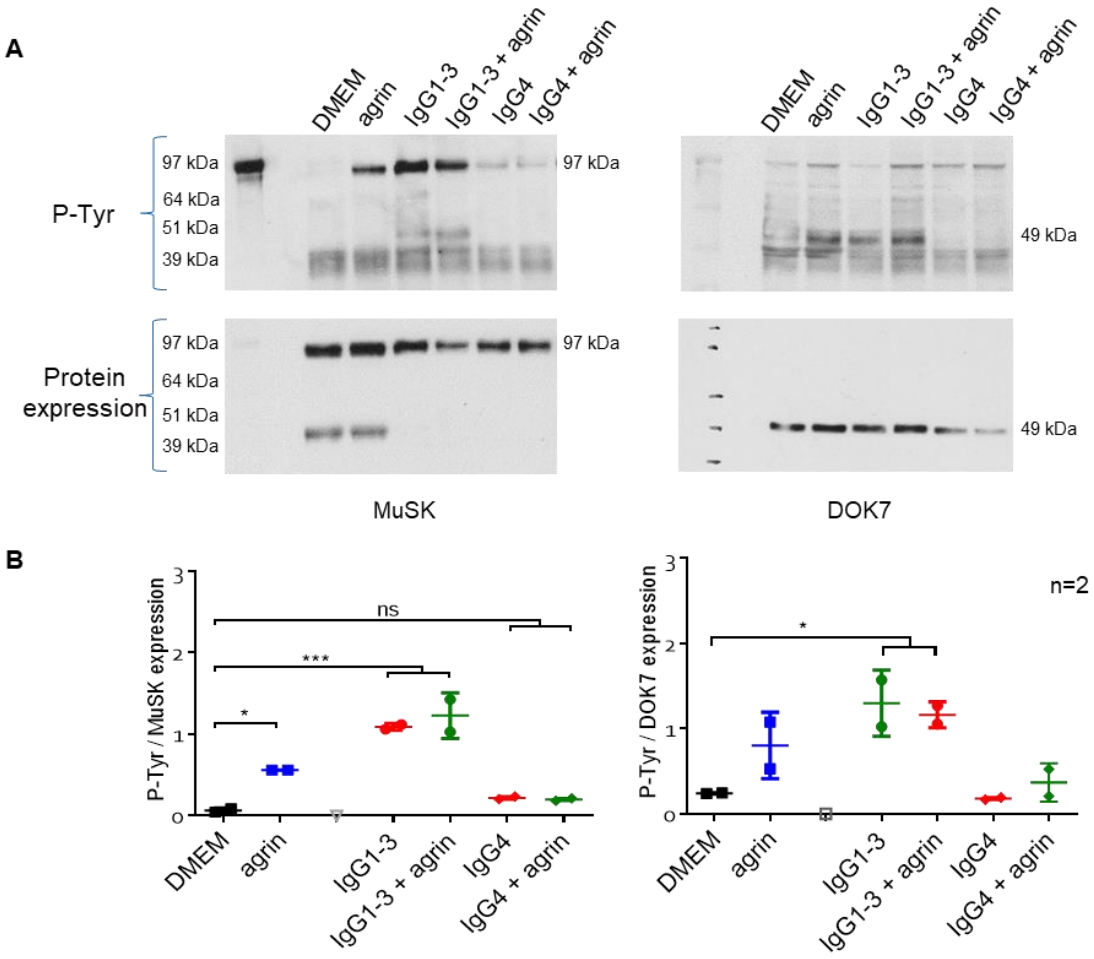


Figure 6.1. IgG1-3 and IgG4 had an opposite effect on MuSK and DOK7 phosphorylation. Myotubes were exposed to MuSK IgG1-3 and IgG4 subclasses in the presence and absence of agrin, which was added 30 minutes after the antibodies. MuSK was immunoprecipitated from the cell lysate using commercial AF562 for DMEM and agrin controls, and patients' purified antibodies for the remaining samples. At the same time, commercial antibody A7 was used to immoprecipitate DOK7. **(A)** Representative western blots showing a strong phosphorylation band for both MuSK (left) and DOK7 (right) in the samples incubated with MuSK IgG1-3. **(B)** Quantification of the density of phosphorylation bands normalised for total protein expression from pooled results of 2 independent experiments shows that MuSK IgG1-3 increased both MuSK and DOK7 phosphorylation even in the absence of agrin. Conversely, as expected, MuSK IgG4 did not induce MuSK phosphorylation and prevented the effect of agrin. One-way ANOVA with multiple comparisons against DMEM was used. Mean + SD are shown.

6.2.2) *Optimisation of AChR pull-down for phosphorylation analysis*

The next question was whether the phosphorylation signal triggered by the IgG1-3 was able to reach the end of the cascade at the level of the AChRs. To study this, preliminary experiments were carried out to optimise the immunoprecipitation of the AChR and to measure reliably the tyrosine phosphorylation of either the δ or β subunits of the receptor. Specifically, two different approaches were tested in parallel using (a) a mouse monoclonal antibody directed against the α subunit of the AChR (D6) (Whiting, Vincent et al. 1985), and (b) streptavidin-conjugated bungarotoxin (BTX).

After inducing the phosphorylation cascade by exposing the myotubes to agrin, immunoprecipitation was attempted on both membrane-expressed and total AChRs by incubating the myotubes with the D6 antibody or the streptavidin-BTX either before or after lysing the cells. Streptavidin and Protein G beads, without BTX and the D6 antibody respectively, were used as control. The western blot was first probed for phosphotyrosine (Figure 6.2A), and then for the β subunit of the AChR on the stripped membrane (Figure 6.2B). In the phosphorylation blot, a strong and clear band was detected at 45 kDa in the agrin-induced myotubes exposed to streptavidin-BTX prior to cell lysis. The same band was not present in the samples incubated with the BTX after lysing the cells, indicating a less efficient immunoprecipitation under these experimental conditions. When the D6 antibody was used, non-specific bands were detected at the same molecular size of 45 kDa irrespective of the presence or absence of agrin. A similar pattern was also observed when the myotubes were incubated with only Protein G without the D6 antibody, suggesting non-specificity of the bands observed in the immunoprecipitated samples.

When probed for the β subunit of the AChR (Figure 6.2B), a clear signal was detectable in almost all samples supporting the overall effectiveness of the

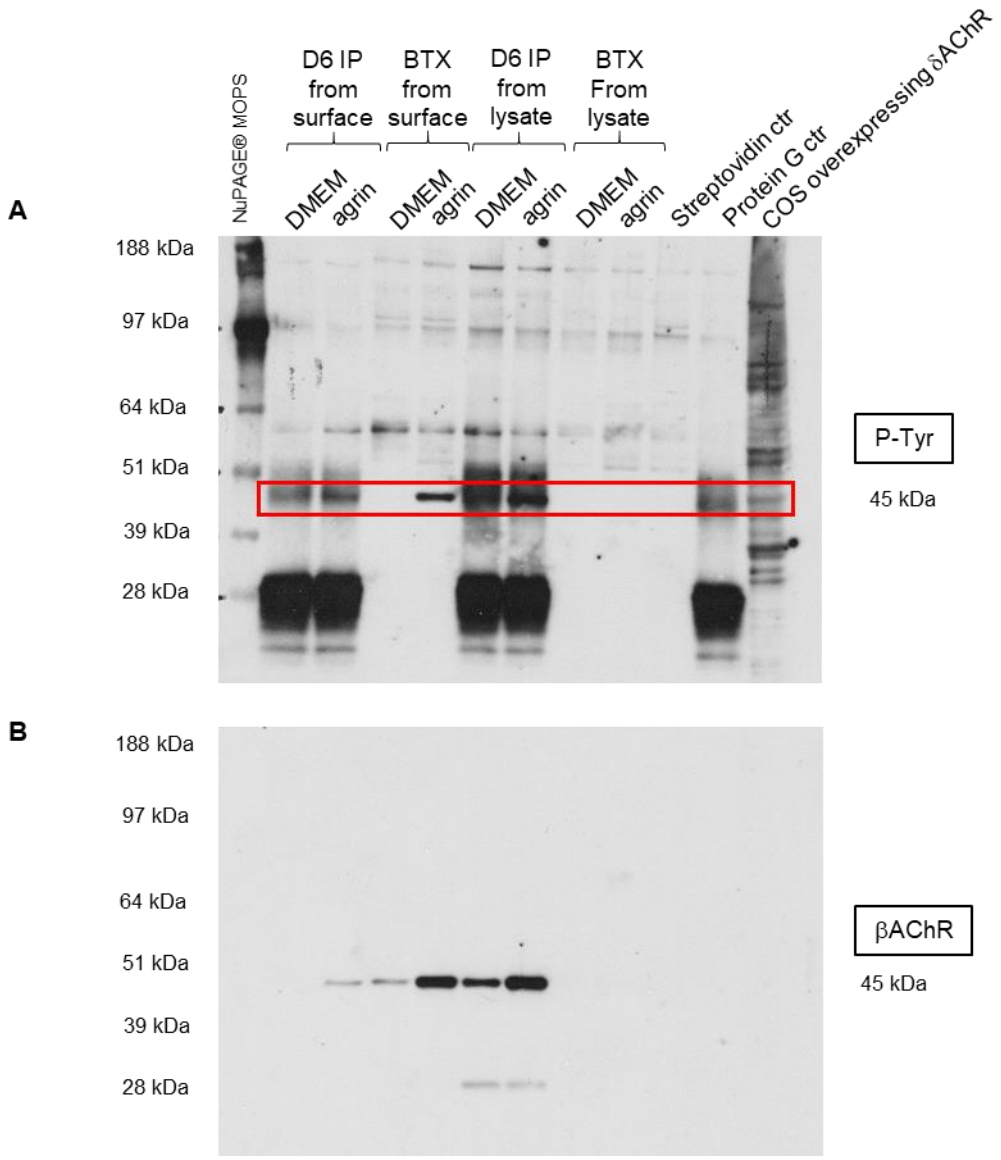


Figure 6.2. Optimisation of AChR pull-down for phosphorylation analysis. Myotubes were exposed to agrin for 40 minutes to induce the phosphorylation. Afterwards, cells were exposed for 1 hour at room temperature to streptavidin conjugated bungarotoxin (BTX) or anti-aAChR antibody D6 to pull-down the AChR from the cell surface. A parallel pull-down was attempted also from the cell lysates using the same principle. Streptavidin and Protein G beads in the absence of BTX and AChR antibody were used as controls. **(A)** In the western blot probed for phosphotyrosine, the pull-down with streptavidin-BTX from the cell surface showed the clearest phosphorylation band induced by agrin at around 45 kDa. The same procedure was less effective on the cell lysate. In the samples where antibody D6 was used, bands corresponding to antibody heavy chains covered potential phosphorylation bands of AChR subunits. **(B)** The phosphorylation blot was stripped and reprobed for the βAChR subunit. The phosphorylation band detected in the first blot corresponds to the size of the βAChR. In the first lane (DMEM-treated cells IP with D6 from the surface) the βAChR band is not detectable. This is likely due the combined effect of the stripping of the nitrocellulose membrane and the less efficient immunoprecipitation observed in general in the DMEM samples compared to those exposed to agrin (as seen also in the other lanes).

immunoprecipitation technique, with the exception of the sample exposed to DMEM and immunoprecipitated with D6 from the membrane (first lane on the left), and those incubated with BTX in the cell lysate (last two lanes on the right). Notably, the β subunit bands appeared stronger in the samples exposed to agrin compared to their DMEM equivalents, suggesting a more efficient immunoprecipitation possibly due to the initial clustering of the AChRs. The phosphorylation band seen at 45 kDa in the agrin-induced samples was consistent with the bands of the β subunit. The stripped membrane was also probed for the δ subunit of the AChR, which runs at a higher molecular weight (around 60 kDa) compared to the β and was effectively immunoprecipitated by both BTX and D6 antibody. Despite a weak phosphorylation signal was detected at the correct size in the phosphorylation blot, no modifications induced by agrin were observed.

According to these results, analysing the phosphorylation of the β subunit after immunoprecipitation of the membrane AChRs with streptavidin-BTX appeared to be the most reliable approach and was therefore used in the subsequent experiments.

6.2.3) Agrin and MuSK IgG1-3 induced a similar phosphorylation time course for MuSK, DOK7 and βAChR

A phosphorylation time course was then performed comparing the effect of MuSK IgG1-3 on MuSK, DOK7 and the βAChR with agrin stimulation.

Myotubes were exposed to MuSK IgG1-3 (0.5 nM), in the presence and absence of agrin (1:800), for 1, 2, 4, and 8 hours. Cells were lysed at each time point and immunoprecipitation of MuSK, DOK7 and βAChR carried out as previously described. A similar phosphorylation course was observed in all the proteins studied with a sharp initial increase of the signal after the first hour of exposure to either agrin, MuSK IgG1-3, or the combination of the two, followed by progressive reduction (Figure 6.3).

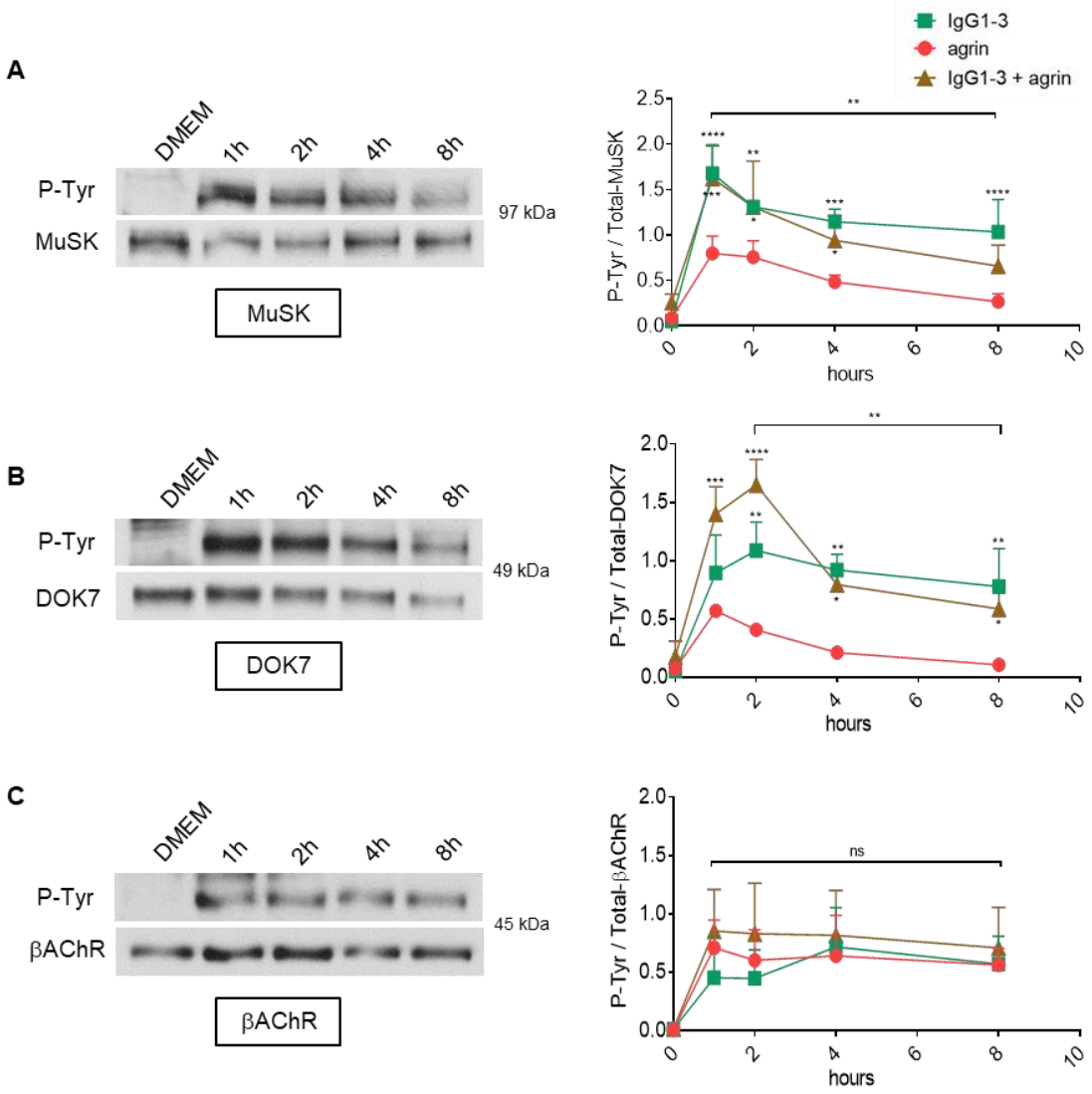


Figure 6.3. Agrin and MuSK IgG1-3 induced a similar phosphorylation time course for MuSK, DOK7 and βAChR. C2C12 myotubes were exposed to MuSK IgG1-3 in the presence and absence of agrin. Incubation was stopped at different time points (1h, 2h, 4h, and 8h). MuSK **(A)** and DOK7 **(B)** were immunoprecipitated from cell lysates as previously described, and the βAChR **(C)** pulled-down from the surface by streptavidin-conjugated bungarotoxin. On the left, representative western blots showing phospho-tyrosine bands (top) and corresponding expression (bottom) of MuSK (97kDa), DOK7 (49 kDa) and βAChR (45 kDa). The representative western blots (left) are from samples incubated with MuSK IgG1-3. On the right, pooled results of 2 experiments showing the variations over time of MuSK, DOK7, and βAChR phosphorylation. Both agrin and IgG1-3 induced a time-dependent increase of phosphorylation which peaked at 1h for MuSK, and at 2h for DOK7, with a subsequent progressive decrease. The phosphorylation of the βAChR rose by one hour and was then stable up to 8h. Notably, the time curves for b phosphorylation were similar for IgG1-3 and agrin, although the IgG1-3 MuSK antibodies induced higher MuSK and DOK7 phosphorylation compared to that for agrin alone at each time point. Two-way ANOVA-multiple comparisons for time was used. Mean + SD are shown.

Notably, in the presence of IgG1-3, MuSK and DOK7 phosphorylation was significantly higher compared to agrin alone at almost each time point (for MuSK: $p<0.0001$ at 1h and 8h; $p<0.01$ at 2h; $p<0.001$ at 4h; for DOK7: $p<0.01$ at 2, 4 and 8h) (Figure 6.3A and B). No differences were detected in the phosphorylation of βAChR between IgG1-3 and agrin and, in this case, the decrease over time of the phosphorylation signal was slower compared to that of MuSK and DOK7 (Figure 6.3C). This is indicated by the absence of statistical difference between each time point of the βAChR phosphorylation and the end time course at 8h in each experimental condition. Conversely, the phosphorylation peak of MuSK and DOK7 at 1h and 2h respectively was significantly higher compared to the level at 8h hour in the samples exposed to IgG1-3, and agrin with IgG1-3 ($p<0.01$).

6.2.4) MuSK antibody subclasses induced AChR microclusters but failed to sustain full cluster maturation

The previous results suggest that MuSK IgG1-3 effectively activate the AChR clustering cascade as, after activating MuSK and DOK7, the phosphorylation signal reached the βAChR at the end of the pathway. However, as described in Chapter 3 and in a previous study by Koneczny et al (Koneczny, Cossins et al. 2013), MuSK IgG1-3 inhibited the formation of AChR clusters. In the attempt to explain these apparently incompatible findings, the number and size of AChR clusters were further analysed after incubation with the different MuSK antibody subclasses.

First, C2C12 myotubes were exposed overnight to MuSK IgG1-3 or IgG4 (0.5 nM) in the presence and absence of agrin (1:800). Clusters were labelled with fluorescent α-bungarotoxin and counted according to their size. A threshold of 3 μm was chosen to separate fully-developed AChR clusters from immature/developing microclusters as used in Chapter 5 (Geng, Zhang et al. 2009). As shown in Figure 6.4, myotubes

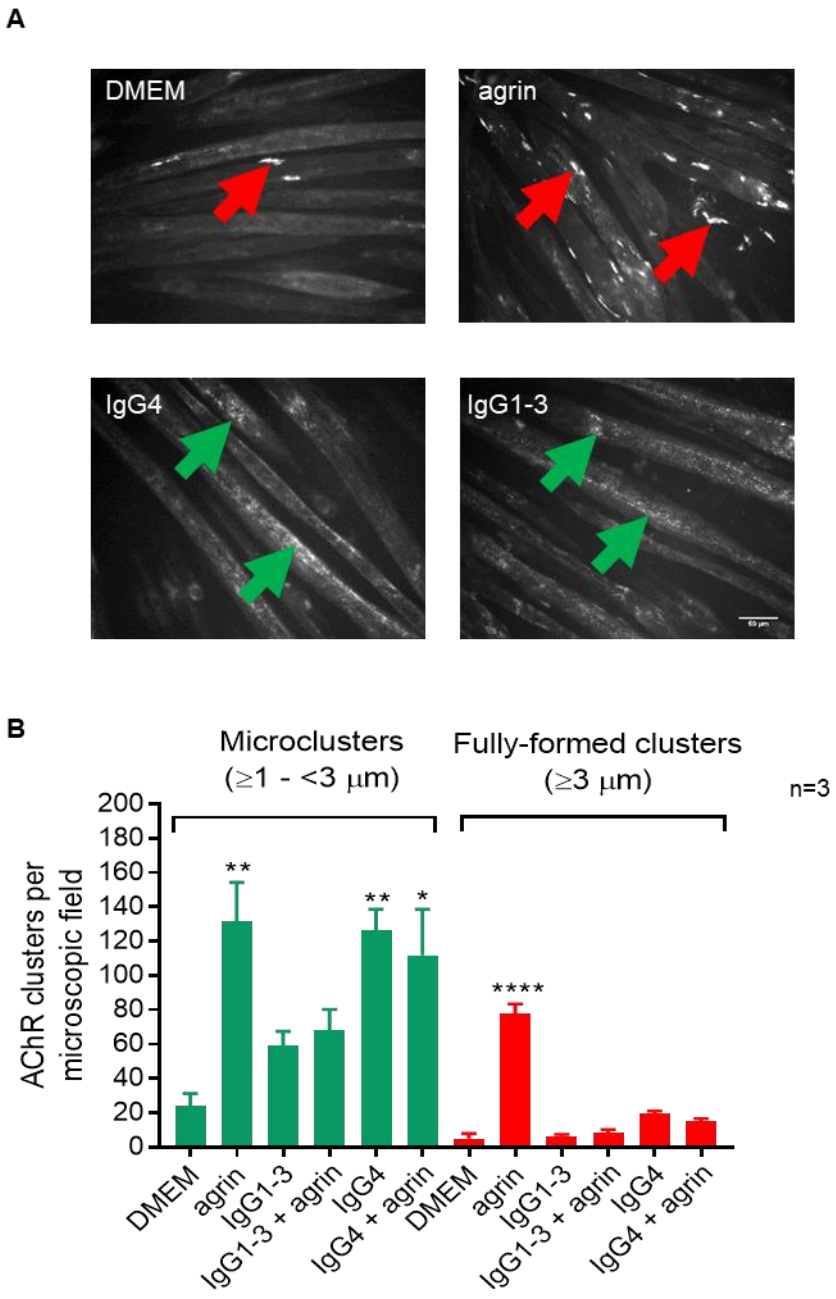


Figure 6.4. MuSK antibody subclasses induced AChR microclusters but failed to sustain full cluster maturation. C2C12 myotubes were exposed to agrin, MuSK IgG4, and IgG1-3 for 16 hours and then AChR clusters stained with Alexa Flour 594 α-bungarotoxin. Clusters were counted with ImageJ software using different thresholds for cluster length (≥1 - <3 μm for microclusters; ≥3 μm for fully formed clusters). (**A**) Representative images of AChR clusters. Fully formed clusters form spontaneously on the myotube surface (DMEM) and their number increased significantly after agrin exposure (red arrows). Conversely, AChR microclusters (green arrows) were present after incubation of MuSK antibodies. In this case, fully formed clusters were rarely detectable. (**B**) Pooled results of 3 experiments showing that MuSK IgG subclasses increased the number of AChR microclusters compared to DMEM, and this was significant for MuSK IgG4. Conversely, only agrin induced a significant increase of fully formed AChR clusters. Scale bar represents 50 μm. One-Way ANOVA with multiple comparisons against DMEM was used. Mean + SEMs are shown.

expressed few spontaneous mature AChR clusters (<10 per field – Figure 6.4A - DMEM) and their number increased to more than 70/field following incubation with agrin (Figure 6.4A - agrin). In the presence of either MuSK IgG1-3 or IgG4, agrin-dependent AChR clustering was severely inhibited ($p<0.0001$, Figure 6.4A – IgG1-3 and IgG4) as the number of AChR clusters was comparable to that observed with DMEM. Fully formed clusters are indicated in Figure 6.4A with the red arrow. However, an increase of microclusters (Figure 6.4A – green arrow) was observed in the presence of each MuSK antibody subclass, and for the IgG4 antibodies this was similar to that induced by agrin (Figure 6.4B).

In order to identify at which stage MuSK IgG1-3 affected the maturation process, AChR clustering was studied over time, exposing the myotubes to the IgG1-3 antibody subclasses in the presence and absence of agrin (Figure 6.5). The number of fully-matured AChR clusters and microclusters was counted at 1, 2, 4, and 8 hours. AChR microclusters increased progressively under all the conditions studied, but their number rose more slowly in the presence of MuSK IgG1-3 and, at the final end-point of 8 hours, it was significantly lower compared to agrin ($p<0.0001$) (Figure 6.5B).

To evaluate additional potential effects of the MuSK antibodies on AChR clusters, the expression of the receptors was estimated through a radioactive assay. After overnight incubation with agrin, MuSK IgG1-3 and IgG4, myotubes were exposed to ^{125}I-bungarotoxin to label the membrane AChRs. Cell were then lysed and total CPM, which provides an estimate of the amount of the expression of the AChRs, were then measured with a γ-counter. Compared to agrin and DMEM, all MuSK IgG subclasses reduced the membrane expression of AChRs with a significant difference observed with the IgG1-3 subclasses ($p<0.05$) (Figure 6.6).

Finally, considering the newly observed effects of MuSK antibodies on AChR microclustering, the effects of SHP2 inhibition described in Chapter 3 were revisited to

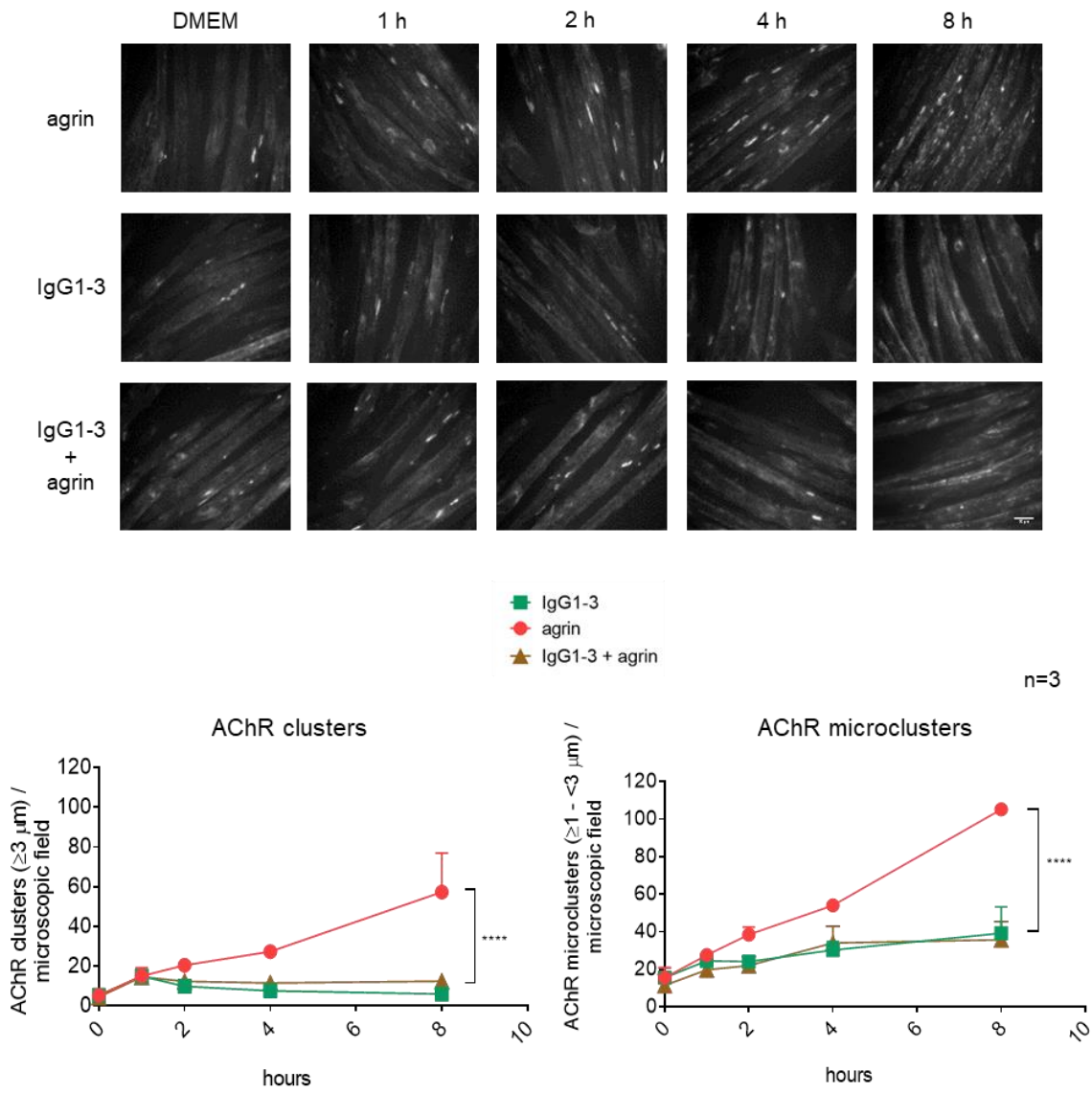


Figure 6.5. MuSK IgG1-3 partially increased AChR microclusters overtime but not fully-matured clusters. C2C12 myotubes were exposed to MuSK IgG1-3 in the presence and absence of agrin. Incubation was stopped at different time points (1h, 2h, 4h, and 8h) and AChR clusters stained with Alexa Flour 594 α-bungarotoxin. Clusters were then counted with ImageJ software using different thresholds for cluster length (≥1 - <3 µm for microclusters; ≥3 µm for fully formed clusters). (**A**) Representative images of AChR clusters. (B) Pooled results of 2 experiments showed that, in the presence of MuSK IgG1-3, the number of fully formed AChR clusters remained comparable to DMEM while progressive increase was observed for agrin. On the other hand, IgG1-3 induced a moderate increase in the number of microclusters although their number was significantly lower compared to those in agrin. Scale bar represents 50 µm. Two-way ANOVA for time was used. Mean + SEMs are shown.

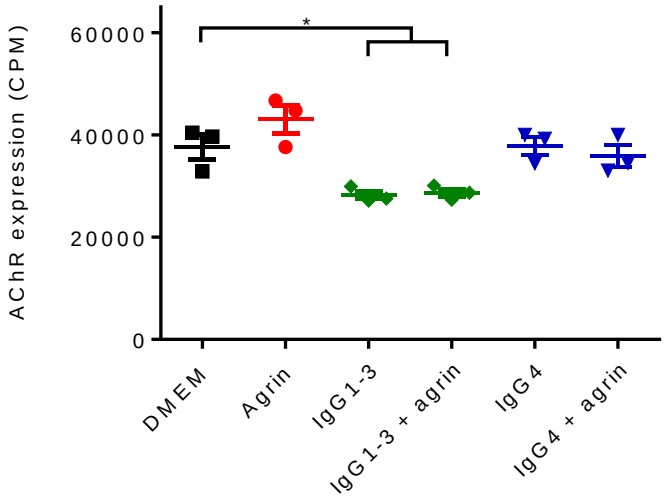


Figure 6.6. MuSK IgG1-3 partially reduced AChR membrane expression. Myotubes were exposed to agrin and MuSK antibody subclasses for 16 hours. AChR membrane expression was estimated pulling down AChRs with ^{125}I bungarotoxin and measuring the total CPM with a g-counter. Both IgG1-3 and IgG4 reduced the average expression of membrane AChRs but this was statistically significant only for IgG1-3. One-Way ANOVA with multiple comparisons against DMEM was used. Mean + SEMs are shown.

evaluate whether NSC-87877 was able to preserve full cluster maturation in the presence of the different antibody subclasses. In this respect, microscopic images from the experiments described in Chapter 3, paragraph 3.2.10, were re-analysed separating clusters according to their size with a threshold of 3 μm for fully-formed clusters (Figure 6.7). First, the number of microclusters induced by MuSK Total IgG, IgG1-3 and IgG4 was not significantly different compared to that observed with agrin, whereas fully-formed clusters were markedly reduced as expected. Notably, NSC-87877 increased significantly the number of both microclusters and fully-formed clusters in the presence of the individual IgG subclasses, indicating that SHP2 inhibition not only induced cluster formation but also supported the physiological maturation of the clusters.

6.2.5) Staining of rapsyn and β-actin on C2C12 myotubes

The next step was to understand in which way the AChR microclusters differ from the fully-formed clusters. Interactions between clusters, intracellular rapsyn and the β-actin microfilament scaffolding were therefore evaluated by immunohistochemistry. Optimisation of the technique, using different fixation/permeabilisation, was required to obtain a reliable staining of the targeted intracellular proteins. After overnight exposure of the cells to agrin, cells were fixed with formaldehyde followed by staining of AChR clusters with fluorescent α-bungarotoxin (red). Afterwards, permeabilisation of the cells were carried out with either triton X (0.1%) or saponin (0.1%). A third sample, not subjected to formaldehyde, was exposed to ice-cold acetone (100%) for combined fixation and permeabilisation. Finally, intracellular rapsyn and β-actin were probed with specific antibodies (as indicated in Chapter 2, Table 2.1) and labelled with fluorescent secondary antibodies (Figure 6.8, in green and blue respectively). Among the different conditions studied, a clear positivity for rapsyn, which co-localises with the AChR

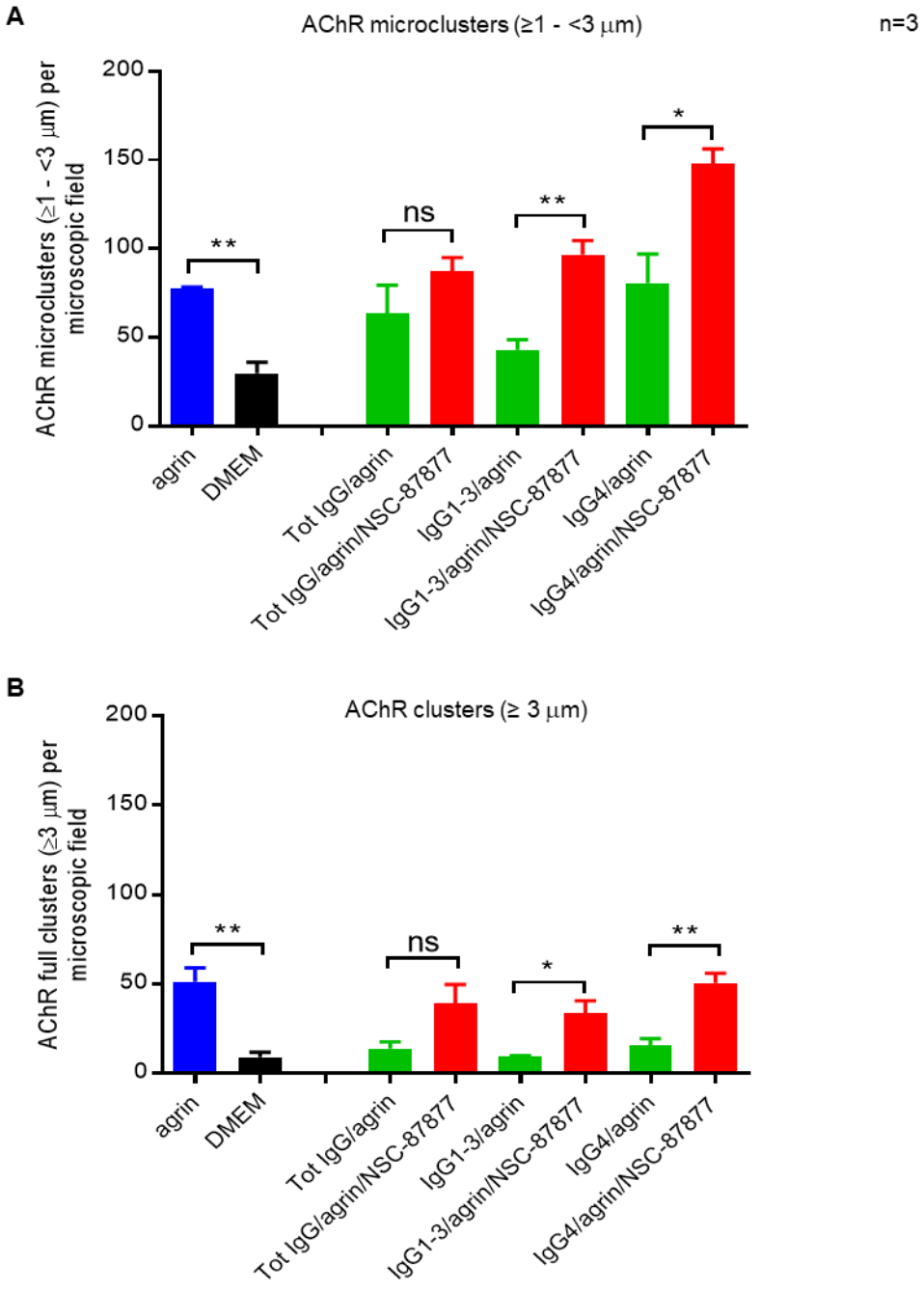


Figure 6.7. SHP2 inhibition increased both micro- and fully-formed AChR clusters in the presence of MuSK antibodies. Agrin-stimulated myotubes were exposed for 16 hours to MuSK IgG antibody subclasses, stained for AChR clustering with fluorescent α-bungarotoxin, and AChR clusters counted with ImageJ software using different thresholds for cluster length (≥1 - <3 μm for microclusters; ≥3 μm for fully formed clusters). Pooled results of 3 experiments show that the number of AChR microclusters **(A)** induced by MuSK antibodies was not significantly different compared to that observed with agrin. As expected, all MuSK antibody subclasses prevented full cluster maturation **(B)**. Notably, in the presence of both MuSK IgG1-3 and IgG4, SHP2 inhibition by NSC-87877 increased the number of microclusters and, more importantly, of fully-formed clusters. Two-sided t tests were used for comparisons at each IgG concentration. Mean + SEMs are shown.

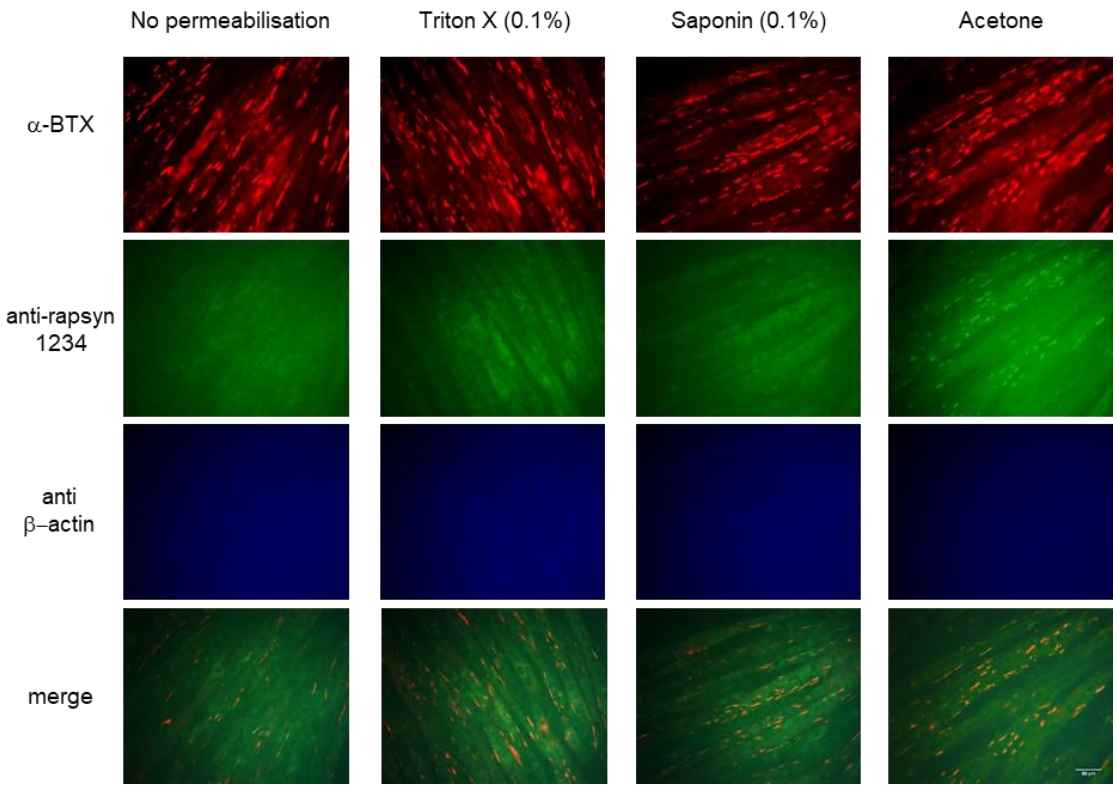


Figure 6.8. Optimisation of rapsyn and b-actin staining on C2C12 myotubes. C2C12 myotubes were exposed to agrin for 16 hours to induce AChR clustering. AChR clusters were stained as previously described with Alexa Fluor 594 α-bungarotoxin before permeabilising the cells with triton X, saponin, or ice-cold acetone. Samples treated with triton X and saponin were then fixed with formaldehyde, whereas further fixing was not required with acetone. Afterward, cells were exposed to primary antibodies against rapsyn and β-actin, and finally probed with secondary fluorescent antibodies Alexa Fluor 488 and 405 respectively. Among all the samples, only the one treated with acetone showed a clear positive staining for rapsyn. Co-localisation between AChR clusters and rapsyn was observed as shown in the merge image. On the other hand, β-actin filaments were not identifiable in any of the different experimental conditions tested. Scale bar represents 50 µm.

clusters, was observed only in the sample exposed to acetone, indicating an effective permeabilisation of the myotubes (Figure 6.8 – merge). However, staining for β-actin was not successful as no positive labelling was observe in any of the samples, suggesting a low efficacy of the antibody used.

A different approach was tested to optimise the staining of the actin filaments. As described above, myotubes were exposed to agrin overnight, stained for AChR clusters, and finally fixed and permeabilised with acetone. The staining of rapsyn was carried out as before and, in parallel, cells were incubated with fluorescent phalloidin which successfully labelled the actin filaments (Figure 6.9 – blue). To better visualise the filament scaffolding, the presence and shape of AChR clusters, high resolution images were acquired with confocal microscopy. The optimisation of this technique, with the acquisition of confocal images, represented a necessary preparatory step for the subsequent qualitative analysis of the cytoskeleton scaffolding after exposure of the myotubes to MuSK antibodies described below.

6.2.6) Co-localization between rapsyn and AChR microclusters is reduced compared to fully-formed clusters

As rapsyn plays a fundamental role in the maturation of AChR clusters by anchoring the AChR subunits to the underlying cytoskeleton, the next question was whether AChR microclusters induced by MuSK antibodies interact with rapsyn molecules as expected for fully-formed AChR clusters. After incubation with either agrin, MuSK IgG1-3, or MuSK IgG4 antibodies, myotubes were stained for AChR clusters and intracellular rapsyn as indicated above and, to achieve greater definition, 20 microscopic fields for each sample were captured using confocal microscopy (Figure 6.10). Co-localisation between AChR clusters and rapsyn was analysed with Fiji-ImageJ software using the

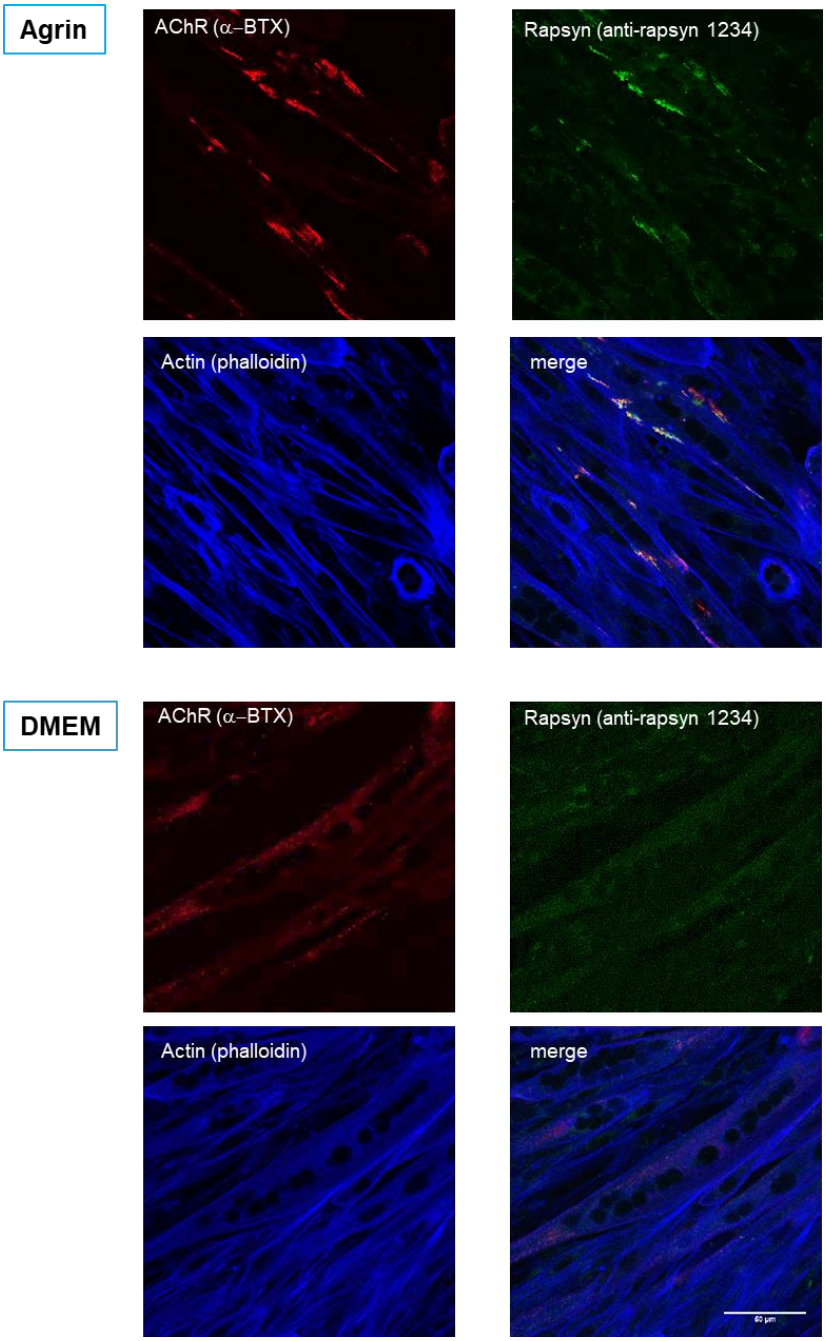


Figure 6.9. O**ptimisation of β-actin staining on C2C12 myotubes**. C2C12 myotubes were exposed to agrin for 16 hours to induce AChR clustering and cells incubated with DMEM only were used as control. AChR clusters were stained as previously described with Alexa Fluor 594 α-bungarotoxin before permeabilising and fixing the cells with ice-cold acetone. Myotubes were then probed with a mouse primary antibody against rapsyn, in parallel with Alexa Flour 405 phalloidin for the actin filaments. Finally, cells were exposed to an anti-mouse secondary fluorescent antibody Alexa Fluor 488 for rapsyn detection. As already described, the staining for rapsyn showed good co-localisation with AChR clusters in the samples incubated with agrin. In addition, fluorescent phalloidin proved to be highly effective in the staining of the intracellular structure of actin filaments. High resolution images were taken with a Zeiss LSM 780 upright multi-photon confocal. Scale bar represents 50 µm.

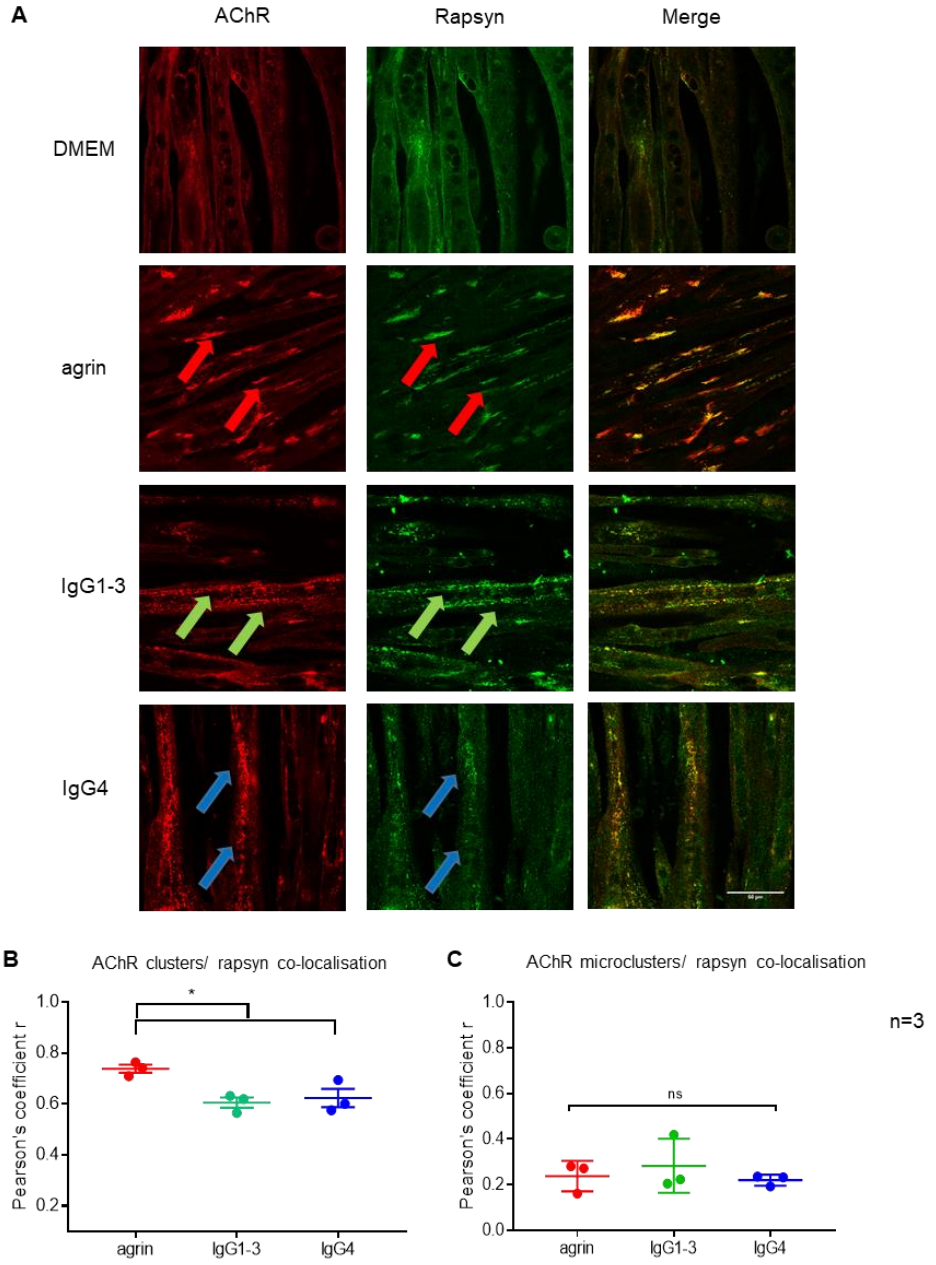


Figure 6.10. Co-localization between rapsyn and AChR microclusters is reduced. C2C12 myotubes were exposed to MuSK antibody sublasses for 16 hours to induce AChR microclusters. Cells incubated with agrin and DMEM only were used as control. AChR clusters were stained as previously described with fluorescent α-bungarotoxin. Rapsyn staining was performed after cell permeabilisation and fixing with acetone. **(A)** Representative microscopy images. In the presence of agrin, fully formed AChR clusters showed a high level of colocalisation with rapsyn (red arrows), whereas it was less evident for microclusters induced by MuSK IgG1-3 (green arrows) or IgG4 (blue arrows). **(B)** Co-localisation between AChR clusters and rapsyn was quantified evaluating the level of correlation (Pearson's r) between the images using JaCoP plug-in for Fiji-ImageJ. Pooled results of 3 experiments showed a significantly higher correlation in agrin-induced clusters compared to that induced by MuSK IgG subclasses. **(C)** When the analysis was restricted to microclusters, no significant co-localisation was found in any of the samples. High resolution images were taken with a Zeiss LSM 780 upright multi-photon confocal microscope. Scale bar represents 50 µm. One-way ANOVA with multiple comparisons was used. Mean + SEMs are shown.

plug-in JaCoP. The software estimates the degree of overlap between two fluorescent images providing a correlation measurement through Pearson's coefficient (r).

When the clusters were analysed irrespective of their size, a correlation was found between AChR clusters and rapsyn in the agrin sample (Pearson's coefficient r=0.73) supporting a significant co-localisation of the two proteins (Figure 6.10 A – agrin, red arrows). On the other hand, in the presence of MuSK antibodies, co-localisation was lower, especially in the samples exposed to IgG1-3 (Figure 6.10 A and B – MuSK IgG1-3 and IgG4, green and blue arrows; r=0.6 for IgG1-3, and 0.62 for IgG4; $p<0.05$ for both antibody subclasses compared to agrin). Notably, when a size threshold for microclusters was applied (Figure 6.10 B), the co-localisation between AChRs and rapsyn was decreased in all samples, with a reduction of the mean r value below 0.5.

6.2.7) β-actin intracytoplasmic inclusions were present after exposure to MuSK antibodies

A potential impairment in the arrangement of actin filaments caused by MuSK antibodies was then evaluated. Myotubes were exposed overnight to either agrin or MuSK IgG1-3 and IgG4, stained for AChR clusters, permeabilised with acetone, and the actin filament finally labelled with phalloidin. A way to digitally quantify potential differences in the cytoskeleton scaffolding among samples was explored, although no reliable methodology was found due to the intrinsic characteristics of the filaments' structure. Therefore, confocal images (20 per sample) were evaluated by two blinded investigators for qualitative differences (Figure 6.11). Notably, both investigators were able to identify the samples incubated with MuSK antibodies due to the presence of intracytoplasmic inclusions positively stained with phalloidin (Figure 6.11 – lower panels, red arrows).

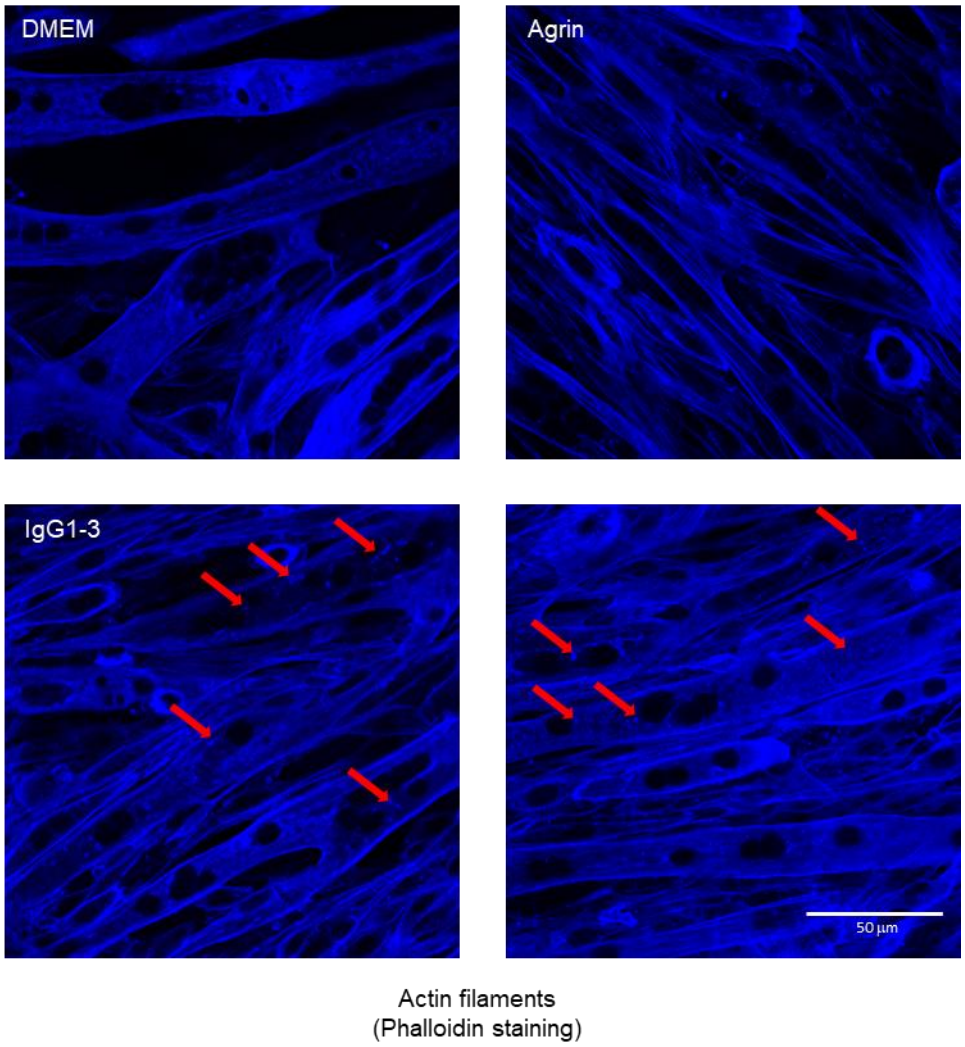


Figure 6.11. Altered structure of β-actin with intracytoplasmatic inclusions was detected in the presence of MuSK antibodies. C2C12 myotubes were exposed for 16 hours to agrin and MuSK antibody subclasses, and cells incubated with DMEM only were used as control. Cells were then permeabilised and fixed with ice-cold acetone, and stained for the actin filaments with Alexa Flour 405 phalloidin. Images from 20 microscopic fields were taken and qualitative evaluated by a blinded investigator. Samples incubated with MuSK antibodies, either IgG1-3 or IgG4, were identified by the investigator as characterised by the appearance of more cytoplasmic inclusions (arrows) compared to agrin, suggesting an involvement of the cytoskeleton structure. High resolution images were taken with a Zeiss LSM 780 upright multi-photon confocal microscope. Scale bar represents 50 µm.

6.2.8) MuSK IgG1-3 and IgG4 activated Rho GTPase

In an attempt to explain the failing of AChR cluster maturation and partial disruption of the structure of actin filaments induced by MuSK IgG1-3 and IgG4, the effects of MuSK antibodies were investigated on the subsidiary GTPase intracellular pathway of Rho and Rac1. As discussed in detail in Chapter 1, the physiological activation of Rho and Rac1 downstream of MuSK determines the cytoskeleton rearrangements required for clusters formation and maturation (Weston, Gordon et al. 2003).

First, to reliably measure the levels of active Rho and Rac1, two commercial kits were tested and optimised. Although different in terms of reagents and detection of the targeted protein (western blotting for Rho, and immunoabsorbance with ELISA for Rac1), both techniques shared the same principle of using a GST-linked protein to pull down the active form of the GTPases.

As GTPase activation is a very labile and fast-occurring event, the first attempt to measure the level of active Rho was carried out after exposing the myotubes to agrin for different periods of time (15, 30 and 45 minutes), after starving the cells for 3 hours to reduce the basal activity of intracellular GTPases. The lysis buffer provided in the commercial kit was initially used, and active Rho was pulled down by incubating the cell lysate with GST-Rhotekin. Protein levels were analysed by western blotting by running two parallel gels, one for the active form of Rho that was pulled down, and the second for the cell lysate for the total protein expression (Figure 6.12 A1). Rho was clearly and equally present in all the cell lysates as indicated by the corresponding 20 kDa band detected in the blot probed for the total protein expression (Figure 6.12 A1 – right). In the blot probed for the active protein, a faint band was detected at the same molecular size, although no changes were evident after agrin incubation at the different time points (Figure 6.12 A1 – left).

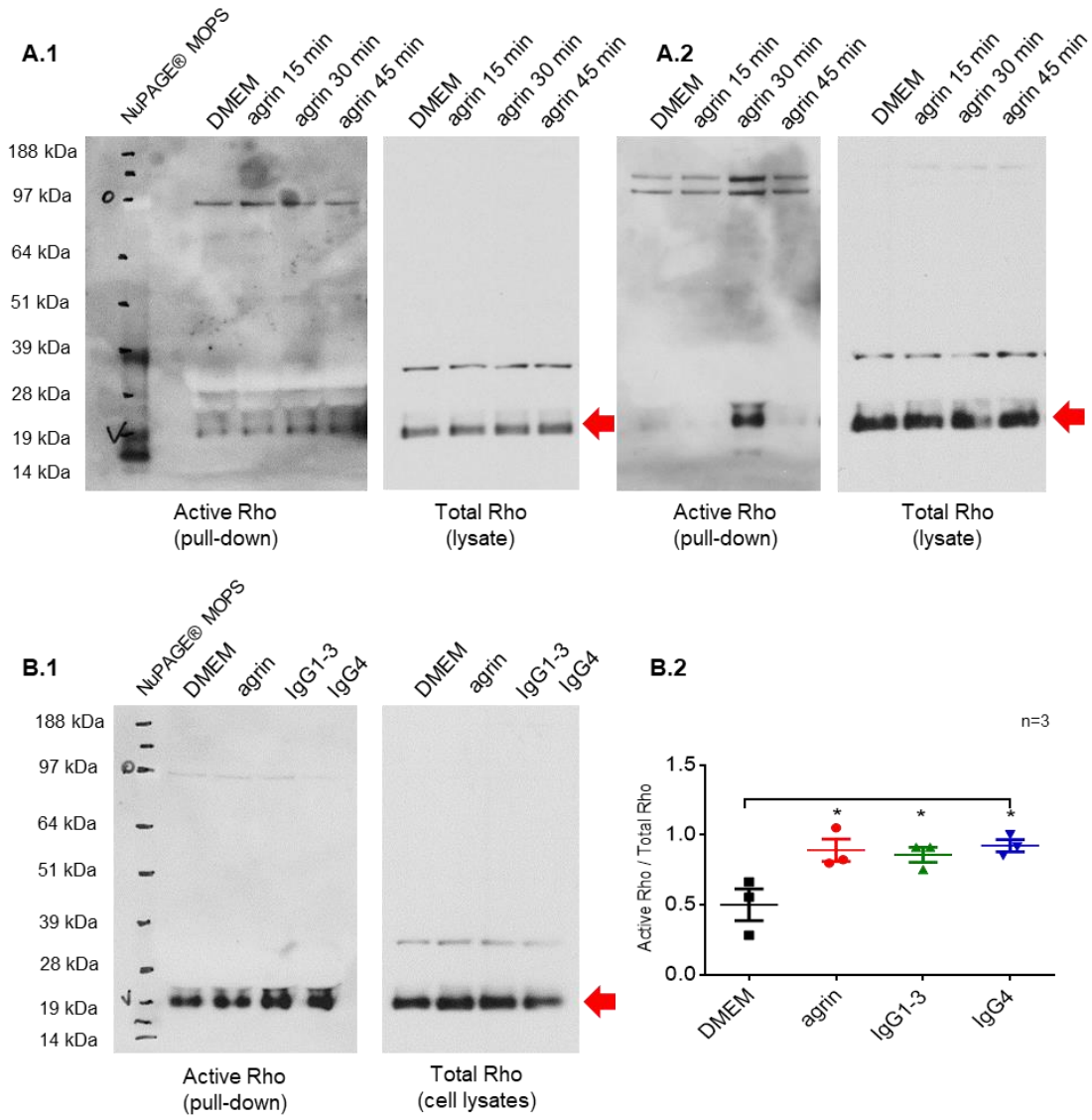


Figure 6.12. MuSK IgG1-3 and IgG4 activate of Rho GTPase. (A) Optimisation of active-Rho pull down. (**A.1)** myotubes were starved for 3 hours to reduced the basal activity of intracellular GTPases, then exposed to agrin and lysed at different incubation times (15, 30 and 45 minutes) with the lysis buffers provided in the commercial kit. Active Rho was pulled down incubating the lysates with GST-Rhotekin, which binds to the active form of the protein, and protein levels analysed by western blotting. Cell lysates not exposed to GST-Rhotekin were used as control for the total Rho expression. Faint 20 kDa bands (consistent with the size of Rho) were detected but no changes induced by agrin were observed at any time point. **(A.2)** Starvation of the cells was prolonged to 24 hours and concentration of Ca++ and Mg++ was increased in the lysis buffers to preserve the GTPase signal. In this case, a strong active-Rho band was detected in the sample exposed to agrin for 30 min. **(B)** Using the same experimental conditions, myotubes were exposed to agrin or MuSK antibody subclasses for 30 minutes, and active-Rho analysed by western blotting. **(B.1)** Representative western blot showing the presence of a strong signal for active-Rho induced by agrin and both IgG1-3 and IgG4. **(B.2)** Pooled results of 3 experiments showing that agrin, IgG1-3 and IgG4 induced a similar increase in the Rho activation compared to DMEM. Levels of active-Rho were normalised to the total Rho expression. One-Way ANOVA with multiple comparisons against DMEM was used. Mean + SEMs are shown. Bands corresponding to Rho are indicated by the red arrow.

In order to improve the sensitivity of the technique, myotubes were starved for 24 hours to further reduce the cell metabolism and increase the GTPase response to agrin stimulation. In addition, the concentration of Ca^{++} and Mg^{++} was increased in the lysis buffer (see Chapter 2, paragraph 2.17) to stabilise the GTPase signal (as indicated in the original study by Weston et al (Weston, Gordon et al. 2003)). Following these methodological changes, an increase in Rho activation was clearly detectable after 30-minute exposure to agrin (Figure 6.12 A2), indicating that this was a reliable time point to use. Myotubes were then incubated with MuSK IgG1-3 and IgG4 under the same experimental conditions, and a strong band corresponding to the active protein was detected in all the samples exposed to either agrin or the MuSK antibody subclasses (Figure 6.12 B1). When the level of active Rho was normalised to the total Rho expression after pooling 3 individual experiments, both agrin and the MuSK antibody subclasses induced a similar increase in the Rho activation compared to medium only ($p<0.05$, Figure 6.12 B2). This suggests that MuSK antibodies, independent of their subclass, have the potential to trigger cytoskeleton modifications through Rho activation, mimicking the physiological activation by agrin.

Finally, to evaluate whether the GTPase signal was forwarded downstream of Rho, the activation of Rac1 was studied after incubation of the myotubes with agrin and MuSK IgG1-3 antibodies at different time points (7, 15, 30, 45 minutes). Due to the limited availability of ELISA plates, the overall cost of the detection kit, and the volatility of the GTPase signal (which limited the number of samples that could be processed for each experiment), precedence was given to the IgG1-3 subclasses with the aim of analysing the IgG4 fraction only in case promising results were observed. As mentioned above, the commercial kit measured Rac1 activation through an immunoabsorbent ELISA rather than western blotting. First, total protein concentration was estimated in the cell lysate by BCA colorimetric assay, and then a normalised volume of lysate was

loaded to an ELISA plate coated with a GTP-binding protein, which interacts specifically with the active form of Rac1. On average, the level of active Rac1 detected in the samples incubated with agrin and MuSK IgG1-3 was a little higher compared to that of medium only (Figure 6.13). However, the difference did not reach statistical significance due to the high variability in the measurements, highlighting the difficulty in maintaining a detectable GTPase signal throughout the experiment and the likely lack of sensitivity of the whole assay. In this respect, even the positive control, which is a constitutively active Rac1 provided in the commercial kit, did not reach significance compared to DMEM.

6.2.9) Optimisation of MuSK-Lrp4 co-immunoprecipitation

One of the suggested pathogenic mechanisms of MuSK IgG4 is the interference in the interaction between MuSK and Lpr4 (Huijbers, Zhang et al. 2013, Koneczny, Cossins et al. 2013) which leads to the inactivation of MuSK. On the contrary, this effect was not observed for the IgG1-3 subclasses as they were not able to disrupt the co-immunoprecipitation of the MuSK-Lrp4 complex in a HEK 293 model (Koneczny, Cossins et al. 2013). Here, a similar set of experiments was attempted to confirm this finding. Transfected HEK 293T cells and the more physiological setting of C2C12 myotubes were used.

First, it was important to verify whether the two antibodies available in our lab (mouse monoclonal antibodies anti-Lrp4 (TA326569 and N207/27) were able to detect reliably Lrp4. HEK 293T were transfected with either *LRP4*, *MUSK*, or a combination of the two, and the cell lysates analysed by western blotting for protein expression (Figure 6.14). The nitrocellulose membrane was first probed for Lrp4 with TA326569 antibody (Figure 6.14 – left), then stripped and reprobed with N207/27 (Figure 6.14 – middle),

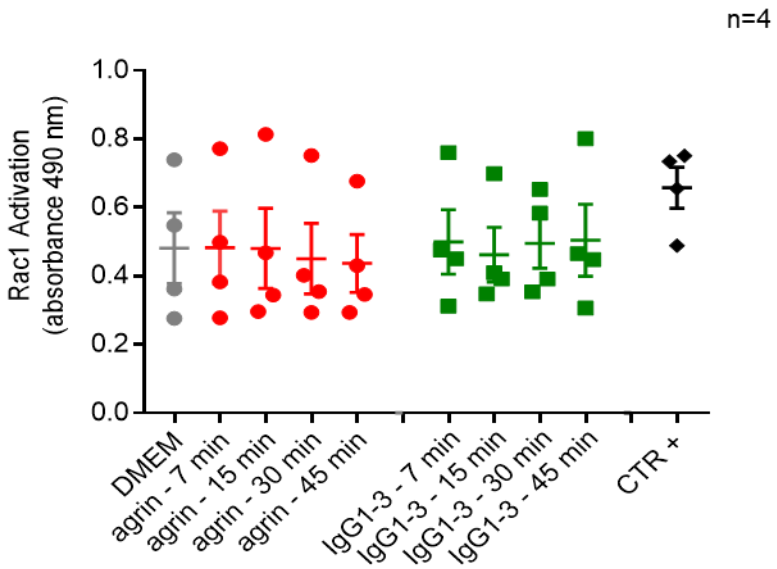


Figure 6.13. Agrin and MuSK IgG1-3 did not activate Rac1 GTPase. Activation of GTPase Rac1, which is downstream of Rho, was studied on myotubes incubated for different times with agrin and MuSK IgG1-3. Total protein concentration in the cell lysate was estimated by BCA colorimetric assay. A normalised volume of lysate was then incubated with the ELISA plate coated with a Rac-GTP-binding protein which is specific for the active form of Rac1. Plates were then probed with an anti-Rac1 antibody and a secondary HRP for the plate reading. Pooled results from 4 experiments are shown. No statistically significant differences were observed over time in samples incubated with either agrin or MuSK IgG1-3, despite in the latter the average level of Rac1 activity was higher compared to DMEM. This was also observed for the positive control, which is a constitutively active Rac1 provided in the commercial kit. The high variability in the measurements, including the positive control, highlights the inner difficulty of preserving the GTPase signal and an overall limited sensitivity of the assay. One-Way ANOVA with multiple comparisons against DMEM was used. Mean + SEMs are shown.

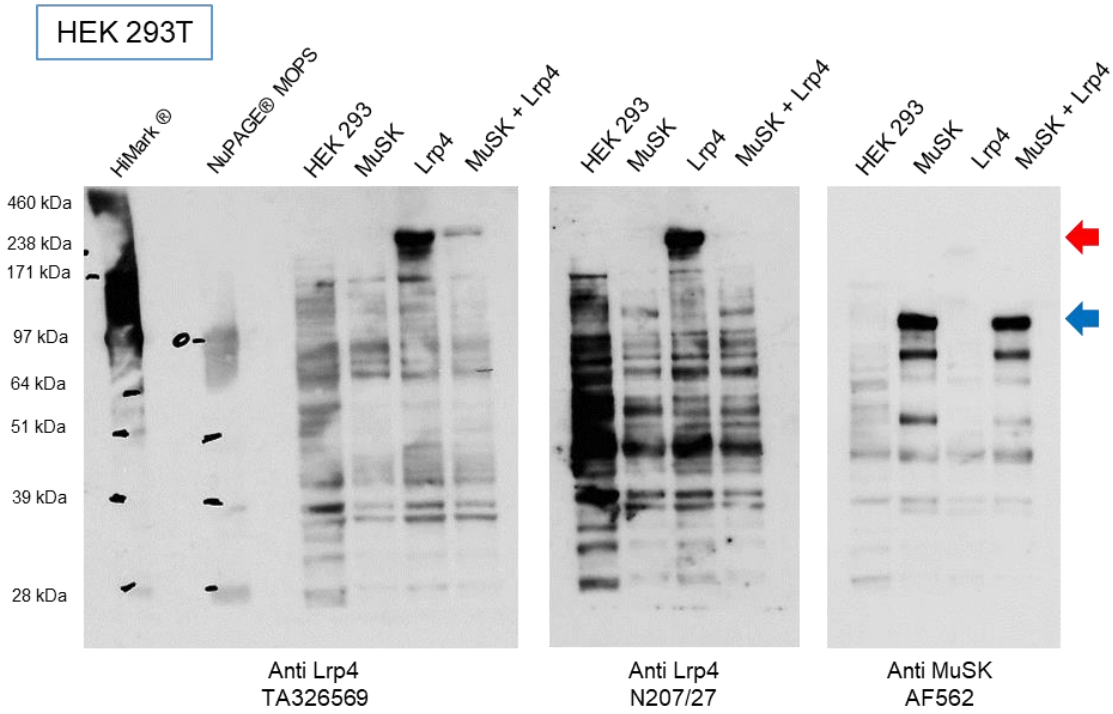


Figure 6.14. Detection of Lrp4 on transfected HEK cells. HEK 293 cells were transfected with recombinant *LRP4*, *MUSK*, and with both the constructs together. Protein expression in the cell lysate was then detected by western blotting. Non-transfected HEK cells were used as control. Two different anti Lrp4 antibodies were tested, TA326569 and N207/27 (the latter on the same nitrocellulose membrane after stripping). Similar results were observed for both antibodies. A strong band at around 213 kDa corresponding to Lrp4 (red arrow) was present in the cells transfected with *LRP4* only, and a fainter one in the cells transfected with both *MUSK* and *LRP4.* The nitrocellulose membrane was then stripped and reprobed for MuSK with the usual anti-MuSK AF562 antibody. A strong band at 97 kDa (blue arrow) was detectable in the samples transfected with *MUSK* alone and together with *LRP4*.

finally stripped for a second time and probed for MuSK with AF562 (Figure 6.14 – right). Both TA326569 and N207/27 detected a strong band at 213 kDa corresponding to the size expected for Lrp4 in the sample transfected only with the *LRP4* plasmid. A fainter band of similar size was observed in the cells co-transfected with *LRP4* and *MUSK* in the blot probed with TA326569, despite using the same amount of *MUSK* and *LRP4* plasmid DNA to transfect the cells. This might be due to the bigger size of the *LRP4* plasmid leading to a more effective transfection of the smaller *MUSK*. Notably, the same band was not detectable with N207/27, likely as a result of the harsh stripping of the nitrocellulose membrane. On the other hand, MuSK was strongly detectable (97 kDa) in all the samples transfected with *MUSK* (either alone or in combination with *LRP4*).

The following experiments aimed to optimise the co-immunoprecipitation of Lrp4 and MuSK. An initial attempt was performed on C2C12 myotubes (Figure 6.15A), in which interaction between MuSK-Lrp4 was first triggered by exposing the cells to agrin for 40 minutes. MuSK immunoprecipitation was carried out as previously described incubating the cell lysate with Protein G magnetic beads and anti-MuSK AF562. Samples incubated with medium only, beads without anti-MuSK antibody, and plain cell lysates were used as control. However, when the blots were probed with anti-Lrp4 TA326569 and N207/27 antibodies (Figure 6.15A, left and right respectively), no bands were detected at the correct size of 213 kDa in either immunoprecipitated samples or controls, including the myotube lysate. As results were similar for both anti-Lrp4 antibodies, in the subsequent experiments only N207/27 was used as it provided clearer blots with less non-specific binding.

Co-immunoprecipitation was then attempted on HEK 293T cells double-transfected with *MUSK* and *LRP4*. Samples transfected with only *MUSK*, *LRP4*, and wild type HEK not subjected to immunoprecipitation were used as control. Initially, the

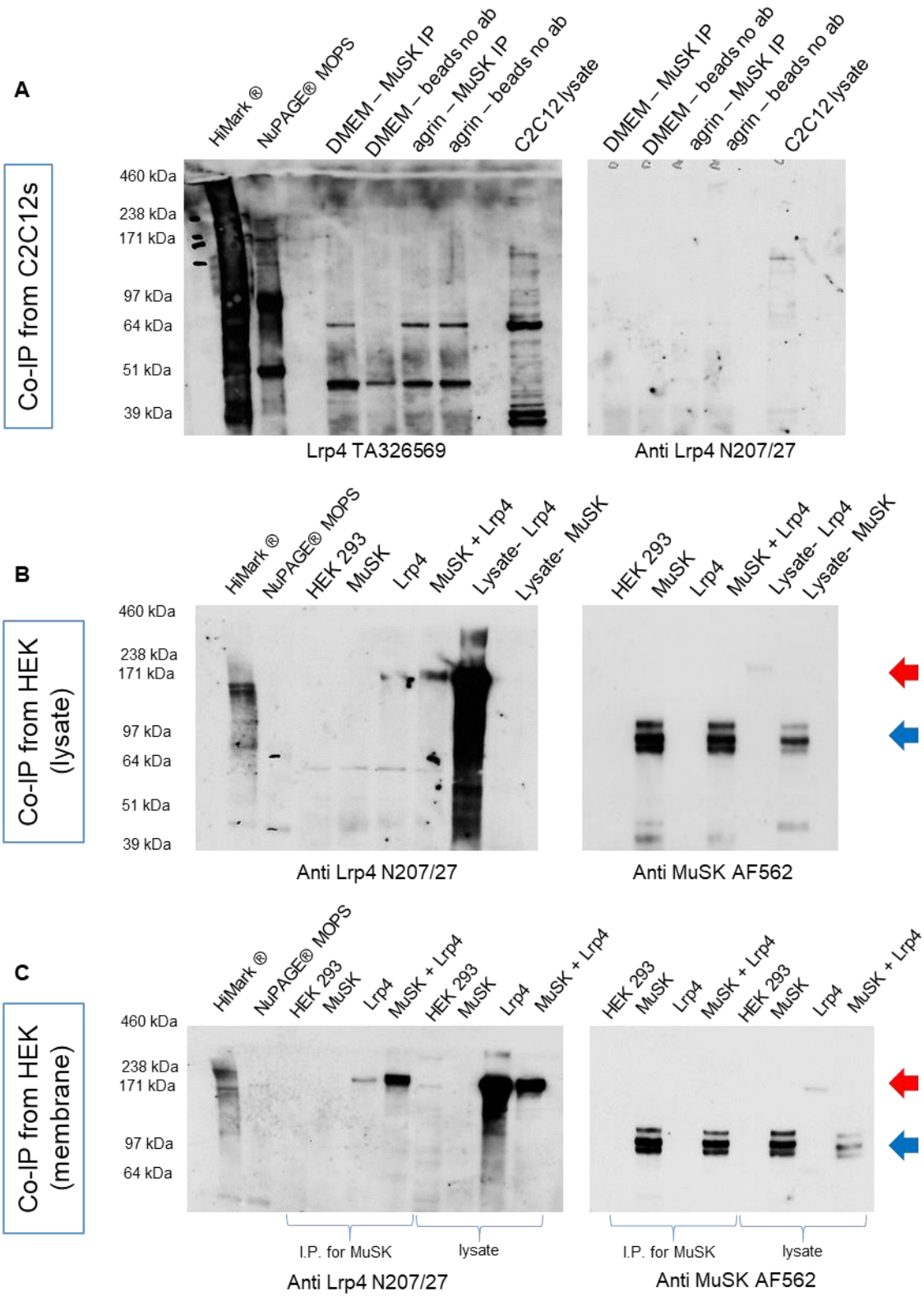

A
Co-IP from C2C12s
HiMark ®
NuPAGE® MOPS
DMEM – MuSK IP
DMEM – beads no ab
agrin – MuSK IP
agrin – beads no ab
C2C12 lysate
460 kDa
238 kDa
171 kDa
97 kDa
64 kDa
51 kDa
39 kDa
Lrp4 TA326569
Anti Lrp4 N207/27
B
Co-IP from HEK (lysate)
HEK 293
MuSK
Lrp4
MuSK + Lrp4
Lysate- Lrp4
Lysate- MuSK
Anti Lrp4 N207/27
Anti MuSK AF562
C
Co-IP from HEK (membrane)
I.P. for MuSK
lysate

Figure 6.15. Optimisation of MuSK-Lrp4 co-immunoprecipitation from HEK 293 cells and C2C12 myotubes. (A) C2C12 myotubes were exposed to agrin for 40 minutes to induce MuSK-Lrp4 interaction. Immunoprecipitation of the MuSK-Lrp4 complex was attempted by incubating the cell lysates with anti-MuSK AF562. Samples incubated with Protein-G beads in the absence of AF562 and cell lysate were used as controls. However, no bands were detected at the correct size of 213 kDa on the western blots probed with the two different anti-Lrp4 antibodies. **(B)** HEK 293 cells were transfected with recombinant *LRP4*, *MUSK*, and with both the constructs together. In this case, a clear band corresponding to Lrp4 (red arrow) was detectable in the cell lysate of the sample co-transfected with both *MUSK* and *LRP4* when anti-MuSK AF562 was used for immunoprecipitation. Cell lysates were used for comparison. **(C)** Co-immunoprecipitation of MuSK and Lrp4 from the membrane was performed by exposing the transfected cell to anti-MuSK AF562 for 1 h before lysing the cells. As observed in (**B)**, a strong band corresponding to Lrp4 was detected in the co-transfected sample, confirming the efficacy of the co-immunoprecipitation. The band at 97 kDa corresponds to MuSK (blue arrow).

experiment was carried out on the total cell lysate (Figure 6.15 B) using the anti-MuSK AF562 for the co-immunoprecipitation. A band at 213 kDa corresponding to Lrp4 was observed in the sample co-transfected with both *MUSK* and *LRP4* indicating effective co-immunoprecipitation.

Finally, the experiment was repeated incubating the anti-MuSK AF562 antibody directly with the cells for 1 hour before lysing, in order to immunoprecipitate only the MuSK-Lrp4 complexes expressed on the cell membrane (Figure 6.15 C). As observed previously, a strong band corresponding to Lrp4 was detected in the co-transfected sample, confirming the efficacy of the co-immunoprecipitation (Figure 6.15C - left). A fainter Lrp4 band was detected also in the sample transfected with only Lrp4, although this seems likely related to the very high expression of Lrp4 as indicated by the strong density of the corresponding band in the cell lysate. As expected, the MuSK band at 97 kDa was present only in the samples transfected with *MUSK* (Figure 6.15 C - right).

6.2.10) MuSK IgG1-3 partially reduced Lrp4-MuSK interaction

Following optimisation of the co-immunoprecipitation technique, the potential disruption of the binding between MuSK and Lrp4 by MuSK IgG1-3 was studied in the HEK cell model. After transfection with *LRP4* and *MUSK*, HEK 293T cells were exposed to the MuSK antibody subclasses (0.5 nM) before cell lysis to immunoprecipitate the MuSK-Lrp4 complexes expressed on the membrane. Samples incubated with either commercial anti-MuSK AF562 or healthy control IgG (at a concentration equivalent to the total protein in the MuSK antibody preparation) were used as control, similar to that described in the previous study by Koneczny et al (Koneczny, Cossins et al. 2013). In addition, double-transfected HEK cells incubated only with DMEM, and exposed to Protein G magnetic beads in the absence of antibodies, were used as an additional control to evaluate potential non-specific binding

and immunoprecipitation of either MuSK or Lrp4 by the beads (Figure 6.16 – DMEM lanes). In the western blots, despite a strong Lrp4 signal when co-immunoprecipitated with anti-MuSK AF562, a fainter band was detectable in all the remaining samples, including the healthy control IgG (Figure 6.16 A – left). This suggests that a proportion of Lrp4 was immunoprecipitated by the different antibody preparations independent of MuSK. Conversely, MuSK was not detectable in the healthy control sample (Figure 6.16 A – right). To correct for this bias, the density value of the control IgG was subtracted from the other samples in the densitometry quantification (Figure 6.16 B). Analysis was then carried out normalising the density of each Lrp4 band to the corresponding MuSK values to estimate the proportion of Lrp4 molecules pulled down together with MuSK. After normalisation and bias correction, the level of Lrp4 co-immunoprecipitated with MuSK was significantly reduced for both IgG1-3 and IgG4 antibodies suggesting that all subclasses impair MuSK-Lrp4 interaction. As expected, this was particularly pronounced for MuSK IgG4.

6.2.11) Transcriptional modifications induced by MuSK antibodies

In the final set of experiments, it was evaluated whether the effects on AChR clustering caused by the MuSK IgG1-3 could be partially related to changes in the gene expression pattern of the muscle cell. Myotubes were exposed for 2.5 h to either DMEM, agrin, MuSK IgG1-3, or total IgG purified from a healthy individual. Intracellular RNA was then extracted and, as described in Chapter 3, samples were sent in triplicate for transcriptomic sequencing to Novogene (UK) Company Ltd. Further analysis (aligning of the RNA sequences, reads counting and comparison among samples) was carried out using the bioinformatic programmes as described in Chapter 2, paragraph 2.8. Modifications in gene transcription of at least 1 log fold were considered significant.

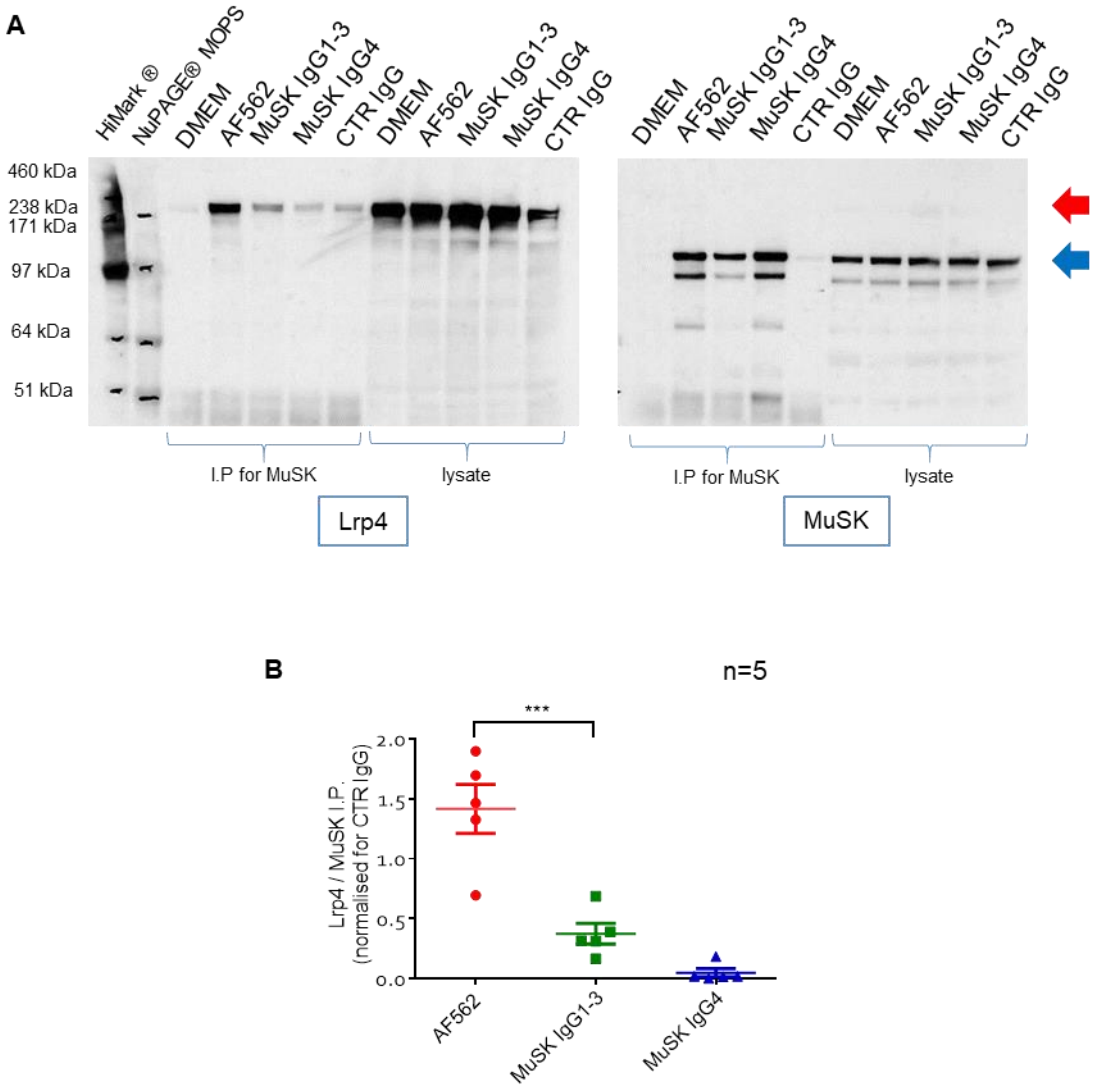


Figure 6.16. MuSK IgG1-3 partially reduced MuSK-Lrp4 interaction. HEK 293 cells were co-transfected with recombinant *LRP4* and *MUSK*, and then exposed to anti-MuSK AF562, and patients' MuSK subclasses, and healthy control IgG for 2.5 hours at 37ºC. Co-immunoprecipitation of the membrane MuSK-Lrp4 complex was analysed by western blotting as previously described. **(A)** The representative western blot shows a much fainter Lrp4 band in the samples immunoprecipitated with patients' MuSK antibody subclasses. A faint band was also present in the healthy control IgG suggesting a mild non specific binding. In comparison, MuSK bands were significantly stronger and there was no binding in the healthy control. Cell lysates were used as comparison for protein expression. DMEM lanes correspond to double-transfected HEK cells exposed to Protein G beads in the absence of IP antibodies. **(B)** Pooled results of 5 experiments shows that all MuSK antibody subclasses reduced the level of Lrp4 co-immunoprecipitatied with MuSK suggesting an impairment in MuSK-Lrp4 interaction, and this was particularly evident for MuSK IgG4. Bands corresponding to Lrp4 and MuSK are indicated with the red and blue arrows respectively.

First, the expression pattern induced by physiological agrin stimulation was analysed and compared against the baseline expression with DMEM (Table 6.1). No genes were modified more than 2 log fold from their basal level. An upregulation between 1 and 2 log fold was however observed in the following genes: Uba52, Rps28, Snrpg, Cxcl5, Cxcl1, Zdhhc14; on the other hand, none of the genes showed a significant downregulation with the only exception of Ngfr which nearly reached the 1 log fold threshold reduction. All these genes are mainly involved in cell growth, replication, signal transduction, and protein synthesis as indicated by the pathway interaction analysis performed with the online platform Reatcome (Figure 6.17). No genes or pathways specifically or exclusively involved in the AChR clustering were found.

When the gene expression was analysed after incubation of the myotubes with MuSK IgG1-3, more than 350 genes were upregulated and 120 downregulated (at least 1 log fold) compared to the DMEM baseline. Conversely, the control IgG induced an upregulation of 45 genes, and a downregulation of other 20. Of these genes, 22 were modified by both MuSK and control IgG (19 upregulated, and 3 downregulated, see Table 6.2) and, therefore, were not considered in the analysis. Cytokines and transcriptional factors (e.g. IL6, TNF, Cxcl5, Fos and Ras) were the gene categories most represented. Notably, Hs3st1 and Rgs2 (a Sulfotransferase and a GTPase regulator respectively) were the only two genes upregulated by the control IgG and downregulated by MuSK IgG1-3. On the other hand, the expression of Hivep3 (a zinc-finger transcription factor associated with NF-Kb) was reduced by control IgG and increased by MuSK IgG1-3.

Due to the high number of genes modified by the antibodies, the expression cut-off was increased to 2 log fold in order to improve the specificity of the analysis. After these considerations, a total of 117 genes were modified by MuSK IgG1-3 (102 upregulated and 15 downregulated, see Table 6.3 and 6.4).

Gene	logFC	P value	Protein
Zdhhc14	1.47551	5.14×10^{-5}	Zinc Finger DHHC-Type Palmitoyltransferase 14
Cxcl1	1.2945	2.82×10^{-08}	C-X-C Motif Chemokine Ligand 1
Cxcl5	1.20594	1.21×10^{-6}	C-X-C Motif Chemokine Ligand 5
Snrpg	1.09073	1.18×10^{-6}	Small Nuclear Ribonucleoprotein Polypeptide G
Rps28	1.02662	2.11×10^{-17}	Ribosomal Protein S28
Uba52	1.01889	2.08×10^{-32}	Ubiquitin A-52 Residue Ribosomal Protein Product 1
Ngfr	-0.89491	0.000827	Nerve Growth Factor Receptor

Table 6.1. Genes modified by agrin compared to DMEM. Log-fold changes (logFC), P value, and encoded protein are indicated for each gene.

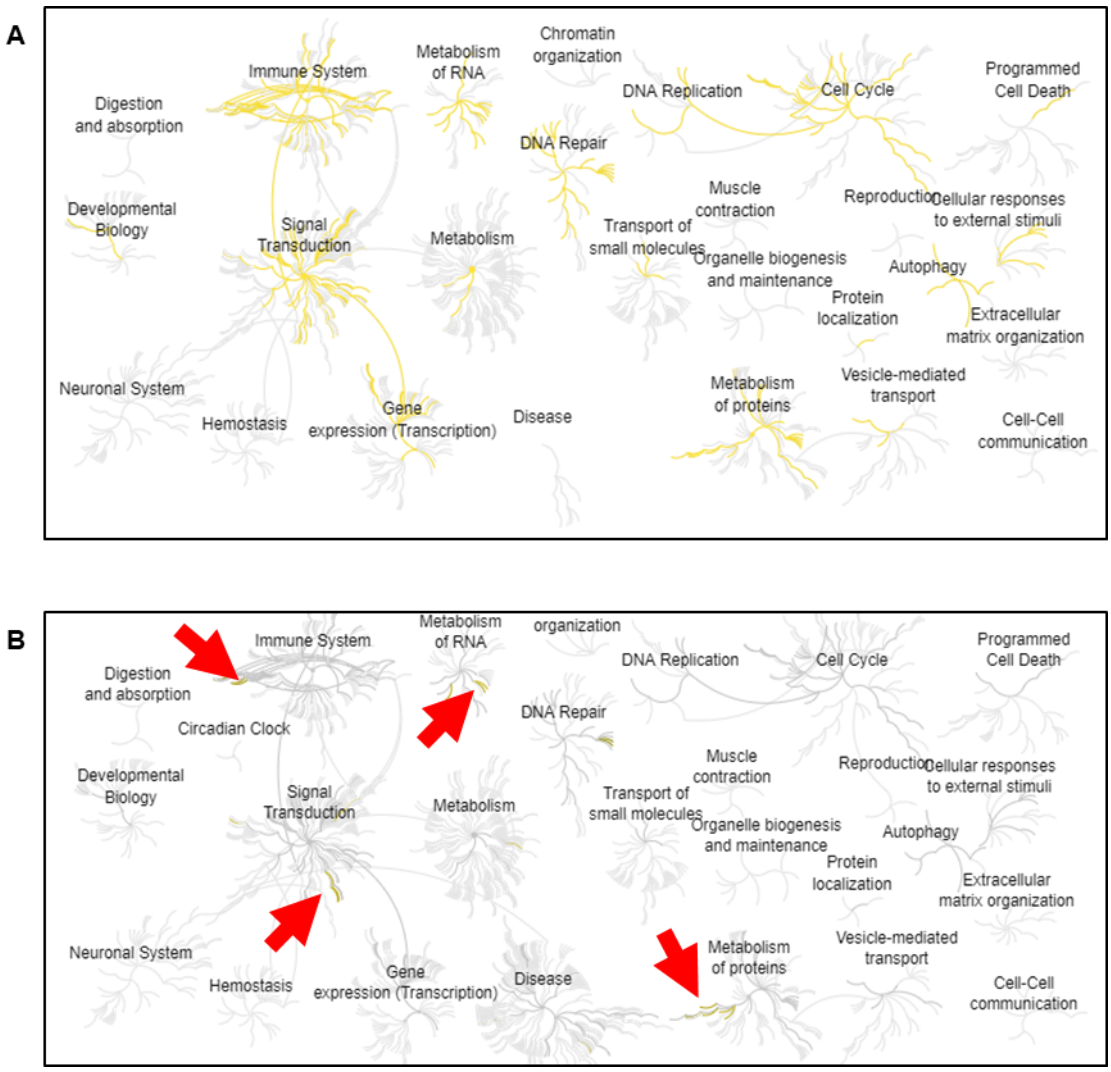


Figure 6.17. Transcriptional modifications induced by agrin on C2C12 myotubes. RNA was extracted from C2C12 myotubes after exposure to agrin for 2.5 hours. Preparation of transcriptomic library and RNA sequencing were performed by Novogene (UK) Company Ltd. Compared to DMEM, gene expression analysis with R software showed that agrin induced upregulation (between 1 and 2 fold) of the following genes: Uba52, Rps28, Snrpg, Cxcl5, Cxcl1, Zdhhc14; and downregulation of Ngfr. The online platform Reatcome was used to analyse the intracellular pathway involvement **(A** – highlighted in yellow**)** and significant interactions within these pathways **(B** – red arrows**)** among the genes modified by agrin.

Gene	Protein
Upregulated	
Il6	Interleukin 6
Serpinb2	Serpin Family B Member 2
Cxcl5	C-X-C Motif Chemokine Ligand 1
Ptgs2	Prostaglandin-Endoperoxide Synthase 2
Cebpd	CCAAT Enhancer Binding Protein Delta
Ch25h	Cholesterol 25-Hydroxylase
Il1rl1	Interleukin 1 Receptor Like 1
Plek	Pleckstrin
Olr1	Oxidized Low Density Lipoprotein Receptor 1
Nr4a3	Nuclear Receptor Subfamily 4 Group A Member 3
Nr4a1	Nuclear Receptor Subfamily 4 Group A Member 1
Fosb	FosB Proto-Oncogene, AP-1 Transcription Factor Subunit
Rasl11a	RAS Like Family 11 Member A
Fos	Fos Proto-Oncogene, AP-1 Transcription Factor Subunit
F12	Coagulation Factor XII
Il18rap	Interleukin 18 Receptor Accessory Protein
Tnfaip2	TNF Alpha Induced Protein 2
Slc39a5	Solute Carrier Family 39 Member 5
Gareml	GRB2 Associated Regulator Of MAPK1 Subtype 2
Downregulated	
Esco2	Establishment Of Sister Chromatid Cohesion N-Acetyltransferase 2
Ar	Androgen Receptor
Trp53inp1	Tumor Protein P53 Inducible Nuclear Protein 1

Table 6.2. Genes and corresponding protein products up- and down-regulated by both MuSK IgG1-3 and total IgG from a healthy individual.

Gene	logFC	P value	Protein *PART 1*
Cxcl2	12.08157	2.75×10^{-208}	C-X-C Motif Chemokine Ligand 2
Icam1	9.91133	9.45×10^{-83}	Intercellular Adhesion Molecule 1
Csf2	9.213115	7.56×10^{-115}	Colony Stimulating Factor 2
Saa3	8.597478	0	Serum Amyloid A3, Pseudogene
Cxcl3	8.482365	6.51×10^{-37}	C-X-C Motif Chemokine Ligand 3
Cxcl1	8.413732	0	C-X-C Motif Chemokine Ligand 1
Ccl20	8.260924	2.29×10^{-29}	C-C Motif Chemokine Ligand 20
Lcn2	7.251566	1.82×10^{-16}	Lipocalin 2
Nlrp3	6.92072	4.58×10^{-41}	NLR Family Pyrin Domain Containing 3
Csf3	6.522277	5.32×10^{-32}	Colony Stimulating Factor 3
Gbp5	6.099334	1.09×10^{-46}	Guanylate Binding Protein 5
Ptx3	5.894471	0	Pentraxin 3
Nos2	5.872333	1.94×10^{-219}	Nitric Oxide Synthase 2
Ccl2	5.867545	0	C-C Motif Chemokine Ligand 2
Ccrl2	4.978135	2.02×10^{-49}	C-C Motif Chemokine Receptor Like 2
Penk	4.676803	4.39×10^{-47}	Proenkephalin
Cyp1a1	4.664173	7.22×10^{-219}	Cytochrome P450 Family 1 Subfamily A Member 1
Lif	4.638999	0	LIF Interleukin 6 Family Cytokine
Cxcl10	4.470844	1.02×10^{-43}	C-X-C Motif Chemokine Ligand 10
Ccl7	4.278011	0	C-C Motif Chemokine Ligand 7
Neurl3	4.207111	5.32×10^{-112}	Neuralized E3 Ubiquitin Protein Ligase 3
Slfn2	4.125361	2.90×10^{-196}	Schlafen Family Member 12
Tnf	4.066445	3.17×10^{-25}	Tumor Necrosis Factor
Rnd1	3.842764	0	Rho Family GTPase 1
Zc3h12a	3.835223	0	Zinc Finger CCCH-Type Containing 12A
Gbp3	3.81094	4.83×10^{-72}	Guanylate Binding Protein 3
Nfkbie	3.794403	0	NFKB Inhibitor Epsilon
Birc3	3.787262	7.51×10^{-27}	Baculoviral IAP Repeat Containing 3
Nfkbiz	3.753533	0	NFKB Inhibitor Zeta
Ccl9	3.66361	1.52×10^{-115}	C-C Motif Chemokine Receptor 3
Socs3	3.590919	0	Suppressor Of Cytokine Signaling 3
Serpina3g	3.554675	3.45×10^{-39}	Serpin Family A Member 3
Ptger2	3.440797	4.36×10^{-39}	Prostaglandin E Receptor 2
Cd69	3.40726	3.32×10^{-20}	CD69 Molecule

Table 6.3 *(Part 1)***.** Genes and corresponding protein products selectively upregulated by MuSK IgG1-3.

Gene	logFC	P value	Protein *PART 2*
Cish	3.402223	9.86×10^{-105}	Cytokine Inducible SH2 Containing Protein
Ccl5	3.301794	1.55×10^{-30}	C-C Motif Chemokine Ligand 5
Nfkbia	3.220861	0	NFKB Inhibitor Alpha
Cxcl16	3.159365	6.24×10^{-114}	C-X-C Motif Chemokine Ligand 16
Tlr2	3.122754	4.50×10^{-261}	Toll Like Receptor 2
Fosl1	3.117372	3.26×10^{-296}	FOS Like 1, AP-1 Transcription Factor Subunit
Ier3	3.085888	4.02×10^{-298}	Immediate Early Response 3
Il15ra	3.044517	1.06×10^{-16}	Interleukin 15 Receptor Subunit Alpha
Rasgef1b	3.021137	2.80×10^{-19}	RasGEF Domain Family Member 1B
Ereg	2.986593	0	Epiregulin
Vcam1	2.864554	0	Vascular Cell Adhesion Molecule 1
Tnfaip3	2.826668	0	TNF Alpha Induced Protein 3
Steap4	2.786027	3.59×10^{-12}	STEAP4 Metalloreductase
Gbp2	2.772562	1.96×10^{-124}	Guanylate Binding Protein 2
Ccrn4l	2.739412	0	Nocturnin
Rgs16	2.691153	2.36×10^{-207}	Regulator Of G Protein Signaling 16
Pbx4	2.638554	1.57×10^{-30}	PBX Homeobox 4
Fas	2.602803	8.64×10^{-90}	Fas Cell Surface Death Receptor
Csf1	2.572402	0	Colony Stimulating Factor 1
Serpine1	2.553472	0	Serpin Family E Member 1
Ddit4	2.543819	2.39×10^{-223}	DNA Damage Inducible Transcript 4
Adamts4	2.543059	1.36×10^{-291}	ADAM Metallopeptidase Thrombospondin 1 Motif 4
Gbp1	2.509877	3.02×10^{-46}	Guanylate Binding Protein 1
Prdm1	2.505143	3.73×10^{-15}	PR/SET Domain 1
Mt2	2.494926	1.18×10^{-277}	Melatonin Receptor 1B
Nod2	2.482524	6.57×10^{-114}	Nucleotide Binding Oligomerization Domain 2
Cilp2	2.464871	1.86×10^{-50}	Cartilage Intermediate Layer Protein 2
Rtn4rl2	2.440753	3.38×10^{-14}	Reticulon 4 Receptor Like 2
Malt1	2.432704	6.10×10^{-158}	MALT1 Paracaspase
Foxs1	2.426599	2.21×10^{-208}	Forkhead Box S1
Stx11	2.369294	7.47×10^{-291}	Syntaxin 11
Pdgfa	2.366416	3.92×10^{-267}	Platelet Derived Growth Factor Subunit A
Nfkb1	2.354795	0	Nuclear Factor Kappa B Subunit 1
Irf5	2.354655	1.96×10^{-13}	Interferon Regulatory Factor 5

Table 6.3 *(Part 2)***.** Genes and corresponding protein products selectively upregulated by MuSK IgG1-3.

Gene	logFC	P value	Protein *PART 3*
Gm129	2.352647	4.64×10^{-60}	Circadian Associated Repressor Of Transcription
Irf1	2.333315	1.12×10^{-232}	Interferon Regulatory Factor 1
Ripk2	2.325697	8.36×10^{-296}	Receptor Interacting Serine/Threonine Kinase 2
Plscr1	2.279415	3.66×10^{-189}	Phospholipid Scramblase 1
D8Ertd82e	2.274875	4.28×10^{-106}	PEAK1 Related, Kinase-Activating Pseudokinase 1
Myc	2.252104	1.62×10^{-148}	MYC Proto-Oncogene, BHLH Transcription Factor
Pdgfb	2.238218	5.64×10^{-202}	Platelet Derived Growth Factor Subunit B
Slc7a2	2.231685	7.43×10^{-136}	Solute Carrier Family 7 Member 2
Tnip1	2.228958	0	TNFAIP3 Interacting Protein 1
Slpi	2.22563	1.41×10^{-24}	Secretory Leukocyte Peptidase Inhibitor
Fam110c	2.224125	1.50×10^{-56}	Family With Sequence Similarity 110 Member C
Gadd45b	2.172086	1.64×10^{-238}	Growth Arrest And DNA Damage Inducible Beta
Dusp5	2.170653	6.68×10^{-152}	Dual Specificity Phosphatase 5
Spry4	2.169578	6.97×10^{-112}	Sprouty RTK Signaling Antagonist 4
Col27a1	2.167372	6.97×10^{-57}	Collagen Type XXVII Alpha 1 Chain
Grem2	2.161828	2.87×10^{-49}	Gremlin 2, DAN Family BMP Antagonist
Gjb2	2.156186	1.77×10^{-18}	Gap Junction Protein Beta 2
Trib3	2.144339	2.02×10^{-56}	Tribbles Pseudokinase 3
Ahrr	2.125043	7.58×10^{-18}	Aryl-Hydrocarbon Receptor Repressor
Slc7a11	2.124533	1.39×10^{-42}	Solute Carrier Family 7 Member 11
Angptl4	2.119972	2.24×10^{-285}	Angiopoietin Like 4
Sesn2	2.103687	5.07×10^{-181}	Sestrin 2
Pik3r5	2.09339	5.76×10^{-29}	Pik3r5
Bcl3	2.080304	4.27×10^{-86}	BCL3 Transcription Coactivator
Parp14	2.075939	4.16×10^{-32}	Poly(ADP-Ribose) Polymerase Family Member 14
Ddit3	2.074582	1.20×10^{-86}	DNA Damage Inducible Transcript 3
Rab20	2.046625	3.77×10^{-46}	RAB20, Member RAS Oncogene Family
Pfkfb3	2.045885	1.91×10^{-108}	Phosphofructo-2-Kinase/Fructose-2,6-Biphosphatase3
Fgf7	2.045008	2.14×10^{-94}	Fibroblast Growth Factor 7
Inhba	2.022624	6.57×10^{-64}	Inhibin Subunit Beta A
Chac1	2.014928	2.24×10^{-77}	ChaC Glutathione Gamma-Glutamylcyclotransferase 1
Smim3	2.013972	4.24×10^{-185}	Small Integral Membrane Protein 3
Gpr68	2.002027	9.87×10^{-16}	G Protein-Coupled Receptor 68

Table 6.3 *(Part 3)***.** Genes and corresponding protein products selectively upregulated by MuSK IgG1-3.

Gene	logFC	P value	Protein
Mn1	-3.74267	6.54×10^{-16}	MN1 Proto-Oncogene, Transcriptional Regulator
Cxcr4	-3.14098	0	C-X-C Motif Chemokine Receptor 4
Rgs2	-2.88794	1.02×10^{-21}	Regulator Of G Protein Signaling 2
Skida1	-2.88039	2.73×10^{-10}	SKI/DACH Domain Containing 1
Bnc1	-2.85973	2.46×10^{-12}	Basonuclin 1
Ccrl1	-2.51137	4.96×10^{-11}	Atypical Chemokine Receptor 4
Ddit4l	-2.49964	2.63×10^{-11}	DNA Damage Inducible Transcript 4 Like
Sox8	-2.49687	1.79×10^{-72}	SRY-Box Transcription Factor 8
Bmf	-2.46093	2.90×10^{-51}	Bcl2 Modifying Factor
Gas1	-2.28353	2.45×10^{-246}	Growth Arrest Specific 1
Ush1g	-2.18009	5.20×10^{-09}	USH1 Protein Network Component Sans
Slc40a1	-2.08028	7.76×10^{-28}	Solute Carrier Family 40 Member 1
Smad6	-2.06208	9.52×10^{-37}	SMAD Family Member 6
Ttc30b	-2.04539	7.64×10^{-28}	Tetratricopeptide Repeat Domain 30B
9930111J21Rik1	-2.0069	2.96×10^{-17}	Interferon-inducible GTPase family member

Table 6.4. Genes and corresponding protein products selectively downregulated by MuSK IgG1-3.

The Reatcome analysis showed that he identified genes were involved in several and widespread intracellular pathways, most prominently involving the signal transduction, metabolism, apoptosis, and immune response of the cell (Figure 6.18). Significant interactions among individual genes within the pathways involved in signal transduction and immune response of the cell were also found (Figure 6.18 B). However, genes specifically involved in the AChR clustering were not detected, except for the Rho GTPase which was upregulated by 3.8 log fold.

6.3) Discussion

Following the observations in Chapters 3 and 5 that the purified MuSK IgG1-3 and monoclonal anti-MuSK antibodies impaired AChR clustering while not inhibiting MuSK phosphorylation, the pathogenic role of these MuSK antibody subclasses was further explored.

Phosphorylation experiments in Chapter 5 showed that the monoclonal anti-MuSK antibodies did not inhibit MuSK phosphorylation but, nevertheless, induced an agrin-independent increase in its phosphorylation. The next experimental step was, therefore, to evaluate whether this effect was shared with the patient-derived MuSK IgG1-3. Indeed, the purified preparations from pooled MuSK-MG patients activated MuSK directly in the absence of agrin. Moreover, DOK7 phosphorylation was also increased, indicating that the IgG1-3 effectively trigger the AChR phosphorylation pathway by forwarding the signal downstream of MuSK. In addition, that the presence of a phosphorylation band corresponding to the size of DOK7 in the samples incubated with MuSK IgG1-3 suggests an effective co-immunoprecipitation of the MuSK-DOK7 complex by these antibody subclasses, something not observed by the IgG4 antibodies. This might indicate that the divalent binding of MuSK IgG1-3 further tightens MuSK-DOK7 interaction.

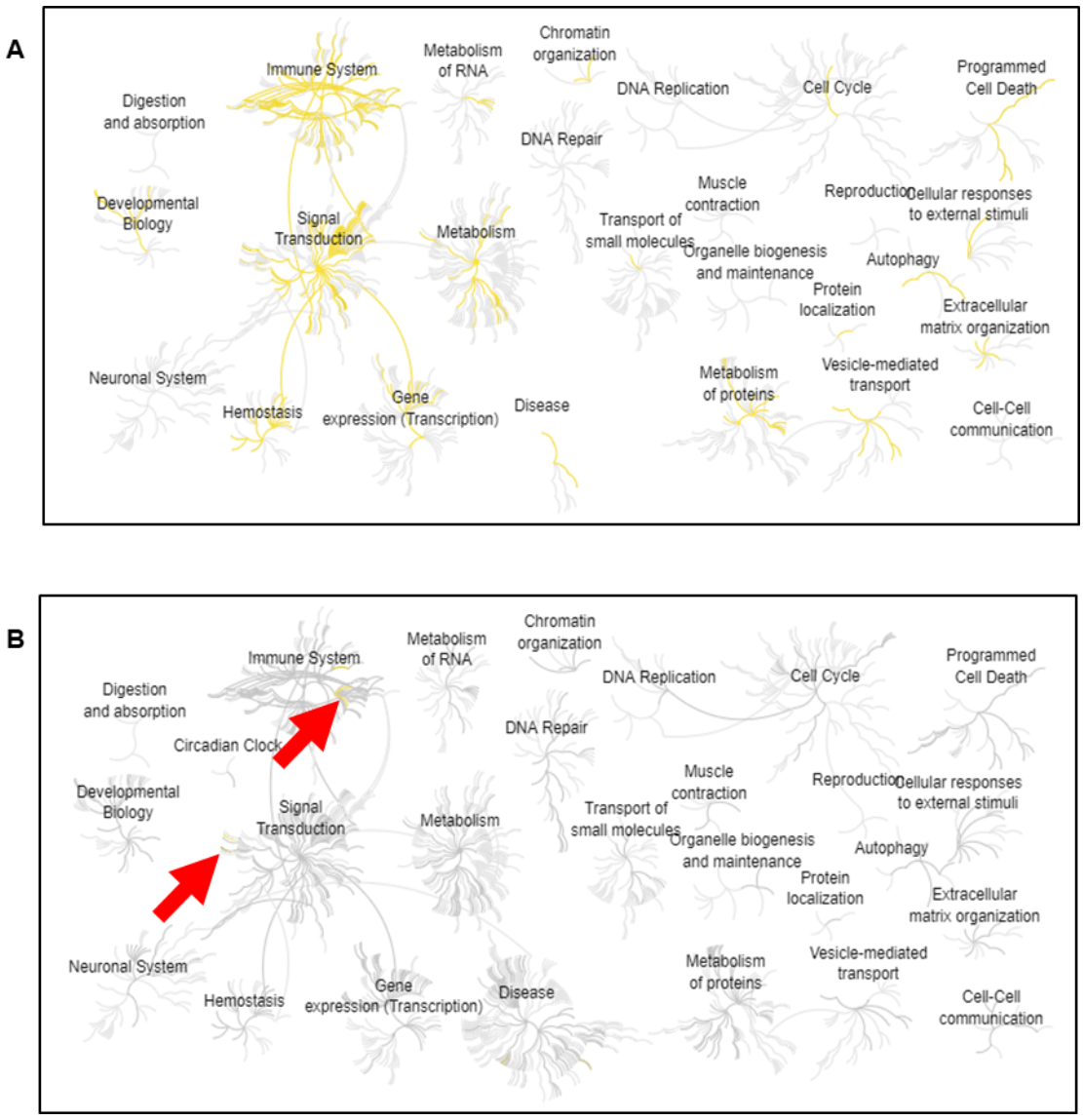


Figure 6.18. Transcriptional modifications induced by MuSK IgG1-3 on C2C12 myotubes. RNA was extracted from C2C12 myotubes after exposure to MuSK IgG1-3 or healthy control IgG for 2.5 hours. Preparation of transcriptomic library and RNA sequencing were performed by the Novogene (UK) Company Ltd. Compared to DMEM and after subtraction of the overlapping findings between MuSK-MG and healthy control samples, gene expression analysis with R software showed that MuSK IgG1-3 modified the transcription (at least by 2 folds) of 81 genes. Of these, Nf-Kb, MAPK, IL6, IL10, NOD1, NOD2 and TNFR1 were the genes subjected to the most significant expression changes. On the other hand, expression of *Musk*, *Chrnd* and *Chrng* was less than 0.5 folds. The online platform Reatcome was used to analyse the intracellular pathways involved **(A** – highlighted in yellow**)** and significant interactions within these pathways **(B** – red arrows**)** among the genes modified by MuSK IgG1-3.

To study whether the phosphorylation signal reached the end of the clustering pathway, a different pull-down technique was required, as the immunoprecipitation of the receptor using an antibody (D6) directed against the α subunit of the AChR was only partially successful. Although the antibody showed partial effectiveness in pulling down the AChR, as indicated by the detection of the β and δ subunits in most of the samples in the western blots, the phosphorylation signal was either not present or obscured by other non-specific bands. In particular, the D6 antibody was less effective in pulling down the AChR from the cell membrane. This might be related to the high selectivity of D6 to the extracellular domain of the human α subunit, with potential lower affinity for the mouse isoform of the C2C12 myotubes (similarly to already observed for the *Torpedo Californica*) (Jacobson, Beeson et al. 1999). More reliable results were obtained with streptavidin-conjugated bungarotoxin which enabled detection of a clear phosphorylation signal corresponding to the β subunit of the AChR. Interestingly, the streptavidin pull-down provided better results when incubated with live myotubes for the detection of membrane expressed AChRs, suggesting less efficient binding after cell lysis.

When the phosphorylation of the AChR pathway was studied over time, MuSK IgG1-3 and agrin induced a similar activation pattern. Moreover, the phosphorylation levels for both DOK7 and MuSK were higher in the presence of MuSK antibodies at each time point compared to agrin alone. However, since agrin was deliberately used at submaximal activity levels (see Chapter 2 and 3), whereas the concentration of MuSK antibodies was the maximum achieved in the purified IgG1-3, this comparison has limitations. Nevertheless, although comparing the phosphorylation levels could be misleading, it is clear that MuSK IgG1-3, independent of agrin, were able to activate the phosphorylation cascade from MuSK to β subunit of the AChR. The phosphorylation of intermediate kinases, such as Crk, Crk-L, Abl, Scr, PAK1, and Sorbs, was not directly

investigated as their activation by MuSK IgG1-3 has been reported to be necessary in order for the phosphorylation signal to reach the βAChR (Mittaud, Marangi et al. 2001, Luo, Wang et al. 2002, Finn, Feng et al. 2003, Hallock, Xu et al. 2010, Hallock, Chin et al. 2016).

When the clustering of the AChRs was analysed, fully-matured clusters were severely impaired by all MuSK antibodies, including the IgG1-3 subclasses despite their concomitant activation of the phosphorylation pathway. This effect on the clusters has been already observed in the initial experiments with the SHP2 inhibitor (see Chapter 3) and is consistent with that previously described (Koneczny, Cossins et al. 2013). When the AChR clusters were analysed according to their size, both MuSK IgG4 and IgG1-3 were found to induce the cluster precursors, so-called microclusters. As MuSK IgG4 do not activate the phosphorylation cascade, unlike IgG1-3, the microcluster formation observed with all the antibody subclasses might be caused by a different – and still unexplored – mechanism rather than the direct stimulation of MuSK.

It is worth noting that raised numbers of microclusters were also present in the samples incubated with agrin. This can be explained by the fact that the formation of clusters is dynamic, and different stages of maturation can be present at the same time. In addition, a technical bias could also count for the microcluster increase in the agrin sample, as the ImageJ software struggled to discriminate the variability of the brightness intensity within fully-formed clusters, which were therefore counted as additional microclusters. With the help of the Wolfson Imaging Centre of our research institute, different settings of ImageJ macro were tested to reduce this bias in the cluster detection. An automatic identification of the threshold for contrast and brightness of each image was tried. However, it failed to discriminate the AChR clusters from the cell background. Therefore, the manual setting of the threshold was chosen as the most reliable way for the cluster counting, and adjusted individually for each experiment. To

reduce possible additional bias created by the manual setting, the background threshold was set using the DMEM control for reference as it features only minimal spontaneous clustering. The parameters for the acquisition of images were kept identical among samples of individual experiments and, therefore, the subsequent automatic counting provided inter- and intra-experimental consistency to estimate and compare the number and size of AChR clusters.

Over the time course, the number of both fully-formed clusters and microclusters increased progressively after agrin stimulation. Conversely, in the presence of MuSK IgG1-3 only the microclusters were induced, which reached a significantly lower number compared to agrin at the final time point of 8 hours. This finding suggests that MuSK IgG1-3 might fail to sustain the transition from microclusters to fully-matured clusters. This hypothesis is supported by two additional observations: a) the co-localisation between AChR microclusters and rapsyn is reduced, indicating that rapsyn has not been yet fully recruited at this stage of the cluster maturation (this is also supported by the similar result observed in the agrin sample when only microclusters were considered); b) the modest reduction of the membrane expression of the AChRs in the presence of MuSK antibodies. This could be related to an increased turnover of the AChRs, possibly induced by the sustained MuSK activation by the divalent IgG1-3, or by the triggering of the "canonical" Wnt pathway through the stimulation of MuSK frizzled domain, which reduces the expression of rapsyn destabilising the AChR clusters (Wang, Ruan et al. 2008). Finally, the inhibition of Shp2 by NSC-87877 was able to preserve cluster maturation in the presence of MuSK antibodies, as the number of micro- and fully-developed AChR clusters was equally increased by the drug despite concomitant exposure to MuSK IgG1-3 and IgG4. This suggests that the increase in MuSK phosphorylation by SHP2 works in a more physiological way compared to the forced activation induced by MuSK IgG1-3, possibly mimicking the stimulation of

neuregulin-1 (believed to be important for full cluster maturation) where the two pathways converge on MuSK (Madhavan, Zhao et al. 2005, Zhao, Qian et al. 2007, Ngo, Cole et al. 2012).

As the maturation of the AChR clusters relies on targeted rearrangements of the cytoskeleton scaffold – which allow for the proper anchoring of high-density clusters – the pathways involved were analysed by measuring the activity of the GTPases Rho and Rac1, and by qualitative evaluation of the structure of the actin filaments. The measurement of the active form of Rho and Rac1 was, however, particularly challenging as the GTPase signal is extremely volatile and difficult to preserve for western blot analysis. Reliable measurements were eventually obtained after optimising the technique by (a) prolonging the starvation of the cells prior to the experiment (to reduce the overall basal GTPase activity and increase the susceptibility of the cells to external stimulation) and (b) increasing the concentration of Mg^{++} and Ca^{++} in the buffers (which stabilised the GTPase signal). Although the ELISA test used to quantify Rac1 activation was quicker and more straightforward to carry out, the pull-down and western blot analysis used for Rho proved to be more sensitive with less interexperimental variability. However, no significant differences were found in the activation pattern of either GTPase between the physiological stimulation by agrin and the MuSK antibody subclasses. This is an unexpected result as Rho and Rac1 are supposed to play a central role in transition from microclusters to fully-developed clusters (Weston, Gordon et al. 2003, Bai, Guo et al. 2018). In this respect, considering the impairment observed in cluster maturation caused by MuSK antibodies, a disruption in the GTPase activation was considered a logical potential explanation for the antibody effects. However, the full activation pattern of Rho and Rac1 has not been fully explored yet due to technical difficulties and reduced availability of materials, and it is possible that it might diverge over time between MuSK antibodies and agrin. For

example, it has been suggested that a timely activation of Rac1 is essential for the proper cytoskeleton rearrangements, which can be disrupted by its hyperactivation (Bai, Guo et al. 2018). This could be a potential effect of MuSK antibodies, especially the divalent IgG1-3 considering their effect on MuSK activation as described above.

The structure of the actin filaments was then evaluated by confocal imaging after permeabilisation of the myotubes and staining with florescent phalloidin. Different approaches to analyse the structure of the actin filaments were reviewed with the help of the Wolfson Imaging Centre of our research Institute. However, due to the intrinsic characteristics of the filaments, a quantitative measurement was deemed not possible and a qualitative assessment by two blinded investigators was therefore chosen. Notably, both investigators were able to recognise visually the presence of intracellular aggregates positively stained with phalloidin in myotubes incubated with MuSK antibodies; this finding is compatible with underlying impairment of the cytoskeleton scaffolding caused by the antibodies with consequent disruption in the formation/maturation of the AChR clusters.

Considering the direct MuSK activation induced by MuSK IgG1-3 and the lack of evidence of an impairment in the intracellular phosphorylation/GTPases pathways, it was possible that a disruption of MuSK-Lrp4 interaction contributed to the pathogenic effects of the MuSK IgG1-3 antibodies on AChR clustering. To evaluate the integrity of the binding between MuSK and Lrp4, the two molecules were co-immunoprecipitated using either the commercial anti-MuSK antibody AF562, or the purified patients' own antibodies. After optimising the technique on HEK cells co-transfected with *MUSK* and *LRP4*, co-immunoprecipitation was attempted on C2C12 myotubes. However, this was not successful as no Lrp4 was detectable in any of the samples. This might be due to the low expression and less stable interaction between MuSK and Lrp4 on the myotubes compared to the transfected HEK cells (in which both molecules can be easily detected

directly on the cell lysates without requiring immunoprecipitation). Indeed, when the co-immunoprecipitation experiment was performed on HEK cells, both MuSK and Lrp4 were reliably detected in all the samples. However, a small amount of Lrp4 was pulled down by the IgG from the healthy control, indicating non-specific binding. To reduce this bias, measurements were corrected by subtracting the density of the Lrp4 band of the control sample from the values obtained in the other MuSK antibody preparations. After this correction, and despite the limitations of the experiment, the level of Lrp4 co-immunoprecipitated with MuSK was found to be reduced in the presence of MuSK IgG1-3, suggesting an impaired interaction of the two proteins caused by the antibodies (and a shared pathological mechanism with MuSK IgG4).

This result was different from that reported by Koneczny et al, where the co-immunoprecipitation of MuSK-Lrp4 was not impaired by MuSK IgG1-3 (Koneczny, Cossins et al. 2013). Although cell transfection, immunoprecipitation, and selection of controls were carried out similarly, two major differences can be pointed out between the studies. First, in the experiments described in this thesis, the MuSK IgG1-3 preparation was obtained from pooled plasma of 5 different MuSK-MG patients, whereas Koneczny et al used two MG samples individually. In this respect, the pooled preparation might be more representative of the disease as a whole being less influenced by potential confounding factors characteristic of each individual patient. On the other hand, the healthy control used in the present study was able to immunoprecipitate non-specifically a small amount of Lrp4, a bias that needed to be compensated during the quantitative analysis of the western blot bands and could be partially responsible for the different results obtained. This was not the case in the study by Koneczny et al where the two healthy controls did not cause any unwanted immunoprecipitation. It is possible that the concentration of HC purified IgG used here was higher compared to the study by Koneczny et al, as it was equivalent to that of the total IgG preparation of the pooled

sample (and therefore more likely to have a non-specific binding effect to Lrp4). Nevertheless, the use of additional controls from other healthy individuals would have been necessary to optimised further the experiment. However, this was not carried out due the limited access of facilities and resources caused by the COVID-19 lockdown.

As the exact mechanism of action of MuSK IgG1-3 remained rather elusive, a final attempt to explain their effect was carried out by analysing the myotube transcriptome to evaluate potential dysregulation in the gene expression. With the initial threshold of 1 log fold change, more than 470 genes were found to be modified by the IgG1-3 preparation, with their level mRNA either up- (352 genes) or down- (120 genes) regulated. However, when the threshold was increased to 2 log fold and the genes commonly dysregulated by both MuSK antibodies and IgG from a healthy control eliminated from the analysis, the number of candidate genes was reduced to 117 (102 upregulated and 15 downregulated). However, when all the corresponding protein products were identified, none of them was strictly involved in the AChR clustering pathway as we currently know it. Apart from the main players (namely MuSK, DOK7, Lrp4, and the AChR subunits), also the other known intracellular effectors (such as Crks, Anxa3, Sorbs-1 and -2, Abl-1 and -2, Scr, Dvl1/PAK1, α-actinin, cortactin), were unchanged in the transcriptomic analysis for the exception of the Rho GTPase, which was upregulated (see Chapter 1, Figure 1.3 for a representation of the AChR pathway and its effectors) (Mittaud, Marangi et al. 2001, Luo, Wang et al. 2002, Finn, Feng et al. 2003, Weston, Gordon et al. 2003, Dobbins, Luo et al. 2008, Madhavan, Gong et al. 2009, Hallock, Xu et al. 2010, Cartaud, Stetzkowski-Marden et al. 2011, Hallock, Chin et al. 2016, Bai, Guo et al. 2018, Wang, Li et al. 2020). In addition, the induction of the atrophy factor Muscle RING-Finger protein-1 (MURF-1) was previously reported in C2C12 myotubes exposed to patients' sera and in the masseter of passive-immunised mice (Benveniste, Jacobson et al. 2005), which supposedly contribute to the selective

muscle atrophy observed in MuSK-MG patient. However, this was not confirmed in the current transcriptomic analysis, further suggesting that the pathogenic effects of MuSK IgG1-3 are more likely confined to post-translational and transductional protein modifications rather than transcriptional.

Most of the genes in which the expression was modified – particularly the production of cytokines (such as the CXC ligands, interferon, and other interleukins), and in the intracellular signal transduction, gene transcription, and cellular growth (e.g. cytochrome P450, NFkB, Fos1, Myc) – are commonly involved in the general immune response of the cell to an external challenge. This non-specific pattern of gene expression is likely due to the high proportion of other IgG not directed against MuSK present in the purified samples. In addition, these preparations were obtained by pooling plasmas from different patients, which further increased the variety of antibodies present in the sample. In this respect, the control IgG was obtained from a single healthy individual creating the comparison even more difficult and limited. Repeating the transcriptomic analysis with the monoclonal anti-MuSK antibodies described in Chapter 5 would have been helpful in increasing the specificity and significance of the experiment. Unfortunately, these preparations were no longer available at this stage of the study.

Chapter 7

Discussion

Introduction

The aim of this thesis was to investigate the potential therapeutic benefit of SHP2 inhibition as a treatment for MuSK myasthenia. In addition, the specific pathogenic mechanisms of the disease were further explored focusing on the role of the less-characterised MuSK IgG1, 2 and 3 antibody subclasses.

MuSK-MG patients usually present a high incidence of life-threatening crises, and low response to steroid and immunosuppressive treatments (Evoli, Tonali et al. 2003, Vincent, Bowen et al. 2003, Evoli 2006, Guptill, Sanders et al. 2011). Therefore, the development of a treatment that targets specifically its pathological mechanisms would offer a potential better control of symptoms, fewer side effects, and might reduce the necessity of long-term immunosuppression.

Targeting the intracellular regulators of the AChR clustering pathway represents a novel therapeutic approach in autoimmune myasthenia. This thesis expands on previous work, which identified the phosphatase SHP2 as a potential candidate in the treatment of MuSK-MG (Zhao, Qian et al. 2007, Huda, Cao et al. 2020).

Furthermore, the pathogenic mechanisms underlying MuSK-MG are still not completely unravelled. Specifically, the IgG4 subclass of MuSK-Abs has been considered to be pathogenic and has been studied to a larger extent than the IgG1-3 subclasses, largely on the basis of a study where the MuSK-Ab levels were undetectable in mice injected with purified total IgG1-3 (Klooster, Plomp et al. 2012). However, a pathogenic effect of the IgG1-3 antibodies was demonstrated to cause a reduction in AChR clusters similar to that induced by MuSK IgG4 (Koneczny, Cossins et al. 2013). In that study the direct effect of IgG1-3 on MuSK phosphorylation was not performed, as it was assumed that it would be decreased. However, during the experiments

described here and carried out to test the effectiveness of SHP2 inhibition with the different MuSK-Ab subclasses, it emerged that MuSK phosphorylation was unchanged in the presence of IgG1-3 and, therefore, warranted further investigation.

SHP2 inhibition by NSC-87877 is effective in counteracting the pathogenicity of MuSK antibodies in vitro

NSC-87877 stimulated a dose-dependent increase of both MuSK phosphorylation and AChR clustering in the myotubes, supporting its potential therapeutic effectiveness in MuSK-MG models. However, a paradoxical effect was observed at high concentrations, potentially related to the loss of the drug specificity with the final outcome of inhibiting the clustering pathway. This finding suggests that NSC-87877 has a narrow therapeutic window that should be taken into account in future *in vivo* testing. MuSK function was, however, not irreversibly suppressed as the addition of agrin reversed the effects of high doses of the drug. This is in keeping with the current physiological model in which SHP2 does not directly compete with agrin, being activated intracellularly downstream of MuSK (Madhavan, Zhao et al. 2005, Zhao, Qian et al. 2007).

The fact that NSC-87877 stimulated AChR clustering did not necessarily mean that the agrin-Lrp4-MuSK-DOK7 pathway was involved; activation of non-specific pathways might coincidentally promote AChR clustering. However, the lack of effect in *MUSK* KO or mutant *DOK7* myotubes supports the initial hypothesis that the drug acts through the direct stimulation of MuSK.

The positive effects on AChR clustering by NSC-87877 was preserved in the presence of purified MuSK antibodies, irrespective of their subclass, supporting the drug potential efficacy for therapeutic purposes. This was particularly clear in the presence of MuSK IgG4 which, as expected, prevented MuSK activation by agrin (Huijbers, Zhang et al. 2013, Koneczny, Cossins et al. 2013). Moreover, for the first time, it was observed

that MuSK IgG1-3 impaired the formation of AChR clusters without inhibiting MuSK phosphorylation. In the presence of MuSK IgG1-3, NCS-87877 did not increase MuSK phosphorylation, although AChR clusters were still protected from dispersal. It is possible that the inhibition of SHP2 restores a more physiological activation of MuSK by acting intracellularly, allowing for a correct transduction of the phosphorylation signal to the downstream pathway. This, associated with a potential increased expression of the AChRs, might explain the efficacy of the NSC-87877 with MuSK IgG1-3 without affecting MuSK phosphorylation.

Despite the encouraging results obtained *in vitro*, NSC-87877 was not equally successful when tested in different animal models. Specifically, in wild type mice, MuSK phosphorylation was not increased despite a wide range of doses were tested. The hepatic metabolism and renal excretion of the drug, and the complexity of the neuromuscular junction regulation itself (which is much more sophisticated compared to the simplistic model represented by the myotubes) should be taken into account. It is also worth noting that SHP2 plays a subsidiary role in the development of the neuromuscular junction (Dong, Li et al. 2006), and its involvement in the mature synapsis might be limited. Another possibility is that MuSK might be phosphorylated *in vivo* already at its maximum level and, consequently, any additional increase is not achievable. A third possibility is that the dosage of NSC-87877 might be too high, reflecting the paradoxical effect on MuSK phosphorylation observed in the myotubes. As literature data is currently very limited, further testing with a wider range of doses of NSC-87877 is required to evaluate the pharmacokinetic properties of the drug and its therapeutic window. In this respect, the successful active-immunisation of the animals, obtained by Prof Erdem Tüzün with our purified MuSK extracellular domain, provides the basis for the creation of the *in vivo* model needed to test the efficacy of NSC-87877 in MuSK-MG.

The therapeutic potential of SHP2 inhibition is limited in congenital myasthenic syndromes

SHP2 inhibition was also tested in both *in vitro* and *in vivo* models of different congenital myasthenic syndromes (CMS). Specifically, the mutations in *MUSK* and *DOK7* chosen to study the specificity of NSC-87877 were selected for their clinical relevance as previously described in CMS patients (Beeson, Higuchi et al. 2006, Rodriguez Cruz, Cossins et al. 2020). However, AChR clustering was not improved by NSC-87877 in either cell lines, and the drug was not able to restore MuSK phosphorylation in the mutant protein.

Additional experiments were carried out in an *in vivo* model of AChR deficiency syndrome (Cossins, Webster et al. 2004) hoping that the activation of MuSK by NSC-87877 might compensate for the deficiency of AChRs by increasing their clusters, also considering the reduced MuSK phosphorylation found in the model animal. However, no improvement in either clinical phenotype or MuSK phosphorylation was induced by the drug. This could be due to the fact that a) a proper dose regime was not identified, and/or b) the pathogenic mechanisms responsible for the AChR deficiency syndrome are not affected by the inhibition of SHP2. All considering, the role of SHP2 inhibition for the treatment of CMS with underlying mutations in *MUSK*, *DOK7* and the ε subunit of the AChR appears to be limited.

MuSK IgG1-3 antibody subclasses are pathogenic showing opposite effects on the phosphorylation cascade compared to MuSK IgG4

The recent creation of MuSK monoclonal antibodies by our collaborator Prof K O'Connor provided the opportunity to study the effects of the different antibody subclasses in the absence of confusing factors present in purified preparations from patients' plasma (which are polyclonal and non-antigen specific). MuSK-mAbs

prevented the formation of agrin-induced AChR clusters on the myotubes while increasing MuSK phosphorylation even in the absence of agrin (likely following a forced dimerization of MuSK caused by the antibody divalent binding). In addition, the number of cluster precursors (microclusters) was increased by the mAbs, suggesting an impairment in cluster maturation. The group of Huijbers et al suggested that divalent MuSK antibodies are less pathogenic, after observing that MuSK-mAbs induced a partial increase in AChR clustering, and a milder phenotype in mice passively immunised with divalent mAbs compared to the their monovalent equivalents (Huijbers, Vergoossen et al. 2019, Vergoossen, Plomp et al. 2021).

Although intriguing, this model fails to explain why our data indicate that, even in the presence of a MuSK activation apparently indistinguishable from agrin, the clustering of AChRs is not equally induced. In this respect, an over-activated MuSK was found to impair AChR clustering as a consequence of a gain-of-function mutation in its gene and was responsible for the development of a congenital myasthenic syndrome (Rodriguez Cruz, Cossins et al. 2020). In addition, it is possible that not all the intracellular tyrosines of MuSK are equally activated by the antibodies, therefore impairing its kinase function and responsiveness to the physiological agrin stimulation (something that was not possible to discriminate with the western blot technique currently used) (Herbst and Burden 2000, Till, Becerra et al. 2002).

The experiments carried out with MuSK IgG1-3 purified from MuSK-MG patients' plasma showed similar effects to that observed with MuSK-mAbs. Moreover, the phosphorylation signal was forwarded effectively downstream of MuSK to DOK7 and the βAChR at the end of the pathway. As MuSK-Abs failed to induce fully-matured AChR clusters while inducing an increase in microclusters, it was initially supposed that the antibodies would have not been able to activate the Rho and Rac1 GTPases, which regulates the rearrangements of cytoskeleton required for the maturation of AChR

clusters (Weston, Gordon et al. 2003, Bai, Guo et al. 2018). However, both MuSK IgG4 and IgG1-3 antibodies had the same effect as agrin on the activation of the GTPases, further complicating a potential explanation in their pathogenic mechanism.

Apart from the classic agrin-MuSK-DOK7 pathway, increasing evidence suggests that, in order to induce the formation and proper maturation of AChR clusters, additional effectors, other than agrin, are required. This opens new and not yet explored possibilities to explain the pathogenic effects of MuSK antibodies. Specifically, different proteins of the Wnt family (in particular Wnt9 and Wnt11) are supposed to sustain the activation of MuSK and positively regulate AChR clustering by binding to MuSK frizzled domain (Luo, Wang et al. 2002, Wang, Jing et al. 2003). Notably, in the absence of agrin, Wnts do not induce full cluster maturation but only AChR microclustering through activation of Rac1 (Henriquez, Webb et al. 2008). In addition, the activation of the "canonical pathway" mediated by β-catenin by some members of the Wnt family induces a downregulation of the AChR clustering by reducing the expression of rapsyn (Wang, Ruan et al. 2008). It is possible that these mechanisms (partial activation of Rac1 and reduced rapsyn expression) are shared by a portion of MuSK antibodies (either IgG4 or IgG1-3) that bind to the frizzle domain of MuSK instead of the more common "main immunogenic region" located in the Ig1-like domain (McConville, Farrugia et al. 2004, Huijbers, Vink et al. 2016). This hypothesis is supported by the activation of the GTPase pathway by both MuSK IgG4 and IgG1-3, the impaired co-localisation between rapsyn and AChR microclusters, and the mild reduction in the number of AChRs expressed on the cell membrane. Moreover, the recently identified BMP4-MuSK pathway could also be disrupted by MuSK antibodies. In this case, antibodies directed to the Ig3-like domain of MuSK might prevent the binding of BMP4 to its transmembrane receptor ALK3, which requires the concomitant interaction with MuSK Ig3 domain to have its effect on AChR clustering by inducing

the expression of *MUSK*, *DOK7* and *Wnt11* genes (Yilmaz, Kattamuri et al. 2016). Additional studies are however needed to further establish a pathogenic role of MuSK antibodies in the Wnt and BMP4 pathways.

The interaction between MuSK and Lrp4 was previously thought to be unaffected by the IgG1-3 (Koneczny, Cossins et al. 2013). However, an impairment of some degree is suggested by the result of the co-immunoprecipitation analysis performed on HEK cells described here, allowing for potential steric clashes between the antibodies and other structural proteins, and contributing in this way to the observed failure in transition from micro- to fully-formed clusters. In this respect, MuSK-Lrp4 tetramer is connected to several other protein complexes of the sarcolemma and extracellular matrix (such as laminin, ColQ, and the sarco- and dystroglycans) which help to maintain the overall structure and function of the NMJ, and contribute indirectly to the formation of AChR clusters (Cartaud, Strochlic et al. 2004, Nishimune, Valdez et al. 2008, Kamimura, Ueno et al. 2013, Zhao, Shen et al. 2018). Further studies are needed to investigate the potential disruption of these inter-protein interactions and their relevance in the pathogenicity of MuSK-MG.

Finally, more traditional pathogenic mechanisms of IgG1-3 were still not fully explored and would require specific characterisation. For example, MuSK internalisation from the muscle membrane has not been demonstrated in a previous study (Koneczny, Cossins et al. 2013) nor in the present work. Moreover, the role of complement activation has been indirectly suggested by the increase in breakdown complement products in MuSK-MG sera (Tuzun, Yilmaz et al. 2011) although not detected on the NMJ from patients' muscle biopsy (Shiraishi, Motomura et al. 2005). A more direct and systematic approach with *in vitro* and *in vivo* models would therefore be helpful to evaluate this potentially important component of the pathogenicity of MuSK IgG1-3 antibodies.

Modifications in gene expression by NSC-87877 might contribute to its effect on AChR clustering, whereas no specific changes have been identified with MuSK IgG1-3 antibodies

Transcriptomic analysis was performed on the myotubes to evaluate additional mechanisms of action triggered by either SHP2 inhibition or MuSK IgG1-3 antibodies.

NSC-87877 induced a marked induction of cytochromes and other detoxicating pathways aimed to metabolise and inactivate the drug. Subtler transcriptional modifications were observed on genes directly linked to the AChR clustering pathway, involving most notably the upregulation of neuregulin-1 and an inhibitor of the Wnt pathway (Nkd2). As both neuregulin-1 and Wnts modulate AChR clustering (Chu, Moscoso et al. 1995, Jo, Zhu et al. 1995, Zhang, Liang et al. 2012), the upregulation of the above genes suggests that NSC-87877 increases AChR clusters not only by activating MuSK phosphorylation, but also by tuning these collateral pathways.

With respect to MuSK-IgG1-3, no specific transcriptional changes were found in the pathways related to the AChR clustering. The cell responded to the allogenic stimuli of the polyclonal IgG1-3 preparations (which contain a mix of antibodies against many proteins, including MuSK) by activating generic effectors of the immune response (e.g. cytokines and other intercellular signalling proteins), and by enhancing protein synthesis and cell metabolism. In order to analyse a MuSK antibody-specific transcriptional response, further studies with monoclonal anti-MuSK antibodies would be appropriate to evaluate the real contribution of transcriptional modifications to the pathogenesis of MuSK-MG.

Finally, it should be considered that MuSK antibodies induces mainly intracytoplasmic post-translational changes. A phosphoproteomic study, similar to those previously carried out to identify the intracellular effectors downstream of MuSK (Durnberger, Camurdanoglu et al. 2014, Wang, Li et al. 2020), would be helpful to

further define the post-translational modification induced by the different subclasses of MuSK antibodies.

Conclusions

The work presented in this thesis shows that modulating the activity of the intracellular regulators of AChR clustering pathway could represent a viable path towards the development of specific treatments for MuSK myasthenia. This is supported by the encouraging results observed *in vitro* by the inhibition of SHP2 in counteracting the pathogenic effects of MuSK antibodies, irrespective of their subclasses. In this respect, the initial *in vivo* testing appears reassuring regarding the safety profile of the drug, although additional studies should be carried out in a proper animal model of autoimmune myasthenia to evaluate the therapeutic efficacy of this pharmacological approach. Finally, the present work provides novel evidence regarding the pathogenic potential of MuSK IgG1-3 antibodies, although the exact mechanism by which these subclasses impair AChR clustering remains elusive. Both MuSK IgG4 and IgG1-3 could equally contribute to the development of MuSK-MG as they impair AChR clustering through different, and apparently opposite, effects on the phosphorylation cascade. Unravelling the precise mechanism of action of each antibody subclass would be an important step for the development of selective treatments and, on a broader scale, to widen our understanding in the physiological processes that regulate the formation and function of the neuromuscular junction.

Bibliography

Aarli, J. A. (2008). "Myasthenia gravis in the elderly - Is it different?" Myasthenia Gravis and Related Disorders: 11th International Conference **1132**: 238-243.

Agius, M. A., S. Zhu, C. A. Kirvan, A. L. Schafer, M. Y. Lin, R. H. Fairclough, J. J. F. Oger, T. Aziz and J. A. Aarli (1998). "Rapsyn antibodies in myasthenia gravis." Myasthenia Gravis and Related Diseases **841**: 516-521.

Aharonov, A., O. Abramsky, R. Tarrabhazdai and S. Fuchs (1975). "Humoral Antibodies to Acetylcholine-Receptor in Patients with Myasthenia-Gravis." Lancet **2**(7930): 340-342.

Alahgholi-Hajibehzad, M., V. Yilmaz, Y. Gulsen-Parman, F. Aysal, P. Oflazer, F. Deymeer and G. Saruhan-Direskeneli (2013). "Association of HLA-DRB1 *14, -DRB1 *16 and -DQB1 *05 with MuSK-myasthenia gravis in patients from Turkey." Hum Immunol **74**(12): 1633-1635.

Alles, V. V., B. Bottazzi, G. Peri, J. Golay, M. Introna and A. Mantovani (1994). "Inducible Expression of Ptx3, a New Member of the Pentraxin Family, in Human Mononuclear Phagocytes." Blood **84**(10): 3483-3493.

Alonso, A., J. Sasin, N. Bottini, I. Friedberg, I. Friedberg, A. Osterman, A. Godzik, T. Hunter, J. Dixon and T. Mustelin (2004). "Protein tyrosine phosphatases in the human genome." Cell **117**(6): 699-711.

Antonio-Santos, A. A. and E. R. Eggenberger (2008). "Medical treatment options for ocular myasthenia gravis." Current Opinion in Ophthalmology **19**(6): 468-478.

Apel, E. D., S. L. Roberds, K. P. Campbell and J. P. Merlie (1995). "Rapsyn May Function as a Link between the Acetylcholine-Receptor and the Agrin-Binding Dystrophin-Associated Glycoprotein Complex." Neuron **15**(1): 115-126.

Arber, S., S. J. Burden and A. J. Harris (2002). "Patterning of skeletal muscle." Current Opinion in Neurobiology **12**(1): 100-103.

Arredondo, J., M. Lara, F. Ng, D. A. Gochez, D. C. Lee, S. P. Logia, J. Nguyen and R. A. Maselli (2014). "COOH-terminal collagen Q (COLQ) mutants causing human deficiency of endplate acetylcholinesterase impair the interaction of ColQ with proteins of the basal lamina." Human Genetics **133**(5): 599-616.

Axelrod, D., P. Ravdin, D. E. Koppel, J. Schlessinger, W. W. Webb, E. L. Elson and T. R. Podleski (1976). "Lateral Motion of Fluorescently Labeled Acetylcholine Receptors in Membranes of Developing Muscle-Fibers." Proceedings of the National Academy of Sciences of the United States of America **73**(12): 4594-4598.

Bai, Y., D. Guo, X. Sun, G. Tang, T. Liao, Y. Peng, J. Xu and L. Shi (2018). "Balanced Rac1 activity controls formation and maintenance of neuromuscular acetylcholine receptor clusters." J Cell Sci **131**(15).

Bartoccioni, E., F. Scuderi, A. Augugliaro, S. Chiatamone Ranieri, D. Sauchelli, P. Alboino, M. Marino and A. Evoli (2009). "HLA class II allele analysis in MuSK-positive myasthenia gravis suggests a role for DQ5." Neurology **72**(2): 195-197.

Bedlack, R. S., D. L. Simel, H. Bosworth, G. Samsa, B. Tucker-Lipscomb and D. B. Sanders (2005). "Quantitative myasthenia gravis score: Assessment of responsiveness and longitudinal validity." Neurology **64**(11): 1968-1970.

Beeson, D., O. Higuchi, J. Palace, J. Cossins, H. Spearman, S. Maxwell, J. Newsom-Davis, G. Burke, P. Fawcett, M. Motomura, J. S. Muller, H. Lochmuller, C. Slater, A. Vincent and Y. Yamanashi (2006). "Dok-7 mutations underlie a neuromuscular junction synaptopathy." Science **313**(5795): 1975-1978.

Benatar, M., D. B. Sanders, G. I. Wolfe, M. P. McDermott and R. Tawil (2012). "Design of the Efficacy of Prednisone in the Treatment of Ocular Myasthenia (EPITOME) trial." Myasthenia Gravis and Related Disorders Ii **1275**: 17-22.

Benveniste, O., L. Jacobson, M. E. Farrugia, L. Clover and A. Vincent (2005). "MuSK antibody positive myasthenia gravis plasma modifies MURF-1 expression in C2C12 cultures and mouse muscle in vivo." J Neuroimmunol **170**(1-2): 41-48.

Bergamin, E., P. T. Hallock, S. J. Burden and S. R. Hubbard (2010). "The cytoplasmic adaptor protein Dok7 activates the receptor tyrosine kinase MuSK via dimerization." Mol Cell **39**(1): 100-109.

Bhanot, P., M. Brink, C. H. Samos, J. C. Hsieh, Y. S. Wang, J. P. Macke, D. Andrew, J. Nathans and R. Nusse (1996). "A new member of the frizzled family from Drosophila functions as a Wingless receptor." Nature **382**(6588): 225-230.

Bilic, J., Y. L. Huang, G. Davidson, T. Zimmermann, C. M. Cruciat, M. Bienz and C. Niehrs (2007). "Wnt induces LRP6 signalosomes and promotes dishevelled-dependent LRP6 phosphorylation." Science **316**(5831): 1619-1622.

Blaes, F., D. Beeson, P. Plested, B. Lang and A. Vincent (2000). "IgG from "seronegative" myasthenia gravis patients binds to a muscle cell line, TE671, but not to human acetylcholine receptor." Ann Neurol **47**(4): 504-510.

Blalock, A., A. M. Harvey, F. R. Ford and J. L. Lilienthal (1941). "The treatment of myasthenia gravis by removal of the thymus gland - Preliminary report." Journal of the American Medical Association **117**: 1529-1533.

Bodis, G., V. Toth and A. Schwarting (2018). "Role of Human Leukocyte Antigens (HLA) in Autoimmune Diseases." Rheumatology and Therapy **5**(1): 5-20.

Boex, M., J. Messeant, S. Bauche, B. Fontaine, C. Legay and L. Strochlic (2018). "Regulation of mammalian neuromuscular junction formation and maintenance by Wnt signaling." Current Opinion in Physiology **4**: 88-95.

Bonifati, D. M. and C. Angelini (1997). "Long-term cyclosporine treatment in a group of severe myasthenia gravis patients." Journal of Neurology **244**(9): 542-547.

Borges, L. S. and M. Ferns (2001). "Agrin-induced phosphorylation of the acetylcholine receptor regulates cytoskeletal anchoring and clustering." J Cell Biol **153**(1): 1-12.

Bromberg, M. B. and D. M. Scott (1994). "Single-Fiber Emg Reference Values - Reformatted in Tabular Form." Muscle & Nerve **17**(7): 820-821.

Bromberg, M. B., J. J. Wald, D. A. Forshew, E. L. Feldman and J. W. Albers (1997). "Randomized trial of azathioprine or prednisone for initial immunosuppressive treatment of myasthenia gravis." Journal of the Neurological Sciences **150**(1): 59-62.

Brunner, E., O. Peter, L. Schweizer and K. Basler (1997). "pangolin encodes a Lef-1 homologue that acts downstream of Armadillo to transduce the Wingless signal in Drosophila." Nature **385**(6619): 829-833.

Buckley, C., D. Douek, J. Newsom-Davis, A. Vincent and N. Willcox (2001). "Mature, long-lived CD4(+) and CD8(+) T cells are generated by the thymoma in myasthenia gravis." Annals of Neurology **50**(1): 64-72.

Buckley, C., J. Newsom-Davis, N. Willcox and A. Vincent (2001). "Do titin and cytokine antibodies in MG patients predict thymoma or thymoma recurrence?" Neurology **57**(9): 1579-1582.

Bunda, S., K. Burrell, P. Heir, L. F. Zeng, A. Alamsahebpour, Y. Kano, B. Raught, Z. Y. Zhang, G. Zadeh and M. Ohh (2015). "Inhibition of SHP2-mediated dephosphorylation of Ras suppresses oncogenesis." Nature Communications **6**.

Burden, S. J. (2002). "Building the vertebrate neuromuscular synapse." Journal of Neurobiology **53**(4): 501-511.

Burges, J., D. W. Wray, S. Pizzighella, Z. Hall and A. Vincent (1990). "A Myasthenia-Gravis Plasma Immunoglobulin Reduces Miniature Endplate Potentials at Human Endplates Invitro." Muscle & Nerve **13**(5): 407-413.

Camilleri, A. A., R. Willmann, G. Sadasivam, S. Lin, M. A. Ruegg, M. Gesemann and C. Fuhrer (2007). "Tyrosine phosphatases such as SHP-2 act in a balance with Src-family kinases in stabilization of postsynaptic clusters of acetylcholine receptors." Bmc Neuroscience **8**.

Camurdanoglu, B. Z., C. Hrovat, G. Durnberger, M. Madalinski, K. Mechtler and R. Herbst (2016). "Musk Kinase Activity is Modulated By A Serine Phosphorylation Site in The Kinase Loop." Scientific Reports **6**.

Cantor, S., W. Zhang, N. Delestree, L. Remedio, G. Z. Mentis and S. J. Burden (2018). "Preserving neuromuscular synapses in ALS by stimulating MuSK with a therapeutic agonist antibody." Elife **7**.

Carr, A. S., C. R. Cardwell, P. O. McCarron and J. McConville (2010). "A systematic review of population based epidemiological studies in Myasthenia Gravis." BMC Neurol **10**: 46.

Carruthers, M. N., M. D. Topazian, A. Khosroshahi, T. E. Witzig, Z. S. Wallace, P. A. Hart, V. Deshpande, T. C. Smyrk, S. Chari and J. H. Stone (2015). "Rituximab for IgG4-related disease: a prospective, open-label trial." Ann Rheum Dis **74**(6): 1171-1177.

Cartaud, A., S. Coutant, T. C. Petrucci and J. Cartaud (1998). "Evidence for in situ and in vitro association between beta-dystroglycan and the subsynaptic 43K rapsyn protein - Consequence for acetylcholine receptor clustering at the synapse." Journal of Biological Chemistry **273**(18): 11321-11326.

Cartaud, A., F. Stetzkowski-Marden, A. Maoui and J. Cartaud (2011). "Agrin triggers the clustering of raft-associated acetylcholine receptors through actin cytoskeleton reorganization." Biology of the Cell **103**(6): 287-301.

Cartaud, A., L. Strochlic, M. Guerra, B. Blanchard, M. Lambergeon, E. Krejci, J. Cartaud and C. Legay (2004). "MuSK is required for anchoring acetylcholinesterase at the neuromuscular junction." J Cell Biol **165**(4): 505-515.

Chen, A. Z., L. Bai, K. K. Zhong, X. Q. Shu, A. L. Wang, Y. T. Xiao, K. J. Zhang and C. Y. Shen (2020). "APC2(CDH1)negatively regulates agrin signaling by promoting the ubiquitination and proteolytic degradation of DOK7." Faseb Journal **34**(9): 12009-12023.

Chen, F., L. Qian, Z. H. Yang, Y. Huang, S. T. Ngo, N. J. Ruan, J. Wang, C. Schneider, P. G. Noakes, Y. Q. Ding, L. Mei and Z. G. Luo (2007). "Rapsyn interaction with calpain stabilizes AChR clusters at the neuromuscular junction." Neuron **55**(2): 247-260.

Chen, L. W., S. S. Sung, M. L. R. Yip, H. R. Lawrence, Y. Ren, W. C. Guida, S. M. Sebti, N. J. Lawrence and J. Wu (2006). "Discovery of a novel Shp2 protein tyrosine phosphatase inhibitor." Molecular Pharmacology **70**(2): 562-570.

Chen, W. H., H. C. Chiu and R. P. Hseih (1993). "Association of Hla-Bw46dr9 Combination with Juvenile Myasthenia-Gravis in Chinese." Journal of Neurology Neurosurgery and Psychiatry **56**(4): 382-385.

Chu, G. C., L. M. Moscoso, M. X. Sliwkowski and J. P. Merlie (1995). "Regulation of the Acetylcholine-Receptor Epsilon-Subunit Gene by Recombinant Aria - an in-Vitro Model for Transynaptic Gene-Regulation." Neuron **14**(2): 329-339.

Chung, H. J. and H. K. Lee (2009). "Constructing a road map from synapses to behaviour Meeting on Synapses: From Molecules to Circuits & Behavior." Embo Reports **10**(9): 958-962.

Ciafaloni, E., N. K. Nikhar, J. M. Massey and D. B. Sanders (2000). "Retrospective analysis of the use of cyclosporine in myasthenia gravis." Neurology **55**(3): 448-450.

Clifford, K. M., L. D. Hobson-Webb, M. Benatar, et al (2019). "Thymectomy may not be associated with clinical improvement in MuSK myasthenia gravis." Muscle Nerve **59**(4): 404-410.

Cole, R. N., N. Ghazanfari, S. T. Ngo, O. L. Gervasio, S. W. Reddel and W. D. Phillips (2010). "Patient autoantibodies deplete postsynaptic muscle-specific kinase leading to disassembly of the ACh receptor scaffold and myasthenia gravis in mice." J Physiol **588**(Pt 17): 3217-3229.

Cole, R. N., S. W. Reddel, O. L. Gervasio and W. D. Phillips (2008). "Anti-MuSK patient antibodies disrupt the mouse neuromuscular junction." Ann Neurol **63**(6): 782-789.

Compston, D. A. S., A. Vincent, J. Newsomdavis and J. R. Batchelor (1980). "Clinical, Pathological, Hla-Antigen and Immunological Evidence for Disease Heterogeneity in Myasthenia-Gravis." Brain **103**(Sep): 579-601.

Cossins, J., K. Belaya, K. Zoltowska, I. Koneczny, S. Maxwell, L. Jacobson, M. I. Leite, P. Waters, A. Vincent and D. Beeson (2012). "The search for new antigenic targets in myasthenia gravis." Myasthenia Gravis and Related Disorders Ii **1275**: 123-128.

Cossins, J., W. W. Liu, K. Belaya, S. Maxwell, M. Oldridge, T. Lester, S. Robb and D. Beeson (2012). "The spectrum of mutations that underlie the neuromuscular junction synaptopathy in DOK7 congenital myasthenic syndrome." Human Molecular Genetics **21**(17): 3765-3775.

Cossins, J., R. Webster, S. Maxwell, G. Burke, A. Vincent and D. Beeson (2004). "A mouse model of AChR deficiency syndrome with a phenotype reflecting the human condition." Human Molecular Genetics **13**(23): 2947-2957.

Coutinho, A. E. and K. E. Chapman (2011). "The anti-inflammatory and immunosuppressive effects of glucocorticoids, recent developments and mechanistic insights." Mol Cell Endocrinol **335**(1): 2-13.

Cruz, P. M. R., M. Al-Hajjar, S. Huda, L. Jacobson, M. Woodhall, S. Jayawant, C. Buckley, D. Hilton-Jones, D. Beeson, A. Vincent, M. I. Leite and J. Palace (2015). "Clinical Features and Diagnostic Usefulness of Antibodies to Clustered Acetylcholine Receptors in the Diagnosis of Seronegative Myasthenia Gravis." Jama Neurology **72**(6): 642-649.

Cunnick, J. M., L. Mei, C. A. Doupnik and J. Wu (2001). "Phosphotyrosines 627 and 659 of Gab1 constitute a bisphosphoryl tyrosine-based activation motif (BTAM) conferring binding and activation of SHP2." Journal of Biological Chemistry **276**(26): 24380-24387.

Dayot, S., D. Speisky, A. Couvelard, P. Bourgoin, V. Gratio, J. Cros, V. Rebours, A. Sauvanet, P. Bedossa, V. Paradis, P. Ruszniewski, A. Couvineau and T. Voisin (2018). "In vitro, in vivo and ex vivo demonstration of the antitumoral role of hypocretin-1/orexin-A and almorexant in pancreatic ductal adenocarcinoma." Oncotarget **9**(6): 6952-6967.

Deb, T. B., L. Wong, D. S. Salomon, G. C. Zhou, J. E. Dixon, J. S. Gutkind, S. A. Thompson and G. R. Johnson (1998). "A common requirement for the catalytic activity and both SH2 domains of SHP-2 in mitogen-activated protein (MAP) kinase activation by the ErbB family of receptors - A specific role for SHP-2 in MAP, but not c-jun

amino-terminal kinase activation." Journal of Biological Chemistry **273**(27): 16643-16646.

Devaux, J. J., Y. Miura, Y. Fukami, T. Inoue, C. Manso, M. Belghazi, K. Sekiguchi, N. Kokubun, H. Ichikawa, A. H. Y. Wong and N. Yuki (2016). "Neurofascin-155 IgG4 in chronic inflammatory demyelinating polyneuropathy." Neurology **86**(9): 800-807.

Deymeer, F., O. Gungor-Tuncer, V. Yilmaz, Y. Parman, P. Serdaroglu, C. Ozdemir, A. Vincent and G. Saruhan-Direskeneli (2007). "Clinical comparison of anti-MuSK- vs anti-AChR-positive and seronegative myasthenia gravis." Neurology **68**(8): 609-611.

Di Stefano, V., A. Lupica, M. G. Rispoli, A. Di Muzio, F. Brighina and C. Rodolico (2020). "Rituximab in AChR subtype of myasthenia gravis: systematic review." J Neurol Neurosurg Psychiatry **91**(4): 392-395.

Diaz-Manera, J., E. Martinez-Hernandez, L. Querol, R. Klooster, R. Rojas-Garcia, X. Suarez-Calvet, J. L. Munoz-Blanco, C. Mazia, K. R. Straasheijm, E. Gallardo, C. Juarez, J. J. Verschuuren and I. Illa (2012). "Long-lasting treatment effect of rituximab in MuSK myasthenia." Neurology **78**(3): 189-193.

Dobbins, G. C., S. W. Luo, Z. H. Yang, W. C. Xiong and L. Mei (2008). "alpha-Actinin interacts with rapsyn in agrin-stimulated AChR clustering." Molecular Brain **1**.

Dong, X. P., X. M. Li, T. M. Gao, E. E. Zhang, G. S. Feng, W. C. Xiong and L. Mei (2006). "Shp2 is dispensable in the formation and maintenance of the neuromuscular junction." Neurosignals **15**(2): 53-63.

Drachman, D. B., C. W. Angus, R. N. Adams, J. D. Michelson and G. J. Hoffman (1978). "Myasthenic Antibodies Cross-Link Acetylcholine Receptors to Accelerate Degradation." New England Journal of Medicine **298**(20): 1116-1122.

Durnberger, G., B. Z. Camurdanoglu, M. Tomschik, M. Schutzbier, E. Roitinger, O. Hudecz, K. Mechtler and R. Herbst (2014). "Global Analysis of Muscle-specific Kinase Signaling by Quantitative Phosphoproteomics." Molecular & Cellular Proteomics **13**(8): 1993-2003.

Eaton, L. M. and E. H. Lambert (1957). "Electromyography and Electric Stimulation of Nerves in Diseases of Motor Unit - Observations on Myasthenic Syndrome Associated with Malignant Tumors." Jama-Journal of the American Medical Association **163**(13): 1117-1124.

Engel, A. G., K. Ohno and S. M. Sine (2003). "Sleuthing molecular targets for neurological diseases at the neuromuscular junction." Nature Reviews Neuroscience **4**(5): 339-352.

Escher, P., E. Lacazette, M. Courtet, A. Blindenbacher, L. Landmann, G. Bezakova, K. C. Lloyd, U. Mueller and H. R. Brenner (2005). "Synapses form in skeletal muscles lacking neuregulin receptors." Science **308**(5730): 1920-1923.

Evoli, A. (2006). "Clinical aspects of neuromuscular transmission disorders." Acta Neurol Scand Suppl **183**: 8-11.

Evoli, A., P. E. Alboini, A. Bisonni, A. Mastrorosa and E. Bartoccioni (2012). "Management challenges in muscle-specific tyrosine kinase myasthenia gravis." Ann N Y Acad Sci **1274**: 86-91.

Evoli, A., P. E. Alboini, V. Damato and R. Iorio (2016). "3,4-Diaminopyridine may improve myasthenia gravis with MuSK antibodies." Neurology **86**(11): 1070-1071.

Evoli, A., P. E. Alboini, R. Iorio, V. Damato and E. Bartoccioni (2017). "Pattern of ocular involvement in myasthenia gravis with MuSK antibodies." J Neurol Neurosurg Psychiatry **88**(9): 761-763.

Evoli, A., M. R. Bianchi, R. Riso, G. M. Minicuci, A. P. Batocchi, S. Servidei, F. Scuderi and E. Bartoccioni (2008). "Response to therapy in myasthenia gravis with anti-MuSK antibodies." Ann N Y Acad Sci **1132**: 76-83.

Evoli, A., P. A. Tonali, L. Padua, M. L. Monaco, F. Scuderi, A. P. Batocchi, M. Marino and E. Bartoccioni (2003). "Clinical correlates with anti-MuSK antibodies in generalized seronegative myasthenia gravis." Brain **126**(Pt 10): 2304-2311.

Farrugia, M. E., R. P. Kennett, D. Hilton-Jones, J. Newsom-Davis and A. Vincent (2007). "Quantitative EMG of facial muscles in myasthenia patients with MuSK antibodies." Clin Neurophysiol **118**(2): 269-277.

Farrugia, M. E., R. P. Kennett, J. Newsom-Davis, D. Hilton-Jones and A. Vincent (2006). "Single-fiber electromyography in limb and facial muscles in muscle-specific kinase antibody and acetylcholine receptor antibody myasthenia gravis." Muscle Nerve **33**(4): 568-570.

Farrugia, M. E., M. D. Robson, L. Clover, P. Anslow, J. Newsom-Davis, R. Kennett, D. Hilton-Jones, P. M. Matthews and A. Vincent (2006). "MRI and clinical studies of facial and bulbar muscle involvement in MuSK antibody-associated myasthenia gravis." Brain **129**(Pt 6): 1481-1492.

Ferns, M. J., J. T. Campanelli, W. Hoch, R. H. Scheller and Z. Hall (1993). "The Ability of Agrin to Cluster Achrs Depends on Alternative Splicing and on Cell-Surface Proteoglycans." Neuron **11**(3): 491-502.

Finn, A. J., G. Feng and A. M. Pendergast (2003). "Postsynaptic requirement for Abl kinases in assembly of the neuromuscular junction." Nat Neurosci **6**(7): 717-723.

Flanagan-Steet, H., M. A. Fox, D. Meyer and J. R. Sanes (2005). "Neuromuscular synapses can form in vivo by incorporation of initially aneural postsynaptic specializations." Development **132**(20): 4471-4481.

Furuta, N., K. Ishizawa, M. Shibata, S. Tsukagoshi, S. Nagamine, K. Makioka, Y. Fujita, M. Ikeda, S. Yoshimura, M. Motomura, K. Okamoto and Y. Ikeda (2015). "Anti-MuSK Antibody-positive Myasthenia Gravis Mimicking Amyotrophic Lateral Sclerosis." Intern Med **54**(19): 2497-2501.

Gallardo, E., E. Martinez-Hernandez, M. J. Titulaer, M. G. Huijbers, M. A. Martinez, A. Ramos, L. Querol, J. Diaz-Manera, R. Rojas-Garcia, C. R. Hayworth, J. J. Verschuuren,

R. Balice-Gordon, J. Dalmau and I. Illa (2014). "Cortactin autoantibodies in myasthenia gravis." Autoimmunity Reviews **13**(10): 1003-1007.

Gao, H., L. Zhao, H. Wang, E. J. Xie, X. H. Wang, Q. Wu, Y. Y. Yu, X. Y. He, H. B. Ji, L. Rink, J. X. Min and F. D. Wang (2017). "Metal transporter Slc39a10 regulates susceptibility to inflammatory stimuli by controlling macrophage survival." Proceedings of the National Academy of Sciences of the United States of America **114**(49): 12940-12945.

Garner, K., A. N. Hunt, G. Koster, P. Somerharju, E. Groves, M. Li, P. Raghu, R. Holic and S. Cockcroft (2012). "Phosphatidylinositol Transfer Protein, Cytoplasmic 1 (PITPNC1) Binds and Transfers Phosphatidic Acid." Journal of Biological Chemistry **287**(38): 32263-32276.

Gasperi, C., A. Melms, B. Schoser, Y. N. Zhang, J. Meltoranta, V. Risson, L. Schaeffer, B. Schalke and S. Kroger (2014). "Anti-agrin autoantibodies in myasthenia gravis." Neurology **82**(22): 1976-1983.

Gaspersic, R., B. Koritnik, N. Crne-Finderle and J. Sketelj (1999). "Acetylcholinesterase in the neuromuscular junction." Chem Biol Interact **119-120**: 301-308.

Geng, L., H. L. Zhang and H. B. Peng (2009). "The formation of acetylcholine receptor clusters visualized with quantum dots." Bmc Neuroscience **10**.

Giraud, M., R. Taubert, C. Vandiedonck, X. Y. Ke, M. Levi-Strauss, F. Pagani, F. E. Baralle, B. Eymard, C. Tranchant, P. Gajdos, A. Vincent, N. Willcox, D. Beeson, B. Kyewski and H. J. Garchon (2007). "An IRF8-binding promoter variant and AIRE control CHRNA1 promiscuous expression in thymus." Nature **448**(7156): 934-U939.

Giraud, M., C. Vandiedonck and H. J. Garchon (2008). "Genetic factors in autoimmune myasthenia gravis." Myasthenia Gravis and Related Disorders: 11th International Conference **1132**: 180-192.

Glass, D. J., D. C. Bowen, T. N. Stitt, C. Radziejewski, J. Bruno, T. E. Ryan, D. R. Gies, S. Shah, K. Mattsson, S. J. Burden, P. S. DiStefano, D. M. Valenzuela, T. M. DeChiara and G. D. Yancopoulos (1996). "Agrin acts via a MuSK receptor complex." Cell **85**(4): 513-523.

Glass, D. J., T. M. DeChiara, T. N. Stitt, P. S. DiStefano, D. M. Valenzuela and G. D. Yancopoulos (1996). "The receptor tyrosine kinase MuSK is required for neuromuscular junction formation and is a functional receptor for agrin." Cold Spring Harb Symp Quant Biol **61**: 435-444.

Godfrey, E. W., R. M. Nitkin, B. G. Wallace, L. L. Rubin and U. J. McMahan (1984). "Components of Torpedo electric organ and muscle that cause aggregation of acetylcholine receptors on cultured muscle cells." J Cell Biol **99**(2): 615-627.

Grob, D., N. Brunner, T. Namba and M. Pagala (2008). "Lifetime course of myasthenia gravis." Muscle & Nerve **37**(2): 141-149.

Gronseth, G. S. and R. J. Barohn (2000). "Practice parameter: Thymectomy for autoimmune myasthenia gravis (an evidence-based review) - Report of the Quality Standards Subcommittee of the American Academy of Neurology." Neurology **55**(1): 7-15.

Grosskopf, S., C. Eckert, C. Arkona, S. Radetzki, K. Bohm, U. Heinemann, G. Wolber, J. P. von Kries, W. Birchmeier and J. Rademann (2015). "Selective Inhibitors of the Protein Tyrosine Phosphatase SHP2 Block Cellular Motility and Growth of Cancer Cells in vitro and in vivo." Chemmedchem **10**(5): 815-826.

Guptill, J. T. and D. B. Sanders (2010). "Update on muscle-specific tyrosine kinase antibody positive myasthenia gravis." Curr Opin Neurol **23**(5): 530-535.

Guptill, J. T., D. B. Sanders and A. Evoli (2011). "Anti-MuSK antibody myasthenia gravis: clinical findings and response to treatment in two large cohorts." Muscle Nerve **44**(1): 36-40.

Hack, A. A., M. E. Groh and E. M. McNally (2000). "Sarcoglycans in muscular dystrophy." Microscopy Research and Technique **48**(3-4): 167-180.

Hain, B., K. Jordan, M. Deschauer and S. Zierz (2006). "Successful treatment of MuSK antibody-positive myasthenia gravis with rituximab." Muscle Nerve **33**(4): 575-580.

Hallock, P. T., S. Chin, S. Blais, T. A. Neubert and D. J. Glass (2016). "Sorbs1 and-2 Interact with CrkL and Are Required for Acetylcholine Receptor Cluster Formation." Molecular and Cellular Biology **36**(2): 262-270.

Hallock, P. T., C. F. Xu, T. J. Park, T. A. Neubert, T. Curran and S. J. Burden (2010). "Dok-7 regulates neuromuscular synapse formation by recruiting Crk and Crk-L." Genes Dev **24**(21): 2451-2461.

Halpern, B., P. Bakouche and C. Martial-Lasfargues (1969). "[Destruction of nerve cells cultured "in vitro" by lymphocytes from patients with multiple sclerosis. Auto-immune pathogenesis of multiple sclerosis]." Presse Med **77**(55): 2103-2106.

Haran, M., A. Schattner, A. Mate, D. Starobin, G. Haran and M. Shtalrid (2013). "Can a rare form of myasthenia gravis shed additional light on disease mechanisms?" Clin Neurol Neurosurg **115**(5): 562-566.

Hehir, M. K., L. D. Hobson-Webb, M. Benatar, et al (2017). "Rituximab as treatment for anti-MuSK myasthenia gravis: Multicenter blinded prospective review." Neurology **89**(10): 1069-1077.

Heinemann, S., S. Bevan, R. Kullberg, J. Lindstrom and J. Rice (1977). "Modulation of Acetylcholine-Receptor by Antibody against Receptor." Proceedings of the National Academy of Sciences of the United States of America **74**(7): 3090-3094.

Heldal, A. T., J. F. Owe, N. E. Gilhus and F. Romi (2009). "Seropositive Myasthenia Gravis: A Nationwide Epidemiologic Study." Neurology **73**(2): 150-151.

Henriquez, J. P., A. Webb, M. Bence, H. Bildsoe, M. Sahores, S. M. Hughes and P. C. Salinas (2008). "Wnt signaling promotes AChR aggregation at the neuromuscular

synapse in collaboration with agrin." Proceedings of the National Academy of Sciences of the United States of America **105**(48): 18812-18817.

Herbst, R. and S. J. Burden (2000). "The juxtamembrane region of MuSK has a critical role in agrin-mediated signaling." Embo Journal **19**(1): 67-77.

Heuser, J. E. and S. R. Salpeter (1979). "Organization of Acetylcholine Receptors in Quick-Frozen, Deep-Etched, and Rotary-Replicated Torpedo Postsynaptic Membrane." Journal of Cell Biology **82**(1): 150-173.

Higuchi, O., J. Hamuro, M. Motomura and Y. Yamanashi (2011). "Autoantibodies to Low-Density Lipoprotein Receptor-Related Protein 4 in Myasthenia Gravis." Annals of Neurology **69**(2): 418-422.

Hoch, W., J. McConville, S. Helms, J. Newsom-Davis, A. Melms and A. Vincent (2001). "Auto-antibodies to the receptor tyrosine kinase MuSK in patients with myasthenia gravis without acetylcholine receptor antibodies." Nat Med **7**(3): 365-368.

Hoffacker, V., A. Schultz, J. J. Tiesinga, R. Gold, B. Schalke, W. Nix, R. Kiefer, H. K. Muller-Hermelink and A. Marx (2000). "Thymomas alter the T-cell subset composition in the blood: a potential mechanism for thymoma-associated autoimmune disease." Blood **96**(12): 3872-3879.

Hong, Y., P. Zisimopoulou, N. Trakas, K. Karagiorgou, C. Stergiou, G. O. Skeie, H. J. Hao, X. Gao, J. F. Owe, X. Zhang, Y. X. Yue, F. Romi, Q. Wang, H. F. Li, N. E. Gilhus and S. J. Tzartos (2017). "Multiple antibody detection in 'seronegative' myasthenia gravis patients." European Journal of Neurology **24**(6): 844-850.

Howard, J. F., V. Bril, T. M. Burns, et al (2019). "Randomized phase 2 study of FcRn antagonist efgartigimod in generalized myasthenia gravis." Neurology **92**(23): E2661-E2673.

Howard, J. F., M. Freimer, F. O'Brien, J. J. Wang, S. R. Collins, J. T. Kissel and M. P. S. Grp (2017). "Qmg and Mg-Adl Correlations: Study of Eculizumab Treatment of Myasthenia Gravis." Muscle & Nerve **56**(2): 328-330.

Howard, J. F., R. J. Nowak, G. I. Wolfe, M. L. Freimer, T. H. Vu, J. L. Hinton, M. Benatar, P. W. Duda, J. E. MacDougall, R. Farzaneh-Far, H. J. Kaminski and Z. M. S. Grp (2020). "Clinical Effects of the Self-administered Subcutaneous Complement Inhibitor Zilucoplan in Patients With Moderate to Severe Generalized Myasthenia Gravis Results of a Phase 2 Randomized, Double-Blind, Placebo-Controlled, Multicenter Clinical Trial." Jama Neurology **77**(5): 582-592.

Howard, J. F., K. Utsugisawa, M. Benatar, et al (2017). "Safety and efficacy of eculizumab in anti-acetylcholine receptor antibody-positive refractory generalised myasthenia gravis (REGAIN): a phase 3, randomised, double-blind, placebo-controlled, multicentre study." Lancet Neurology **16**(12): 976-986.

Huda, S., M. Cao, A. De Rosa, M. Woodhall, P. M. Rodriguez Cruz, J. Cossins, M. Maestri, R. Ricciardi, A. Evoli, D. Beeson and A. Vincent (2020). "SHP2 inhibitor protects AChRs from effects of myasthenia gravis MuSK antibody." Neurol Neuroimmunol Neuroinflamm **7**(1).

Huda, S., P. Waters, M. Woodhall, M. I. Leite, L. Jacobson, A. De Rosa, M. Maestri, R. Ricciardi, J. M. Heckmann, A. Maniaol, A. Evoli, J. Cossins, D. Hilton-Jones and A. Vincent (2017). "IgG-specific cell-based assay detects potentially pathogenic MuSK-Abs in seronegative MG." Neurol Neuroimmunol Neuroinflamm **4**(4): e357.

Hughes, T. (2005). "The early history of myasthenia gravis." Neuromuscular Disorders **15**(12): 878-886.

Huijbers, M. G., E. H. Niks, R. Klooster, M. de Visser, J. B. Kuks, J. H. Veldink, P. Klarenbeek, P. Van Damme, M. H. de Baets, S. M. van der Maarel, L. H. van den Berg and J. J. Verschuuren (2016). "Myasthenia gravis with muscle specific kinase antibodies mimicking amyotrophic lateral sclerosis." Neuromuscul Disord **26**(6): 350-353.

Huijbers, M. G., D. L. Vergoossen, Y. E. Fillie-Grijpma, I. E. van Es, M. T. Koning, L. M. Slot, H. Veelken, J. J. Plomp, S. M. van der Maarel and J. J. Verschuuren (2019). "MuSK myasthenia gravis monoclonal antibodies: Valency dictates pathogenicity." Neurol Neuroimmunol Neuroinflamm **6**(3): e547.

Huijbers, M. G., A. F. D. Vink, E. H. Niks, R. H. Westhuis, E. W. van Zwet, R. H. de Meel, R. Rojas-Garcia, J. Diaz-Manera, J. B. Kuks, R. Klooster, K. Straasheijm, A. Evoli, I. Illa, S. M. van der Maarel and J. J. Verschuuren (2016). "Longitudinal epitope mapping in MuSK myasthenia gravis: implications for disease severity." Journal of Neuroimmunology **291**: 82-88.

Huijbers, M. G., W. Zhang, R. Klooster, E. H. Niks, M. B. Friese, K. R. Straasheijm, P. E. Thijssen, H. Vrolijk, J. J. Plomp, P. Vogels, M. Losen, S. M. Van der Maarel, S. J. Burden and J. J. Verschuuren (2013). "MuSK IgG4 autoantibodies cause myasthenia gravis by inhibiting binding between MuSK and Lrp4." Proc Natl Acad Sci U S A **110**(51): 20783-20788.

Irani, S. R., P. Pettingill, K. A. Kleopa, N. Schiza, P. Waters, C. Mazia, L. Zuliani, O. Watanabe, B. Lang, C. Buckley and A. Vincent (2012). "Morvan syndrome: Clinical and serological observations in 29 cases." Annals of Neurology **72**(2): 241-255.

Jacob, S., S. Viegas, M. I. Leite, R. Webster, J. Cossins, R. Kennett, D. Hilton-Jones, B. P. Morgan and A. Vincent (2012). "Presence and Pathogenic Relevance of Antibodies to Clustered Acetylcholine Receptor in Ocular and Generalized Myasthenia Gravis." Archives of Neurology **69**(8): 994-1001.

Jacobson, L., D. Beeson, S. Tzartos and A. Vincent (1999). "Monoclonal antibodies raised against human acetylcholine receptor bind to all five subunits of the fetal isoform." Journal of Neuroimmunology **98**(2): 112-120.

Janer, M., A. Cowland, J. Picard, D. Campbell, P. Pontarotti, J. Newsom-Davis, M. Bunce, K. Welsh, A. Demaine, A. G. Wilson and N. Willcox (1999). "A susceptibility region for myasthenia gravis extending into the HLA-class I sector telomeric to HLA-C." Human Immunology **60**(9): 909-917.

Jha, S., K. P. Xu, T. Maruta, M. Oshima, D. R. Mosier, M. Z. Atassi and W. Hoch (2006). "Myasthenia gravis induced in mice by immunization with the recombinant

extracellular domain of rat muscle-specific kinase (MuSK)." Journal of Neuroimmunology **175**(1-2): 107-117.

Jo, S. A., X. J. Zhu, M. A. Marchionni and S. J. Burden (1995). "Neuregulins Are Concentrated at Nerve-Muscle Synapses and Activate Ach-Receptor Gene-Expression." Nature **373**(6510): 158-161.

Jonsson, D. I., R. Pirskanen and F. Piehl (2017). "Beneficial effect of tocilizumab in myasthenia gravis refractory to rituximab." Neuromuscul Disord **27**(6): 565-568.

Kaegi, C., B. Wuest, J. Schreiner, U. C. Steiner, A. Vultaggio, A. Matucci, C. Crowley and O. Boyman (2019). "Systematic Review of Safety and Efficacy of Rituximab in Treating Immune-Mediated Disorders." Front Immunol **10**: 1990.

Kamimura, K., K. Ueno, J. Nakagawa, R. Hamada, M. Saitoe and N. Maeda (2013). "Perlecan regulates bidirectional Wnt signaling at the Drosophila neuromuscular junction." Journal of Cell Biology **200**(2): 219-233.

Kamisawa, T. and K. Okazaki (2017). "Diagnosis and Treatment of IgG4-Related Disease." Curr Top Microbiol Immunol **401**: 19-33.

Katarzyna, M. Z., K. Belaya, M. Leite, W. Patrick, A. Vincent and D. Beeson (2015). "Collagen Q - A potential target for autoantibodies in myasthenia gravis." Journal of the Neurological Sciences **348**(1-2): 241-244.

Katz, B. and R. Miledi (1965). "Release of Acetylcholine from a Nerve Terminal by Electric Pulses of Variable Strength and Duration." Nature **207**(5001): 1097-&.

Kawakami, Y., M. Ito, M. Hirayama, K. Sahashi, B. Ohkawara, A. Masuda, H. Nishida, N. Mabuchi, A. G. Engel and K. Ohno (2011). "Anti-MuSK autoantibodies block binding of collagen Q to MuSK." Neurology **77**(20): 1819-1826.

Keesey, J. C. (2002). ""Crisis" in myasthenia gravis: An historical perspective." Muscle & Nerve **26**(1): 1-3.

Kerty, E., A. Elsais, Z. Argov, A. Evoli and N. E. Gilhus (2014). "EFNS/ENS Guidelines for the treatment of ocular myasthenia." European Journal of Neurology **21**(5): 687-693.

Keung, B., K. R. Robeson, D. B. DiCapua, J. B. Rosen, K. C. O'Connor, J. M. Goldstein and R. J. Nowak (2013). "Long-term benefit of rituximab in MuSK autoantibody myasthenia gravis patients." J Neurol Neurosurg Psychiatry **84**(12): 1407-1409.

Khan, M. M., D. Lustrino, W. A. Silveira, et a;l (2016). "Sympathetic innervation controls homeostasis of neuromuscular junctions in health and disease." Proc Natl Acad Sci U S A **113**(3): 746-750.

Khosroshahi, A., D. B. Bloch, V. Deshpande and J. H. Stone (2010). "Rituximab therapy leads to rapid decline of serum IgG4 levels and prompt clinical improvement in IgG4-related systemic disease." Arthritis Rheum **62**(6): 1755-1762.

Kishida, S., H. Yamamoto and A. Kikuchi (2004). "Wnt-3a and Dvl induce neurite retraction by activating Rho-associated kinase." Molecular and Cellular Biology **24**(10): 4487-4501.

Klein, R., A. Marx, P. Strobel, B. Schalke, W. Nix and N. Willcox (2013). "Autoimmune associations and autoantibody screening show focused recognition in patient subgroups with generalized myasthenia gravis." Human Immunology **74**(9): 1184-1193.

Klooster, R., J. J. Plomp, M. G. Huijbers, E. H. Niks, K. R. Straasheijm, F. J. Detmers, P. W. Hermans, K. Sleijpen, A. Verrips, M. Losen, P. Martinez-Martinez, M. H. De Baets, S. M. van der Maarel and J. J. Verschuuren (2012). "Muscle-specific kinase myasthenia gravis IgG4 autoantibodies cause severe neuromuscular junction dysfunction in mice." Brain **135**(Pt 4): 1081-1101.

Koneczny, I. (2018). "A New Classification System for IgG4 Autoantibodies." Front Immunol **9**: 97.

Koneczny, I. (2018). "A New Classification System for IgG4 Autoantibodies." Frontiers in Immunology **9**.

Koneczny, I., J. Cossins, P. Waters, D. Beeson and A. Vincent (2013). "MuSK myasthenia gravis IgG4 disrupts the interaction of LRP4 with MuSK but both IgG4 and IgG1-3 can disperse preformed agrin-independent AChR clusters." PLoS One **8**(11): e80695.

Koneczny, I., D. Rennspiess, F. Marcuse, et al (2019). "Characterization of the thymus in Lrp4 myasthenia gravis: Four cases." Autoimmunity Reviews **18**(1): 50-55.

Koneczny, I., J. A. Stevens, A. De Rosa, et al (2017). "IgG4 autoantibodies against muscle-specific kinase undergo Fab-arm exchange in myasthenia gravis patients." J Autoimmun **77**: 104-115.

Konig, N., H. R. Stetefeld, C. Dohmen, et al (2021). "MuSK-antibodies are associated with worse outcome in myasthenic crisis requiring mechanical ventilation." Journal of Neurology.

Krejci, E., F. Coussen, N. Duval, J. M. Chatel, C. Legay, M. Puype, J. Vandekerckhove, J. Cartaud, S. Bon and J. Massoulie (1991). "Primary structure of a collagenic tail peptide of Torpedo acetylcholinesterase: co-expression with catalytic subunit induces the production of collagen-tailed forms in transfected cells." EMBO J **10**(5): 1285-1293.

Kucukerden, M., R. Huda, E. Tuzun, A. Yilmaz, L. Skriapa, N. Trakas, R. T. Strait, F. D. Finkelman, S. Kabadayi, P. Zisimopoulou, S. Tzartos and P. Christadoss (2016). "MuSK induced experimental autoimmune myasthenia gravis does not require IgG1 antibody to MuSK." J Neuroimmunol **295-296**: 84-92.

Kummer, T. T., T. Misgeld and J. R. Sanes (2006). "Assembly of the postsynaptic membrane at the neuromuscular junction: paradigm lost." Current Opinion in Neurobiology **16**(1): 74-82.

Kurihara, Y., J. Yamagami, T. Funakoshi, M. Ishii, J. Miyamoto, Y. Fujio, R. Kakuta, A. Tanikawa, Y. Aoyama, K. Iwatsuki, N. Ishii, T. Hashimoto, W. Nishie, H. Shimizu, K. Kouyama and M. Amagai (2019). "Rituximab therapy for refractory autoimmune bullous diseases: A multicenter, open-label, single-arm, phase 1/2 study on 10 Japanese patients." J Dermatol **46**(2): 124-130.

Laemmli, U. K. (1970). "Cleavage of Structural Proteins during Assembly of Head of Bacteriophage-T4." Nature **227**(5259): 680-+.

Lee, M., D. Beeson and J. Palace (2018). "Therapeutic strategies for congenital myasthenic syndromes." Ann N Y Acad Sci **1412**(1): 129-136.

Lee, W. Y., C. R. Free and S. M. Sine (2009). "Binding to gating transduction in nicotinic receptors: Cys-loop energetically couples to pre-M1 and M2-M3 regions." J Neurosci **29**(10): 3189-3199.

Lee, Y., J. Rudell and M. Ferns (2009). "RAPSYN INTERACTS WITH THE MUSCLE ACETYLCHOLINE RECEPTOR VIA alpha-HELICAL DOMAINS IN THE alpha, beta, AND epsilon SUBUNIT INTRACELLULAR LOOPS." Neuroscience **163**(1): 222-232.

Leite, M. I., S. Jacob, S. Viegas, J. Cossins, L. Clover, B. P. Morgan, D. Beeson, N. Willcox and A. Vincent (2008). "IgG1 antibodies to acetylcholine receptors in 'seronegative' myasthenia gravis." Brain **131**(Pt 7): 1940-1952.

Lennon, V. A. and E. H. Lambert (1981). "Monoclonal Autoantibodies to Acetylcholine-Receptors - Evidence for a Dominant Idiotype and Requirement of Complement for Pathogenicity." Annals of the New York Academy of Sciences **377**(Dec): 77-96.

Li, J., Y. J. Kang, L. G. Wei, W. J. Liu, Y. P. Tian, B. Z. Chen, X. D. Lin, Y. Li, G. S. Feng and Z. X. Lu (2014). "Tyrosine Phosphatase Shp2 Mediates the Estrogen Biological Action in Breast Cancer via Interaction with the Estrogen Extranuclear Receptor." Plos One **9**(7).

Li, M., J. Han, Y. Zhang, J. Lv, J. Zhang, X. Zhao, L. Ren, H. Fang, J. Yang, Y. Zhang, X. Cui, Q. Zhang, Q. Li, Y. Du and F. Gao (2019). "Clinical analysis of Chinese anti-LRP4 antibodies in patients with myasthenia gravis." European Journal of Immunology **49**: 952-952.

Lin, W., B. Dominguez, J. Yang, P. Aryal, E. P. Brandon, F. H. Gage and K. F. Lee (2005). "Neurotransmitter acetylcholine negatively regulates neuromuscular synapse formation by a Cdk5-dependent mechanism." Neuron **46**(4): 569-579.

Lindstrom, J. M., M. E. Seybold, V. A. Lennon, S. Whittingham and D. D. Duane (1976). "Antibody to acetylcholine receptor in myasthenia gravis. Prevalence, clinical correlates, and diagnostic value." Neurology **26**(11): 1054-1059.

Littleton, E., M. Dreger, J. Palace and A. Vincent (2009). "Immunocapture and identification of cell membrane protein antigenic targets of serum autoantibodies." Mol Cell Proteomics **8**(7): 1688-1696.

Luo, Z. G., Q. Wang, J. Z. Zhou, J. B. Wang, Z. J. Luo, M. Y. Liu, X. He, A. Wynshaw-Boris, W. C. Xiong, B. Lu and L. Mei (2002). "Regulation of AChR clustering by dishevelled interacting with MuSK and PAK1." Neuron **35**(3): 489-505.

Lustig, L. R., H. Peng, H. Hiel, T. Yamamoto and P. A. Fuchs (2001). "Molecular cloning and mapping of the human nicotinic acetylcholine receptor alpha 10 (CHRNA10)." Genomics **73**(3): 272-283.

MacLennan, C., D. Beeson, A. M. Buijs, A. Vincent and J. Newsom-Davis (1997). "Acetylcholine receptor expression in human extraocular muscles and their susceptibility to myasthenia gravis." Ann Neurol **41**(4): 423-431.

Maddison, P., J. McConville, M. E. Farrugia, N. Davies, M. Rose, F. Norwood, H. Jungbluth, S. Robb and D. Hilton-Jones (2011). "The use of rituximab in myasthenia gravis and Lambert-Eaton myasthenic syndrome." J Neurol Neurosurg Psychiatry **82**(6): 671-673.

Madhavan, R., Z. L. L. Gong, J. J. Ma, A. W. S. Chan and H. B. Peng (2009). "The Function of Cortactin in the Clustering of Acetylcholine Receptors at the Vertebrate Neuromuscular Junction." Plos One **4**(12).

Madhavan, R., X. T. T. Zhao, M. A. Ruegg and H. B. Peng (2005). "Tyrosine phosphatase regulation of MuSK-dependent acetylcholine receptor clustering." Molecular and Cellular Neuroscience **28**(3): 403-416.

Manikandan, P. and S. Nagini (2018). "Cytochrome P450 Structure, Function and Clinical Significance: A Review." Current Drug Targets **19**(1): 38-54.

Mao, Z. F., L. X. Yang, X. A. Mo, C. Qin, Y. R. Lai, N. Y. He, T. Li and M. L. Hackett (2011). "Frequency of Autoimmune Diseases in Myasthenia Gravis: A Systematic Review." International Journal of Neuroscience **121**(3): 121-129.

Marino, M., F. Scuderi, D. Samengo, G. Saltelli, M. T. Maiuri, C. Y. Shen, L. Mei, M. Sabatelli, G. Pani, G. Antonini, A. Evoli and E. Bartoccioni (2015). "Flow Cytofluorimetric Analysis of Anti-LRP4 (LDL Receptor-Related Protein 4) Autoantibodies in Italian Patients with Myasthenia Gravis." Plos One **10**(8).

Marx, A., F. Pfister, B. Schalke, G. Saruhan-Direskeneli, A. Melms and P. Strobel (2013). "The different roles of the thymus in the pathogenesis of the various myasthenia gravis subtypes." Autoimmun Rev **12**(9): 875-884.

Matsui, N., S. Nakane, Y. Nakagawa, K. Kondo, T. Mitsui, T. Matsumoto, K. Arisawa and R. Kaji (2009). "Increasing incidence of elderly onset patients with myasthenia gravis in a local area of Japan." Journal of Neurology Neurosurgery and Psychiatry **80**(10): 1168-1171.

Matsuki, K., T. Juji, K. Tokunaga, M. Takamizawa, H. Maeda, M. Soda, Y. Nomura and M. Segawa (1990). "Hla Antigens in Japanese Patients with Myasthenia-Gravis." Journal of Clinical Investigation **86**(2): 392-399.

Matthews, I., S. Chen, R. Hewer, V. McGrath, J. Furmaniak and B. R. Smith (2004). "Muscle-specific receptor tyrosine kinase (MuSK) autoantibodies - a new immunoprecipitation assay." Journal of Neuroimmunology **154**(1-2): 96-96.

McConville, J., M. E. Farrugia, D. Beeson, U. Kishore, R. Metcalfe, J. Newsom-Davis and A. Vincent (2004). "Detection and characterization of MuSK antibodies in seronegative myasthenia gravis." Ann Neurol **55**(4): 580-584.

McMahan, U. J. (1990). "The agrin hypothesis." Cold Spring Harb Symp Quant Biol **55**: 407-418.

Meriggioli, M. N., E. Ciafaloni, K. A. Al-Hayk, J. Rowin, B. Tucker-Lipscomb, J. M. Massey and D. B. Sanders (2003). "Mycophenolate mofetil for myasthenia gravis - An analysis of efficacy, safety, and tolerability." Neurology **61**(10): 1438-1440.

Meriggioli, M. N. and D. B. Sanders (2009). "Autoimmune myasthenia gravis: emerging clinical and biological heterogeneity." Lancet Neurology **8**(5): 475-490.

Misgeld, T., T. T. Kummer, J. W. Lichtman and J. R. Sanes (2005). "Agrin promotes synaptic differentiation by counteracting an inhibitory effect of neurotransmitter." Proceedings of the National Academy of Sciences of the United States of America **102**(31): 11088-11093.

Mishina, M., T. Takai, K. Imoto, M. Noda, T. Takahashi, S. Numa, C. Methfessel and B. Sakmann (1986). "Molecular Distinction between Fetal and Adult Forms of Muscle Acetylcholine-Receptor." Nature **321**(6068): 406-411.

Missias, A. C., J. Mudd, J. M. Cunningham, J. H. Steinbach, J. P. Merlie and J. R. Sanes (1997). "Deficient development and maintenance of postsynaptic specializations in mutant mice lacking an 'adult' acetylcholine receptor subunit." Development **124**(24): 5075-5086.

Mittaud, P., P. A. Marangi, S. Erb-Vogtli and C. Fuhrer (2001). "Agrin-induced activation of acetylcholine receptor-bound Src family kinases requires Rapsyn and correlates with acetylcholine receptor clustering." J Biol Chem **276**(17): 14505-14513.

Mori, S., S. Kubo, T. Akiyoshi, S. Yamada, T. Miyazaki, H. Hotta, J. Desaki, M. Kishi, T. Konishi, Y. Nishino, A. Miyazawa, N. Maruyama and K. Shigemoto (2012). "Antibodies against muscle-specific kinase impair both presynaptic and postsynaptic functions in a murine model of myasthenia gravis." Am J Pathol **180**(2): 798-810.

Morsch, M., S. W. Reddel, N. Ghazanfari, K. V. Toyka and W. D. Phillips (2013). "Pyridostigmine but not 3,4-diaminopyridine exacerbates ACh receptor loss and myasthenia induced in mice by muscle-specific kinase autoantibody." J Physiol **591**(10): 2747-2762.

Moscoso, L. M., G. C. Chu, M. Gautam, P. G. Noakes, J. P. Merlie and J. R. Sanes (1995). "Synapse-Associated Expression of an Acetylcholine Receptor-Inducing Protein, Aria/Heregulin, and Its Putative Receptors, Erbb2 and Erbb3, in Developing Mammalian Muscle." Developmental Biology **172**(1): 158-169.

Mossman, S., A. Vincent and J. Newsom-Davis (1986). "Myasthenia gravis without acetylcholine-receptor antibody: a distinct disease entity." Lancet **1**(8473): 116-119.

Mukhtasimova, N., W. Y. Lee, H. L. Wang and S. M. Sine (2009). "Detection and trapping of intermediate states priming nicotinic receptor channel opening." Nature **459**(7245): 451-U172.

Mullis, K., F. Faloona, S. Scharf, R. Saiki, G. Horn and H. Erlich (1986). "Specific Enzymatic Amplification of DNA Invitro - the Polymerase Chain-Reaction." Cold Spring Harbor Symposia on Quantitative Biology **51**: 263-273.

Nath, N., B. Godat, C. Zimprich, S. J. Dwight, C. Corona, M. McDougall and M. Urh (2016). "Homogeneous plate based antibody internalization assay using pH sensor fluorescent dye." Journal of Immunological Methods **431**: 11-21.

Nations, S. P., G. I. Wolfe, A. A. Amato, C. E. Jackson, W. W. Bryan and R. J. Barohn (1999). "Distal myasthenia gravis." Neurology **52**(3): 632-634.

Neel, B. G., H. H. Gu and L. Pao (2003). "The 'Shp'ing news: SH2 domain-containing tyrosine phosphatases in cell signaling." Trends in Biochemical Sciences **28**(6): 284-293.

Ngo, S. T., R. N. Cole, N. Sunn, W. D. Phillips and P. G. Noakes (2012). "Neuregulin-1 potentiates agrin-induced acetylcholine receptor clustering through muscle-specific kinase phosphorylation." Journal of Cell Science **125**(6): 1531-1543.

Nikolic, A. V., G. G. Bacic, M. Z. Dakovic, S. D. Lavrnic, V. M. Rakocevic Stojanovic, I. Z. Basta and D. V. Lavrnic (2015). "Myopathy, muscle atrophy and tongue lipid composition in MuSK myasthenia gravis." Acta Neurol Belg **115**(3): 361-365.

Niks, E. H., J. B. Kuks, B. O. Roep, G. W. Haasnoot, W. Verduijn, B. E. Ballieux, M. H. De Baets, A. Vincent and J. J. Verschuuren (2006). "Strong association of MuSK antibody-positive myasthenia gravis and HLA-DR14-DQ5." Neurology **66**(11): 1772-1774.

Niks, E. H., J. B. Kuks and J. J. Verschuuren (2007). "Epidemiology of myasthenia gravis with anti-muscle specific kinase antibodies in The Netherlands." J Neurol Neurosurg Psychiatry **78**(4): 417-418.

Nishimune, H., G. Valdez, G. Jarad, C. L. Moulson, U. Muller, J. H. Miner and J. R. Sanes (2008). "Laminins promote postsynaptic maturation by an autocrine mechanism at the neuromuscular junction." Journal of Cell Biology **182**(6): 1201-1215.

Noakes, P. G., M. Gautam, J. Mudd, J. R. Sanes and J. P. Merlie (1995). "Aberrant differentiation of neuromuscular junctions in mice lacking s-laminin/laminin beta 2." Nature **374**(6519): 258-262.

Noordermeer, J., J. Klingensmith, N. Perrimon and R. Nusse (1994). "Dishevelled and Armadillo Act in the Wingless Signaling Pathway in Drosophila." Nature **367**(6458): 80-83.

Norris, P. A. A., G. Kaur and A. H. Lazarus (2020). "New insights into IVIg mechanisms and alternatives in autoimmune and inflammatory diseases." Current Opinion in Hematology **27**(6): 392-398.

Nowak, R. J., D. B. Dicapua, N. Zebardast and J. M. Goldstein (2011). "Response of patients with refractory myasthenia gravis to rituximab: a retrospective study." Ther Adv Neurol Disord **4**(5): 259-266.

Oger, J., R. Kaufman and K. Berry (1987). "Acetylcholine-Receptor Antibodies in Myasthenia-Gravis - Use of a Qualitative Assay for Diagnostic Purposes." Canadian Journal of Neurological Sciences **14**(3): 297-302.

Oh, S. J., M. B. Morgan, L. Lu, Y. Hatanaka, S. Hemmi, A. Young and G. C. Claussen (2009). "Racial differences in myasthenia gravis in Alabama." Muscle Nerve **39**(3): 328-332.

Ohta, K., K. Shigemoto, A. Fujinami, N. Maruyama, T. Konishi and M. Ohta (2007). "Clinical and experimental features of MuSK antibody positive MG in Japan." Eur J Neurol **14**(9): 1029-1034.

Okada, K., A. Inoue, M. Okada, Y. Murata, S. Kakuta, T. Jigami, S. Kubo, H. Shiraishi, K. Eguchi, M. Motomura, T. Akiyama, Y. Iwakura, O. Higuchi and Y. Yamanashi (2006). "The muscle protein Dok-7 is essential for neuromuscular synaptogenesis." Science **312**(5781): 1802-1805.

Otsuka, K., M. Ito, B. Ohkawara, A. Masuda, Y. Kawakami, K. Sahashi, H. Nishida, N. Mabuchi, A. Takano, A. G. Engel and K. Ohno (2015). "Collagen Q and anti-MuSK autoantibody competitively suppress agrin/LRP4/MuSK signaling." Sci Rep **5**: 13928.

Oury, J., Y. Liu, A. Topf, S. Todorovic, E. Hoedt, V. Preethish-Kumar, T. A. Neubert, W. Lin, H. Lochmuller and S. J. Burden (2019). "MACF1 links Rapsyn to microtubule- and actin-binding proteins to maintain neuromuscular synapses." J Cell Biol **218**(5): 1686-1705.

Owen, D., A. Topf, V. Preethish-Kumar, et al (2018). "Recessive variants of MuSK are associated with late onset CMS and predominant limb girdle weakness." Am J Med Genet A **176**(7): 1594-1601.

Pakzad, Z., T. Aziz and J. Oger (2011). "Increasing Incidence of Myasthenia Gravis among Elderly in British Columbia, Canada." Neurology **76**(17): 1526-1528.

Palace, J., J. Newsom-Davis, B. Lecky and M. G. S. Grp (1998). "A randomized double-blind trial of prednisolone alone or with azathioprine in myasthenia gravis." Neurology **50**(6): 1778-1783.

Panzer, J. A., Y. Song and R. J. Balice-Gordon (2006). "In vivo imaging of preferential motor axon outgrowth to and synaptogenesis at prepatterned acetylcholine receptor clusters in embryonic zebrafish skeletal muscle." J Neurosci **26**(3): 934-947.

Pasnoor, M., J. H. He, L. Herbelin, T. M. Burns, et al (2016). "A randomized controlled trial of methotrexate for patients with generalized myasthenia gravis." Neurology **87**(1): 57-64.

Pasnoor, M., G. I. Wolfe, S. Nations, J. Trivedi, R. J. Barohn, L. Herbelin, A. McVey, M. Dimachkie, J. Kissel, R. Walsh, A. Amato, T. Mozaffar, M. Hungs, L. Chui, J. Goldstein, S. Novella, T. Burns, L. Phillips, G. Claussen, A. Young, T. Bertorini and S. Oh (2010). "Clinical findings in MuSK-antibody positive myasthenia gravis: a U.S. experience." Muscle Nerve **41**(3): 370-374.

Patel, V., A. Oh, A. Voit, L. G. Sultatos, G. J. Babu, B. A. Wilson, M. Ho and J. J. McArdle (2014). "Altered active zones, vesicle pools, nerve terminal conductivity, and morphology during experimental MuSK myasthenia gravis." PLoS One **9**(12): e110571.

Patrick, J., J. Lindstrom, B. Culp and J. Mcmillan (1973). "Studies on Purified Eel Acetylcholine-Receptor and Anti-Acetylcholine Receptor Antibody." Proceedings of the National Academy of Sciences of the United States of America **70**(12): 3334-3338.

Patton, B. L., J. M. Cunningham, J. Thyboll, J. Kortesmaa, H. Westerblad, L. Edstrom, K. Tryggvason and J. R. Sanes (2001). "Properly formed but improperly localized synaptic specializations in the absence of laminin alpha4." Nat Neurosci **4**(6): 597-604.

Pearce, J. M. S. (2005). "Mary Broadfoot Walker (1888-1974): A historic discovery in myasthenia gravis." European Neurology **53**(1): 51-53.

Perez-Fernandez, A., G. Lopez-Ruano, R. Prieto-Bermejo, C. Ijurko, M. Diez-Campelo, F. Sanchez-Guijo and A. Hernandez-Hernandez (2019). "SHP1 and SHP2 inhibition enhances the pro-differentiative effect of phorbol esters: an alternative approach against acute myeloid leukemia." Journal of Experimental & Clinical Cancer Research **38**.

Pevzner, A., B. Schoser, K. Peters, N. C. Cosma, A. Karakatsani, B. Schalke, A. Melms and S. Kroger (2012). "Anti-LRP4 autoantibodies in AChR- and MuSK-antibody-negative myasthenia gravis." Journal of Neurology **259**(3): 427-435.

Phillips, L. H. and J. C. Torner (1996). "Epidemiologic evidence for a changing natural history of myasthenia gravis." Neurology **47**(5): 1233-1238.

Plomp, J. J., G. T. H. Vankempen, M. H. Debaets, Y. M. F. Graus, J. B. M. Kuks and P. C. Molenaar (1995). "Acetylcholine-Release in Myasthenia-Gravis - Regulation at Single End-Plate Level." Annals of Neurology **37**(5): 627-636.

Porter, C. W. and E. A. Barnard (1975). "The density of cholinergic receptors at the endplate postsynaptic membrane: ultrastructural studies in two mammalian species." J Membr Biol **20**(1-2): 31-49.

Punga, A. R., S. O. Lin, F. Oliveri, S. Meinen and M. A. Ruegg (2011). "Muscle-selective synaptic disassembly and reorganization in MuSK antibody positive MG mice." Experimental Neurology **230**(2): 207-217.

Qian, Y. K., A. W. Chan, R. Madhavan and H. B. Peng (2008). "The function of Shp2 tyrosine phosphatase in the dispersal of acetylcholine receptor clusters." BMC Neurosci **9**: 70.

Ran, F. A., P. D. Hsu, J. Wright, V. Agarwala, D. A. Scott and F. Zhang (2013). "Genome engineering using the CRISPR-Cas9 system." Nature Protocols **8**(11): 2281-2308.

Rivner, M. H., B. M. Quarles, J. X. Pan, et al (2020). "Clinical features of LRP4/agrin-antibody-positive myasthenia gravis: A multicenter study." Muscle Nerve **62**(3): 333-343.

Rodolico, C., A. Toscano, M. Autunno, S. Messina, C. Nicolosi, M. Aguennouz, M. Laura, P. Girlanda, C. Messina and G. Vita (2002). "Limb-girdle myasthenia: clinical, electrophysiological and morphological features in familial and autoimmune cases." Neuromuscular Disorders **12**(10): 964-969.

Rodriguez Cruz, P. M., J. Cossins, J. Cheung, S. Maxwell, S. Jayawant, R. Herbst, D. Waithe, A. P. Kornev, J. Palace and D. Beeson (2020). "Congenital myasthenic syndrome due to mutations in MUSK suggests that the level of MuSK phosphorylation is crucial for governing synaptic structure." Hum Mutat **41**(3): 619-631.

Rojas, M., P. Restrepo-Jimenez, D. M. Monsalve, Y. Pacheco, Y. Acosta-Ampudia, C. Ramirez-Santana, P. S. C. Leung, A. A. Ansari, M. E. Gershwin and J. M. Anaya (2018). "Molecular mimicry and autoimmunity." Journal of Autoimmunity **95**: 100-123.

Romi, F., G. O. Skeie, J. A. Aarli and N. E. Gilhus (2000). "Muscle autoantibodies in subgroups of myasthenia gravis patients." Journal of Neurology **247**(5): 369-375.

Ronager, J., M. Ravnborg, I. Hermansen and S. Vorstrup (2001). "Immunoglobulin treatment versus plasma exchange in patients with chronic moderate to severe myasthenia gravis." Artif Organs **25**(12): 967-973.

Rosso, S. B., D. Sussman, A. Wynshaw-Boris and P. C. Salinas (2005). "Wnt signaling through Dishevelled, Rac and JNK regulates dendritic development." Nature Neuroscience **8**(1): 34-42.

Ruff, R. L. and V. A. Lennon (1998). "End-plate voltage-gated sodium channels are lost in clinical and experimental myasthenia gravis." Annals of Neurology **43**(3): 370-379.

Sanders, D. B. and A. Evoli (2010). "Immunosuppressive therapies in myasthenia gravis." Autoimmunity **43**(5-6): 428-435.

Sanders, D. B. and E. V. Stalberg (1996). "AAEM minimonograph .25. Single-fiber electromyography." Muscle & Nerve **19**(9): 1069-1083.
Sapru, M. K. (2001). "Neuregulin-1 regulates expression of the Ets-2 transcription factor." Life Sciences **69**(22): 2663-2674.

Sarrigiannis, P. G., R. P. Kennett, S. Read and M. E. Farrugia (2006). "Single-fiber EMG with a concentric needle electrode: Validation in myasthenia gravis." Muscle & Nerve **33**(1): 61-65.

Schneeberger, V. E., Y. Ren, N. Luetteke, Q. L. Huang, L. W. Chen, H. R. Lawrence, N. J. Lawrence, E. B. Haura, J. M. Koomen, D. Coppola and J. Wu (2015). "Inhibition of Shp2 suppresses mutant EGFR-induced lung tumors in transgenic mouse model of lung adenocarcinoma." Oncotarget **6**(8): 6191-6202.

Scuderi, F., M. Marino, L. Colonna, F. Mannella, A. Evoli, C. Provenzano and E. Bartoccioni (2002). "Anti-p110 autoantibodies identify a subtype of "seronegative" myasthenia gravis with prominent oculobulbar involvement." Lab Invest **82**(9): 1139-1146.

Shen, C. Y., Y. S. Lu, B. Zhang, D. Figueiredo, J. Bean, J. Jung, H. T. Wu, A. Barik, D. M. Yin, W. C. Xiong and L. Mei (2013). "Antibodies against low-density lipoprotein receptor-related protein 4 induce myasthenia gravis." Journal of Clinical Investigation **123**(12): 5190-5202.

Shi, Y., I. T. Ma, R. H. Patel, et al (2015). "NSC-87877 inhibits DUSP26 function in neuroblastoma resulting in p53-mediated apoptosis." Cell Death & Disease **6**.

Shigemoto, K., S. Kubo, N. Maruyama, N. Hato, H. Yamada, C. Jie, N. Kobayashi, K. Mominoki, Y. Abe, N. Ueda and S. Matsuda (2006). "Induction of myasthenia by immunization against muscle-specific kinase." J Clin Invest **116**(4): 1016-1024.

Shiraishi, H., M. Motomura, T. Yoshimura, T. Fukudome, T. Fukuda, Y. Nakao, M. Tsujihata, A. Vincent and K. Eguchi (2005). "Acetylcholine receptors loss and postsynaptic damage in MuSK antibody-positive myasthenia gravis." Ann Neurol **57**(2): 289-293.

Siegfried, E., E. L. Wilder and N. Perrimon (1994). "Components of Wingless Signaling in Drosophila." Nature **367**(6458): 76-80.

Simon, N. G., S. W. Reddel, M. C. Kiernan and R. Layzer (2013). "Muscle-specific kinase antibodies: a novel cause of peripheral nerve hyperexcitability?" Muscle Nerve **48**(5): 819-823.

Skjei, K. L., V. A. Lennon and N. L. Kuntz (2013). "Muscle specific kinase autoimmune myasthenia gravis in children: a case series." Neuromuscul Disord **23**(11): 874-882.

Slater, C. R. (2015). "The functional organization of motor nerve terminals." Progress in Neurobiology **134**: 55-103.

Somnier, F. E. (2005). "Increasing incidence of late-onset anti-AChR antibody seropositive myasthenia gravis." Neurology **65**(6): 928-930.

Stathopoulos, P., A. Kumar, J. A. Vander Heiden, E. Pascual-Goni, R. J. Nowak and K. C. O'Connor (2018). "Mechanisms underlying B cell immune dysregulation and autoantibody production in MuSK myasthenia gravis." Annals of the New York Academy of Sciences **1412**(1): 154-165.

Stiegler, A. L., S. J. Burden and S. R. Hubbard (2006). "Crystal structure of the agrin-responsive immunoglobulin-like domains 1 and 2 of the receptor tyrosine kinase MuSK." Journal of Molecular Biology **364**(3): 424-433.

Strobel, P., W. Y. Chuang, S. Chuvpilo, et al (2008). "Common cellular and diverse genetic basis of thymoma-associated myasthenia gravis - Role of MHC class II and

AIRE genes and genetic polymorphisms." Myasthenia Gravis and Related Disorders: 11th International Conference **1132**: 143-156.

Strochlic, L., J. Falk, E. Goillot, S. Sigoillot, F. Bourgeois, P. Delers, J. Rouviere, A. Swain, V. Castellani, L. Schaeffer and C. Legay (2012). "Wnt4 Participates in the Formation of Vertebrate Neuromuscular Junction." Plos One **7**(1).

Takamori, M., T. Nakamura and M. Motomura (2013). "Antibodies against Wnt receptor of muscle-specific tyrosine kinase in myasthenia gravis." Journal of Neuroimmunology **254**(1-2): 183-186.

Takata, K., P. Stathopoulos, M. Cao, M. Mane-Damas, M. L. Fichtner, E. S. Benotti, L. Jacobson, P. Waters, S. R. Irani, P. Martinez-Martinez, D. Beeson, M. Losen, A. Vincent, R. J. Nowak and K. C. O'Connor (2019). "Characterization of pathogenic monoclonal autoantibodies derived from muscle-specific kinase myasthenia gravis patients." JCI Insight **4**(12).

Tan, C. S. and I. J. Koralnik (2010). "Progressive multifocal leukoencephalopathy and other disorders caused by JC virus: clinical features and pathogenesis." Lancet Neurology **9**(4): 425-437.

Tang, H. B., P. Macpherson, L. S. Argetsinger, D. Cieslak, S. T. Suhr, C. Carter-Su and D. Goldman (2004). "CaM kinase II-dependent phosphorylation of myogenin contributes to activity-dependent suppression of nAChR gene expression in developing rat myotubes." Cellular Signalling **16**(5): 551-563.

Tanowitz, M., J. T. Si, D. H. Yu, G. S. Feng and L. Mei (1999). "Regulation of neuregulin-mediated acetylcholine receptor synthesis by protein tyrosine phosphatase SHP2." Journal of Neuroscience **19**(21): 9426-9435.

Tansey, M. G., G. C. Chu and J. P. Merlie (1996). "ARIA/HRG regulates AChR epsilon subunit gene expression at the neuromuscular synapse via activation of phosphatidylinositol 3-kinase and Ras/MAPK pathway." Journal of Cell Biology **134**(2): 465-476.

Tendijke, P., H. Yamashita, T. K. Sampath, A. H. Reddi, M. Estevez, D. L. Riddle, H. Ichijo, C. H. Heldin and K. Miyazono (1994). "Identification of Type-I Receptors for Osteogenic Protein-1 and Bone Morphogenetic Protein-4." Journal of Biological Chemistry **269**(25): 16985-16988.

Thiruppathi, M., J. Rowin, B. Ganesh, J. R. Sheng, B. S. Prabhakar and M. N. Meriggioli (2012). "Impaired regulatory function in circulating CD4(+)CD25(high)CD127(low/-) T cells in patients with myasthenia gravis." Clinical Immunology **145**(3): 209-223.

Till, J. H., M. Becerra, A. Watty, Y. Lu, Y. L. Ma, T. A. Neubert, S. J. Burden and S. R. Hubbard (2002). "Crystal structure of the MuSK tyrosine kinase: Insights into receptor autoregulation." Structure **10**(9): 1187-1196.

Tindall, R. S. A., J. T. Phillips, J. A. Rollins, L. Wells and K. Hall (1993). "A Clinical Therapeutic Trial of Cyclosporine in Myasthenia-Gravis." Annals of the New York Academy of Sciences **681**: 539-551.

Topakian, R., F. Zimprich, S. Iglseder, N. Embacher, M. Guger, K. Stieglbauer, D. Langenscheidt, J. Rath, S. Quasthoff, P. Simschitz, J. Wanschitz, D. Windisch, P. Muller, D. Oel, G. Schustereder, S. Einsiedler, C. Eggers and W. Loscher (2019). "High efficacy of rituximab for myasthenia gravis: a comprehensive nationwide study in Austria." J Neurol **266**(3): 699-706.

Trinidad, J. C. and J. B. Cohen (2004). "Neuregulin inhibits acetylcholine receptor aggregation in myotubes." J Biol Chem **279**(30): 31622-31628.

Tsiamalos, P., G. Kordas, A. Kokla, K. Poulas and S. J. Tzartos (2009). "Epidemiological and immunological profile of muscle-specific kinase myasthenia gravis in Greece." Eur J Neurol **16**(8): 925-930.

Tuzun, E., S. Berrih-Aknin, T. Brenner, L. L. Kusner, R. Le Panse, H. Yang, S. Tzartos and P. Christadoss (2015). "Guidelines for standard preclinical experiments in the mouse model of myasthenia gravis induced by acetylcholine receptor immunization." Experimental Neurology **270**: 11-17.

Tuzun, E. and P. Christadoss (2013). "Complement associated pathogenic mechanisms in myasthenia gravis." Autoimmunity Reviews **12**(9): 904-911.

Tuzun, E., B. G. Scott, E. Goluszko, S. Higgs and P. Christadoss (2003). "Genetic evidence for involvement of classical complement pathway in induction of experimental autoimmune myasthenia gravis." Journal of Immunology **171**(7): 3847-3854.

Tuzun, E., V. Yilmaz, Y. Parman, P. Oflazer, F. Deymeer and G. Saruhan-Direskeneli (2011). "Increased complement consumption in MuSK-antibody-positive myasthenia gravis patients." Med Princ Pract **20**(6): 581-583.

Tzartos, S. J. and J. M. Lindstrom (1980). "Monoclonal-Antibodies Used to Probe Acetylcholine-Receptor Structure - Localization of the Main Immunogenic Region and Detection of Similarities between Subunits." Proceedings of the National Academy of Sciences of the United States of America-Biological Sciences **77**(2): 755-759.

Ulusoy, C., F. Cavus, V. Yilmaz and E. Tuzun (2017). "Immunization with Recombinantly Expressed LRP4 Induces Experimental Autoimmune Myasthenia Gravis in C57BL/6 Mice." Immunological Investigations **46**(5): 490-499.

Ulusoy, C., E. Kim, E. Tuzun, R. Huda, V. Yilmaz, K. Poulas, N. Trakas, L. Skriapa, A. Niarchos, R. T. Strait, F. D. Finkelman, S. Turan, P. Zisimopoulou, S. Tzartos, G. Saruhan-Direskeneli and P. Christadoss (2014). "Preferential production of IgG1, IL-4 and IL-10 in MuSK-immunized mice." Clinical Immunology **151**(2): 155-163.

Usmani, A., L. Kwan, D. Wahib-Khalil, J. Trivedi, S. Nations and R. Sarode (2019). "Excellent response to therapeutic plasma exchange in myasthenia gravis patients irrespective of antibody status." J Clin Apher **34**(4): 416-422.

van Amerongen, R. and R. Nusse (2009). "Towards an integrated view of Wnt signaling in development." Development **136**(19): 3205-3214.

van der Neut Kolfschoten, M., J. Schuurman, M. Losen, W. K. Bleeker, P. Martinez-Martinez, E. Vermeulen, T. H. den Bleker, L. Wiegman, T. Vink, L. A. Aarden, M. H. De Baets, J. G. van de Winkel, R. C. Aalberse and P. W. Parren (2007). "Anti-inflammatory activity of human IgG4 antibodies by dynamic Fab arm exchange." Science **317**(5844): 1554-1557.

Vergoossen, D. L. E., J. J. Plomp, C. Gstottner, Y. E. Fillie-Grijpma, R. Augustinus, R. Verpalen, M. Wuhrer, P. W. H. I. Parren, E. Dominguez-Vega, S. M. van der Maarel, J. J. Verschuuren and M. G. Huijbers (2021). "Functional monovalency amplifies the pathogenicity of anti-MuSK IgG4 in myasthenia gravis." Proceedings of the National Academy of Sciences of the United States of America **118**(13).

Vidarsson, G., G. Dekkers and T. Rispens (2014). "IgG subclasses and allotypes: from structure to effector functions." Front Immunol **5**: 520.

Viegas, S., L. Jacobson, P. Waters, J. Cossins, S. Jacob, M. I. Leite, R. Webster and A. Vincent (2012). "Passive and active immunization models of MuSK-Ab positive myasthenia: electrophysiological evidence for pre and postsynaptic defects." Exp Neurol **234**(2): 506-512.

Vincent, A. (2002). "Unravelling the pathogenesis of myasthenia gravis." Nature Reviews Immunology **2**(10): 797-804.

Vincent, A., J. Bowen, J. Newsom-Davis and J. McConville (2003). "Seronegative generalised myasthenia gravis: clinical features, antibodies, and their targets." Lancet Neurol **2**(2): 99-106.

Vincent, A., L. Clover, C. Buckley, J. G. Evans, P. M. Rothwell and U. M. G. Survey (2003). "Evidence of underdiagnosis of myasthenia gravis in older people." Journal of Neurology Neurosurgery and Psychiatry **74**(8): 1105-1108.

Vincent, A., S. G. Cullcandy, J. Newsomdavis, A. Trautmann, P. C. Molenaar and R. L. Polak (1981). "Congenital Myasthenia - Endplate Acetylcholine-Receptors and Electrophysiology in 5 Cases." Muscle & Nerve **4**(4): 306-318.

Vincent, A. and M. I. Leite (2005). "Neuromuscular junction autoimmune disease: muscle specific kinase antibodies and treatments for myasthenia gravis." Curr Opin Neurol **18**(5): 519-525.

Vincent, A., M. I. Leite, M. E. Farrugia, S. Jacob, S. Viegas, H. Shiraishi, O. Benveniste, B. P. Morgan, D. Hilton-Jones, J. Newsom-Davis, D. Beeson and N. Willcox (2008). "Myasthenia gravis seronegative for acetylcholine receptor antibodies." Ann N Y Acad Sci **1132**: 84-92.

Vincent, A. and J. Newsom-Davis (1982). "Acetylcholine receptor antibody characteristics in myasthenia gravis. I. Patients with generalized myasthenia or disease restricted to ocular muscles." Clin Exp Immunol **49**(2): 257-265.

Vincent, A. and J. Newsomdavis (1985). "Acetylcholine-Receptor Antibody as a Diagnostic-Test for Myasthenia-Gravis - Results in 153 Validated Cases and 2967 Diagnostic Assays." Journal of Neurology Neurosurgery and Psychiatry **48**(12): 1246-1252.

Wallace, B. G., Z. C. Qu and R. L. Huganir (1991). "Agrin Induces Phosphorylation of the Nicotinic Acetylcholine-Receptor." Neuron **6**(6): 869-878.

Wang, B. B., Y. Li, M. Sui, Q. Q. Qi, T. Wang, D. Liu, M. L. Zhou, Y. J. Zheng, L. Q. Zhu and B. Zhang (2020). "Identification of the downstream molecules of agrin/Dok-7 signaling in muscle." Faseb Journal **34**(4): 5144-5161.

Wang, J., N. J. Ruan, L. Qian, W. L. Lei, F. Chen and Z. G. Luo (2008). "Wnt/beta-catenin signaling suppresses Rapsyn expression and inhibits acetylcholine receptor clustering at the neuromuscular junction." Journal of Biological Chemistry **283**(31): 21668-21675.

Wang, J. M., Z. Jing, L. L. Zhang, G. D. Zhou, J. Braun, Y. Yao and Z. Z. Wang (2003). "Regulation of acetylcholine receptor clustering by the tumor suppressor APC." Nature Neuroscience **6**(10): 1017-1018.

Waters, M. J., D. Field and J. Ravindran (2019). "Refractory myasthenia gravis successfully treated with ofatumumab." Muscle & Nerve **60**(6): E45-E47.

Weidoff, P. M., M. G. Mcnamee and B. W. Wilson (1981). "Alteration of Acetylcholine-Receptor and Acetylcholinesterase Metabolism by Actinomycin-D in Cultured Muscle-Cells." Canadian Journal of Physiology and Pharmacology **59**(6): 580-585.

Wendell, L. C. and J. M. Levine (2011). "Myasthenic crisis." Neurohospitalist **1**(1): 16-22.

Weston, C., C. Gordon, G. Teressa, E. Hod, X. D. Ren and J. Prives (2003). "Cooperative regulation by Rac and Rho of agrin-induced acetylcholine receptor clustering in muscle cells." J Biol Chem **278**(8): 6450-6455.

Whiting, P., A. Vincent and J. Newsomdavis (1985). "Monoclonal-Antibodies to Torpedo Acetylcholine-Receptor - Characterization of Antigenic Determinants within the Cholinergic Binding-Site." European Journal of Biochemistry **150**(3): 533-539.

Willcox, N., M. I. Leite, Y. Kadota, M. Jones, A. Meager, P. Subrahmanyam, B. Dasgupta, B. P. Morgan and A. Vincent (2008). "Autoimmunizing mechanisms in thymoma and thymus." Myasthenia Gravis and Related Disorders: 11th International Conference **1132**: 163-173.

Wolfe, G. I., H. J. Kaminski, I. B. Aban, et al (2019). "Long-term effect of thymectomy plus prednisone versus prednisone alone in patients with non-thymomatous myasthenia gravis: 2-year extension of the MGTX randomised trial." Lancet Neurology **18**(3): 259-268.

Wolfe, G. I., H. J. Kaminski, J. R. Sonnett, I. B. Aban, H. C. Kuo and G. R. Cutter (2016). "Randomized trial of thymectomy in myasthenia gravis." Journal of Thoracic Disease **8**(12): E1782-E1783.

Wu, H., Y. Lu, C. Shen, N. Patel, L. Gan, W. C. Xiong and L. Mei (2012). "Distinct roles of muscle and motoneuron LRP4 in neuromuscular junction formation." Neuron **75**(1): 94-107.

Wyatt, R. M. and R. J. Balice-Gordon (2003). "Activity-dependent elimination of neuromuscular synapses." Journal of Neurocytology **32**(5-8): 777-794.

Xing, G., H. Jing, L. Zhang, Y. Cao, L. Li, K. Zhao, Z. Dong, W. Chen, H. Wang, R. Cao, W. C. Xiong and L. Mei (2019). "A mechanism in agrin signaling revealed by a prevalent Rapsyn mutation in congenital myasthenic syndrome." Elife **8**.

Xu, K., S. Jha, W. Hoch and S. E. Dryer (2006). "Delayed synapsing muscles are more severely affected in an experimental model of MuSK-induced myasthenia gravis." Neuroscience **143**(3): 655-659.

Yamamoto, J., K. Ihara, H. Nakayama, S. Hikino, K. Satoh, N. Kubo, T. Iida, Y. Fujii and T. Hara (2004). "Characteristic expression of aryl hydrocarbon receptor repressor gene in human tissues: Organ-specific distribution and variable induction patterns in mononuclear cells." Life Sciences **74**(8): 1039-1049.

Yang, X. L., Y. Z. Huang, W. C. Xiong and L. Mei (2005). "Neuregulin-induced expression of the acetylcholine receptor requires endocytosis of ErbB receptors." Molecular and Cellular Neuroscience **28**(2): 335-346.

Yilmaz, A., C. Kattamuri, R. N. Ozdeslik, C. Schmiedel, S. Mentzer, C. Schorl, E. Oancea, T. B. Thompson and J. R. Fallon (2016). "MuSK is a BMP co-receptor that shapes BMP responses and calcium signaling in muscle cells." Science Signaling **9**(444).

Yu, Y. L., B. R. Hawkins, M. S. M. Ip, V. Wong and E. Woo (1992). "Myasthenia-Gravis in Hong-Kong Chinese .1. Epidemiology and Adult Disease." Acta Neurologica Scandinavica **86**(2): 113-119.

Yumoto, N., N. Kim and S. J. Burden (2012). "Lrp4 is a retrograde signal for presynaptic differentiation at neuromuscular synapses." Nature **489**(7416): 438-442.

Zambelis, T., P. Kokotis and N. Karandreas (2011). "Repetitive Nerve Stimulation of Facial and Hypothenar Muscles: Relative Sensitivity in Different Myasthenia Gravis Subgroups." European Neurology **65**(4): 203-207.

Zhang, B., C. Liang, R. Bates, Y. M. Yin, W. C. Xiong and L. Mei (2012). "Wnt proteins regulate acetylcholine receptor clustering in muscle cells." Molecular Brain **5**.

Zhang, B., S. Luo, Q. Wang, T. Suzuki, W. C. Xiong and L. Mei (2008). "LRP4 serves as a coreceptor of agrin." Neuron **60**(2): 285-297.

Zhang, B., C. Y. Shen, B. Bealmear, S. Ragheb, W. C. Xiong, R. A. Lewis, R. P. Lisak and L. Mei (2014). "Autoantibodies to Agrin in Myasthenia Gravis Patients." Plos One **9**(3).

Zhang, B., J. S. Tzartos, M. Belimezi, S. Ragheb, B. Bealmear, R. A. Lewis, W. C. Xiong, R. P. Lisak, S. J. Tzartos and L. Mei (2012). "Autoantibodies to Lipoprotein-

Related Protein 4 in Patients With Double-Seronegative Myasthenia Gravis." Archives of Neurology **69**(4): 445-451.

Zhang, W., A. S. Coldefy, S. R. Hubbard and S. J. Burden (2011). "Agrin binds to the N-terminal region of Lrp4 protein and stimulates association between Lrp4 and the first immunoglobulin-like domain in muscle-specific kinase (MuSK)." J Biol Chem **286**(47): 40624-40630.

Zhang, X. F., M. S. Yang, J. Z. Xu, M. Zhang, B. Lang, W. Wang and A. Vincent (2007). "Clinical and serological study of myasthenia gravis in HuBei Province, China." Journal of Neurology Neurosurgery and Psychiatry **78**(4): 386-390.

Zhao, K., C. Y. Shen, L. Li, H. T. Wu, G. L. Xing, Z. Q. Dong, H. Y. Jing, W. B. Chen, H. S. Zhang, Z. B. Tan, J. X. Pan, L. Xiong, H. S. Wang, W. P. Cui, X. D. Sun, S. H. Li, X. P. Huang, W. C. Xiong and L. Mei (2018). "Sarcoglycan Alpha Mitigates Neuromuscular Junction Decline in Aged Mice by Stabilizing LRP4." Journal of Neuroscience **38**(41): 8860-8873.

Zhao, X. T., Y. K. Qian, A. W. Chan, R. Madhavan and H. B. Peng (2007). "Regulation of ACh receptor clustering by the tyrosine phosphatase Shp2." Dev Neurobiol **67**(13): 1789-1801.

Zinman, L., E. Ng and V. Bril (2007). "IV immunoglobulin in patients with myasthenia gravis - A randomized controlled trial." Neurology **68**(11): 837-841.

Zisimopoulou, P., P. Evangelakou, J. Tzartos,et al (2014). "A comprehensive analysis of the epidemiology and clinical characteristics of anti-LRP4 in myasthenia gravis." Journal of Autoimmunity **52**: 139-145.

Zong, Y., B. Zhang, S. Gu, K. Lee, J. Zhou, G. Yao, D. Figueiredo, K. Perry, L. Mei and R. Jin (2012). "Structural basis of agrin-LRP4-MuSK signaling." Genes Dev **26**(3): 247-258.

Zuber, B. and N. Unwin (2013). "Structure and superorganization of acetylcholine receptor-rapsyn complexes." Proc Natl Acad Sci U S A **110**(26): 10622-10627.